AD633019

REPORT NUMBER 163

NOVEMBER 1965

PRELIMINARY FLUTTER ANALYSIS

VOLUME I WING

XV-5A

LIFT FAN FLIGHT RESEARCH AIRCRAFT PROGRAM

CONTRACT NUMBER DA44-177-TC-715

GENERAL ELECTRIC

NASA Scientific and Technical Information Facility

operated for the National Aeronautics and Space Administration by Documentation Incorporated

Post Office Box 33
College Park, Md. 20740

Telephone | Area Code 301
779-2121

FACILITY CONTROL NO. 52749

DATE 5/31/66

ATTACHED IS A DOCUMENT ON LOAN

FROM: NASA Scientific and Technical Information Facility

TO: Defense Documentation Center
Attn: DDC-IRC (Control Branch)
Cameron Station
Alexandria, Va. 22314

In accordance with the NASA-DOD Cooperative AD Number Assignment Agreement it is requested that an AD number be assigned to the attached report.

☑ As this is our only available copy the return of the document (with AD number and any applicable distribution limitations) to the address below is essential.

☐ This document may be retained by DDC. If retained, please indicate AD number and any applicable distribution limitations on the reproduced copy of the title page and return to the address below.

Return Address: NASA Scientific and Technical Information Facility
Attention: INPUT BRANCH
P. O. Box 33
College Park, Maryland 20740

ACCESSION for
CFSTI WHITE SECTION ☒
DDC BUFF SECTION ☐
UNANNOUNCED ☐
JUSTIFICATION .....
BY .....
DISTRIBUTION/AVAILABILITY CODES
DIST. AVAIL. and/or SPECIAL
1

Report Number 163

PRELIMINARY FLUTTER ANALYSIS

VOLUME I - WING

XV-5A Lift Fan
Flight Research Aircraft

Contract DA 44-177-TC-715

December 1965

DDC
MAY 24 1966
A

OK for CFSTI per telecon Mr. Spooner 1 June 66 jwade

ADVANCED ENGINE & TECHNOLOGY DEPARTMENT
GENERAL ELECTRIC COMPANY
CINCINNATI, OHIO 45215

32749

CONTENTS

SECTION		PAGE
1.0	SUMMARY	1
2.0	INTRODUCTION	3
3.0	METHOD OF APPROACH	5
3.1	Idealization of Aircraft	9
3.1.1	Structural Representation	9
3.1.1.1	Beam Elements	9
3.1.1.2	Torque Tube Elements	10
3.1.1.3	Torque Box Elements	11
3.1.2	Aerodynamic Representation	11
3.1.2.1	Development - Wing	12
3.1.2.1.1	Aerodynamic Center	21
3.1.2.2	Development - Empennage	22
3.1.3	Mass Representation	22
3.2	Vibration (Modal) Analysis	23
3.2.1	Vibration Modes (Normal)	23
3.2.2	Vibration Modes with Gyroscopic Effects	23
3.3	Flutter Analysis	25
4.0	DISCUSSION AND RESULTS	27
4.1	Idealization of Aircraft	31
4.1.1	Structural Representation	31
4.1.1.1	Wing - Aileron	31
4.1.1.2	Fuselage - Empennage	32
4.1.2	Aerodynamic Representation	33
4.1.2.1	Wing - Aileron	33
4.1.2.2	Horizontal-Vertical Stabilizer	34
4.1.3	Mass Representation	34
4.2	Vibration (Modal) Analysis	35
4.2.1	Vibration Modes (Normal)	35
4.2.2	Vibration Modes with Gyroscopic Effects	35

SECTION PAGE

4.3 Flutter Analysis 37

4.3.1 Phase I - Basic Structural Evaluation 37

4.3.1.1 Results 37

4.3.2 Phase II - Wing Front and Rear Spar Flexibility Studies 38

4.3.2.1 Results 38

4.3.3 Phase III - Aileron Mass-Balance Studies 38

4.3.3.1 Results 39

4.3.4 Phase IV - Re-evaluation of Nominal and Optimum Stiffness Configurations 39

4.3.4.1 Results 39

4.3.5 Phase V - Flight Envelope Evaluation 40

4.3.5.1 Results 40

4.3.6 Phase VI - Wing Structural Nose Box Evaluation 40

4.3.6.1 Results 41

4.3.7 Phase VII - Aileron Equivalent Spring Restraint Studies 41

4.3.7.1 Results 41

4.3.8 Phase VIII - Aircraft Simulation Studies 41

4.3.8.1 Results 42

4.3.9 Phase IX - Aerodynamic Simulation Studies 42

4.3.9.1 Results 42

5.0 CONCLUSIONS 43

5.1 Vibration (Modal) Analysis 43

5.1.1 Vibration Modes (Normal) 43

5.1.2 Vibration Modes with Gyroscopic Effects 44

5.2 Flutter Analysis 44

5.2.1 Phase I - Basic Structural Evaluation 44

5.2.2 Phase II - Wing Front and Rear Spar Flexibility Studies 45

5.2.3 Phase III - Aileron Mass-Balance Studies 45

5.2.4 Phase IV - Re-evaluation of Nominal and Optimum Stiffness Configurations 46

5.2.5 Phase V - Flight Envelope Evaluation 46

5.2.6 Phase VI - Wing Structural Nose Box Evaluation 47

SECTION			PAGE
	5.2.7	Phase VII - Aileron Equivalent Spring Restraint Studies	47
	5.2.8	Phase VIII - Aircraft Simulation Studies	47
	5.2.9	Phase IX - Aerodynamic Simulation Studies	48
	5.2.10	Overall Evaluation	49
6.0	APPENDIX		51
	6.1	List of References	51

LIST OF FIGURES

FIGURE		PAGE
1.	Three View of XV-5A	53
2.	Beam Element	55
3.	Torque Tube Element	55
4.	Torque Box Element	56
5.	Definition of Aerodynamic Coordinates	56
6.	XV-5A Cutaway View	57
7.	Idealized Structure Used in Symmetric Analysis	59
8.	Vertical Model Used in Antisymmetric Analysis	60
9.	Lateral Model Used in Antisymmetric Analysis	61
10.	Wing Geometry	62
11.	Aileron Geometry	63
12.	Front Wing Spar-Bending Stiffness Distribution	64
13.	Rear Wing Spar-Bending Stiffness Distribution	64
14.	Wing Rib-Bending Stiffness Distribution	65
15.	Wing Ficticious Spar-Bending Stiffness Distribution	66
16.	Idealized Wing - Skin, Spar and Rib Web Average Thickness	66
17.	Equivalent Torque Tube - Torsional Stiffness Distribution	67
18.	Aileron - Bending and Torsional Stiffness Distribution	68
19.	Fuselage Geometry	69
20.	Horizontal Stabilizer Geometry	70
21.	Vertical Stabilizer Geometry	71
22.	Fuselage - Bending and Torsional Stiffness Distribution	72
23.	Horizontal Stabilizer - Bending and Torsional Stiffness Distribution	73
24.	Vertical Stabilizer - Bending and Torsional Stiffness Distribution	74
25.	Proposed Flight Envelope	75
26.	Wing Planform - Aerodynamic Simulation	76
27.	$C_{L_\alpha}\left[Q^{L\alpha}\right]$	77
28.	$C_{L_\beta}\left[Q^{L\beta}\right]$	78

BLANK PAGE

LIST OF FIGURES (Continued)

FIGURE		PAGE
29.	$C_{L_\beta} \left\lfloor Q^{L\beta} \right\rfloor$	79
30.	$C_{M_\beta} \left\lfloor Q^{M\beta} \right\rfloor$	80
31.	$C_{M_\beta} \left\lfloor Q^{M\beta} \right\rfloor$	81
32.	$C_{H_\alpha} \left\lfloor Q^{H\alpha} \right\rfloor$	82
33.	$C_{H_\beta} \left\lfloor Q^{H\beta} \right\rfloor$	83

Symmetric Mode Shapes - Stiffness Configuration 5A-Gyroscopic Forces Out

34.	Mode 1	84
35.	Mode 2	85
36.	Mode 3	86
37.	Mode 4	87
38.	Mode 5	88
39.	Mode 6	89
40.	Mode 7	90
41.	Mode 8	91

Antisymmetric Mode Shapes - Stiffness Configuration 5A - Gyroscopic Forces Out

42.	Mode 1	92
43.	Mode 2	93
44.	Mode 3	94
45.	Mode 4	95
46.	Mode 5	96
47.	Mode 6	97
48.	Mode 7	98
49.	Mode 8	99
50.	Mode 9	100

Symmetric Mode Shapes - Stiffness Configuration 5A - Gyroscopic Forces In

51.	Mode 1	101
52.	Mode 2	102
53.	Mode 3	103

LIST OF FIGURES (Continued)

FIGURE		PAGE
54.	Mode 4	104
55.	Mode 5	105
56.	Mode 6	106
57.	Mode 7	107
58.	Mode 8	108
Antisymmetric Mode Shapes - Stiffness Configuration 5A - Gyroscopic Forces In		
59.	Mode 1	109
60.	Mode 2	110
61.	Mode 3	111
62.	Mode 4	112
63.	Mode 5	113
64.	Mode 6	114
65.	Mode 7	115
66.	Mode 8	116
67.	Mode 9	117
Phase I Studies		
68.	Symmetric: Flight Condition D (M = 0.75 at sea-level)	118
69.	Symmetric: Flight Condition D (M = 0.75 at sea-level)	119
70.	Antisymmetric: Flight Condition D (M = 0.75 at sea-level)	120
71.	Antisymmetric: Flight Condition D (M = 0.75 at sea-level)	121
Phase II Studies		
72.	Symmetric: Flight Condition D (M = 0.75 at sea-level)	122
73.	Symmetric: Flight Condition D (M = 0.75 at sea-level)	123
74.	Symmetric: Flight Condition D (M = 0.75 at sea-level)	124
75.	Antisymmetric: Flight Condition D (M = 0.75 at sea-level)	125
76.	Antisymmetric: Flight Condition D (M = 0.75 at sea-level)	126

LIST OF FIGURES (Continued)

FIGURE		PAGE
77.	Antisymmetric: Flight Condition D (M = 0.75 at sea-level)	127
Phase III Studies		
78.	Symmetric: Flight Condition D (M = 0.75 at sea-level)	128
79.	Antisymmetric: Flight Condition D (M = 0.75 at sea-level)	129
Phase IV Studies		
80.	Antisymmetric: Flight Condition D (M = 0.75 at sea-level)	130
81.	Symmetric: Flight Condition D (M = 0.75 at sea-level)	131
82.	Antisymmetric: Flight Condition D (M = 0.75 at sea-level)	132
Phase V Studies		
83.	Symmetric: Flight Condition D (M = 0.75 at sea-level)	133
84.	Symmetric: Flight Condition A (M = 0.82 at sea-level)	134
85.	Symmetric: Flight Condition E (M = 0.90 at 5,000')	135
86.	Symmetric: Flight Condition B (M = 0.98 at 9,500')	136
87.	Symmetric: Flight Conditions D, A, E and B	137
88.	Antisymmetric: Flight Condition D (M = 0.75 at sea-level)	138
89.	Antisymmetric: Flight Condition A (M = 0.82 at sea-level)	139
90.	Antisymmetric: Flight Condition E (M = 0.90 at 5,000')	140
91.	Antisymmetric: Flight Condition B (M = 0.98 at 9,500')	141
92.	Antisymmetric: Flight Conditions, D, A, E and B	142

LIST OF FIGURES (Continued)

FIGURE		PAGE
Phase VI Studies		
93.	Symmetric: Flight Condition D (M = 0.75 at sea-level)	143
94.	Antisymmetric: Flight Condition D (M = 0.75 at sea-level)	144
Phase VII Studies		
95.	Symmetric: Flight Condition D (M = 0.75 at sea-level)	145
96.	Antisymmetric: Flight Condition D (M = 0.75 at sea-level)	146
Phase VIII Studies		
97.	Cantilevered Wing - Flight Condition D (M = 0.75 at sea-level)	147
98.	Rigid Fuselage and Empennage - Flight Condition D (M = 0.75 at sea-level)	148
99.	Rigid Fuselage and Empennage - Flight Condition A (M = 0.82 at sea-level)	149
100.	Rigid Fuselage and Empennage - Flight Condition E (M = 0.90 at 5,000')	150
101.	Rigid Fuselage and Empennage - Flight Condition B (M = 0.98 at 9,500')	151
Phase IX Studies		
102.	Lag Function Effects - Flight Condition D (M = 0.75 at sea-level)	152
103.	Lag Function Effects - Flight Condition A (M = 0.82 at sea-level)	153
104.	Lag Function Effects - Flight Condition E (M = 0.90 at 5,000')	154
105.	Lag Function Effects - Flight Condition B (M = 0.98 at 9,500')	155
106.	C_{M_q} Effects - Flight Condition D (M = 0.75 at sea-level)	156
107.	C_{M_q} Effects - Flight Condition A (M = 0.82 at sea-level)	157

LIST OF FIGURES (Continued)

FIGURE		PAGE
108.	C_{M_q} Effects - Flight Condition E (M = 0.90 at 5,000')	158
109.	C_{M_q} Effects - Flight Condition B (M = 0.98 at 9,500')	159
Overall Evaluation		
110.	Flutter Boundary Envelope	160

TABLES

TABLE		PAGE
1.	Aerodynamic Data	161
2.	Stiffness Configurations	161
3.	Flight Conditions	162
4.	Mass and Inertia Distribution (Symmetric Idealization)	163
5.	Mass and Inertia Distribution (Antisymmetric Idealization)	165
6.	Aileron - Mass and Inertia Configurations	167
7.	Modal Data Stiffness Configuration 5A Mass Condition 9 No Gyroscopic Forces	170
8.	Modal Data Stiffness Configuration 5P Mass Condition 8 No Gyroscopic Forces	171
9.	Modal Data Stiffness Configuration 5A Mass Condition 9 Gyroscopic Forces	172
10.	Modal Data Stiffness Configuration 5P Mass Condition 8 Gyroscopic Forces	173

SYMBOLS AND AXES

SYMBOLS

A_{ij}	Element of matrix of aerodynamic influence coefficients, $\sigma \bar{A}_{ij}$
a.c.	Aerodynamic center
b_o	Reference half-chord
$\bar{c}$	Mean aerodynamic chord
c	Aerodynamic chord
c_ℓ	Local sectional lift coefficient
C_{ij}	Element of matrix of flexibility influence coefficients
C(k)	Theodorsen's Lag Function
C_{L_α}, C_{M_β}, C_{H_α}, C_{H_β}, C_{M_q}	- Aerodynamic coefficients
d_2, d_4	Dimensions of shear panel of length ℓ
E	Young's modulus of elasticity
EI	Equivalent beam flexural stiffness
$e^{i\omega t}$	Harmonic motion notation
f	Trailing edge flap
f	Frequency (cycles per second)
$F_{1,2}$	Force
$F_{1,2,3,4}$	Shear flow
g	Coefficient of structural damping or overall damping (structural and aerodynamic)

BLANK PAGE

SYMBOLS (Continued)

G	Shear modulus
GJ	Equivalent beam torsional stiffness
G_{ij}	Element of matrix of gyroscopic terms
h	Aerodynamic hinge-moment per unit span; beam height for vertical shear; vertical displacement of airfoil at a reference axis
$H, \overline{H}$	Aerodynamic hinge-moment
i	Station i; $\sqrt{-1}$
I_{zz}	Mass moment of inertia of wing fan about axis of rotation (lb-in-sec^2)
I	Mass or area moment of inertia
j	Station j
J_{ii}	Element of the mass matrix
k_o	Reduced frequency parameter, $\frac{b_o\omega}{V}$
k	Downwash angle
K_{ij}	Element of matrix of stiffness influence coefficients
K_β	Aileron overall spring restraint
ℓ	Length of beam or torque-tube element; aerodynamic lift per unit span; semi-span
$L, \overline{L}$	Aerodynamic Lift
m	Aerodynamic moment per unit span
$M, \overline{M}$	Mach Number; Aerodynamic moment
$M_{1,2}$	Moment

SYMBOLS (Continued)

$M_{\theta_x}, M_{\theta_y}$	Gyroscopic moments
p	Laplace transformation variable
q	Dynamic pressure; generalized displacement; dimensionless pitch velocity of airfoil
q_β	Dimensionless pitch velocity of control surface
Q	Generalized force
Q_{ij}	Element of matrix of aerodynamic influence coefficients
R_{ii}	Element of aerodynamic integration matrix
t	Web or shear panel thickness
V	Forward velocity
V_o	Velocity corresponding to the Mach Number at a particular altitude
U	Strain Energy
W_1, W_2, etc.	Control surface aerodynamic functions
X_o	Distance from leading edge of airfoil to moment center as a fraction of the total chord
X_1	Distance from leading edge of airfoil to rotation center as a fraction of the total chord
X_a	Distance from leading edge of airfoil to control surface hinge location as a fraction of the total chord
α	Angle of rotation
β	Angle of rotation of control surface relative to airfoil
$\bar{\alpha}$	Angle of attack, $\alpha + h/V$

SYMBOLS (Continued)

$\bar{\beta}$	Effective angle of rotation of control surface, $\beta + c/V\ W_2/W_1\ \dot{\beta}$
γ	Aerodynamic loading
δ_1, δ_2	Inclination of sides of shear panel with respect to Y axis
σ	Aerodynamic parameter for aerodynamic influence coefficient matrix, $4\pi\rho b_o^2 \ell^2 / k_o^2$
Ω	Complex frequency in forced vibration equation; complex eigenvalue for flutter
Ω_z	Fan rotation velocity (rpm)
ϕ	Aileron aerodynamic parameter, $\cos^{-1}(2X_a - 1)$
ω	Angular frequency (radians per second)
ρ	Air density
θ	Angular deflection, bending slope or twist
υ	Poisson's Ratio
o	Identifies maximum amplitude or maximum force in sinusoidal motion
*	Indicial notation
{ }	Column matrix
[ ]	Rectangular matrix
⌈ ⌋	Diagonal matrix
[I]	Unit matrix
$[\ ]^{-1}$	Inverse matrix

AXES

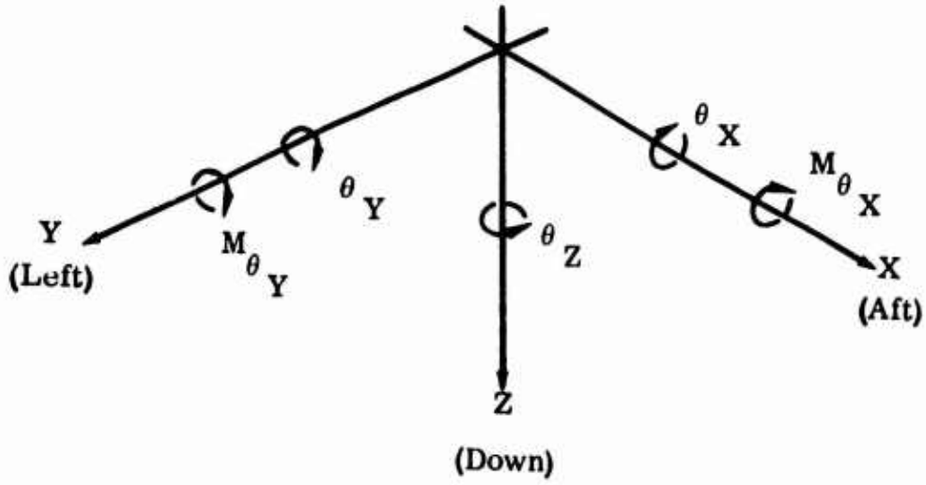

M_{θ_X}, M_{θ_Y} - Gyroscopic Moment Sense

1.0 SUMMARY

The overall preliminary theoretical flutter analysis of the XV-5A Lift Fan Aircraft is presented in three volumes. This is Volume I which reports the investigation of the flutter characteristics of the wing. Volumes II and III detail the analysis of the empennage and control surfaces respectively.

The wing theoretical flutter analysis was a joint effort by Ryan Aerospace and Computer Engineering Associated (CEA), an affiliate of Susquehanna Sciences, Inc., Pasadena, California. The program occupied the CEA direct analog computer during the period of 3 May to 25 May, 1962. The primary concern of the program was that of flutter evaluation of the XV-5A wing in the conventional flight mode. In addition, vibration mode shapes and frequencies were obtained for several wing configurations (stiffness variations) both with and without gyroscopic forces due to the rotating fans in the wings.

Results of the overall CEA analysis have indicated that the XV-5A aircraft (wing), on the basis of the preliminary data utilized in the analysis, is free of flutter within the proposed flight envelope. Studies have shown that mass-balancing of the aileron is a critical factor, and must be carefully evaluated for future design efforts on the XV-5A aircraft. Similarly, the overall spring restraint (K_β) does affect the flutter characteristics, but the variation, at most, will still lie above 15% on V_L or M_L. The flutter mode, that of antisymmetric wing bending coupled with aileron rotation, indicates that proper aircraft simulation must be used in future flutter evaluation of the XV-5A aircraft with due attention given to fuselage and/or aircraft degrees of freedom.

BLANK PAGE

2.0 INTRODUCTION

This report is the final presentation of the preliminary wing flutter and vibration (modal) analysis of the U.S. Army XV-5A Lift Fan Research Aircraft, illustrated in Figure 1.0 performed on the CEA direct analog computer. The XV-5A is a V/STOL aircraft designed for research flight testing of the General Electric X353-5 Lift Fan Propulsion System.

The use of a direct analog computer such as the CEA computer was dictated by close scheduling called for on the XV-5A Program and, consequently, required quicker answers relating to flutter evaluation than would have been possible via conventional means, (e.g. solution of the appropriate equations of motion via digital computer techniques). As stated in Reference 2, a direct analog computer offers an advantage over other computational procedures, since it permits the analyst to observe immediately the effect of design changes on the solution. The formulation of an aeroelastic problem for solution by the direct analog computer is accomplished by first representing electrically the idealized mechanical model of the structure under investigation, i.e. the circuit is a direct analogy of the structure. Next, the external forces acting on the structure, (in this case aerodynamic forces), are simulated by an electronic circuit which generates an electrical analogy for the aerodynamic forces as a function of structural deflections and solution parameters, such as aircraft velocity. Combining both the circuit which is analogous to the structure to that which is analogous to the aerodynamic forces, results in an analog simulation of an airborne elastic vehicle. References 3 through 5 provide additional references related to the use of direct analog computers.

Equations, following the technique of Reference 6, are developed in Section 3.0, Method of Approach. These equations are presented as an analogy to the actual flutter and vibration analysis performed on the CEA direct analog computer.

It is to be emphasized that these equations are not solved by the direct analog computer, and are offered only as a mathematical guide for an understanding of the analysis.

BLANK PAGE

3.0 METHOD OF APPROACH

Of the several methods of determining the flutter characteristics of lifting surfaces, the influence-coefficient method of analysis for calculating the response of a flexible surface to an oscillating disturbing force is similar to that performed by direct electronic analog treatment. The commonly used Rayleigh-Ritz technique, (formulating the equations directly in terms of chosen modal functions), is essentially redundant for the method of approach chosen for flutter analysis of the wing.

The deflection q of a point x, y on a structure subjected to a set of discrete forces or moments acting normal to the surface (assumed lying in the x-y plane and acting in the direction of z may be expressed as

$$\{q\} = [C]\{Q\} \tag{1}$$

Equation 1 is the matrix form of a set of simultaneous equations where an element c_{ij} relates the generalized displacement q_i to the generalized force Q_j. In structural nomenclature, the element c_{ij} is a flexibility influence coefficient which expresses the linear or angular deflection at point i due to the unit force or moment acting at point j. The use of generalized displacements and forces in Equation 1 implies that these may be either linear and/or angular deflections and corresponding forces and/or moments with appropriate flexibility influence coefficients.

In general, the forces to be considered in Equation 1 are an impressed sinusoidal force, inertia forces, structural damping forces, aerodynamic forces and gyroscopic forces.

Consider now each of the above forces:

Impressed Sinusoidal Force

The impressed sinusoidal force considered herein is simply a discrete force or moment applied at a node (point on the surface in the x-y plane) used for purposes of determining the flutter and modal response, as will be discussed later. In general, the force may be expressed as

$$Q_j = Q_{oj}\, e^{i\omega t} \tag{2}$$

where the subscript j denotes the node at which the force or moment is applied.

BLANK PAGE

Inertia Forces

The inertia forces considered herein are the forces set up by consequence of the accelerations developed in the structure. Since for flutter and modal analyses, we are concerned with harmonic motion, the inertia forces may be expressed as

$$\{Q\} = -[J]\{\ddot{q}\} = \omega^2 e^{i\omega t}[J]\{q_o\} \tag{3}$$

where ω is the angular frequency and the matrix $[J]$ is a diagonal matrix of masses and mass inertias lumped at the nodes.

Structural Damping Forces

The structural damping forces acting in the structure are forces in phase with the velocity and proportional to the restoring force. Therefore, we may write for the damping forces,

$$\{Q\} = -g/_{\omega}[K]\{\dot{q}\} = -ige^{i\omega t}[K]\{q_o\} \tag{4}$$

where g is the coefficient of structural damping and the matrix $[K]$ is the matrix of stiffness influence coefficients. The stiffness matrix shown in Equation 4 is the inverse of the flexibility matrix shown in Equation 1, i.e., $[K] = [C]^{-1}$.

Aerodynamic Forces

The aerodynamic forces to be considered herein may be represented by an expression also called an influence coefficient, although it is of a different nature than that denoted by Equation 1. Therefore,

$$\{Q\} = [A]\{q\} = e^{i\omega t}[A]\{q_o\} \tag{5}$$

where the matrix $[A]$ contains aerodynamic influence coefficients whose element A_{ij} represents the aerodynamic force and moment induced at point i by a unit deflection at point j. The above matrix $[A]$ is a complex matrix having real and imaginary parts.

Gyroscopic Forces

The gyroscopic forces (moments) developed on the wing structure are due to the wing fan and may be expressed as

$$\{Q_k\} = [G]\{\dot{q}_k\} = i\omega e^{i\omega t}[G]\left|q_{o_k}\right| \tag{6}$$

where the subscript k denotes the node at which the gyroscopic moments act and the matrix [G] is simply a matrix expressing the angular momentum of the rotating mass.

Substituting Equations 2 through 6 into Equation 1 results in the following matrix equation for forced vibration in an airstream:

$$\{q_o\} = [C]\left|Q_{o_j}\right| + \omega^2[C]\lceil J\rfloor\{q_o\} - ig\{q_o\} + [C][A]\{q_o\}$$
$$+ i\omega[C][G]\left|q_{o_k}\right| \tag{7}$$

Since $Q_{o_j} = J_j\omega^2 q_{o_j}$, where J_j is either the mass or mass-inertia lumped at point j, Equation 7 may be written as

$$\{q_o\} = \omega^2[C]\lceil J\rfloor\{q_o\} - ig\{q_o\} + \omega^2[C]\lceil J\rfloor\left|q_{o_j}\right| + [C][A]\{q_o\}$$
$$+ i\omega[C][G]\left|q_{o_k}\right| \tag{8}$$

where the column matrix $\left|q_{o_j}\right|$ is composed of zeros plus one finite element which is q_{o_j}, the displacement at point j due to the impressed sinusoidal force Q_{o_j} and the column matrix $\left|q_{o_k}\right|$ is composed of zeros, plus two finite elements which are the angular displacements about the x and y axes at point k.

Rearranging Equation 8 results in an expression for the column of generalized displacements:

$$\{q_o\} = {}^{\omega^2}[C][J] - {}^{ig}[I] + [C][A] \; \{q_o\} + {}^{\omega^2}[C][J] \left\{q_{o_j}\right\}$$

$$+ {}^{i\omega}[C] \; [G] \left\{q_{o_k}\right\}$$

$$[I] = {}^{\omega^2}[C] \; [J] - [C] \; [A] + {}^{ig}[I] \; \{q_o\} = {}^{\omega^2}[C] \; [J] \left\{q_{o_j}\right\}$$

$$+ {}^{i\omega}[C] \; [G] \left\{q_{o_k}\right\}$$

Dividing through by ω^2

$$\left[\frac{1}{\omega^2} [I] = [C] \; [J] - \frac{1}{\omega^2} [C] \; [A] + \frac{ig}{\omega^2} \; [I]\right] \left\{q_o\right\} = [C] \; [J] \left\{q_{o_j}\right\}$$

$$+ \frac{1}{\omega} [C] \; [G] \left\{q_{o_k}\right\}$$

or, letting $\Omega = \frac{1}{\omega^2}(1 + ig)$ and $[A] = \sigma[\bar{A}]$

$$\left[{}^{\Omega}[I] - [C] \; [J] - {}^{\sigma}[C][A]\right]\{q_o\} = [C][J] \left\{q_{o_j}\right\} + \frac{i}{\omega}[C] \; [G] \left\{q_{o_k}\right\}$$

and

$$\{q_o\} = \left[{}^{\Omega}[I] - [C] \; [J] - {}^{\sigma}[C] \; [\bar{A}]\right]^{-1} \left[[C] \; [J] \left\{q_{o_j}\right\} + \frac{i}{\omega}[C] \; [G] \left\{q_{o_k}\right\}\right] \quad (9)$$

Equation 9 is written in a general sense, and is applicable to either modal analysis or flutter analysis, as will be shown in subsequent sections.

3.1 IDEALIZATION OF AIRCRAFT

The technique of performing both a flutter and vibration analysis of an aircraft usually requires an idealization of the basic structure and its external loading which is amenable to analytical treatment. The idealization must be of sufficient rigor to meet the demands of engineering accuracy, yet be consistent with the capability of available digital or analog computers. Reference 1 presents the idealization as used in the Computer Engineering Associates' flutter and vibration simulation. However, for purposes of completeness, the discussion will be repeated here with added commentaries on the applicability of passive analog computers to the present problem.

3.1.1 Structural Representation

Since the wing of the XV-5A aircraft is of low aspect-ratio (AR=3.4) and of unusual structural arrangement, (i.e., with a large cutout for wing fan), it was decided to consider the wing more as a deforming plate with a possible elastic curvature of appreciable magnitude in two directions, (spanwise and chord-wise). Secondly, the root restraint, that of two spars with a forward nose box, presented peculiarities which play an important part in the deformations of the surface. For these reasons, it was also decided to consider the wing as an assemblage of a finite number of elastic components, e.g., flexural members, torque tubes and torque boxes. The analysis was primarily concerned with the wing dynamic characteristics, with allowance for fuselage and empennage effects. However, these latter structures were treated as simple beams, subject to engineering beam theory, in order to keep within the capabilities of the analog.

The following discussion interprets each component. These were then set up on the analog computer by passive elements.

3.1.1.1 Beam Elements (Flexure Members)

The beam elements of the idealized structure can be divided into four categories. These are:

1. Beams flexible in bending and shear

2. Beams flexible in bending but rigid in shear

3. Beams flexible in bending but with no shear carrying capability (no shear web)

4. Rigid beams

Beams of Types 2, 3 and 4 are special cases of flexibility of the general beam element of Type 1.

Consider now the beam shown in Figure 2 which represents the beam element of Type 1 above. The beam is deformed by forces and moments applied at panel points 1 and 2. Panel points 1 and 2 represent the nodes of a lumped parameter system resulting from the idealization of the actual continuous structure.

The load-deflection relationships of the beam may be expressed by the following matrix equation,

$$\begin{Bmatrix} h_2 \\ \Theta_2 \\ F_1 \\ M_1 \end{Bmatrix} = \left[\begin{array}{c|c|cc} \ell^2 \int_0^\ell \frac{(1-x/\ell)^2}{EI}\,dx + \ell \int_0^\ell \frac{dx}{Gth} & \ell \int_0^\ell \frac{(1-x/\ell)}{EI}\,dx & 1 & \ell \\ \hline \ell \int_0^\ell \frac{(1-x/\ell)}{EI}\,dx & \int_0^\ell \frac{dx}{EI} & 0 & 1 \\ \hline -1 & 0 & 0 & 0 \\ \hline -\ell & -1 & 0 & 0 \end{array}\right] \begin{Bmatrix} F_2 \\ M_2 \\ h_1 \\ \theta_1 \end{Bmatrix} \quad (10)$$

The above equation was evaluated with the assumption that the flexibility (1/EI) varies linearly over each beam segment and that the beam height (h) was constant over the segment.

3.1.1.2 Torque Tube Elements

The torque tube elements as shown in Figure 3 of the idealized structure may be expressed by the following matrix equation,

$$\begin{Bmatrix} \Theta_2 \\ M_1 \end{Bmatrix} = \left[\begin{array}{c|c} \int_0^\ell \frac{dx}{GJ} & 1 \\ \hline -1 & 0 \end{array}\right] \begin{Bmatrix} M_2 \\ \Theta_1 \end{Bmatrix} \quad (11)$$

The equation was evaluated with the assumption that the flexibility (1/GJ) varies linearly over each torque tube element.

3.1.1.3 Torque Box Elements

The torque box is best described as an element composed of two shear panels, symmetrically located above and below the neutral plane of the structure. Assuming that loads and displacements of the shear panels are antisymmetric about the neutral plane, then shear loads on the boundaries of the panels are moments about the neutral plane and displacements of the panels are rotations about the neutral plane.

Considering a typical shear panel as shown in Figure 4, the basic equations are:

For equilibrium,

$$\frac{F_1}{\ell \cos \delta_1} = \frac{F_3}{\ell \cos \delta_2} \; ; \; \frac{F_2}{d_4} = \frac{F_4}{d_2} \tag{12}$$

The strain energy stored in the panel is,

$$U = \frac{1}{2} F_4^2 \frac{\ell}{Gtd_2} \left(\frac{d_2 + d_4}{2d_2} \right) \left[1 + \frac{2}{3(1+\upsilon)} (\tan^2 \delta_1 + \tan \delta_1 \tan \delta_2 + \tan^2 \delta_2) \right] \tag{13}$$

3.1.2 Aerodynamic Representation

For analog computation, simulation of the unsteady aerodynamics for a flutter analysis of a lifting surface requires the use of assumptions or empirical approximations. As stated in Reference 1, reasonably reliable methods are available for the calculation of steady state aerodynamic loads. However, due to the greater complexity of the nonstationary problem, available methods for computing oscillating aerodynamic forces are less exact. Therefore, the aerodynamic representation used in the flutter analysis of the XV-5A aircraft was accomplished by a rational combination of the following:

A. Mathematical expressions derived for incompressible flow over an infinite aspect ratio surface.

B. Steady state aerodynamic influence coefficients relating force and/or moments to linear and/or angular deflections, calculated on a digital computer.

C. Various approximations, proved reasonable in the general flutter analysis experience.

3.1.2.1 Development - Wing

With reference to statement "A" of Paragraph 3.1.2, the following wing motion of a rigid chord is defined (see Figure 5):

$$\bar{\alpha} = \alpha + \dot{h}/V \tag{14}$$

$$q = c/V\,\dot{\alpha} \tag{15}$$

$$q_\beta = c/V\,\dot{\beta} \tag{16}$$

where:

V = Airstream velocity

c = Aerodynamic chord

α = Angle of rotation (+ L.E. up)

$\dot{h}$ = Vertical airfoil velocity at a reference axis (+ down)

$\bar{\alpha}$ = Angle of attack (at the specific reference axis)

q = Dimensionless pitch velocity

β = Angle of rotation of control surface (+ T.E. down)

x_o = Distance from leading edge to moment axis as a fraction of the total chord (c)

x_1 = Distance from leading edge to rotation center as a fraction of the total chord (c)

q_β = Dimensionless control surface pitch velocity

x_a = Control surface hinge location with respect to the leading edge

From Equations 72, 73 and 74 of Reference 7, the lift, moment and control surface hinge moment per unit span may be written as

$$L = \left(\frac{1}{2}\rho V^2\right)(c)\left[\left\{C_{L_\alpha} * \bar{\alpha}\right\} + \left\{C_{L_q} * q\right\} + \left\{C_{L_\beta} * \beta\right\} + \left\{C_{L_{q_\beta}} * q_\beta\right\}\right] \tag{17}$$

$$M = \left(\frac{1}{2}\rho V^2\right)(c^2)\left[\left\{C_{M_\alpha} * \bar{\alpha}\right\} + \left\{C_{M_q} * q\right\} + \left\{C_{M_\beta} * \beta\right\} + \left\{C_{M_{q_\beta}} * q_\beta\right\}\right] \tag{18}$$

$$H = \left(\frac{1}{2}\rho V^2\right)(c^2)\left[\left\{C_{H_\alpha} * \bar{\alpha}\right\} + \left\{C_{H_q} * q\right\} + \left\{C_{H_\beta} * \beta\right\} + \left\{C_{H_{q_\beta}} * q_\beta\right\}\right] \tag{19}$$

where the asterisk between the coefficient (C_{L_α}, etc.) and the particular coordinate ($\bar{\alpha}$, etc.) represents the indicial response, i.e., the coefficients (C_{L_α}, etc.) represent the indicial response to a unit step change in the particular coordinate involved. The indicial response of a physical system is the time variation of response to a step input if the system is initially at rest.

Following the procedure developed in Reference 7, Equations 17 through 19 may be written as

$$L = L_1 + L_2 + L_3 + L_4 \tag{20}$$

$$M = M_1 + M_2 + M_3 + M_4 \tag{21}$$

$$H = H_1 + H_2 + H_3 + H_4 \tag{22}$$

where the subscript 1 stands for the circulation components; 2 for the camber components; 3 for the first derivative impulsive terms and 4 for the equivalent inertia terms.

Therefore, as in Reference 7, the components are:

<u>Circulation Components</u> ($X_o = 1/4$; $X_1 = 3/4$)

$$L_1 = -\left(\frac{1}{2}\rho V^2\right)(c)(2\pi)\left|C(k)\left(\alpha + \frac{\dot{h}}{V} + W_1\beta + W_2\frac{c}{V}\dot{\beta}\right)\right| \tag{23}$$

$$M_1 = 0 \tag{24}$$

$$H_1 = W_3\,(c)\,L_1 \tag{25}$$

<u>Camber Components</u>

$$L_2 = 0 \tag{26}$$

$$M_2 = -\left(\frac{1}{2}\rho V^2\right)\left(\frac{c^3}{V}\right)\left(\frac{\pi}{8}\right)\left[\dot{\alpha} + W_4\frac{V}{c}\beta + W_5\dot{\beta}\right] \tag{27}$$

$$H_2 = -\left(\frac{1}{2}\rho V^2\right)\left(\frac{c^3}{V}\right)\left(\frac{\pi}{8}\right)\left[W_6\dot{\alpha} + W_7\frac{V}{c}\beta + W_8\dot{\beta}\right] \tag{28}$$

<u>First Derivative Impulsive Terms</u>

$$L_3 = -\left(\frac{1}{2}\rho V^2\right)\left(\frac{c^2}{V}\right)\left(\frac{\pi}{2}\right)\left[\dot{\alpha} + W_9\dot{\beta}\right] \tag{29}$$

$$M_3 = -\left(\frac{1}{2}\rho V^2\right)\left(\frac{c^3}{V}\right)\left(\frac{\pi}{2}\right)\left[\left(\frac{1}{2} - X_o\right)\dot{\alpha} + \{W_{11} + (X_a - X_o)\,W_9\}\,\dot{\beta}\right] \tag{30}$$

$$H_3 = -\left(\frac{1}{2}\rho V^2\right)\left(\frac{c^3}{V}\right)\left(\frac{\pi}{2}\right)\left[W_{10}\dot{\alpha} + W_{13}\dot{\beta}\right] \tag{31}$$

<u>Equivalent Inertia Terms</u>

$$L_4 = -\frac{\pi\rho c^2}{4}\left[\ddot{h} + \left(\frac{1}{2} - X_1\right)c\ddot{\alpha} + W_{10}\,c\,\ddot{\beta}\right] \tag{32}$$

$$M_4 = -\left(\frac{\pi \rho c^2}{4}\right)\left[\left(\frac{1}{2} - X_o\right) c\ddot{h} + \left\{\frac{1}{32} + \left(\frac{1}{2} - X_o\right)\left(\frac{1}{2} - X_1\right)\right\} c^2 \ddot{\alpha}\right] \tag{33}$$

$$H_4 = -\left(\frac{\pi \rho c^2}{4}\right)\left[W_{10}\, c\ddot{h} + \left\{W_{12} + (X_a - X_1)\, W_{10}\right\} c^2 \ddot{\alpha} + W_{14}\, c^2 \ddot{\beta}\right] \tag{34}$$

where the W functions are all functions of X_a and are similar to Theodorsen's T functions, but expressed as explicit functions of the parameter $\varphi = \cos^{-1}(2X_a - 1)$.

With reference to Statement "C" of Paragraph 3.1.2, the following approximations will be made to the control surface "W" coefficients:

$$W_2/W_1 = .8 \quad W_5/W_4 = .4 \quad W_8/W_7$$

$$W_6 = .2\, W_5$$

Numerical values of the above constants are presented in Reference 7, and the above approximations are reasonable for the range of values of X_a to be used in the analysis. Table 1 lists the possible range of X_a with the appropriate W relationships.

The following effective control surface rotation is now defined:

$$\bar{\beta} = \beta + C/_V \; W_2/W_1 \; \dot{\beta} \tag{35}$$

Substituting the above approximations and Equations 35 and 14 into the circulation and camber components, (i.e., Equations 23 through 28),

$$L_1 = -\left(\frac{1}{2}\rho V^2\right)(c)\,(2\pi)\left[C(k)\,(\bar{\alpha} + W_1 \bar{\beta})\right] \tag{36}$$

$$M_1 = 0 \tag{37}$$

$$H_1 = W_3\,(c)\,L_1 \tag{38}$$

$$L_2 = 0 \tag{39}$$

$$M_2 = -\left(\frac{1}{2}\rho V^2\right)(c^2)\left(\frac{\pi}{8}\right)\left|\frac{c}{V}\dot{\alpha} + W_4\bar{\beta} + 0.2\,W_5\frac{c}{V}\dot{\beta}\right| \tag{40}$$

$$H_2 = -\left(\frac{1}{2}\rho V^2\right)(c^2)\left(\frac{\pi}{8}\right)\left|\frac{c}{V}\,0.2\,W_5\,\dot{\alpha} + W_7\,\bar{\beta} + 0.6\,W_8\frac{c}{V}\dot{\beta}\right| \tag{41}$$

The total circulatory and camber terms then, are:

$$L = L_1 + L_2$$

$$= -\left(\frac{1}{2}\rho V^2\right)(c)\,(2\pi)\{C(k)\,[\bar{\alpha} + W_1\,\bar{\beta}]\} \tag{42}$$

$$M = M_1 + M_2$$

$$= -\left(\frac{1}{2}\rho V^2\right)(c^2)\left(\frac{\pi}{8}\right)\left|\frac{c}{V}\dot{\alpha} + W_4\bar{\beta} + 0.2\,W_5\frac{c}{V}\dot{\beta}\right| \tag{43}$$

$$H = H_1 + H_2$$

$$= -\left(\frac{1}{2}\rho V^2\right)(c^2)\left(\frac{\pi}{8}\right)\Big|16W_3\,C(k)\,\bar{\alpha} + (16W_3\,C(k)\,W_1 + W_7)\,\bar{\beta}$$

$$+ 0.2\,W_5\frac{c}{V}\dot{\alpha} + 0.6\,W_8\frac{c}{V}\dot{\beta}\Big| \tag{44}$$

The first derivative impulsive terms (Equations 29 through 31) are known to "smear" out due to compressibility effects. At the speeds to be considered in the analysis, these terms were neglected.

The equivalent inertia terms (Equations 2 through 34) define "aerodynamic mass" which is added to the structural mass of the surface. Since it is small relative to the mass of the wing, these terms are neglected.

Now with reference to Statement "B" of Paragraph 3.1.2, aerodynamic influence coefficient matrices [Q], will be defined in steady-state level flight as follows:

For the lift at the ith section (strip) in pounds,

$$\{L_i\} = -\left(\frac{1}{2}\rho V^2\right)\left(C_{L_\alpha}\,[Q_{ij}^{L\alpha}]\{\alpha_j\} + C_{L_\beta}\,[Q_{ij}^{L\beta}]\,\{\beta_j\}\right) \tag{45}$$

For the moment at the ith section about the aerodynamic center in inch-pounds,

$$\{M_i\} = -\left(\frac{1}{2}\rho V^2\right) C_{M_\beta} \, [Q_{ij}^{M\beta}] \{\beta_j\} \tag{46}$$

For the control surface hinge moment in inch-pounds,

$$\{H_i\} = -\left(\frac{1}{2}\rho V^2\right)\left(C_{H_\alpha} \, [Q_{ij}^{H\alpha}] \{\alpha_j\} + C_{H_\beta} \, [Q_{ij}^{H\beta}] \{\beta_j\} \right) \tag{47}$$

In the above expressions, the subscripts i and j refer to the strips into which the wing has been divided for purposes of aerodynamic simulation.

Equations 45 through 47 define the steady-state aerodynamic forces on the surface and are presumed to include the effects of spanwise coupling between strips (i. e., influence of strip j on strip i), compressibility, aerodynamic balance on the aileron, etc.

Looking now at the development of Equations 45 through 47, the aerodynamic matrices $[Q^{L\alpha}]$, etc. may be defined as weighted numbers which when multiplied by the value of the effective angle of attack, etc. at the jth station, will give the contribution of the jth station to the ith station angle of attack, etc. Integration of the running lift, etc. is implied in the above influence coefficient matrices. However, for purposes of the following discussion, an aerodynamic influence coefficient matrix will be defined as a matrix which relates local lift coefficient and local angle of attack. These coefficients may be thought of as operators which have the property of being able to operate on an arbitrary angle of attack distribution to produce the resultant span loading.

The steady-state loads for the analysis were derived on the basis of strip theory and also by the lifting-line concept of treating aerodynamic loading (i.e., the distributed loading is replaced by a spanwise lift, and moment distribution assumed to act along the line of chordwise centers of pressure).

The lifting-line aerodynamic influence coefficient matrix may be defined as follows:

$$\{\gamma\} = \left\{\frac{cc_\ell}{\bar{c}}\right\} = [Q] \{\alpha, \beta\} \tag{48}$$

where c_ℓ is the local sectional lift coefficient and c is the local chord. The term $cc_\ell/\bar{c}$ represents the nondimensional loading resulting from an arbitrary angular deflection α or β distribution.

Consider now the following loading due to an angle of attack distribution and due to a trailing edge flap rotation distribution:

The loading due to an angle of attack is:

$$\{\gamma_\alpha\} = \left\{\gamma_{w_\alpha}\right\} + \left\{\gamma_{f_\alpha}\right\} \tag{49}$$

where each individual loading may be expressed in terms of influence coefficients as,

$$\left\{\gamma_{w_\alpha}\right\} = [Q_{w\alpha}]\,\{\alpha\} \tag{50}$$

$$\{\gamma_{f\alpha}\} = [Q_{f\alpha}]\,\{\alpha\} \tag{51}$$

The loading due to a flap rotation is:

$$\{\gamma_\beta\} = \{\gamma_{w\beta}\} + \{\gamma_{f\beta}\} \tag{52}$$

and expressing each component in terms of influence coefficients as,

$$\{\gamma_{w\beta}\} = [Q_{w\beta}]\,\{\beta\} \tag{53}$$

$$\{\gamma_{f\beta}\} = [Q_{f\beta}]\,\{\beta\} \tag{54}$$

The total loading on the wing is therefore:

$$\{\gamma_w\} = \{\gamma_{w\alpha}\} + \{\gamma_{w\beta}\}$$

$$= [Q_{w\alpha}]\,\{\alpha\} + [Q_{w\beta}]\,\{\beta\} \tag{55}$$

The running lift in pounds per unit span may be written as:

$$\{\ell_w\} = -\bar{c}\, q\, \{\gamma_w\} \tag{56}$$

The total lift force acting at each of the specified panel points is:

$$\{L\} = \lceil R_w \rfloor \{\ell_w\} \tag{57}$$

where $\lceil R_w \rfloor$ is simply an integrating matrix.

Substituting Equations 56 and 55 into Equation 57 results in a final expression for the lift,

$$\{L\} = -\bar{c}\, q \lceil R_w \rfloor [Q_{w\alpha}]\{\alpha\} - \bar{c}\, q \lceil R_w \rfloor [Q_{w\beta}]\{\beta\} \tag{58}$$

The $[Q_{w\alpha}]$ and $[Q_{w\beta}]$ matrices were computed by the method of References 8 and 9.

The loading on the flap due to an angle of attack and to a flap deflection was computed on a two-dimensional (strip theory) basis. Accordingly, we may write for the resultant hinge moment in lbs-ft. per unit span,

$$h = -q\, c_a^2 \left[\frac{\partial C_h}{\partial \beta}\beta + \frac{\partial C_h}{\partial \alpha}\alpha \right] \tag{59}$$

For all stations,

$$\{h\} = -q \lceil C_a^2 \rfloor \lceil C_{h_\alpha} \rfloor \{\alpha\} - q \lceil C_a^2 \rfloor \lceil C_{h_\beta} \rfloor \{\beta\} \tag{60}$$

The total moment acting at each of the specified panel points is:

$$\{H\} = -q \lceil R_f \rfloor \lceil C_a^2 \rfloor \lceil C_{h_\alpha} \rfloor \{\alpha\} - q \lceil R_f \rfloor \lceil C_a^2 \rfloor \lceil C_{h_\beta} \rfloor \{\beta\} \tag{61}$$

The loading on the wing due to a flap deflection also gives rise to a moment about the panel aerodynamic center (a.c.). Accordingly, by analogy with Equation 48, we may write the loading (moment) produced by a flap rotation as,

$$\{\gamma\} = \left\{\frac{c^2 C_m}{\bar{c}}\right\} = [\bar{Q}_{w\beta}] \{\beta\} \tag{62}$$

Therefore, the running moment about the a.c. is:

$$\{m\} = -q\,\bar{c}\,\{\gamma\} = -q\,\bar{c}\,[\bar{Q}_{w\beta}]\,\{\beta\} \tag{63}$$

And the total moment acting at each panel point is:

$$\{M\} = -q\,\bar{c}\,\lceil R_w \rfloor\,[\bar{Q}_{w\beta}]\,\{\beta\} \tag{64}$$

Computation of the matrix product $\lceil R_w \rfloor\,[Q_{w\beta}]$ was done by the method of Reference 9, and therefore was based upon the lifting-line concept.

Comparing Equations 45 through 47 with Equations 58, 61 and 64, shows the following equalities:

$$\bar{c}\,\lceil R_w \rfloor\,[Q_{w\alpha}] = C_{L\alpha}\,[Q_{ij}^{L\alpha}]$$

$$\bar{c}\,\lceil R_w \rfloor\,[Q_{w\beta}] = C_{L\beta}\,[Q_{ij}^{L\beta}]$$

$$\bar{c}\,\lceil R_w \rfloor\,[\bar{Q}_{w\beta}] = C_{M\beta}\,[Q_{ij}^{M\beta}]$$

$$\lceil R_f \rfloor\lceil C_a^2 \rfloor\lceil C_{h\alpha} \rfloor = C_{H\alpha}\,[Q_{ij}^{H\alpha}]$$

$$\lceil R_f \rfloor\lceil C_a^2 \rfloor\lceil C_{h\beta} \rfloor = C_{H\beta}\,[Q_{ij}^{H\beta}]$$

By analogy with Equations 42 and 58, the nonstationary aerodynamic lift expression, exclusive of the damping terms (velocity dependent) to be used is:

$$\{\bar{L}_1\} = -\left(\frac{1}{2}\rho V^2\right) C(k) \left[C_{L_\alpha}\,[Q_{ij}^{L\alpha}]\{\bar{\alpha}_j\} + C_{L_\beta}\,[Q_{ij}^{L\beta}]\,\{\bar{\beta}_j\}\right] \tag{65}$$

Similarly, the moment is:

$$\{\bar{M}_1\} = \left(-\frac{1}{2}\rho V^2\right) C_{M\beta}\,[Q_{ij}^{M\beta}]\,\{\bar{\beta}_j\} \tag{66}$$

And the hinge moment is:

$$\left|\bar{H}_1\right| = -\left(\frac{1}{2}\rho V^2\right)\left[C_{H_\alpha}\left[Q_{ij}^{H\alpha}\right]\left|\bar{\alpha}_j\right| + C_{H_\beta}\left[Q_{ij}^{H\beta}\right]\left|\bar{\beta}_j\right|\right] \tag{67}$$

The aerodynamic damping terms will not include the effect of spanwise coupling of strips, but will include the effect of Mach number by the use of a proper pitch damping coefficient, C_{M_q}. The aerodynamic damping terms for each strip are then:

$$\bar{L}_2 = 0 \tag{68}$$

$$\begin{aligned}\bar{M}_2 &= -\left(\frac{1}{2}\rho V^2\right)c^2\, C_{M_q}\left[\frac{c}{v}\dot{\alpha} + 0.2W_5\,\frac{C}{V}\dot{\beta}\right] \\ &= -\left(\frac{1}{2}\rho V^2\right)\frac{C^3}{V}\, C_{M_q}\left[\dot{\alpha} + 0.2W_5\dot{\beta}\right]\end{aligned} \tag{69}$$

$$\begin{aligned}\bar{H}_2 &= -\left(\frac{1}{2}\rho V^2\right)c^2\, C_{M_q}\left[0.2W_5\frac{C}{V}\dot{\alpha} + 0.6\, W_8\frac{C}{V}\dot{\beta}\right] \\ &= -\left(\frac{1}{2}\rho V^2\right)\frac{C^3}{V}\, C_{M_q}\left[0.2W_5\,\dot{\alpha} + 0.6W_8\dot{\beta}\right]\end{aligned} \tag{70}$$

3.1.2.1.1 Aerodynamic Center

With additional reference to Statement "C" of Paragraph 3.1.2, several assumptions will be made concerning the location of the aerodynamic center. Theory does not adequately define this parameter, therefore the analysis will be made by varying the a.c. location within reasonable limits. The flutter speeds determined will correspond to the lowest, within the defined a.c. limits. The following assumptions will therefore be made:

A. The a.c. is located at a constant percent chord on all strips.

B. The rotation center, defined by X_1 on Figure 5 is always located the same distance from the midchord as the a.c., therefore:

$$X_1 + X_0 = 1$$

This assumption is exact for incompressible flow when $X_0 = 1/4$, $X_1 = 3/4$ and also at very high Mach numbers, when $X_0 = X_1 = 1/2$.

3.1.2.2 Development - Empennage

Aerodynamic representation of the empennage is used mainly to obtain the aerodynamic contribution of the empennage on the wing flutter characteristics. In addition, without tail effects, the airplane would be unstable in the analog simulation, since, in effect, the simulation is a model of the airplane in free flight. The above aerodynamic effects will be simulated by a lift force acting at the aerodynamic centers of the horizontal and vertical stabilizers. The lift force therefore may be written as

$$L_{a.c.} = \frac{1}{2} \rho V^2 c \, C_{L_\alpha} \bar{\alpha}_T \, C(k) \tag{71}$$

where C_{L_α} is a variable and $\bar{\alpha}_T$ is the effective tail angle of attack and is equal to $(\alpha_T - k\alpha_W)$ where k is the downwash angle.

3.1.3 Mass Representation

The mass distribution of the aircraft was broken up into a number of lumped masses as is usual in aeroelastic studies (lumped parameter system). Figures 7, 8 and 9 show the locations on the aircraft at which masses were lumped. These masses were derived from a zoning of the wing, etc., into small sections, and assuming that the mass was concentrated at the center of mass of the section. Also considered are lumped mass moments of inertia wherever it was felt neglecting them would invalidate a proper simulation.

3.2 VIBRATION (MODAL) ANALYSIS

Vibration modes were obtained from the analog simulation by connecting a variable frequency voltage source which corresponds to a sinusoidal velocity of fixed amplitude to a point in the circuit where large displacements were expected. The frequency of the voltage source was varied until the criterion for the presence of a normal mode was satisfied - i.e., until the input current to the circuit (force applied to the airplane) was a minimum. At each minimum of current, the frequency of vibration and the voltages at all nodes were recorded. By appropriate scale factors, the mode shapes were determined.

3.2.1 Vibration Modes (Normal)

For determining the normal modes of vibration, the appropriate equation is Equation 9 with the aerodynamic and gyroscopic matrices set equal to zero. Equation 9 therefore reduces to an expression governing forced vibration in a vacuum with structural damping:

$$\left|q_o\right| = \left[\Omega\left|I\right| - \left|c\right|\left|J\right|\right]^{-1}\left|c\right|\left|J\right|\left\{q_{o_j}\right\} \tag{72}$$

When the impressed sinusoidal force $Q_j = O$, $q_{o_j} = O$ upon resonance and Equation 72 reduces to

$$\Omega\left|q_o\right| = \left|c\right|\left|J\right|\left|q_o\right| \tag{73}$$

which is the standard equation for normal modes with Ω now equal to $1/\omega^2$ for undamped vibrations and equal to $(1 + ig)/\omega^2$ for damped vibrations.

3.2.2 Vibration Modes with Gyroscopic Effects

For determining the aircraft modes of vibration with gyroscopic effects, the appropriate equation also is Equation 9 with the aerodynamic matrix set equal to zero. Following the same procedure with the impressed sinusoidal force Q_j as in Paragraph 3.2.1, the equation finally reduces to

$$\left|q_o\right| = \frac{i}{\omega}\left[\Omega\left|I\right| - \left|c\right|\left|J\right|\right]^{-1}\left|c\right|\left|G\right|\left\{q_{o_k}\right\} \tag{74}$$

which is an expression for vibration modes with gyroscopic effects with Ω equal to $1/\omega^2$ for undamped vibrations, and equal to $(1 + ig)/\omega^2$ for damped vibrations.

3.3 FLUTTER ANALYSIS

The flutter analysis of the XV-5A was programmed to investigate several speed-altitude combinations that would adequately represent the proposed flight boundary. Flutter plots of damping versus speed were constructed by setting up the appropriate circuits corresponding to a particular speed and by imparting a transient, and then measuring the transient decay rate of free oscillation. With those data, plus the appropriate speed, a point on the curve of structural damping versus speed was obtained. Several speeds were selected in order to define adequately the curve. The recorded transient decay represented the least damped component of free vibration. The oscillations were excited by the application of a pulse at a point in the aerodynamic circuit which represented one component or section. This point was chosen to give a maximum amplitude for the least damped component.

The overall flutter analysis included the effects of varying the following:

1. Aileron mass-balance
2. Aileron spring restraint
3. Distribution of wing bending material
4. Torsional stiffness of the wing leading edge box

For determining the flutter speeds, the analogous equation is again Equation 9 with the gyroscopic matrix set equal to zero. When the impressed sinusoidal force $Q_j = O$, $q_{o_j} = O$ and the equation reduces to

$$\Omega \left|q_o\right| = \left[\left|c\right| \left|J\right| + \sigma \left|c\right| \left|\bar{A}\right| \right] \left|q_o\right| \tag{75}$$

Equation 75 shows that there will be as many roots as the number of physical coordinates (q_o) used, to described the motion of the structure. The root found from the analog, as previously described, usually will be the lowest damped root.

4.0 DISCUSSION

Since a plane of symmetry exists on the airplane, it is convenient and logical to break down the motion of the airplane into symmetric and antisymmetric motions. Therefore, in the analog studies covered by this report, vibration (modal) and flutter are treated as two separate studies for the symmetric and antisymmetric vibration and flutter analyses. The following sections present the input and the output, (vibration and flutter). The results of the flutter analysis may be conveniently divided into nine phases. Each phase has a particular emphasis on some aspect of the problem. These phases are outlined as follows:

Phase I - Basic Structural Evaluation

A. Variable stiffness configurations

1.0 Nominal Stiffness Configuration 5A

2.0 Stiffness Configuration 5B

B. Nominal mass condition

1.0 Mass Condition 1.0

C. Flight Condition D

1.0 M = 0.75; altitude = sea level

Phase II - Wing Front and Rear Spar Flexibility Studies

A. Variable stiffness configurations

1.0 See Table 2

B. Nominal mass condition

1.0 Mass Condition 1.0

C. Flight Condition D

1.0 M = 0.75; altitude = sea level

BLANK PAGE

Phase III - Aileron Mass-Balance Studies

A. Optimum stiffness configuration

1.0 Resulting from Phase II studies

B. Variable mass conditions

1.0 See Table 6

C. Flight Condition D

1.0 M = 0.75; altitude = sea level

Phase IV - Re-evaluation of Nominal and Optimum Stiffness Configurations

A. Realistic stiffness configuration

1.0 Resulting from Phase II

B. Variable mass conditions

1.0 See Table 6

C. Flight Condition D

1.0 M = 0.75; altitude = sea level

Phase V - Flight Envelope Evaluation

A. Variable stiffness configurations

1.0 Nominal Stiffness Configuration 5A

2.0 Realistic stiffness configuration resulting from Phase IV studies

B. Optimum mass conditions

1.0 Resulting from Phase IV studies

C. Variable flight conditions

1.0 See Table 3

Phase VI - Wing Structural Nose Box Evaluation

A. Realistic stiffness configuration

1.0 Resulting from Phase IV studies

B. Optimum mass condition

1.0 Resulting from Phase IV studies

C. Flight Condition D

1.0 M = 0.75; altitude = sea level

Phase VII - Aileron Equivalent Spring Restraint Studies

A. Realistic stiffness configuration

1.0 Resulting from Phase IV studies

B. Optimum mass condition

1.0 Resulting from Phase IV studies

C. Flight Condition D

1.0 M = 0.75; altitude = sea level

Phase VIII - Aircraft Simulation Studies

A. Variable stiffness configuration

1.0 Nominal Stiffness Configuration 5A

2.0 Realistic stiffness configuration resulting from Phase IV studies

B. Optimum mass conditions

1.0 Resulting from Phase IV studies

C. Variable flight conditions

1.0 See Table 3

Phase IX - Aerodynamic Simulation Studies

A. Nominal stiffness configuration 5A

B. Optimum mass condition

1.0 Resulting from Phase IV studies

C. Variable flight conditions

1.0 See Table 3

4.1 IDEALIZATION OF AIRCRAFT

As mentioned in Paragraph 3.1, the aircraft for analysis purposes must be idealized to be amenable to analytical treatment, yet be of sufficient rigor to meet the demands of engineering accuracy, while consistent with the capability of the analog computer. Figure 6 shows the actual aircraft structure to be idealized.

4.1.1 Structural Representation

Since the airplane may be thought of as a number of components assembled to form the complete airplane, e.g., wing, fuselage, horizontal and vertical stabilizers and control surfaces, the following sections will deal with the components as they were treated during the analog analysis.

4.1.1.1 Wing - Aileron

Subject to the preceding discussions, the actual wing structure shown in Figure 6 was idealized into the structure shown in Figure 7 for the symmetric analysis, and Figures 8 and 9 for the antisymmetric analysis. Figures 7, 8 and 9 show the discrete components which represented the idealized model. Spar I on the outer wing panel is a dummy spar assumed for the structural idealization, so as to permit representation of chordwise bending. As such, it was represented as a beam without webs.

The basic structural configurations were designated as Stiffness Configuration 5A and 5B. Configuration 5A represented the structure in a 4g maneuver where very little of the skin is considered effective in bending. Configuration 5B represented the structure in a 1g flight condition where most of the skin is considered effective in bending. All other stiffness configurations studied were identical to Stiffness Configuration 5A, except for the front and rear spar stiffness inboard of BL 100.38. Table 2 lists the various stiffness configurations studied other than the basic configuration. The listing is in terms of a flexibility factor which was applied to the basic configuration 5A -- i.e. $\frac{1}{EI} = \left(\frac{1}{EI}\right)_{nominal} \times$ Flexibility Factor.

Figure 10 depicts the geometry of the wing as used in the structural idealization of the aircraft. The lengths shown represent average values of the mid-plane lengths of Stiffness Configuration 5. Due to the small sweep of the aileron and for simplification of analysis, the

hinge-line was assumed unswept as shown in the aileron geometry sketch, Figure 11. The elastic restraint, represented by the overall control circuit, was assumed to act at aileron station A55. The calculated spring rates which were classified as the nominal values were $K_\beta = 3.761 \times 10^4$ in-#/rad, symmetric and $K_\beta = 2.614 \times 10^4$ in-#/rad, antisymmetric. These values used in conjunction with the nominal aileron mass condition (Mass Condition 1.0) gave 16.0 cps and 13.4 cps as the aileron uncoupled frequency, symmetric and antisymmetric respectively. Figures 12 and 13 show the variation in bending stiffness of the front and rear wing spars respectively, for the two basic stiffness configurations studied in the analysis. Figure 14 depicts the rib bending stiffnesses for the outer panel. As can be seen with a comparison with Figures 12 and 13, which are spar stiffness plots, the chordwise stiffness varies from 1.5 to 5.0 times the spanwise stiffness, indicating the possibility of neglecting chordwise bending. Figure 15 depicts the variation in bending stiffness for the center spar or ficticious stringer utilized in the structural idealization. The values shown are for Stiffness Configuration 5B wherein all the skin is considered effective in bending. Figure 16 presents the idealized wing configuration as developed by the Structures Group. This idealization was followed closely in the analysis with the exception of the leading edge box inboard of BL 100.38 (Rib No. 50) which, in this analysis, was further idealized into an equivalent torque tube as shown in Figures 7 and 8. This equivalent torque tube represented the same torsional stiffness as that of the single cell box. The variation in stiffness is shown in Figure 17. Figure 16 also presents the skin, spar and rib web average thicknesses for use in the torque box simulation. Figure 18 presents the stiffness values for the aileron which was treated as a beam flexible in bending and torsion with the beam simply supported at the hinges. The actual hinge locations shown in Figure 18 were moved to that shown in Figure 11 for analysis purposes. The difference in beam length between hinges was of the order of 1.3 inches, which is negligible.

4.1.1.2 Fuselage-Empennage

Figures 19 through 21 depict the geometry of the fuselage and of the horizontal and vertical stabilizers as used in the structural idealization of the aircraft. For purposes of analog representation, these components of the aircraft were treated as simple beams with assumed elastic axes. The fuselage and empennage idealization was accomplished in a less sophisticated manner than the wing, due to analog circuit limitations. This was felt to be a minor drawback, since the emphasis was to be wing flutter and vibration characteristics, rather than the complete aircraft. Normally,

empennage and wing dynamic analyses can be separate due to the small coupling between wing coordinates and those of the empennage. In conjunction with the less sophisticated representation of the empennage, the swept horizontal stabilizer was assumed to be unswept with the elastic axis of the horizontal stabilizer intersecting the vertical stabilizer elastic axis. With this representation, the root chord plus the closure rib chord at BL 70.16 defined the planform as shown in Figure 20. Empennage control surfaces, (elevator and rudder), were not considered for the analysis. Figures 22 through 24 show the stiffness distributions for the horizontal and vertical stabilizers respectively, as used in the analysis. The torsional stiffness (GJ) plots of both the horizontal and vertical stabilizers reflect a flight condition wherein all the skin was considered effective in determining the stiffness, whereas the bending stiffness (EI) reflects a flight condition where only the tension skin is utilized in the computation. The incapability of the torsional and bending stiffnesses was felt to have a negligible effect in determining the wing flutter speeds.

4.1.2 Aerodynamic Representation

As explained in Paragraph 3.1.2, the aerodynamic representation was accomplished through the use of steady-state aerodynamic influence coefficients modified by an appropriate lag function. Four flight conditions, (constant Mach-altitude) were chosen for analysis purposes that would adequately represent the proposed flight boundary, (Figure 25). These flight conditions are tabulated in Table 3 with accompanying pertinent data related to each condition. Also shown in Table 3 is the lag function, and lag function coefficients for each flight condition.

4.1.2.1 Wing-Aileron

Establishment of aerodynamic strips at which the aerodynamic loads were to be applied led to the planform breakdown as shown in Figures 26 and 11 for the wing and aileron respectively. Figures 27 through 33 present the matrices of aerodynamic influence coefficients as explained by Equations 45, 46, and 47. These matrices are included herein more as a documentation effort than as an aid in evaluating the overall wing flutter analysis. The wing-alone pitch damping coefficients as explained by Equations 69 and 70 are shown in Table 3.

4.1.2.2 Horizontal and Vertical Stabilizer

In line with the less sophisticated representation of the empennage due to analog circuit limitations, the aerodynamic strips chosen for the horizontal and vertical stabilizers are shown in Figures 20 and 21 respectively. Table 3 also presents the aerodynamic lift curve slope coefficient (C_{L_α}) used in the aerodynamic simulation for the tail load as explained by Equation 71.

4.1.3 Mass Representation

Only one gross weight condition was studied during the course of the analysis. This was the design gross weight of approximately 9200 pounds. In line with the usual lumped parameter systems normal for such studies, the breakdown for both the wing, fuselage and empennage are shown in Tables 4 and 5 for the symmetric and antisymmetric idealization respectively. Since mass-balancing of the aileron was studied as a means of evaluating flutter fixes, various aileron mass configurations were used. These configurations are shown in Table 6 with the amount and location of the balancing masses.

4.2 VIBRATION (MODAL) ANALYSIS

As explained in Paragraph 3.2, zero airspeed vibration modes of the airplane were obtained with and without wing fan gyroscopic effects. In order to show relative magnitudes of deflections at various points on the airplane, these mode shapes for the nominal stiffness configuration were plotted in pictorial form.

4.2.1 Vibration Modes (Nominal)

Figures 34 through 50 depict in pictorial form the normal mode shapes (without gyroscopic forces) for Stiffness Configuration 5A and Mass Condition 9, symmetric and antisymmetric. The mode shapes have been normalized to unity at the point of maximum amplitude, and are plotted as such, or as one-half inch to the inch. Table 7 lists for comparative purposes, the frequencies, structural damping and the panel point at which the airplane was excited, as explained in Paragraph 3.2. Damping values were measured from the analog simulation as in an actual ground shake test, since the simulation represented a model of the airplane.

During the flutter analysis of the airplane, structural changes in the wing were studied (Phase II, III and IV studies) and Stiffness Configuration 5P represents one such configuration as is explained in the following Paragraph 4.3. The normal modes of this configuration are not shown pictorially in this report. However, Table 8 lists for comparative purposes. the frequencies, damping, etc. of these modes.

4.2.2 Vibration Modes With Gyroscopic Effects

Figures 51 through 67 depict also in pictorial form the mode shapes with gyroscopic forces for Stiffness Configuration 5A and Mass Condition 9, both symmetric and antisymmetric. Table 9 lists the frequencies, structural damping, etc. As stated in Reference 1, the deflections shown for the modes with gyroscopic forces are the component of deflection in phase with the panel point chosen as the point of excitation. The phase angles between recorded deflections due to gyroscopic forces were generally small (less than 10°, except for deflections of very small amplitude). The in-phase component of deflections were recorded because the phase angles were small, and because deflection data including phase angles cannot be represented pictorially.

Modal data for Stiffness Configuration 5P with gyroscopic forces are listed in Table 10. Modal deflection data for this latter stiffness configuration both with and without gyroscopic forces are presented in Reference 1.

4.3 FLUTTER ANALYSIS

This section is the flutter analysis portion of the CEA program, and is divided into a number of phases which logically depict the dynamic studies of the XV-5A wing. The basic structural configurations herein are Stiffness Configurations 5A and 5B, with Stiffness Configuration 5A being termed nominal. The nominal mass condition pertains to Mass Condition 1.0 (See Table 6), and all other mass conditions reflect changes in aileron mass-balance only. Any changes in wing structural mass due to an increase and/or decrease in stiffness were neglected in the interests of simplicity of analysis. Such neglect was felt to be justified in view of the broad nature of this preliminary analysis. All analyses include the appropriate aileron degrees of freedom such as rotation about the hinge-line, deflection in the z direction, etc.

In general, most of the results of the flutter analysis are plotted in the conventional sense, i.e. overall damping (g) versus Mach number (M). In addition, a solution parameter (V/V_0) is plotted where V_0 corresponds to the Mach speed at the particular altitude (V_0 = Ma, where a is the speed of sound at altitude). The roots plotted represent different branches of typical V-g plots, in that each group of symbols represents the response of the aircraft in a different vibration mode. Although there are an infinite number of aircraft modes, only those modes of interest to the flutter analysis have been plotted. The first subscript with each point represents the frequency of oscillation in cycles per second. The second, if any, represents some variable as explained on each plot.

4.3.1 Phase I - Basic Structural Evaluation

Phase I of the flutter analysis pertained to the evaluation of the basic structural configurations with nominal mass conditions. Since Flight Condition D represented a 5% flutter margin point (see Figure 25), this condition was chosen for the initial evaluation of the basic wing. During this phase of the studies, simultaneous studies of a portion of Phase IX were carried out. These were the effects of aerodynamic center shifts on the flutter characteristics of the aircraft.

4.3.1.1 Results

Figures 68 through 71 present the symmetric and antisymmetric V-g plots for both basic structural configurations, which are Stiffness Configurations 5A and 5B with nominal Mass Condition 1.0 and nominal aileron spring. In this particular case, V_0 is equal to (0.75) (a), and a is the speed of sound at sea level.

4.3.2 Phase II - Wing Front and Rear Spar Flexibility Studies

During this phase of the analysis, studies were directed to evaluating the effects of reducing the stiffness (increasing the flexibility) and thereby reducing weight on the flutter characteristics of the wing. Since Phase I studies showed a flutter velocity in an antisymmetric mode, but above 15% V_L, it was decided to determine what effects a stiffness reduction on the front and rear wing spars between BL 0 and BL 100.38 would have on this flutter velocity. The criterion used was that flutter requirements would be met at 1.05 V_L (M = 0.75 at sea level) with nominal aileron (mass-balance). Once this condition (marginal stability at this point) is met, an attempt to raise the flutter speed by aileron mass-balancing would be made.

4.3.2.1 Results

Figures 75 through 77 present the results of the antisymmetric analysis with Figures 75 and 76 plotted as discussed in Section 4.3. Figure 75 shows the effect of increasing the flexibility of the rear spar from nominal to 220% of nominal while holding the flexibility of the front spar constant. Figure 76 shows the effect of varying the flexibility of both front and rear spars an equal amount varying from 85% of the nominal values to 132.5% of the nominal. Figure 77 shows the damping (g) for various flexibility combinations for both front and rear spars for V/V_o ratios of 1.0 and 1.1. Only the roots of the flutter mode ($f \approx 9.0$-12.0 cps) have been plotted, since this mode showed a marked change in overall damping (g) with stiffness changes. Figures 72 through 74 present the equivalent results for the symmetric case as was shown for the antisymmetric.

4.3.3 Phase III - Aileron Mass-Balance Studies

As explained in Paragraph 4.3.2, aileron mass-balancing was studied to determine its effect on the flutter mode and consequently the flutter velocity. From Phase II studies, Figures 75 and 76, it can be seen that Stiffness Configurations 5N and 5J fulfill the criterion stated in Paragraph 4.3.2. However, since Stiffness Configuration 5N represented a decrease of about 55% (120% increase in flexibility) in rear spar stiffness, while Stiffness Configuration 5J represented a decrease of approximately 25% in both front and rear spar stiffness (32.5% increase in flexibility), it was decided to use Stiffness Configuration 5J and by means of aileron mass-balance, raise the flutter speed. This

was done according to a modified criterion which was sufficient mass-balance, properly located, so that neutral stability is achieved at $V/V_0 = 1.1$ (approximately $1.15\ V_L$).

4.3.3.1 Results

Figure 79 presents the results of these studies. From this figure, it can be seen that Mass Conditions 4.0 and 7.0 both fulfill the stated criteria. Figure 78 presents similar results for the symmetric case, but only for these latter two mass conditions. Other mass conditions were not studied during the symmetric analysis, since it was an anti-symmetric flutter that was evident.

4.3.4 Phase IV - Re-evaluation of Nominal and Optimum Stiffness Configurations

From Phase II and III studies, the optimum stiffness configuration was shown to be 5J $[1.325\ (1/EI_{nominal})]$ with either Mass Condition 4.0 or 7.0. After due consideration, it was decided that a 25% decrease in spar stiffness was more than could be realistically tolerated. Therefore, a closer examination was made in order to reduce structural weight and still maintain the specified 15% margin on flutter speed. After due consideration, it was decided to reduce the stiffness of both spars, maintaining an overall damping (g) of approximately 0.02, the average value of structural damping in aircraft structures at a solution parameter (V/V_0) of 1.1 (approximately $1.15\ V_L$ at sea level). Once this criterion was met, mass-balancing of the aileron at the tip, (since the flutter mode was sensitive to this type), would be resorted to in raising the flutter speed until neutral stability ($g \approx 0$) was reached at a solution parameter of 1.1. Furthermore, aileron tip balancing would be investigated for the nominal Stiffness Configuration 5A, with a view toward optimizing the balance requirements for this configuration.

4.3.4.1 Results

Figure 80 presents the overall damping (g) for various flexibility combinations for both front and rear spars for a solution parameter (V/V_0) of 1.1. The modes shown are antisymmetric, since again this was shown to be the sense of the flutter mode. From the plot, it can be seen that approximately a 10% increase in front spar flexibility and approximately a 15% increase in rear spar flexibility would give the desired results as explained in Paragraph 4.3.4. Figure 82 presents

the actual results obtained from the study. Results have been plotted for both the realistic Stiffness Configuration 5P and the nominal Stiffness Configuration 5A, both with tip balanced ailerons, Mass Condition 8.0 and 9.0, respectively. Stiffness Configuration 5P represents an 11% increase in front spar flexibility (15% decrease in stiffness). The slight discrepancy is due to the manner in which the overall damping was determined. Figure 81 presents the equivalent results for the symmetric case, except that no data was taken with Mass Condition 1.0 for Stiffness Configuration 5P.

4.3.5 Phase V - Flight Envelope Evaluation

Having established the final stiffness configurations with revised aileron mass-balance, the flight envelope was evaluated using the aerodynamics available for the other flight conditions (see Table 3). Since the aerodynamic center is a function of Mach Number, this parameter (a portion of Phase IX studies) was simultaneously evaluated for the three remaining flight conditions.

4.3.5.1 Results

Presented in Figures 83 through 86 are the V-g plots, symmetric sense for Stiffness Configurations 5A and 5P for the four flight conditions studied in the analysis. Flight Conditions A, E and B represent points on the flight envelope which encompass a 15% flutter margin on Mach Number or limit dive speed at sea level, 5,000' and 9,500' altitude, respectively (see Figure 25). Flight Condition D represents a 5% flutter margin point at sea level. Presented on each plot for the latter three flight conditions are the effects of aerodynamic center shifts on the overall damping (g). Figure 87 presents a composite plot of the four flight conditions' V-g plots for an aerodynamic center of 0.20c. Figures 88 through 92 present equivalent results for the antisymmetric analysis. On all plots, only the root or mode of concern has been plotted.

4.3.6 Phase VI - Wing Structural Nose Box Evaluation

During the course of the analysis, design problems arose on a needed cutout on the leading edge structural box on the wing inner panel. Consequently, it was decided to investigate the effect of reduced stiffness on the equivalent torque tube (see Figure 7) lying between BL 61.00 and BL 100.38. Since a flutter point occurred during the analysis of Flight Condition D (M = 0.75 at sea level), this condition was chosen for study.

4.3.6.1 Results

Figures 93 and 94 present the results of reducing the nose box stiffness in the usual V-g plot, symmetric and antisymmetric, respectively. The factors shown are percentages of the nominal torsional stiffness of the equivalent torque tube given in Figure 17. The stiffness configuration chosen, as basic for this particular study, had no relationship with the problem, other than using one or the other (i.e. Stiffness Configuration 5A or 5P, as the base configuration upon which to perform the study).

4.3.7 Phase VII - Aileron Equivalent Spring Restraint Studies

Since in most cases of basic surface flutter, some degree of control surface coupling with basic surface motion is involved, it was decided to investigate the effects of a variable aileron spring restraint. As mentioned in Paragraph 4.1, the aileron restraint, (control circuit) was idealized into an equivalent spring acting at the aileron hinge line. Again, as during the Phase VI studies, Flight Condition D (M = 0.75 at sea level) was chosen for study.

4.3.7.1 Results

Plotted in Figures 95 and 96 are the results of varying the overall spring rate ($K\beta$), symmetric and antisymmetric, respectively. The factors shown are various percentages of the nominal spring rates given in Paragraph 4.1.1.1. Stiffness Configuration 5P was used in conjunction with these studies as in Phase VI studies providing a base configuration.

4.3.8 Phase VIII - Aircraft Simulation Studies

Since a case of wing flutter occurred during the course of analysis, it was decided to investigate the fuselage degrees of freedom involved. Since a free-free airplane was simulated on the analog, it was felt investigations along the line of aircraft simulation would aid in providing insight into the instability, and furthermore provide direction toward future wind tunnel flutter model simulation. Studies covered the range whereby the fuselage presented an infinite restraint to the wing (cantilevered wing) to a fuselage and empennage free in space, but having infinite stiffness in addition to the nominal stiffness present in the fuselage and empennage (see Figures 22, 23 and 24). All flight conditions were covered with Stiffness Configuration 5P, providing the base configuration with the exception of the cantilevered case which included Stiffness Configuration 5A and which was restricted to Flight Condition D (M = 0.75 at sea level).

4.3.8.1 Results

Presented in Figures 97 through 101 are the resulting V-g plots for the aircraft simulation studies, both symmetric and antisymmetric analyses. Figure 97 gives the comparison between a cantilevered wing and a free-free aircraft with flexible fuselage and empennage for both Stiffness Configurations 5A and 5P for Flight Condition D (M = 0.75 at sea level). Figures 98 through 101 present the comparisons between a free-free aircraft with both infinite and nominal fuselage and empennage stiffness for all four flight conditions studied.

4.3.9 Phase IX - Aerodynamic Simulation Studies

As stated in Paragraph 3.1.2, simulation of the unsteady aerodynamics required for a flutter analysis requires the use of assumptions or empirical approximations. The aerodynamic center is one such parameter which is not known adequately from theory. Therefore, this parameter was varied throughout the analysis. Secondly, the lag function C(k) (see Equation 65 and Table 1) is of importance in analog simulation for flutter, and thus was varied in the analysis from in and out of the circuit. Thirdly, the pitch damping coefficient (C_{M_q}), wing-alone, was not known too well for the XV-5A wing at the time. Studies were included in the analysis which also varied this parameter. A full discussion of the preceding items is presented in Reference 7.

4.3.9.1 Results

Variations in aerodynamic center locations have been shown throughout the preceding results and will not be duplicated here. Figures 102 through 105 present the results of removing the lag function from the aerodynamic circuits for the four flight conditions. Figure 106 presents the effect of varying the wing alone pitch damping coefficient (C_{M_q}) for Flight Condition D (M = 0.75 at sea level). A value of $\pi/8$ per rad. for this coefficient is the theoretical value at M = 0. Figures 107 through 109 present similar results for the remaining three flight conditions, with the coefficient being varied from 0 to $\pi/8$, wing alone for Flight Condition A (M = 0.82 at sea level); $\pi/8$, wing alone for Flight Condition E (M = 0.90 at 5,000'), and finally zero, wing plus tail for Flight Condition B (M = 0.98 at 9,500'). The basic curves shown on each plot of Figures 106 through 109 include the values of the pitch damping coefficient (C_{M_q}), wing alone listed in Table 3.

5.0 CONCLUSIONS

Referring to Figure 25, the proposed flight envelope, it is to be noted that during the course of the program at CEA, a revised flight envelope came into being. The four flight conditions used in the flutter analysis do not include a portion of the revised envelope, M = 0.90 at 12,500' altitude (M = 1.035 for 1.15 on V_L). However, it is felt that the analysis does adequately represent the revised envelope, except for the point of maximum q and Mach Number, since Flight Condition B (M = 0.98 at 9,500') represents the same q with the Mach Number difference being 0.055.

5.1 VIBRATION (MODAL) ANALYSIS

Figures 34 through 67 had presented the modes for Stiffness Configuration 5A and Mass Condition 1.0, with and without gyroscopic forces. These modes include the effect of a flexible empennage, which in the CEA analysis was represented somewhat crudely due to equipment limitations. It is felt that the modes which have a large contribution of empennage motion should be viewed somewhat critically, and not taken as being representative of the actual structure. Since this analysis is concerned with wing characteristics, for which analog representation was quite thorough, emphasis must be placed on wing results.

5.1.1 Vibration Modes (Normal)

The normal modes of concern in the analysis are those shown in Figures 35 and 38 for the symmetric case, and those shown in Figures 44 and 46 for the antisymmetric case, all for Stiffness Configuration 5A and Mass Condition 9.0. Figure 35, frequency 8.50 cycles per second, depicts the mode which might be termed first wing bending. Figure 38, frequency 16.55 cycles per second, depicts the mode which might be termed first wing torsion. Similarly, for the antisymmetric case, Figure 44, frequency 11.66 cycles per second; and Figure 46, frequency 16.55 cycles per second, depicts what might be termed the first wing bending and torsional modes, respectively. Some of the other modes shown are also wing modes, but of a higher frequency with the remaining exhibiting large amounts of coupling with the other components, i.e. aileron, fuselage and empennage. Aileron modes which should be mentioned are those of Figure 37, frequency 12.38 cycles per second, and Figure 43, frequency 10.34 cycles per second, symmetric and antisymmetric, respectively. The above modes have been emphasized, since in normal

cases, it is these modes that comprise the mode of flutter, as will be shown in subsequent sections.

5.1.2 Vibration Modes with Gyroscopic Effects

Figure 52, frequency 8.42 cycles per second and Figure 55, frequency 16.34 cycles per second, are the important modes of concern for the symmetric case, whereas Figure 61, frequency 11.65 cycles per second and Figure 63, frequency 16.32 cycles per second depict the equivalent antisymmetric wing modes, again for Stiffness Configuration 5A and Mass Condition 9.0. The aileron modes are shown in Figure 54, frequency 12.40 cycles per second and Figure 60, frequency 10.32 cycles per second, symmetric and antisymmetric, respectively. From a comparison of the above modes with the modes discussed in Paragraph 5.1.1, it is apparent that gyroscopic forces are not too significant in causing radical modal changes. This is so, since the gyroscopic moments are small. The effective mass moment of inertia of the fan rotating parts about the fan rotor axis is 30.20 slug-ft^2 and the fan speed for 100% power is 2640 rpm.

5.2 FLUTTER ANALYSIS

To adequately evaluate the flutter characteristics of the XV-5A aircraft from the overall CEA analysis, it is best to follow the results of each phase of the flutter analysis as presented in Paragraph 4.3.

5.2.1 Phase I - Basic Structural Evaluation

Figures 68 through 71 depict the V-g (or M-g) plots for the basic stiffness configurations of the XV-5A aircraft for various aerodynamic center (a.c.) locations for Flight Condition D (M = 0.75 at sea level). The range of a.c. locations, 0.20c to 0.30c differ slightly from that presented in Figure 30 (C_{M_β} [$Q^{M\beta}$]), in that it was felt the wider range in a.c. travel would better define the dependence, if any, of the flutter speed on the a.c. travel. However, as Figures 68 and 69 show, a.c. location is insignificant in altering the trends of the symmetric case. This is not the case in the antisymmetric analysis as shown in Figures 70 and 71, in which a flutter point does occur, indicating that a.c. travel is significant when a forward location, 0.20c produces the lowest flutter speed (extrapolated in Figure 71). The difference in speeds between the most forward and the most aft location is small, yet this study does point out the need for correctly estimating the aerodynamic center location. In addition, as Figure 70 shows, the more critical stiffness configuration

is 5A (4g representation). It is this configuration that is used as the nominal configuration throughout the entire analysis. The flutter mode is comprised of antisymmetric wing bending coupled with aileron rotation. Although the flutter frequency is about 11.6 cycles per second, and the antisymmetric wing mode was shown to be 11.66 cycles per second with antisymmetric aileron 10.34 cycles per second, it must be remembered that the predominant motion is as mentioned, which implies coupling with aileron, fuselage and empennage. The flutter speed shown in Figure 70, M = 0.845 does not represent the true flutter speed, since M = 0.75 aerodynamics were used in the analysis. Therefore, additional Mach Numbers must be run. The results when plotted on an auxiliary plot, as in Figure 110, will define the true flutter speed, if any, at sea level. Conclusions reached on a true flutter speed are discussed in Paragraph 5.2.5.

5.2.2 Phase II - Wing Front and Rear Spar Flexibilities Studies

Phase I studies have shown that a flutter margin in excess of 15% on V_L does exist and therefore a weight reduction study was instigated. Phase I had shown that the critical mode of flutter was an antisymmetric bending coupled with aileron rotation. Obviously, a reduction in bending stiffness would lower the flutter speed. As mentioned in Paragraph 4.3.2, the criterion was to have neutral stability at 1.05 V_L (M = 0.75 at sea level), this now being a true flutter speed, and then attempt to raise the flutter speed by proper aileron mass-balancing. The significant reduction in flutter speed is shown in Figures 75 and 76. The flutter frequency reduced to 9.5 cycles per second for a 120% reduction in rear spar flexibility, and 10.5 cycles per second for a 32.5% reduction in both front and rear spar flexibilities. The symmetric results are not altered appreciably as shown by Figures 72 through 74.

5.2.3 Phase III - Aileron Mass-Balance Studies

Figure 79 shows the results of applying proper aileron mass-balance to Stiffness Configuration 5J (32.5% increase in front and rear spar flexibilities). These results show the definite inertial coupling between the wing bending mode and the aileron rotational mode. Mass Condition 4.0 (see Table 6.0) fulfills the criterion stated in Paragraph 4.3.3, and also points out the established fact that for a flutter mode involving coupling between main surface bending and control surface rotation, mass-balance at the outboard tip of the control is the optimum position.

5.2.4 Phase IV - Re-evaluation of Nominal and Optimum Stiffness Configurations

Phase II and III studies have shown that a stiffness reduction and consequently a weight savings was feasible. These studies are mainly academic in that a 32.5% increase in spar flexibilities (1/EI) or a 25% reduction in I (E being constant) is more than could be tolerated from a practicality standpoint. However, these studies do indicate that some reduction in stiffness is feasible. Figure 80 is a plot of damping versus front spar flexibility factor, and it shows that a small increase in flexibility within the range of practicality, is feasible for neutral stability with adequate aileron mass-balance at 1.15 V_L (1.15 M_L). Stiffness Configuration 5P with Mass Condition 8.0, as shown in Figure 82, fulfills the criterion stated in Paragraph 4.3.4. The 11% front spar and 18% rear spar flexibility increase represents, respectively, a 10% and 15% decrease in I for the front and rear spars (inboard panel). The weight savings thus gained represent the weight of the spar reduction (in moment of inertia), plus the difference in total mass-balance per aileron (7.0 lb. for Mass Condition 8.0 versus 11.08 lb. for Mass Condition 1.0). Figure 82 also depicts the results of applying the information gained during the Phase III studies to the nominal stiffness configuration (5A). Here, proper mass-balancing of the aileron resulted in a weight savings of 6.08 pounds per aileron, with a slight reduction in flutter speed, but still at 15% above V_L as shown in Figure 82.

5.2.5 Phase V - Flight Envelope Evaluation

Having established the optimum stiffness configuration and mass condition, an analysis was performed for all flight conditions. Figures 87 and 92 show the results of the symmetric and antisymmetric analyses, respectively, for both the optimum Stiffness Configuration 5P and the nominal Stiffness Configuration 5A, both with aileron tip mass-balance. Figure 92 depicts the trend of the antisymmetric flutter mode. A flutter point occurs only at Flight Condition D (M = 0.75 at sea level).

All other flight conditions are free of flutter, with no flutter occurring during the symmetric analysis for all flight conditions as depicted in Figure 87. Plotting of the flutter point, occurring during Flight Condition D (M = 0.75 at sea level), on an auxiliary plot as in Figure 110, shows that no true flutter speed exists for either stiffness configuration with aileron tip mass-balance. A true flutter speed would occur, for example, if neutral stability was reached at a flight parameter of $V/V_O = 1.0$, for example, when M = 0.75 at sea level. Figure 79 shows a flutter point

occurring at $V/V_0 = 1.0$ for $M = 0.75$ at sea level. This was shown to be a flutter point corresponding to a stiffness configuration with increased spar flexibilities (Stiffness Configuration 5J) and Mass Condition 1.0. This point is plotted in Figure 110 to demonstrate the meaning of this auxiliary plot.

5.2.6 Phase VI - Wing Structural Nose Box Evaluation

Studies of the reduction in the wing structural nose box, Figure 94, have shown that a slight decrease in flutter speed occurs in going from nominal torsional stiffness to zero torsional stiffness. This is so, since the flutter mode is one of wing bending coupled with aileron rotation and the nose box contributes more to the overall torsional stiffness of the wing. The torsional stiffness of the wing inner panel is generated mainly by differential bending of both front and rear spars, and reductions in spar stiffness would affect the torsional mode (see Tables 7 and 8 for modal frequency comparisons). However, Phase II studies (see Figures 75 and 76) have shown that the wing torsional mode is not critical, even with such reductions.

5.2.7 Phase VII - Aileron Equivalent Spring Restraint Studies

Phase VII investigated the effects of varying the aileron spring restraint, since in essence this value is somewhat difficult to calculate accurately. Figure 96 depicts the variation in flutter speed obtained by reducing, and also increasing, the overall spring constant (K_β). Also shown are the effects of having a free-floating aileron and a rigidly fixed aileron. The flutter frequencies indicate a change in flutter mode from the basic wing bending-aileron rotation mode, to one involving wing bending coupled with another mode in going from a free-floating aileron to a rigidly fixed aileron. The trend shown in Figure 96, (that of a minimum flutter speed for some factor of the nominal spring constant (K_β) and then increasing flutter speeds above and below this minimum), is common when dealing with basic surface-control surface flutter.

5.2.8 Phase VIII - Aircraft Simulation Studies

This phase of the overall analysis indicates that a proper aircraft simulation must be made in order to determine the contribution of component degrees of freedom that go into making up the mode of flutter. Figure 97 adequately demonstrates this. By simply cantilevering the wing, flutter does not exist, indicating that fuselage or aircraft degrees of freedom contribute to the flutter mode. Furthermore, Figure 98 indicates that by simply including aircraft rigid body degrees of freedom (side translation,

yaw and roll for the antisymmetric case), the mode of flutter is preserved, with a slight decrease in flutter speed due to rigidizing of the fuselage and empennage.

5.2.9 Phase IX - Aerodynamic Simulation Studies

This section is presented more as a discussion on the importance of properly simulating certain terms in the aerodynamic representation, rather than as a discussion on the flutter characteristics of the XV-5A aircraft.

Effects of aerodynamic center shifts have been discussed in Paragraph 5.2.1, with the more critical a.c. location being taken as 0.20c, as shown in Figures 70 and 71 for Flight Condition D (M = 0.75 at sea level). This location corresponds to the lowest flutter speed and is felt to be reasonable for this flight condition. The percentage change from that obtained with the a.c. location at 0.25c, the theoretical subsonic value, is very small, yet this study does indicate a need for correct simulation of this parameter. Figures 84 through 86 present the effects of a.c. location in the symmetric sense for the remaining three flight conditions, whereas similar results for the antisymmetric analyses are presented in Figures 89 through 91. Here, the aerodynamic center locations range from 0.20c to 0.32c. The aft location is more indicative of the trend with increasing Mach Number.

Figure 102 demonstrates the importance of adequately representing the lag function when undergoing an analog flutter analysis. With the lag function completely removed from the circuit, the flutter speed is drastically reduced in the antisymmetric case, and a flutter point occurs (extrapolated) in the symmetric case for Flight Condition (M = 0.75 at sea level). The symmetric case appears to be in error when considering the change in flutter frequency from results obtained with and without the lag function, when compared with the results obtained for the other flight conditions, Figures 103 through 105. The overall trend, though, is to diminish the effect of the lag function as the Mach Number is increased as mentioned in Reference 1.0.

The third aerodynamic parameter to be varied, that of the pitch damping coefficient (C_{M_q}), shows the effect of reducing this value from that used in the analysis (see Table 3) to $\pi/8$, the theoretical value at M = 0, and finally reducing it to zero. As reference 7, Figure 11, depicts, the value of C_{M_q} increases from $\pi/8$ at M = 0 to infinity as M = 1.0 is

approached. The simulation of a proper pitch damping coefficient is apparent when one examines Figures 106 through 109 in which flutter results are plotted for four flight conditions. Taking into account the trend of C_{M_q} as M = 1.0 is approached, and the existence of a flutter trend as shown in Figures 106 and 107, it can be seen that correct simulation of this coefficient is apparent. With the reduction of the value of the coefficient to $\pi/16$ and to zero, a second flutter mode emerges as depicted in Figure 107, antisymmetric with the critical mode showing a marked decrease in flutter speed. In addition, from Figure 107 with the inclusion of reduced values of C_{M_q}, a flutter mode appears for a configuration which is essentially stable in the symmetric sense.

5.2.10 Overall Evaluation

The results of Phase I through IX have indicated that the XV-5A aircraft (wing), on the basis of the preliminary data utilized in the analysis is free of flutter within the proposed flight envelope and revised envelope as shown in Figure 110. Studies have shown that mass-balancing of the aileron is a critical factor and must be carefully evaluated for future design efforts on the XV-5A aircraft. Similarly, the overall spring restraint (K_β) does affect the flutter characteristics, but the variation, at most, will result in flutter speeds above 15% on V_L of M_L. The flutter mode, that of antisymmetric wing bending, coupled with aileron rotation, indicates that proper aircraft simulation must be used in future flutter evaluation of the XV-5A aircraft with due regard given to fuselage and/or aircraft degrees of freedom.

BLANK PAGE

6.0 APPENDIX

6.1 LIST OF REFERENCES

1. Schwendler, R.G., "Flutter Analysis of VZ-11 Aircraft for Ryan Aeronautical Company, San Diego, California." Computer Engineering Associates CEA Project ES 191. July 23, 1962.

2. No Author, "A Proposal Concerning Aeroelastic Analysis of the 'Vertifan' Aircraft for Ryan Aerospace". Computer Engineering Associates ND 333. November 6, 1961.

3. MacNeal, R.H.; McCann, G.D., and Wilts, C.H., "The Solution of Aeroelastic Problems by Means of Electrical Analogies". Journal of the Aeronautical Sciences, Vol. 18, No. 12, December, 1951.

4. McCann, G.D., "The Direct Analogy Electric Analog Computer; Electric Analogies for Mechanical Structures; Designing Analogy Circuits from Test Data". ISA Journal. April, May, June, 1956.

5. Brignac, W.J.; Schwendler, R.G., "Aircraft Structural Analysis On An Analog Computer". Journal of the Engineering Mechanics Division, Proceedings of the American Society of Civil Engineers. June, 1960.

6. Sewall, J.L.; Herr, R.W., and Watkins, C.E., "Use of Subsonic Kernel Function in an Influence - Coefficient Method of Aeroelastic Analysis and Some Comparisons with Experiment". NASA TN D-515. October, 1960.

7. Wilts, C.H., "Aerodynamic Forces in Analog Computation". California Institute of Technology Computing Center, Technical Report No. 116. September, 1959.

8. Gray, W.L., Schenk, K.M.; "A Method for Calculating The Subsonic Steady-State Loading on an Airplane With a Wing of Arbitrary Plan-Form and Stiffness". NACA TN 3030. December, 1953.

9. Campbell, G.S.; "A Finite-Step Method For the Calculation of Span Loadings of Unusual Plan-Forms". NACA RM L50L13. July, 1951.

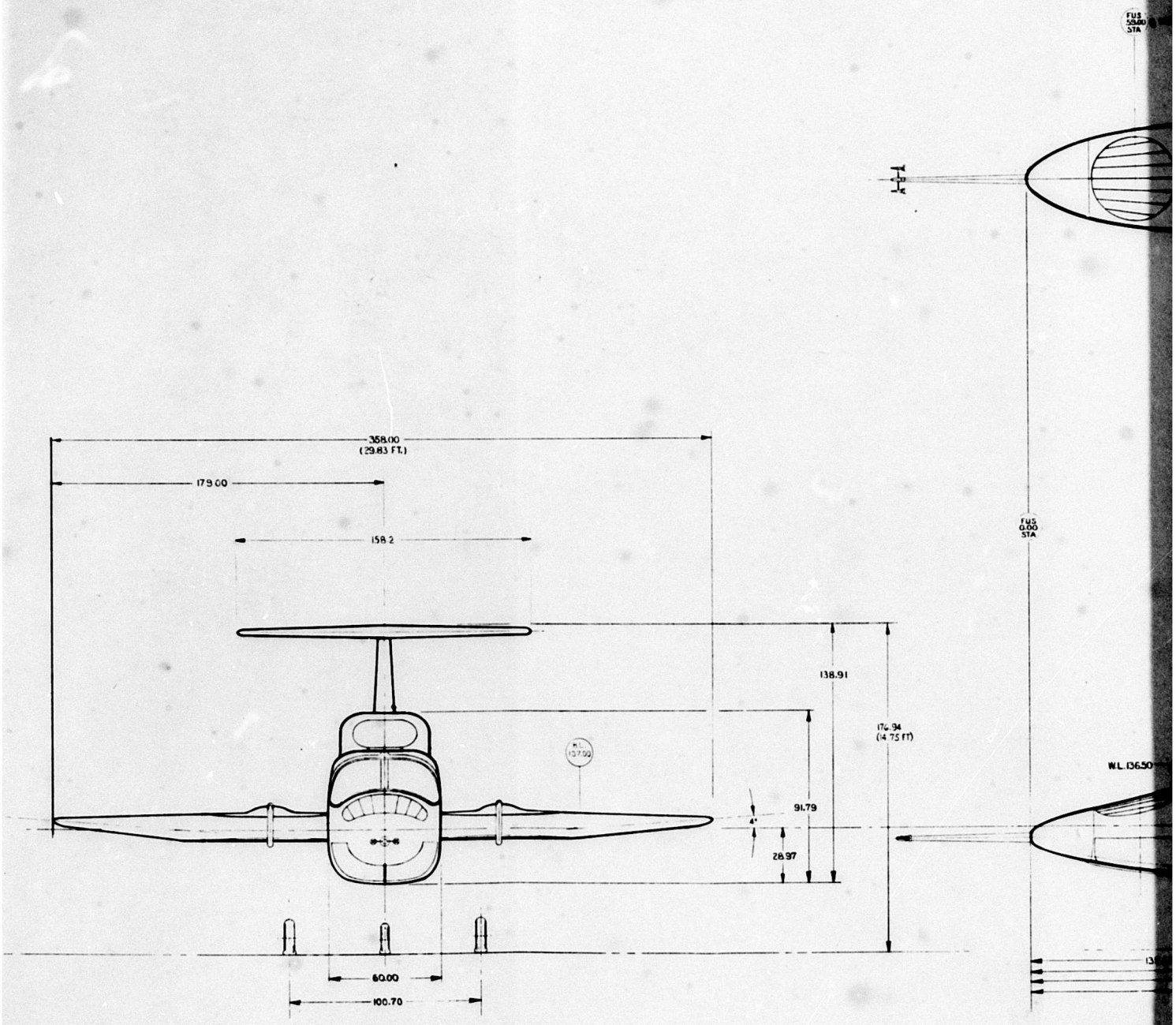
358.00
(29.83 FT.)
179.00
158.2
138.91
176.94
(14.75 FT)
91.79
4°
28.97
60.00
100.70
FUS.
0.00
STA
W.L. 136.50

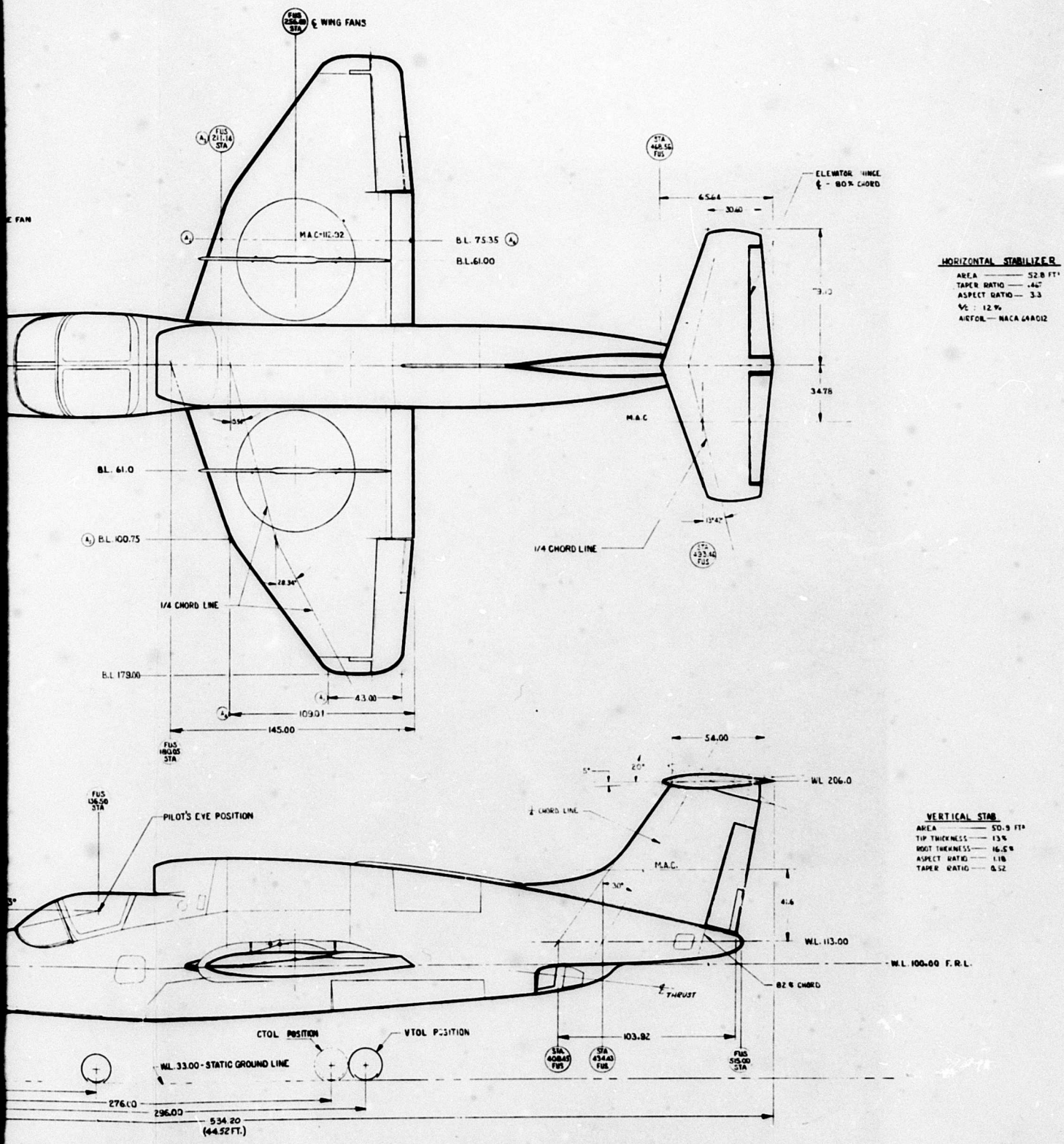

Figure 1 Three-View of XV-5A

B

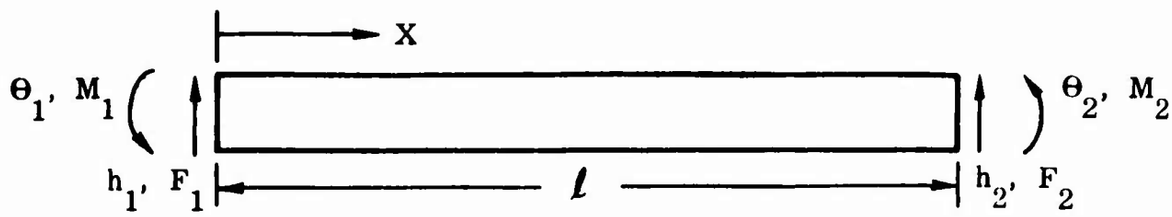

Figure 2 Beam Element

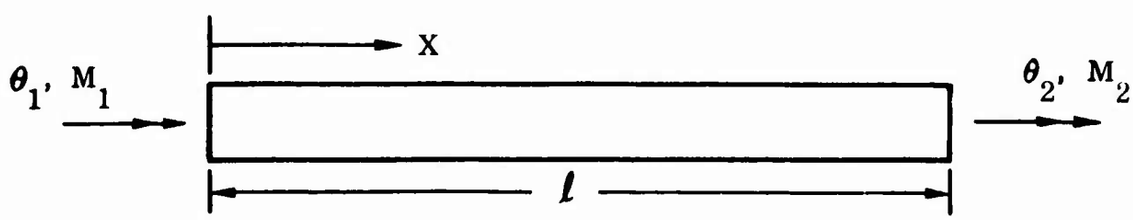

Figure 3 Torque Tube Element

BLANK PAGE

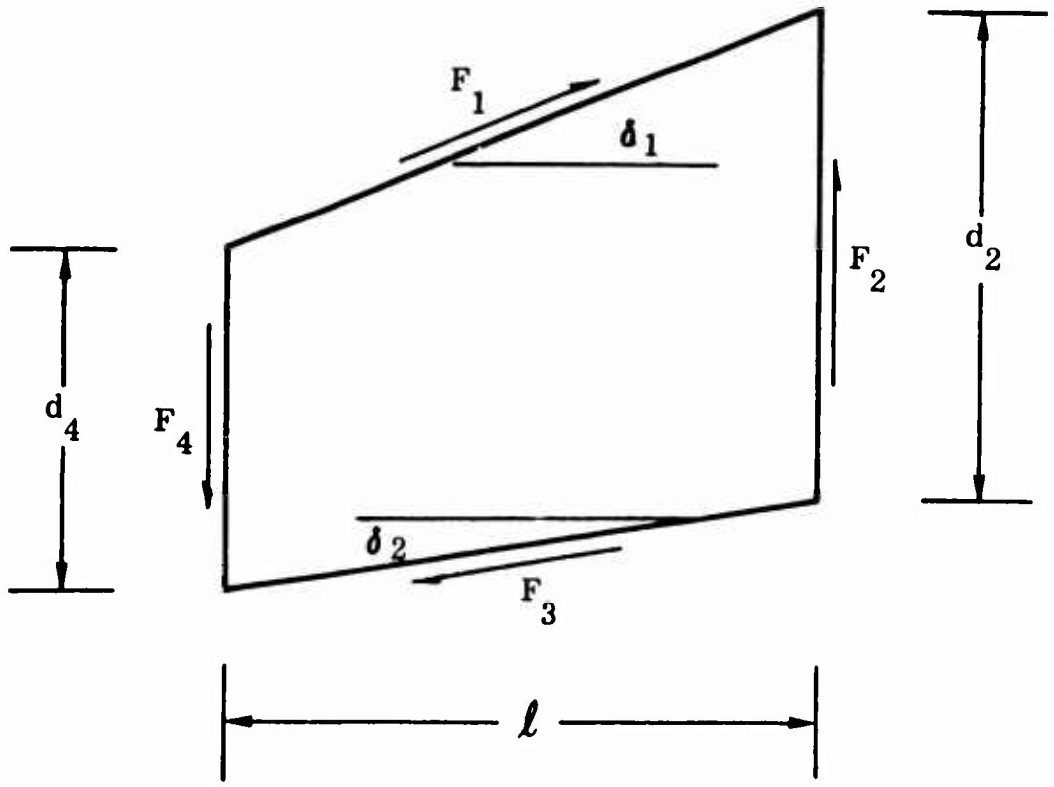

Figure 4 Torque Box Element

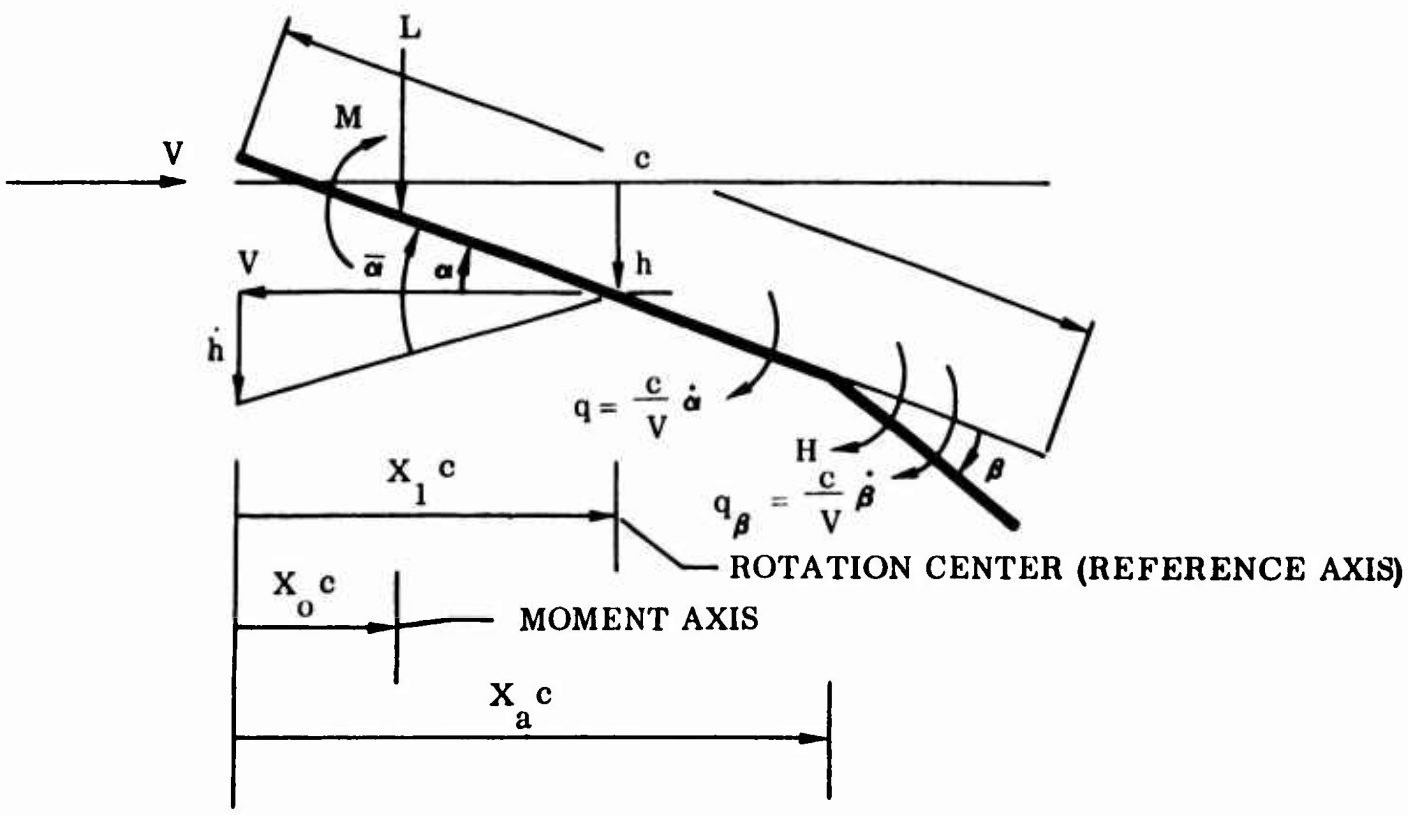

Figure 5 Definition of Aerodynamic Coordinates

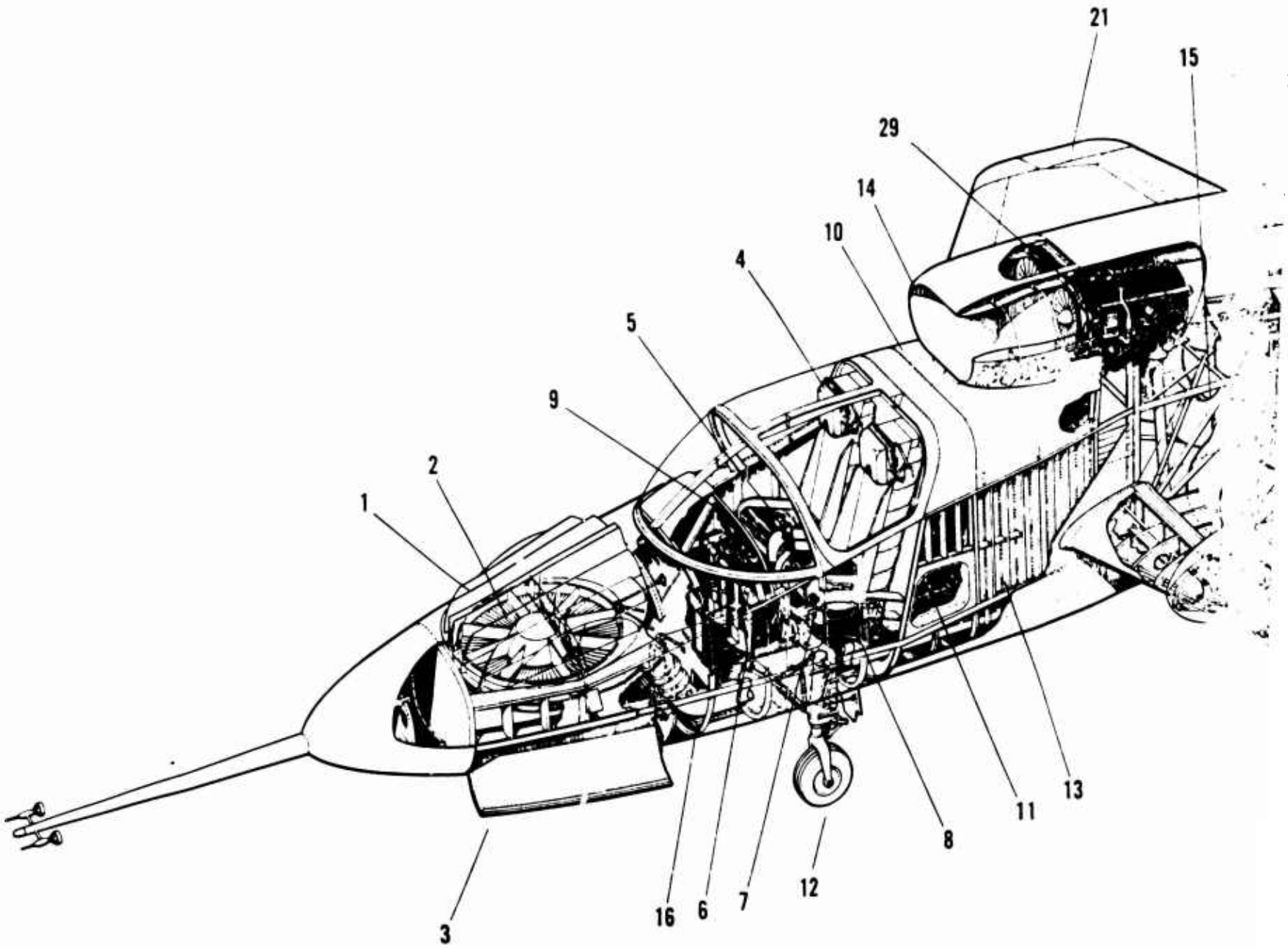
21
15
29
14
10
4
5
9
2
1
3
16
6
7
12
8
11
13

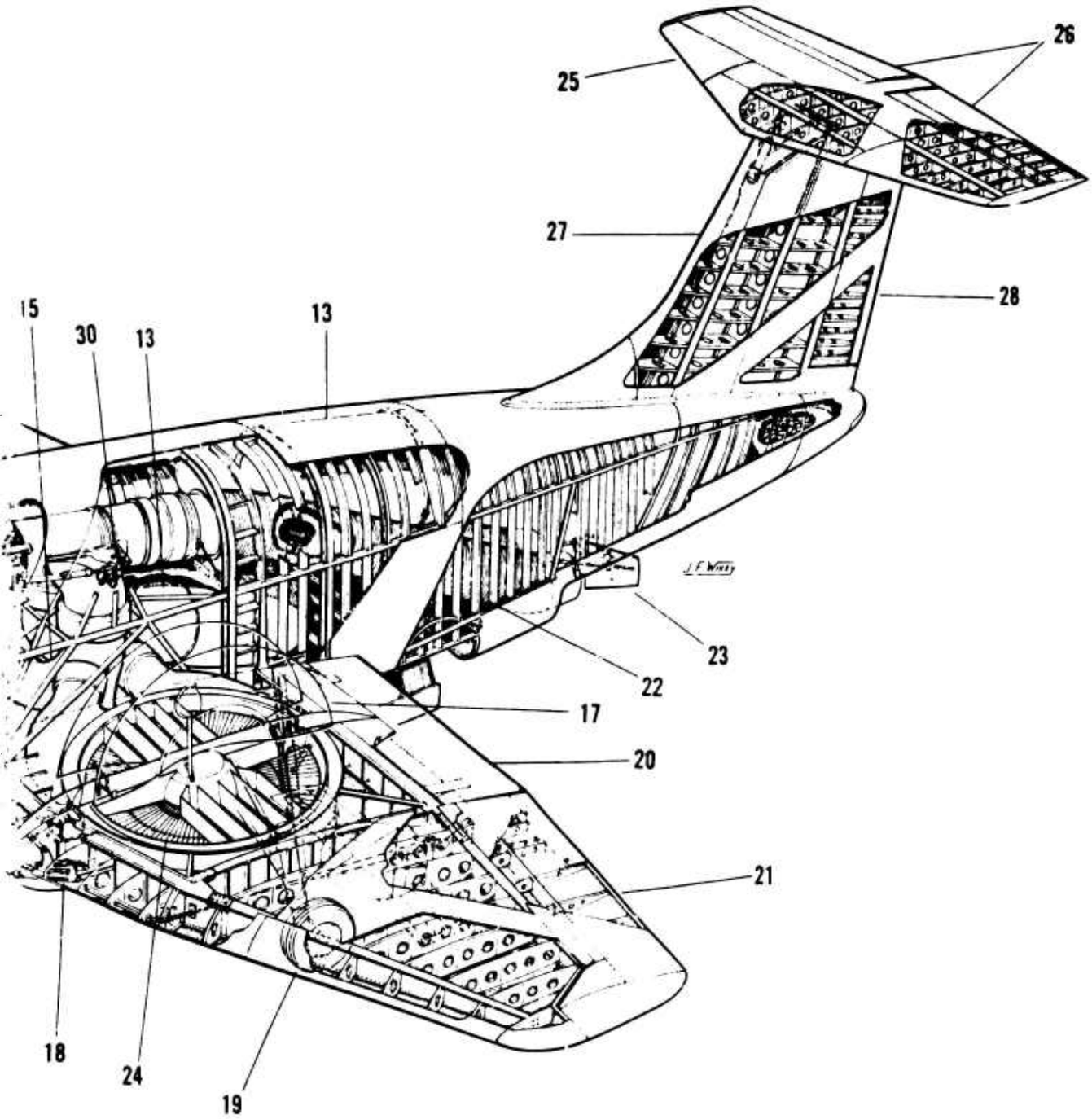

1.
2.
3.
4.
5.
6.
7.
8.
9.
10.
11.
12.
13.
14.
15.
16.
17.
18.
19.
20.
21.
22.
23.
24.
25.
26.
27.
28.
29.
30.

Figure 6 XV-5A Cutaway

B

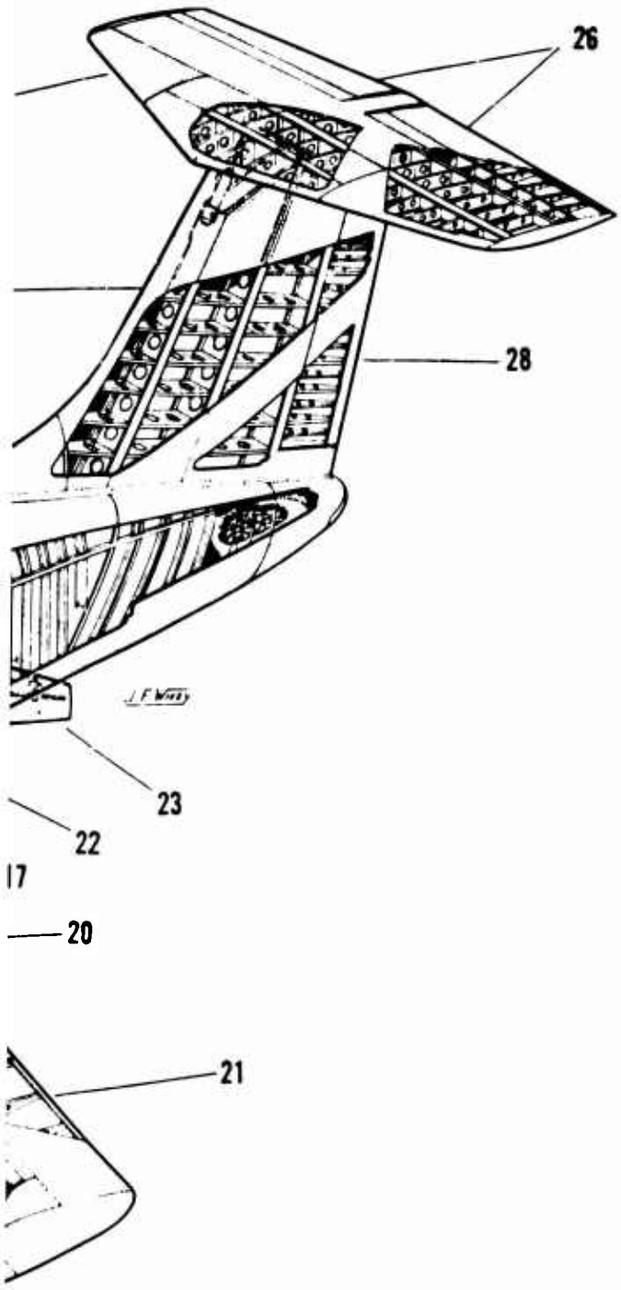

1. NOSE FAN INLET LOUVERS
2. GE-X376 PITCH CONTROL FAN
3. NOSE FAN THRUST REVERSERS AND NOSE FAIRINGS
4. ZERO-ZERO EJECTION SEAT
5. CONVENTIONAL CONTROL STICK
6. RUDDER PEDALS
7. THROTTLES
8. LIFT CONTROL STICK
9. INSTRUMENT PANEL
10. HYDRAULIC COMPARTMENT
11. ELECTRICAL COMPARTMENT
12. NOSE GEAR
13. FUEL TANK
14. SINGLE SPLIT INTAKE
15. CROSSOVER DUCT
16. NOSE FAN SUPPLY DUCT
17. MAIN FAN CLOSURE
18. EXIT LOUVER ACTUATORS
19. TWO POSITION LANDING GEAR
20. FLAP
21. AILERON
22. ENGINE TAIL PIPES
23. THRUST SPOILERS
24. GE-X353-5 LIFT FAN
25. FULL MOVEABLE HORIZONTAL STABILIZER
26. ELEVATORS
27. VERTICAL FIN
28. RUDDER
29. GE J85 GAS GENERATOR
30. DIVERTER VALVE

Figure 6 XV-5A Cutaway View

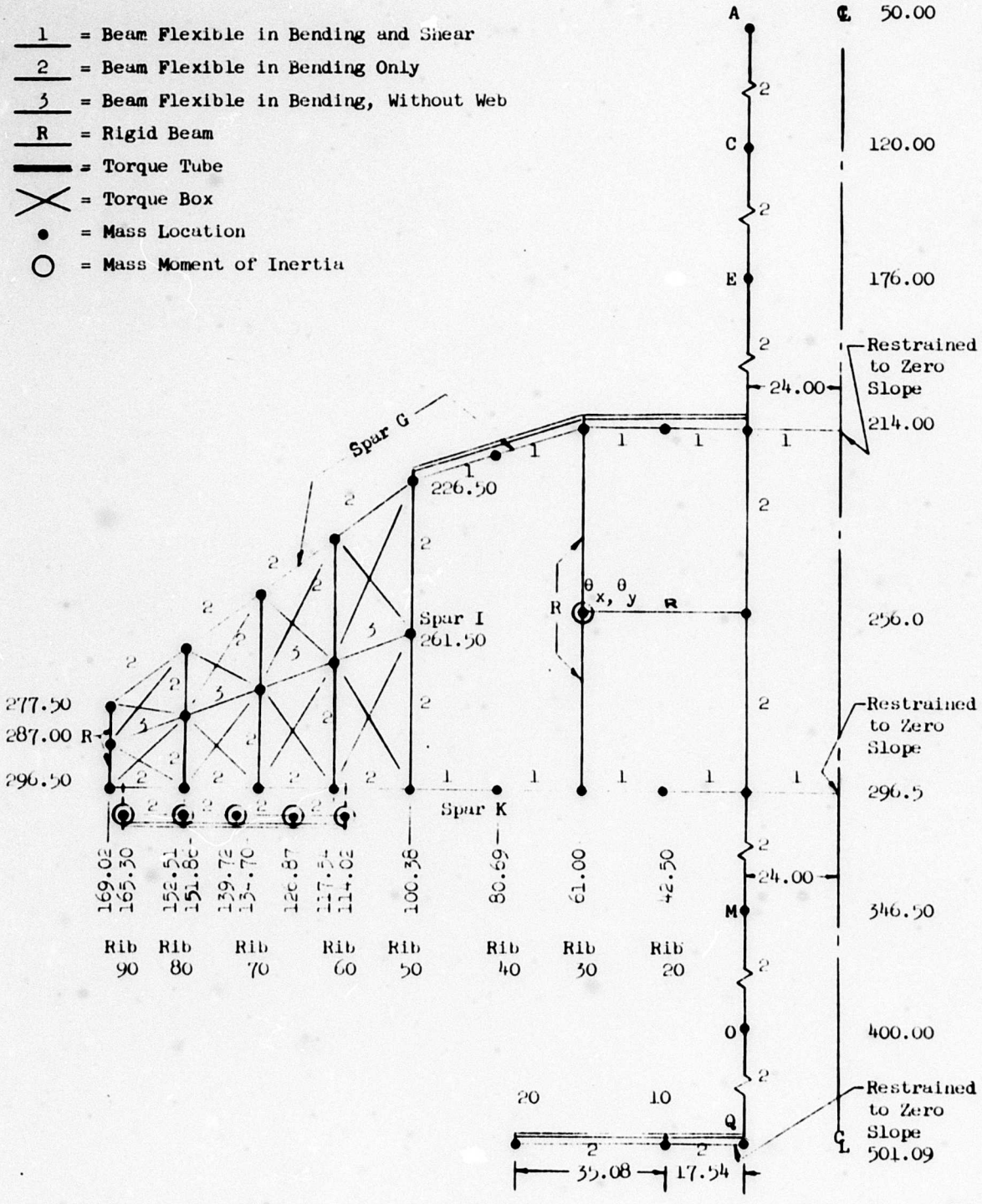

Figure 7 Idealized Structure Used in Symmetric Analysis

BLANK PAGE

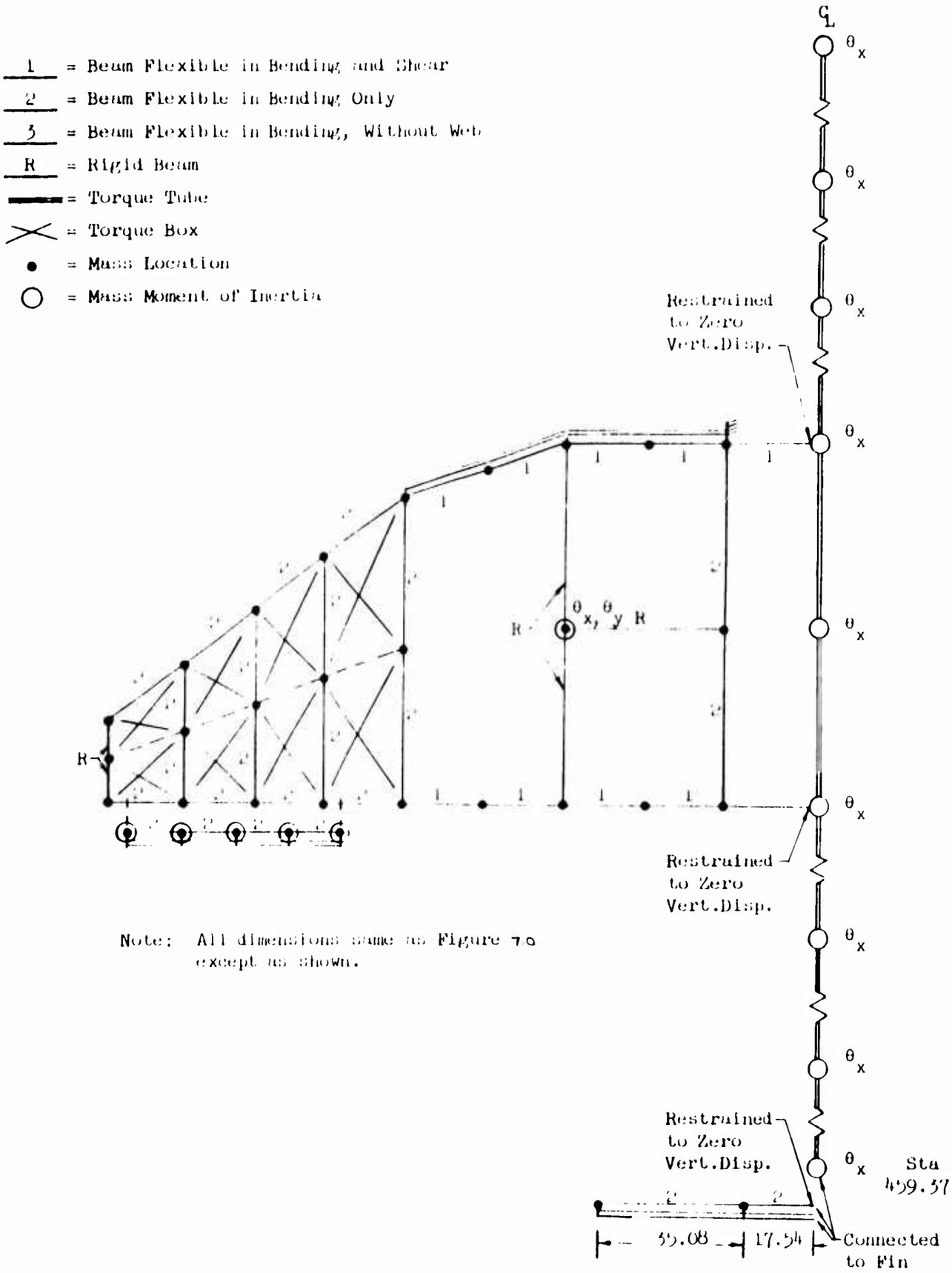

Note: All dimensions same as Figure 7a except as shown.

Figure 8 Vertical Model Used in Antisymmetric Analysis

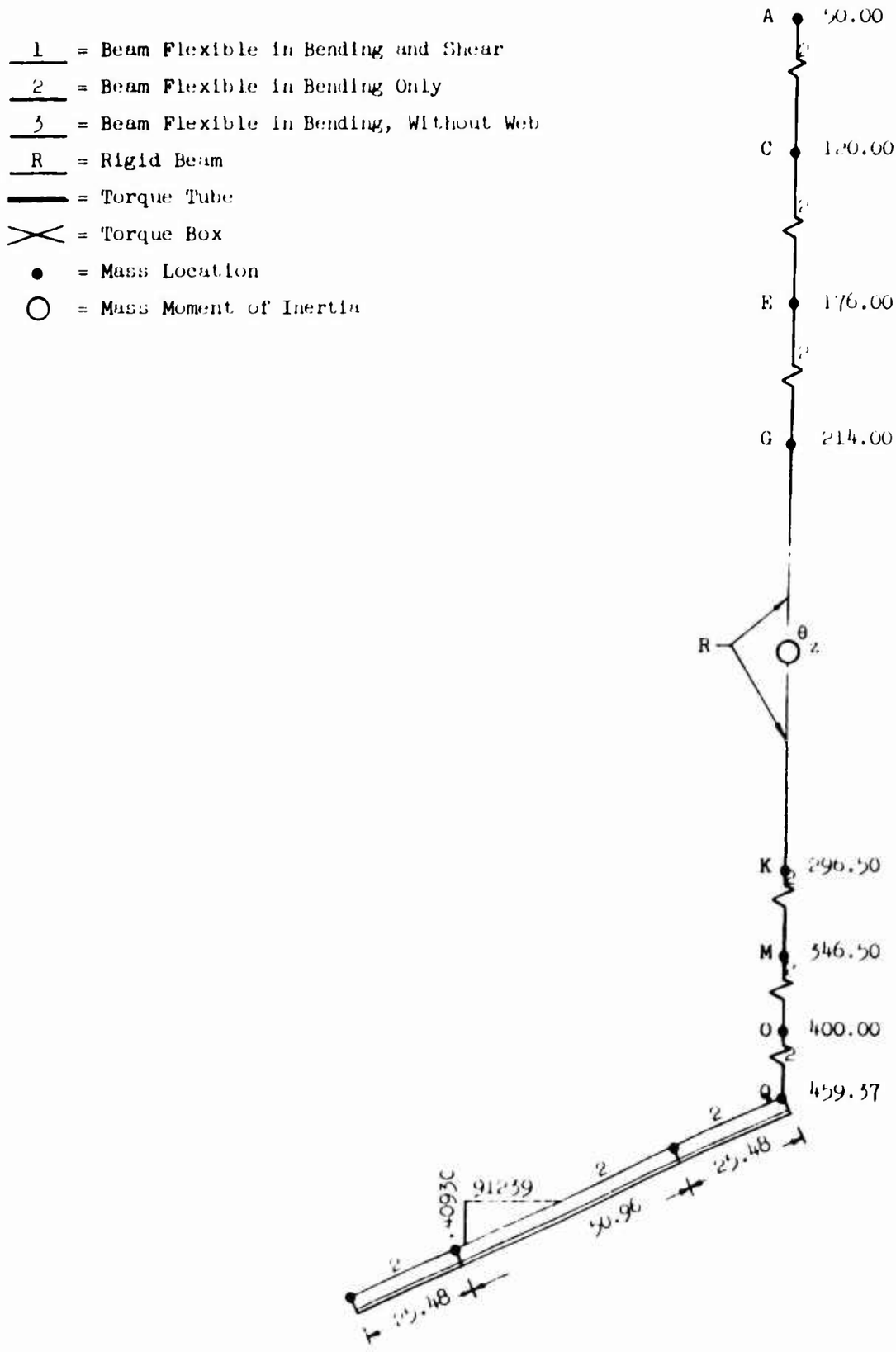

Figure 9 Lateral Model Used in Antisymmetric Analysis

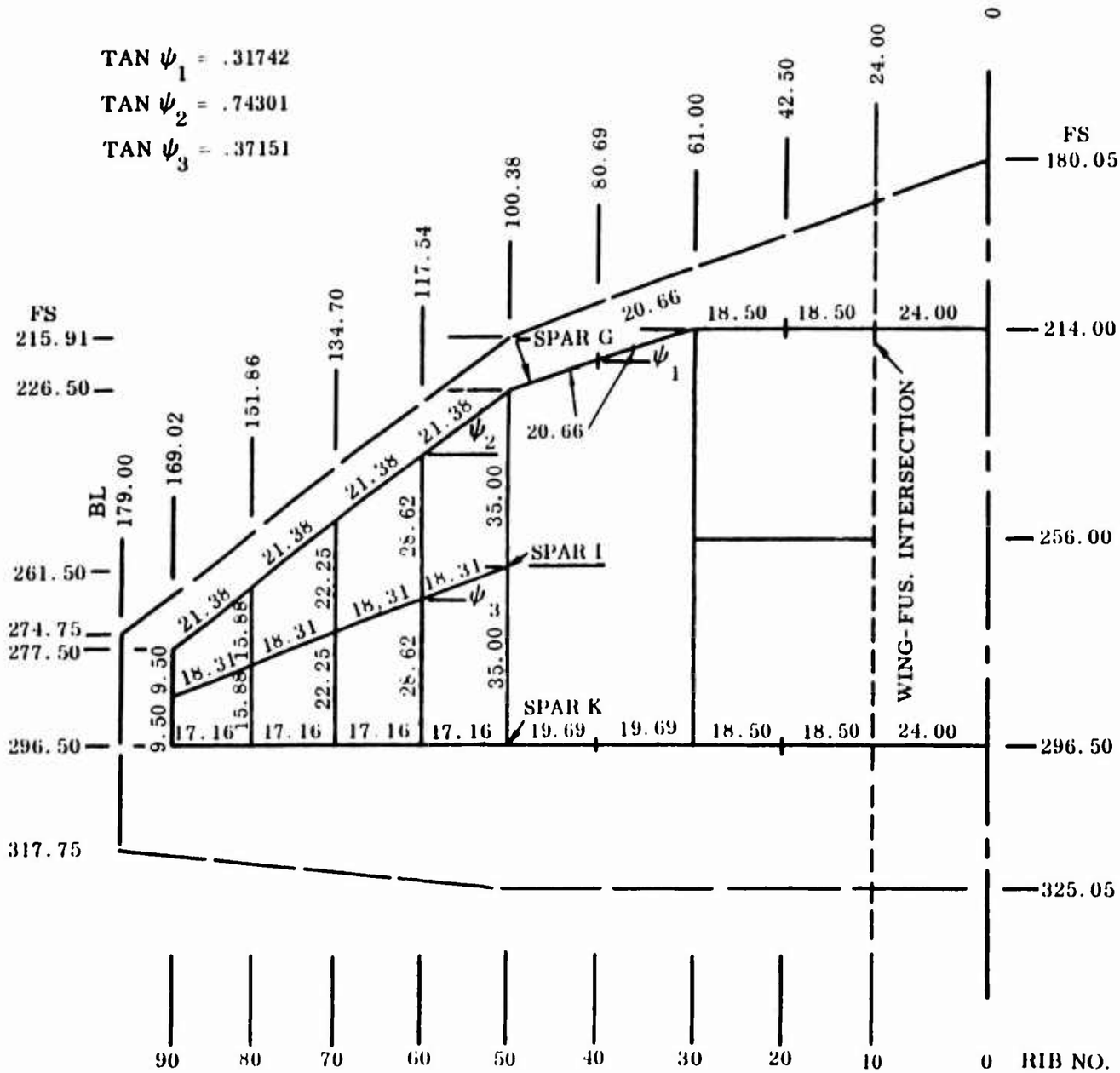

Figure 10 Wing Geometry

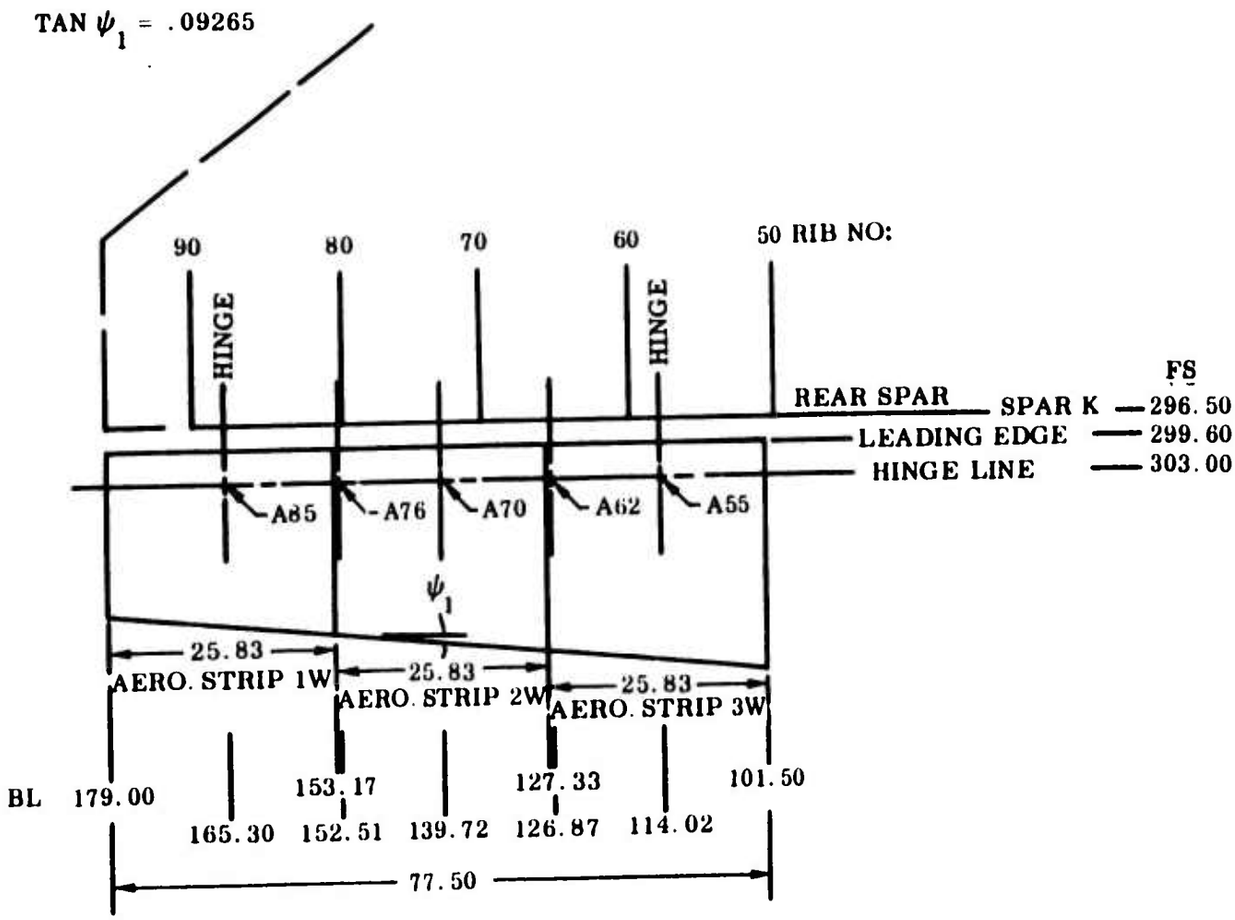

AERO. STRIP		1	2	3
WING CHORD		54.58	76.08	97.67
DISTANCE WING LE	AIL. HL	38.55	57.68	76.89
X_a		0.7063	0.7581	0.7872
COS ϕ		0.4126	0.5162	0.5744

Figure 11 Aileron Geometry

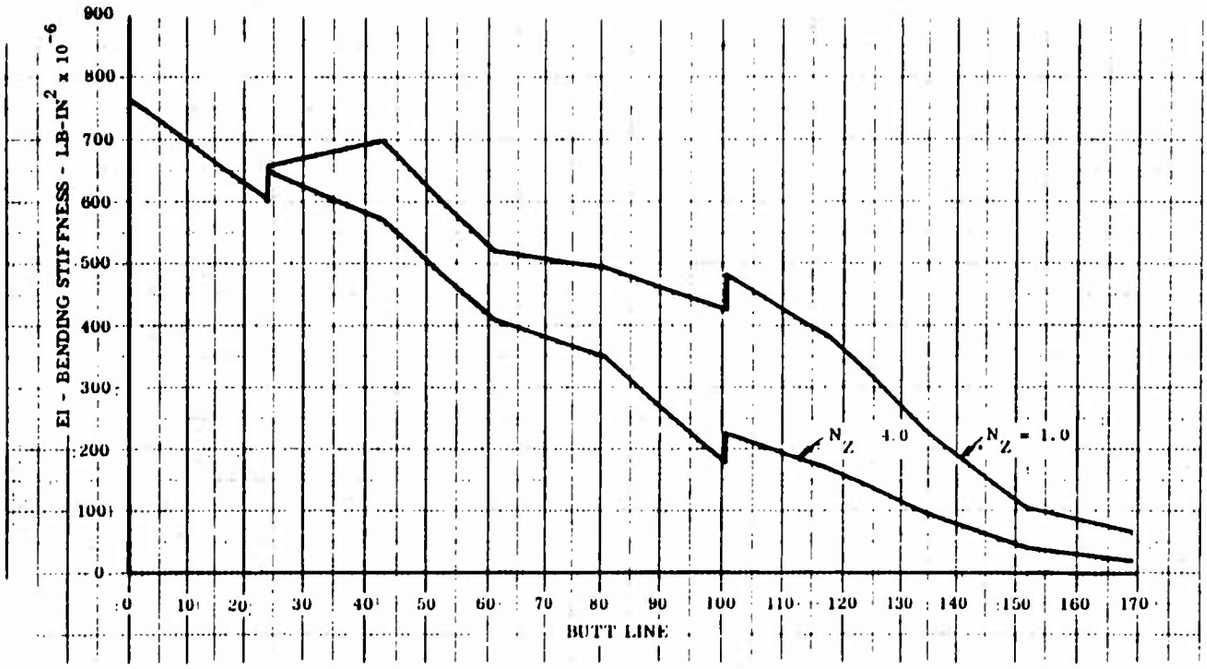

Figure 12 Front Wing Spar - Bending Stiffness Distribution

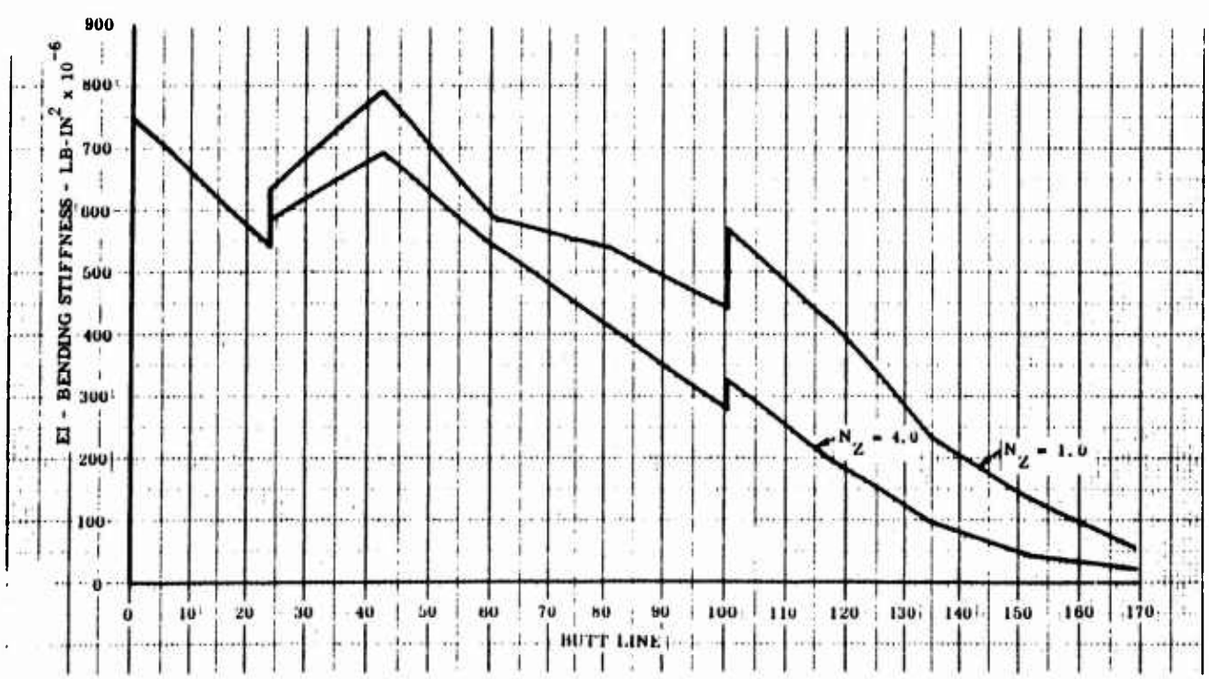

Figure 13 Rear Wing Spar - Bending Stiffness Distribution

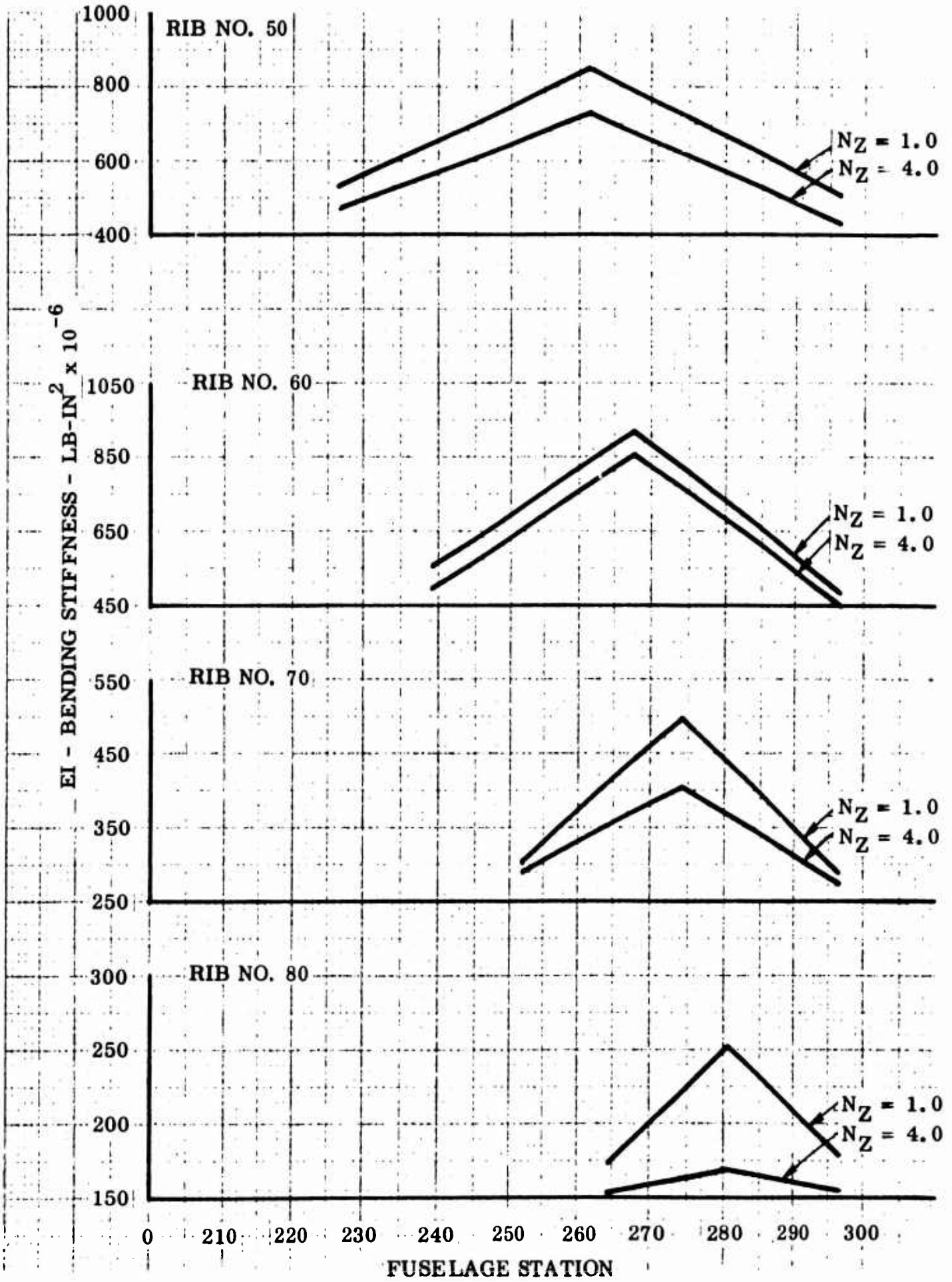

Figure 14 Wing Rib - Bending Stiffness Distribution

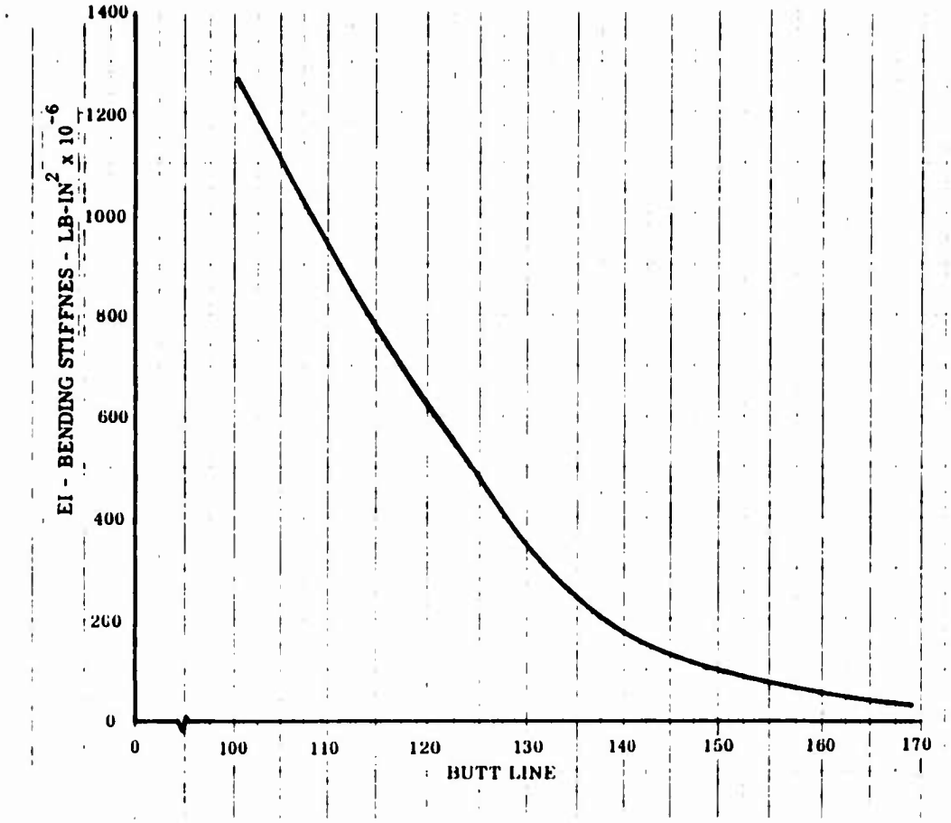

Figure 15 Wing Ficticious Spar - Bending Stiffness Distribution

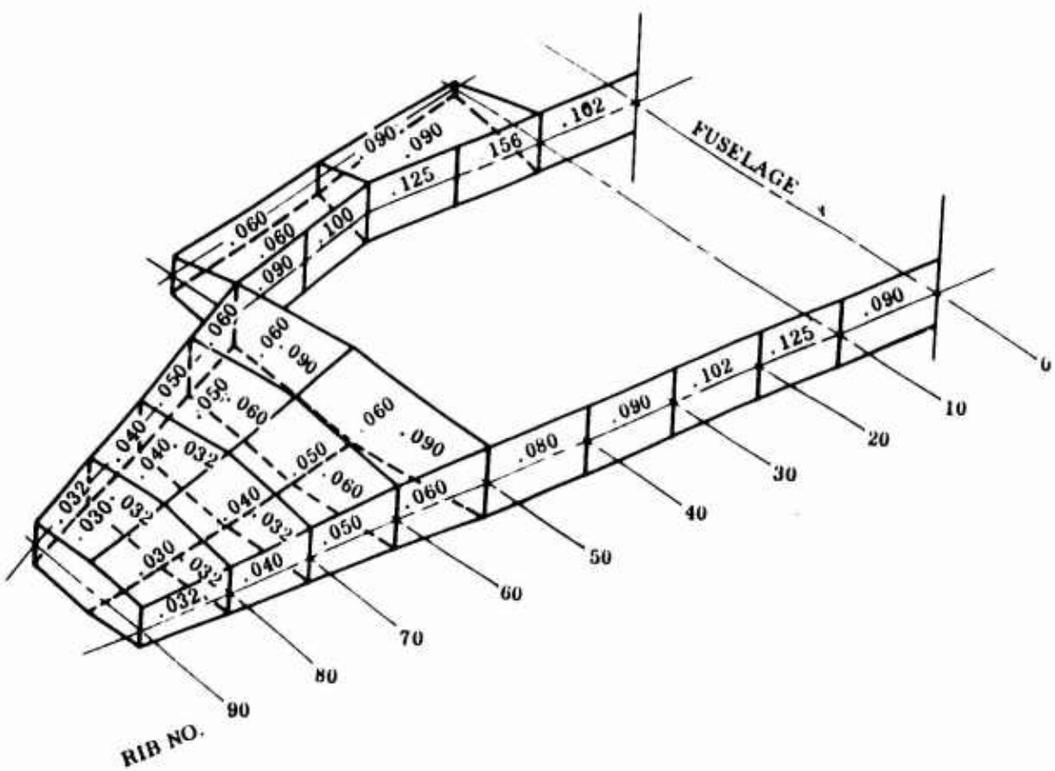

Figure 16 Idealized Wing - Skin, Spar and Rib Web Average Thickness

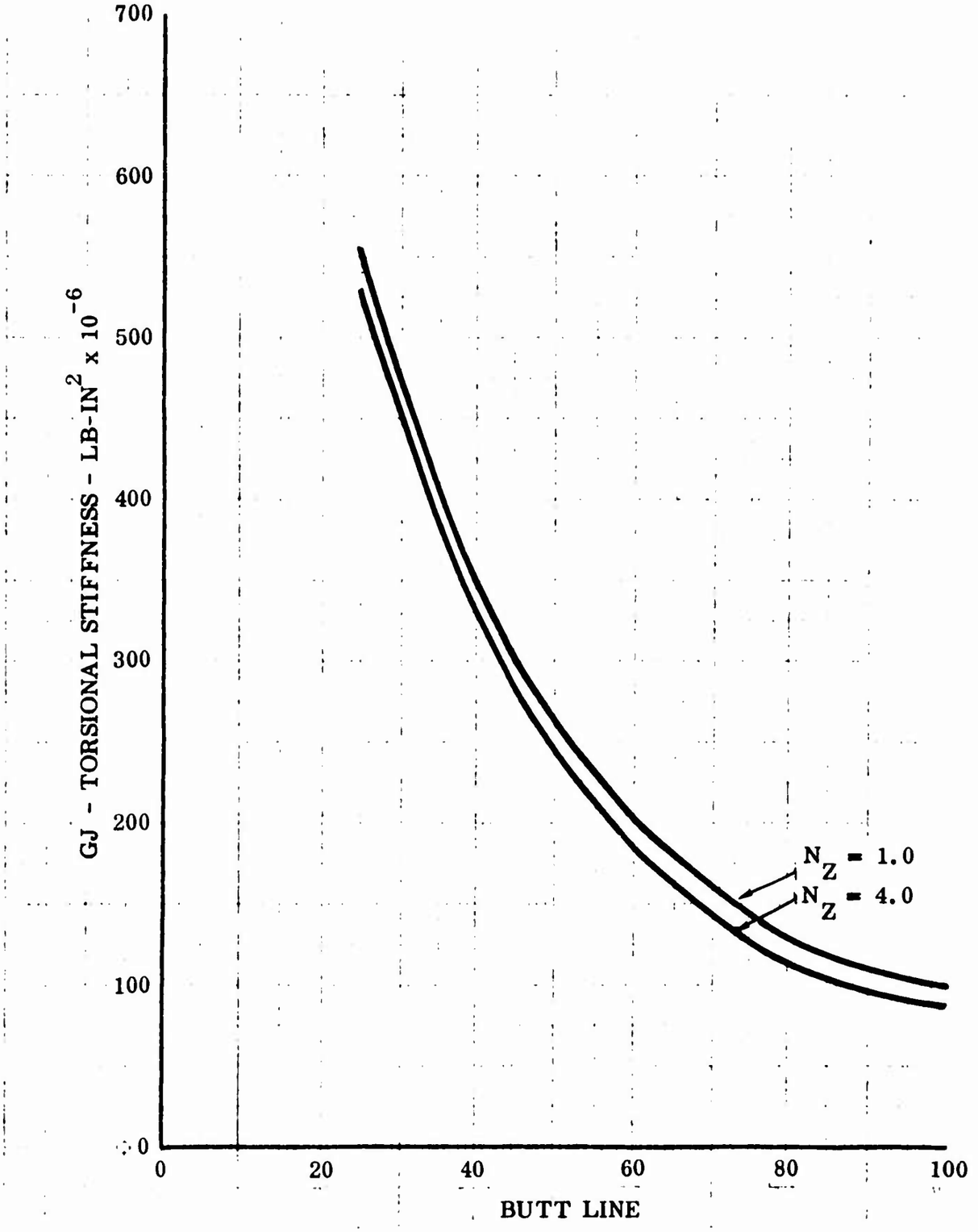

Figure 17 Equivalent Torque Tube - Torsional Stiffness Distribution

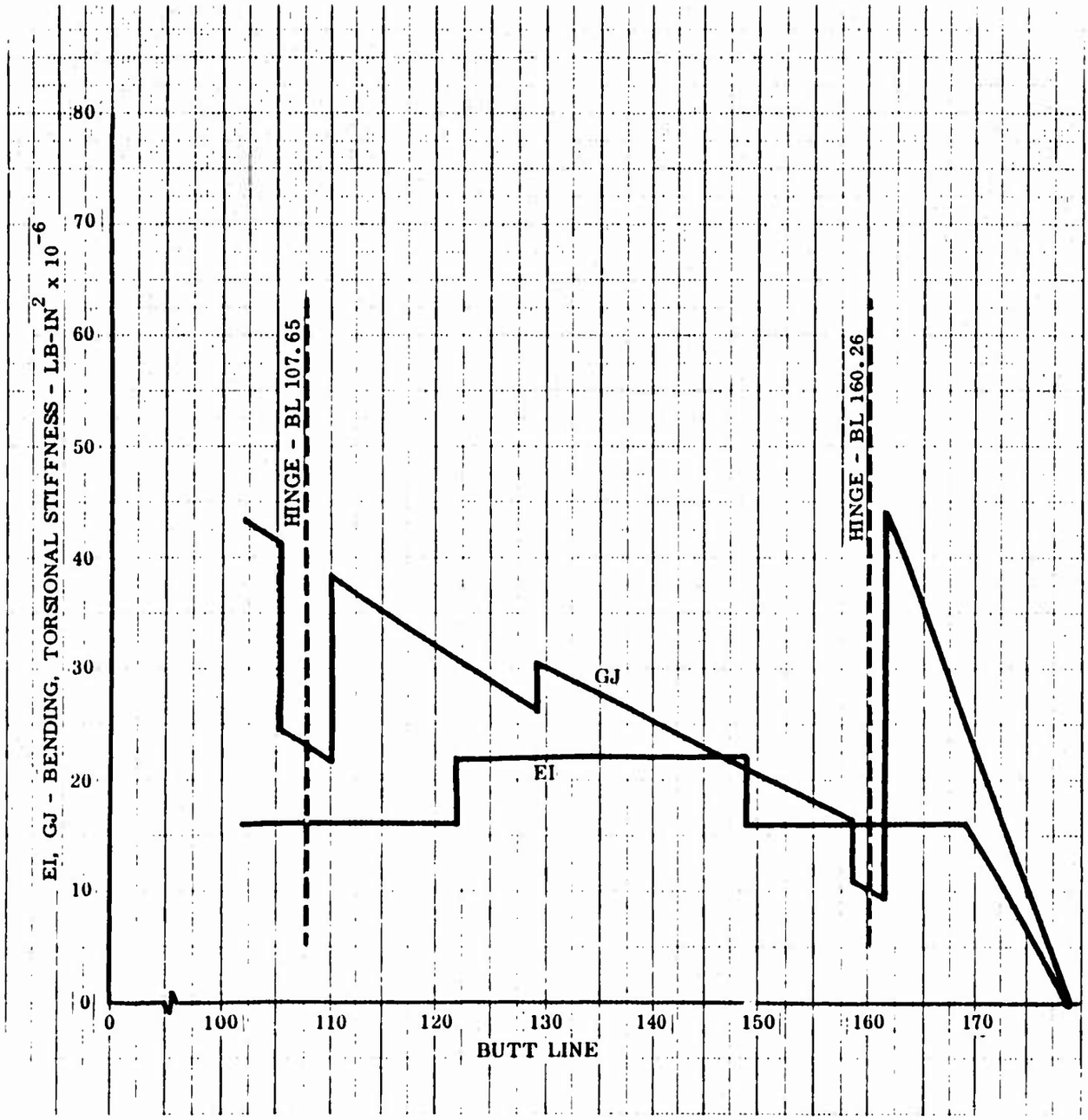

Figure 18 Aileron - Bending and Torsional Stiffness Distribution

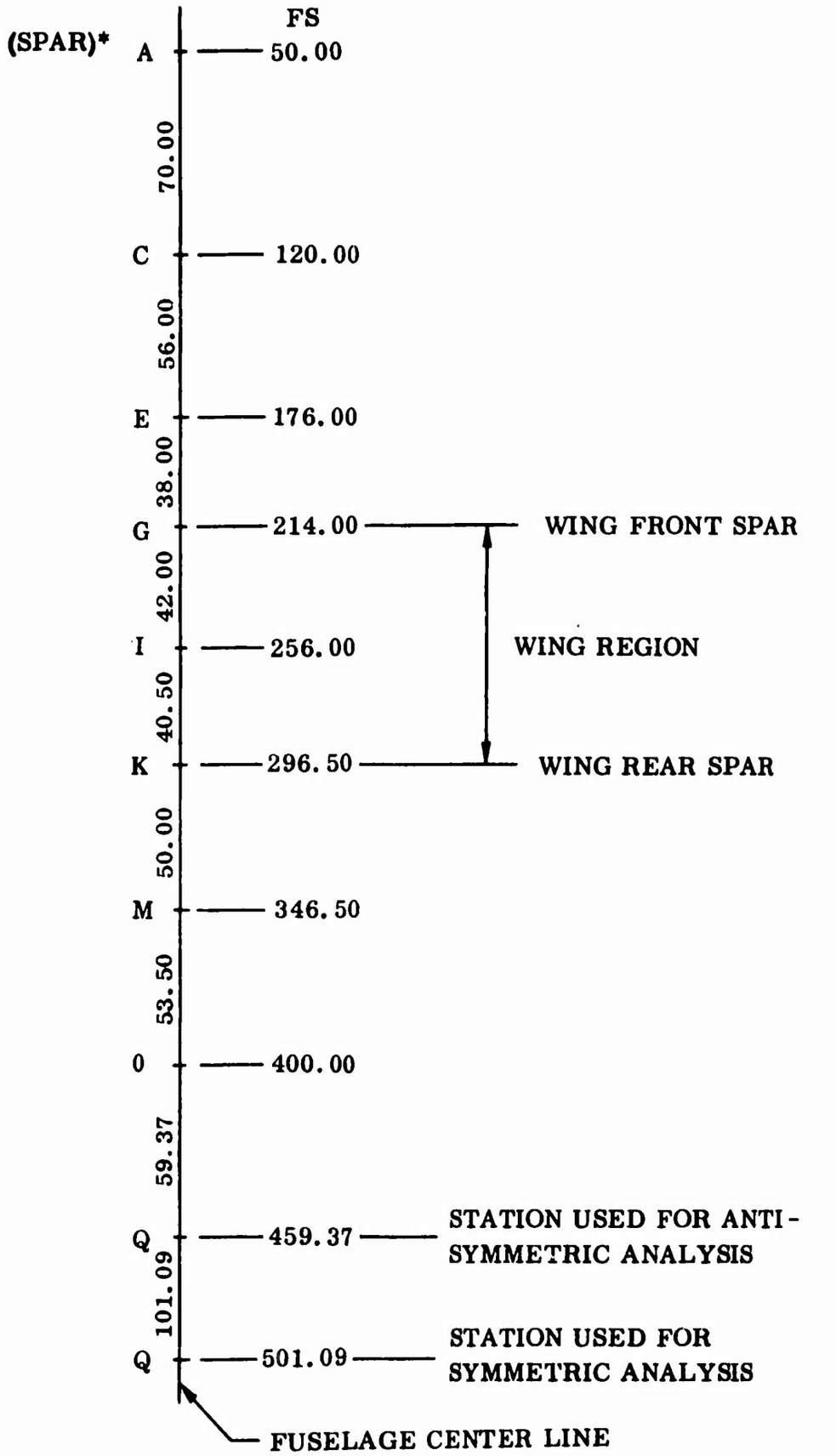

* See Figure 7

Figure 19 Fuselage Geometry

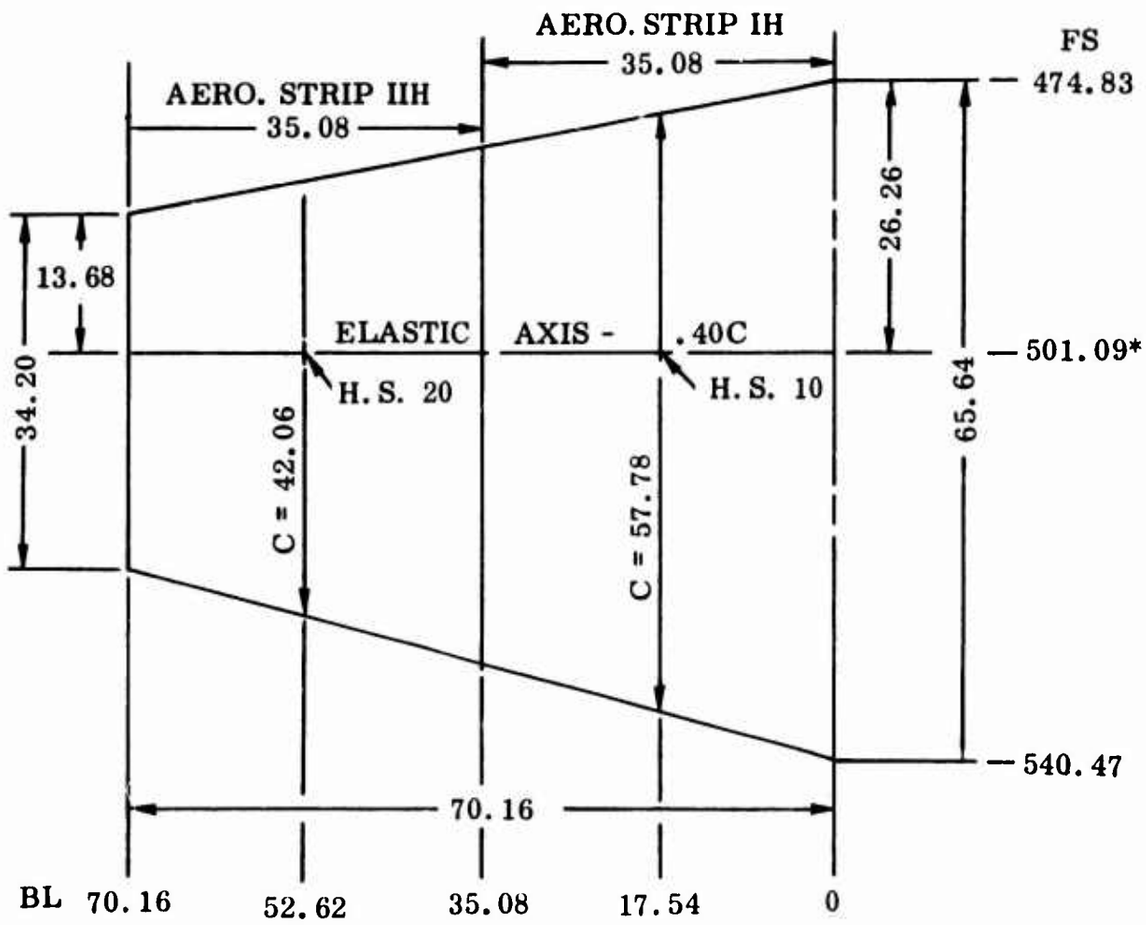

* See Figure 19

Figure 20 Horizontal Stabilizer Geometry

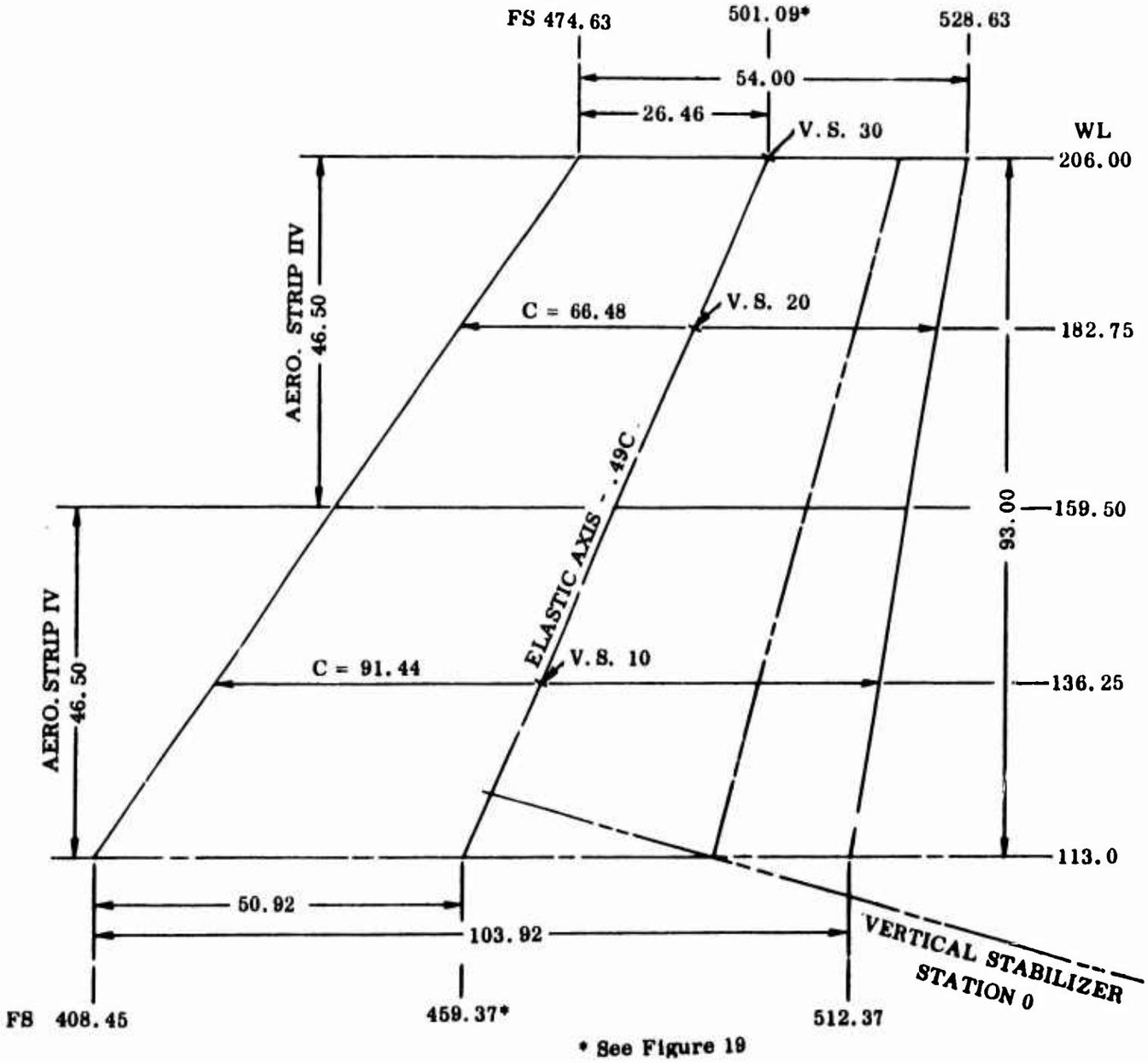

Figure 21 Vertical Stabilizer Geometry

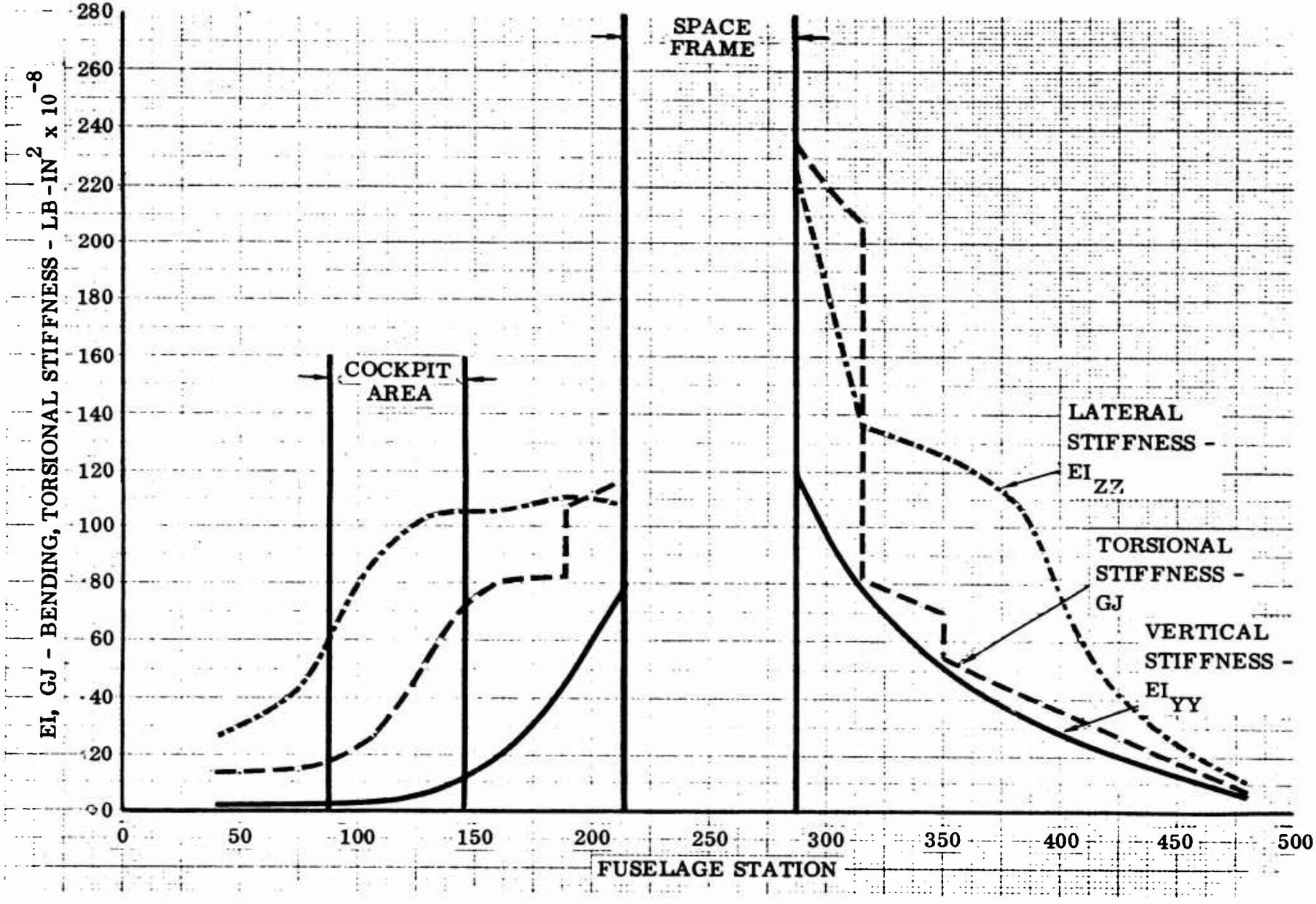

Figure 22 Fuselage - Bending and Torsional Stiffness Distribution

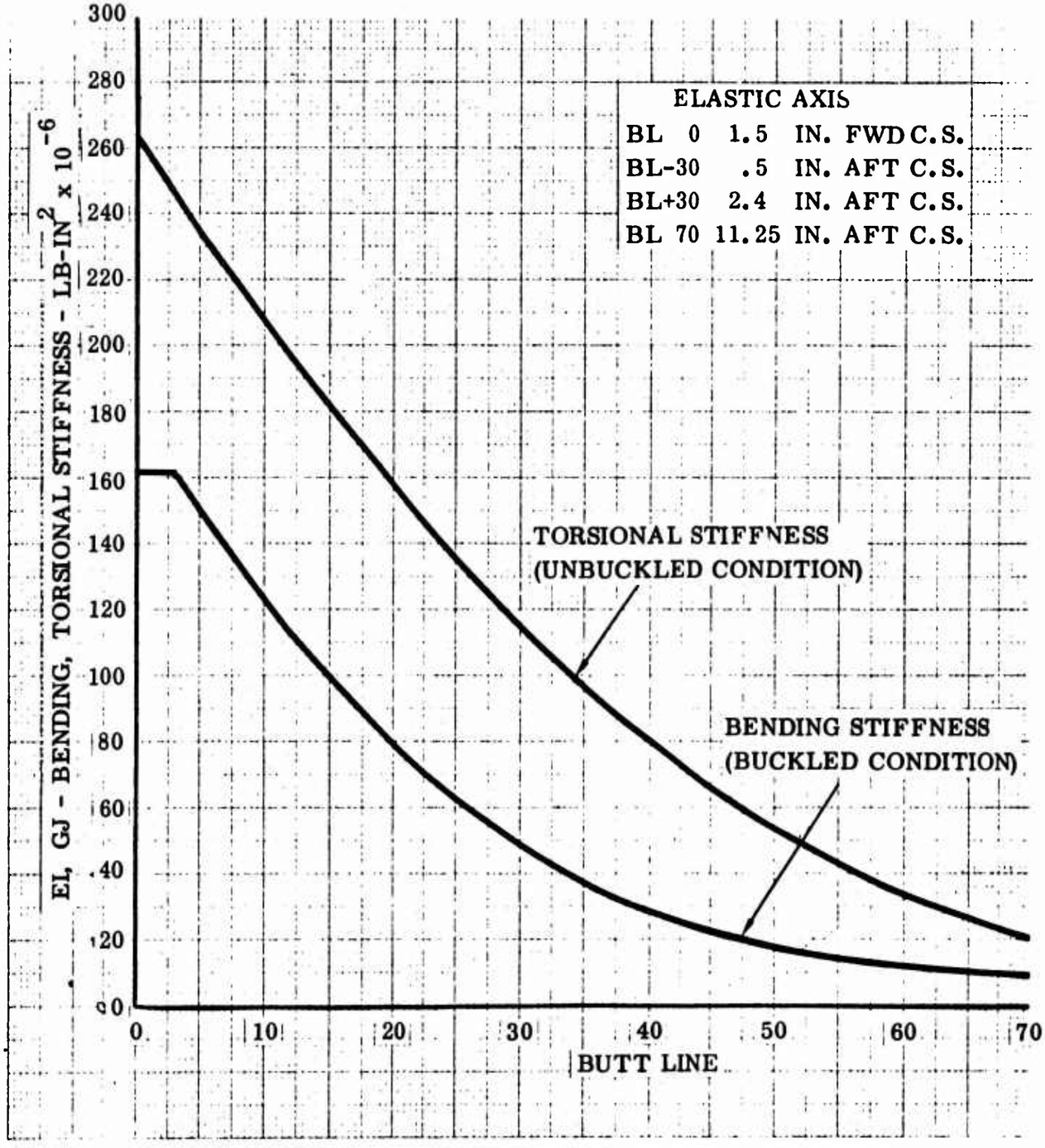

Figure 23 Horizontal Stabilizer - Bending and Torsional Stiffness Distribution

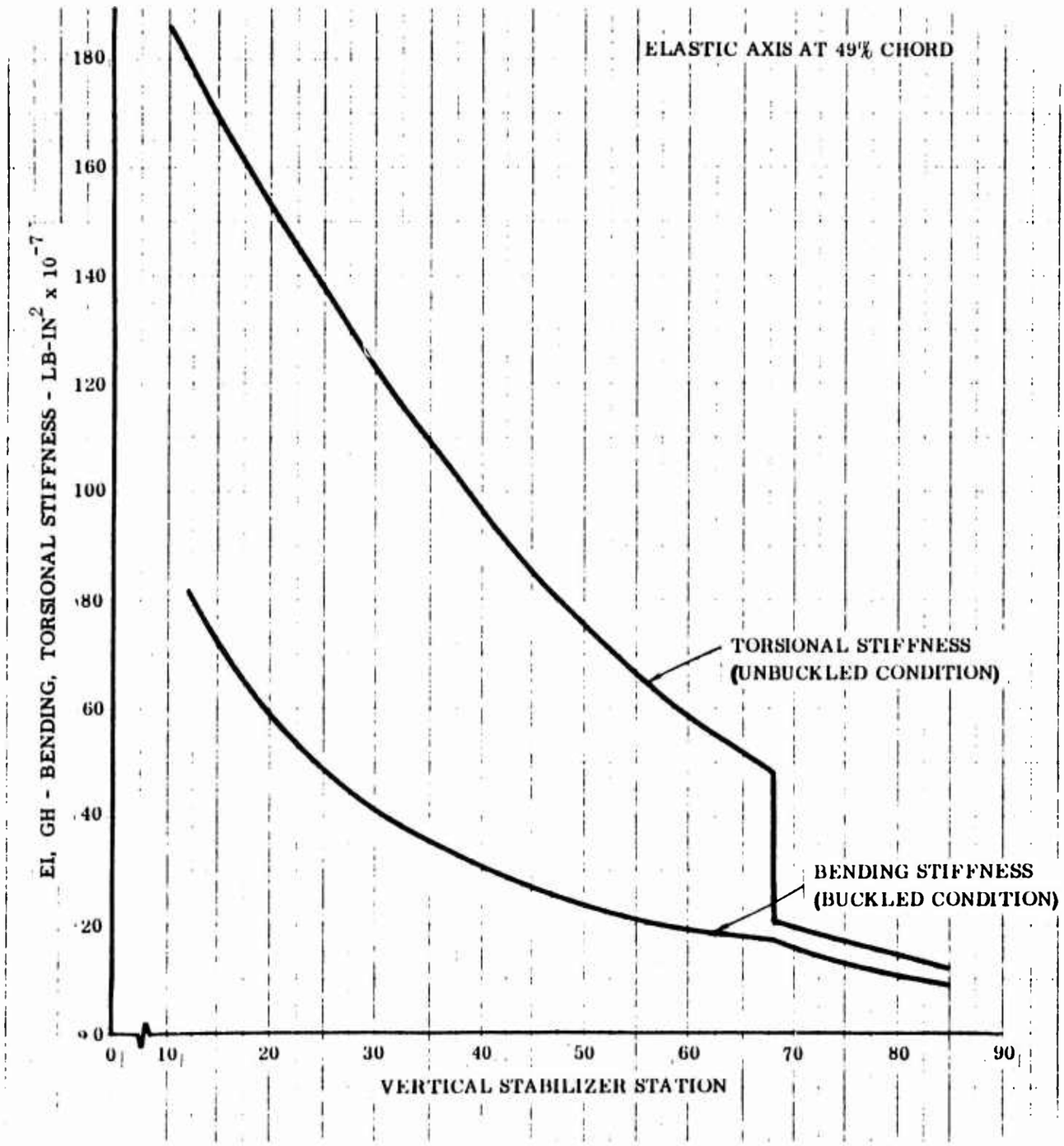

Figure 24 Vertical Stabilizer - Bending and Torsional Stiffness Distribution

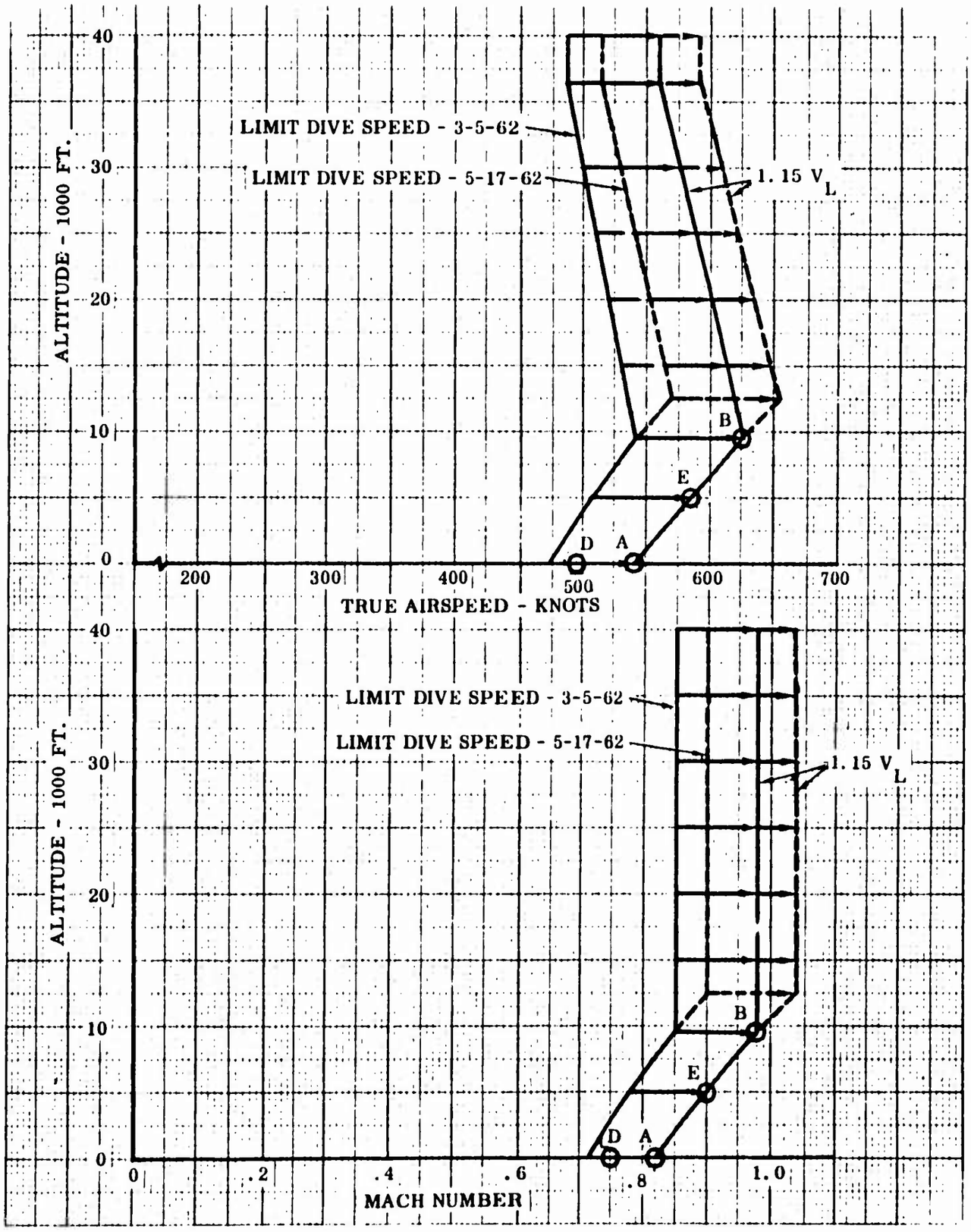

Figure 25 Proposed Flight Envelope

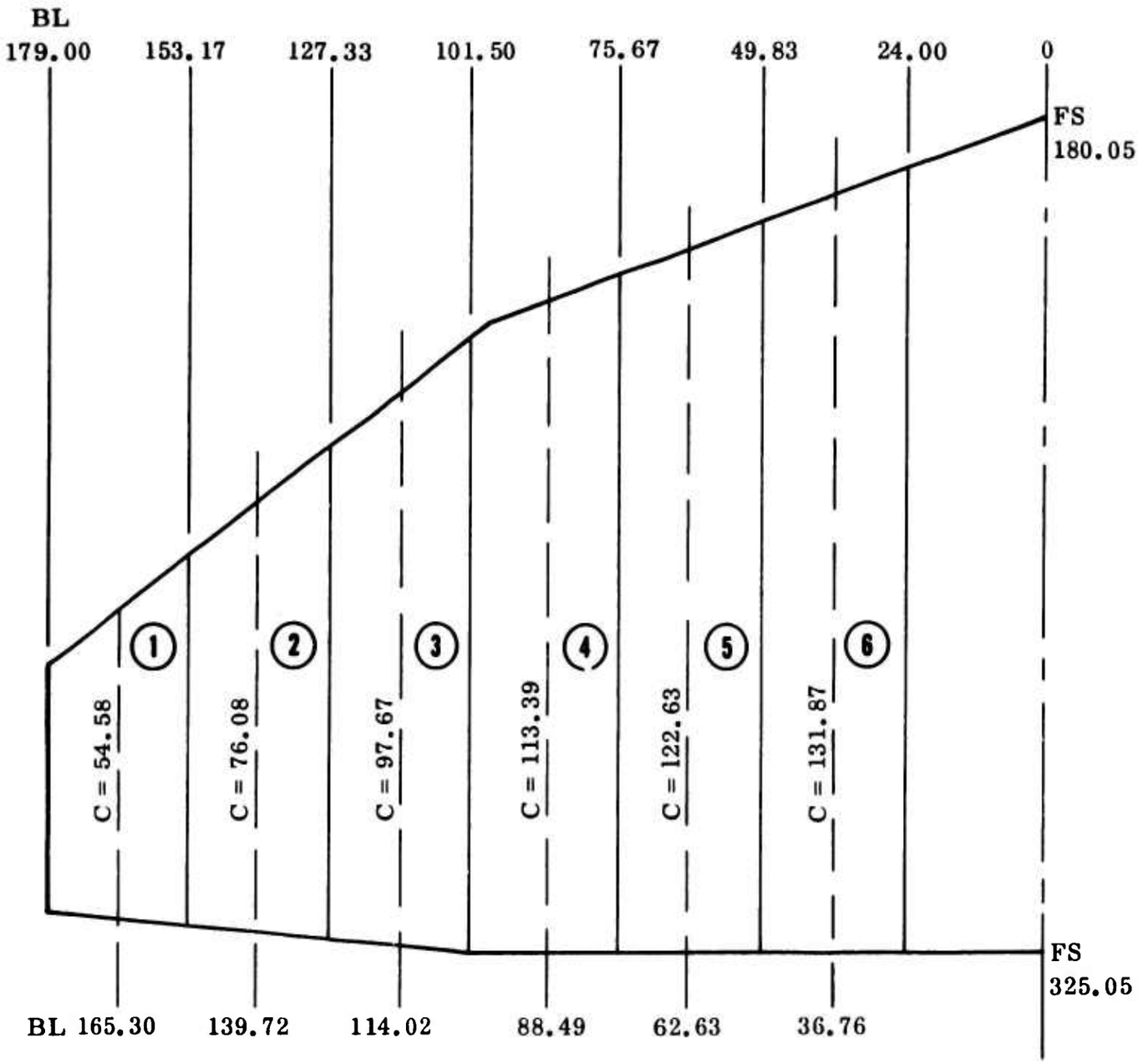

Figure 26 Wing Planform - Aerodynamic Simulation

Ft^2/Rad

M = 0.75

17.0384	7.81180	5.67568	4.74313	4.28343	4.09799
8.20979	23.2431	12.0956	9.30778	8.12293	7.66499
5.73957	11.9179	26.6667	15.1139	12.2848	11.3161
4.65199	8.96941	15.0203	29.9720	18.4378	16.0838
4.12418	7.70494	12.1017	18.4654	34.1800	23.5159
3.88467	7.16314	11.0100	15.9740	23.4523	41.7835

M = 0.82

14.2413	6.15041	4.34307	3.56990	3.19505	3.05238
0.587142	18.2772	8.45940	6.19969	5.27862	4.94057
1.35570	8.61810	23.5338	12.4172	9.77816	8.90982
1.21849	6.07844	12.2477	27.3106	15.8871	13.6162
1.13882	5.10838	9.55989	16.0954	32.2868	21.3926
1.11821	4.79748	8.73456	13.9266	21.8768	41.5071

M = 0.90

11.7379	3.82413	2.38429	1.83808	1.58372	1.52834
1.22477	14.4434	5.48752	3.61923	2.89274	2.70238
0.517137	2.62713	17.6234	7.42730	5.20815	4.62750
0.384860	1.39340	5.64150	21.0380	9.91384	8.01136
0.340226	1.04355	3.37358	8.82843	25.0024	14.3873
0.322637	0.921116	2.69514	6.29286	13.2644	33.6418

M = 0.98

11.3669	3.89184	2.66256	2.28179	2.13320	2.11172
0.470716	13.4096	5.54607	4.08017	3.57049	3.44413
0.200438	1.50555	19.7133	9.27819	7.21120	6.67823
0.164904	0.786618	6.38046	23.7647	12.8138	10.9925
0.153008	0.594425	3.73244	11.1677	28.7529	18.3157
0.146820	0.524584	2.94495	8.24610	17.2724	38.5517

Figure 27 $C_{L_\alpha}\left[Q^{L\alpha}\right]$

Symmetric

Ft^2/Rad

M = 0.75

$$\begin{bmatrix} 6.80178 & 3.54007 & 1.50342 & 0 & 0 & 0 \\ 4.40775 & 8.62577 & 3.41775 & 0 & 0 & 0 \\ 2.64298 & 5.35436 & 6.40975 & 0 & 0 & 0 \\ 2.04053 & 3.72972 & 4.19895 & 0 & 0 & 0 \\ 1.74903 & 3.00274 & 3.06621 & 0 & 0 & 0 \\ 1.57413 & 2.63925 & 2.61702 & 0 & 0 & 0 \end{bmatrix}$$

M = 0.82

$$\begin{bmatrix} 6.80178 & 3.45577 & 1.33390 & 0 & 0 & 0 \\ 3.55247 & 8.40767 & 3.17948 & 0 & 0 & 0 \\ 1.94725 & 4.58945 & 6.18320 & 0 & 0 & 0 \\ 1.25930 & 2.92688 & 3.55251 & 0 & 0 & 0 \\ 1.10772 & 2.19558 & 2.51156 & 0 & 0 & 0 \\ 0.956136 & 1.87750 & 1.98230 & 0 & 0 & 0 \end{bmatrix}$$

M = 0.90

$$\begin{bmatrix} 5.30927 & 2.20958 & 0.728469 & 0 & 0 & 0 \\ 1.50028 & 6.04025 & 1.96081 & 0 & 0 & 0 \\ 0.384786 & 2.03258 & 4.54658 & 0 & 0 & 0 \\ 0.225430 & 0.764909 & 1.86121 & 0 & 0 & 0 \\ 0.159356 & 0.499403 & 0.921816 & 0 & 0 & 0 \\ 0.132149 & 0.338203 & 0.611289 & 0 & 0 & 0 \end{bmatrix}$$

M = 0.98

$$\begin{bmatrix} 5.56968 & 2.46225 & 0.882756 & 0 & 0 & 0 \\ 1.38368 & 6.28679 & 2.30063 & 0 & 0 & 0 \\ 0.291505 & 1.96600 & 4.78876 & 0 & 0 & 0 \\ 0.151582 & 0.714336 & 2.03698 & 0 & 0 & 0 \\ 0.112715 & 0.429866 & 1.03704 & 0 & 0 & 0 \\ 0.0855081 & 0.316078 & 0.706986 & 0 & 0 & 0 \end{bmatrix}$$

Figure 28 $C_{L_\beta}\left[Q^{L_\beta}\right]$

Antisymmetric

Ft^2/Rad

M = 0.75

$$\begin{bmatrix} 5.83010 & 2.84786 & 0.952673 & 0 & 0 & 0 \\ 3.61466 & 7.67437 & 2.53890 & 0 & 0 & 0 \\ 1.98223 & 4.70324 & 5.35903 & 0 & 0 & 0 \\ 1.24375 & 2.59184 & 3.07402 & 0 & 0 & 0 \\ 0.757912 & 1.53298 & 1.66005 & 0 & 0 & 0 \\ 0.411993 & 0.821803 & 0.859320 & 0 & 0 & 0 \end{bmatrix}$$

M = 0.82

$$\begin{bmatrix} 5.81843 & 2.92151 & 1.03802 & 0 & 0 & 0 \\ 3.65353 & 6.97900 & 2.34360 & 0 & 0 & 0 \\ 1.71016 & 4.07741 & 5.01921 & 0 & 0 & 0 \\ 0.971682 & 2.10950 & 2.82013 & 0 & 0 & 0 \\ 0.563576 & 1.24851 & 1.47647 & 0 & 0 & 0 \\ 0.310938 & 0.632156 & 0.734328 & 0 & 0 & 0 \end{bmatrix}$$

M = 0.90

$$\begin{bmatrix} 4.81566 & 2.04502 & 0.601524 & 0 & 0 & 0 \\ 1.70627 & 5.84112 & 1.81922 & 0 & 0 & 0 \\ 0.357579 & 1.99540 & 4.01342 & 0 & 0 & 0 \\ 0.178790 & 0.730140 & 1.83426 & 0 & 0 & 0 \\ 0.120489 & 0.316078 & 0.691557 & 0 & 0 & 0 \\ 0.089395 & 0.146028 & 0.300762 & 0 & 0 & 0 \end{bmatrix}$$

M = 0.98

$$\begin{bmatrix} 4.88951 & 2.19896 & 0.676714 & 0 & 0 & 0 \\ 1.83065 & 6.40374 & 2.01354 & 0 & 0 & 0 \\ 0.349806 & 2.26881 & 4.33566 & 0 & 0 & 0 \\ 0.116602 & 0.695372 & 1.92156 & 0 & 0 & 0 \\ 0.058301 & 0.316078 & 0.717142 & 0 & 0 & 0 \\ 0.019434 & 0.126431 & 0.328104 & 0 & 0 & 0 \end{bmatrix}$$

Figure 29 $C_{L_\beta}\left[{}_Q L_\beta\right]$

Symmetric

Ft^3/Rad

M = 0.75 a.c. 0.24c

$$\begin{bmatrix} 17.66 & 5.740 & 0.8856 & 0 & 0 & 0 \\ 12.90 & 30.18 & 8.356 & 0 & 0 & 0 \\ 7.656 & 17.35 & 27.69 & 0 & 0 & 0 \\ 5.167 & 10.62 & 13.72 & 0 & 0 & 0 \\ 3.012 & 6.347 & 7.612 & 0 & 0 & 0 \\ 1.519 & 3.738 & 4.730 & 0 & 0 & 0 \end{bmatrix}$$

a.c. 0.28c

$$\begin{bmatrix} 16.44 & 5.105 & 0.6154 & 0 & 0 & 0 \\ 11.80 & 28.01 & 7.500 & 0 & 0 & 0 \\ 6.797 & 15.61 & 25.60 & 0 & 0 & 0 \\ 4.394 & 9.205 & 12.13 & 0 & 0 & 0 \\ 2.296 & 5.118 & 6.354 & 0 & 0 & 0 \\ 0.8262 & 2.576 & 3.579 & 0 & 0 & 0 \end{bmatrix}$$

M = 0.82 a.c. 0.23c

$$\begin{bmatrix} 17.49 & 7.672 & 2.477 & 0 & 0 & 0 \\ 11.57 & 28.18 & 8.525 & 0 & 0 & 0 \\ 5.618 & 15.62 & 24.54 & 0 & 0 & 0 \\ 2.673 & 8.674 & 13.09 & 0 & 0 & 0 \\ 1.048 & 4.360 & 6.570 & 0 & 0 & 0 \\ 0.8697 & 2.317 & 0.5724 & 0 & 0 & 0 \end{bmatrix}$$

a.c. 0.30c

$$\begin{bmatrix} 15.35 & 6.591 & 2.060 & 0 & 0 & 0 \\ 10.02 & 24.49 & 7.133 & 0 & 0 & 0 \\ 4.504 & 13.01 & 21.01 & 0 & 0 & 0 \\ 1.846 & 6.737 & 10.74 & 0 & 0 & 0 \\ 0.2453 & 2.793 & 4.761 & 0 & 0 & 0 \\ 0.1282 & 0.8742 & 0.9509 & 0 & 0 & 0 \end{bmatrix}$$

M = 0.90 a.c. 0.12c

$$\begin{bmatrix} 12.13 & 4.576 & 1.502 & 0 & 0 & 0 \\ 4.743 & 22.64 & 7.221 & 0 & 0 & 0 \\ 1.147 & 8.369 & 24.02 & 0 & 0 & 0 \\ 0.5014 & 2.170 & 8.434 & 0 & 0 & 0 \\ 0.2454 & 0.9234 & 1.773 & 0 & 0 & 0 \\ 0.1867 & 0.6703 & 1.200 & 0 & 0 & 0 \end{bmatrix}$$

a.c. 0.34c

$$\begin{bmatrix} 6.888 & 2.391 & 0.7815 & 0 & 0 & 0 \\ 2.660 & 14.31 & 4.530 & 0 & 0 & 0 \\ 0.4483 & 4.733 & 15.86 & 0 & 0 & 0 \\ 0.01288 & 0.5954 & 4.579 & 0 & 0 & 0 \\ \bar{0}.1065 & \bar{0}.1909 & \bar{0}.2798 & 0 & 0 & 0 \\ \bar{0}.1283 & \bar{0}.1485 & \bar{0}.2489 & 0 & 0 & 0 \end{bmatrix}$$

M = 0.98 a.c. 0.15c

$$\begin{bmatrix} 11.61 & 4.956 & 1.820 & 0 & 0 & 0 \\ 3.754 & 23.12 & 8.481 & 0 & 0 & 0 \\ 0.7430 & 8.182 & 27.27 & 0 & 0 & 0 \\ 0.3551 & 2.058 & 8.674 & 0 & 0 & 0 \\ 0.1507 & 0.7763 & 2.689 & 0 & 0 & 0 \\ 0.1054 & 0.5521 & 1.555 & 0 & 0 & 0 \end{bmatrix}$$

a.c. 0.37c

$$\begin{bmatrix} 6.104 & 2.539 & 0.9455 & 0 & 0 & 0 \\ 1.850 & 14.43 & 5.321 & 0 & 0 & 0 \\ 0.2303 & 4.639 & 18.70 & 0 & 0 & 0 \\ 0.02947 & 0.5376 & 4.438 & 0 & 0 & 0 \\ \bar{0}.08393 & \bar{0}.1621 & 0.3434 & 0 & 0 & 0 \\ \bar{0}.08359 & \bar{0}.2038 & \bar{0}.1461 & 0 & 0 & 0 \end{bmatrix}$$

Figure 30 $C_{M_\beta}\left[{}_Q M_\beta\right]$

Antisymmetric

Ft^3/Rad

M = 0.75 a.c. 0.24c

$$\begin{bmatrix} 13.97 & 4.902 & 0.5633 & 0 & 0 & 0 \\ 10.04 & 24.05 & 6.206 & 0 & 0 & 0 \\ 5.511 & 14.38 & 20.86 & 0 & 0 & 0 \\ 3.014 & 7.049 & 9.679 & 0 & 0 & 0 \\ 1.273 & 3.103 & 3.985 & 0 & 0 & 0 \\ 0.3832 & 1.103 & 1.503 & 0 & 0 & 0 \end{bmatrix}$$

a.c. 0.28c

$$\begin{bmatrix} 12.92 & 4.392 & 0.5923 & 0 & 0 & 0 \\ 9.129 & 22.13 & 5.568 & 0 & 0 & 0 \\ 4.865 & 12.85 & 19.12 & 0 & 0 & 0 \\ 2.543 & 6.065 & 8.512 & 0 & 0 & 0 \\ 0.9627 & 2.474 & 3.303 & 0 & 0 & 0 \\ 0.2022 & 0.7411 & 1.125 & 0 & 0 & 0 \end{bmatrix}$$

M = 0.82 a.c. 0.23c

[Not Available]

a.c. 0.30c

[Not Available]

M = 0.90 a.c. 0.12c

[Not Available]

a.c. 0.34c

[Not Available]

M = 0.98 a.c. 0.15c

[Not Available]

a.c. 0.37c

[Not Available]

Figure 31 $C_{M_\beta}\left[{}_Q M\beta\right]$

Antisymmetric

(Symmetric = 1.16 Antisymmetric)

M = 0.75

Ft^3/Rad

$$\begin{bmatrix} \bar{1}.81188 & & & & & \\ & 0.260077 & & & & \\ & & 0.188912 & & & \\ & & & 0 & & \\ & & & & 0 & \\ & & & & & 0 \end{bmatrix}$$

M = 0.82

$$\begin{bmatrix} \bar{1}.77147 & & & & & \\ & 0.323382 & & & & \\ & & 0.266596 & & & \\ & & & 0 & & \\ & & & & 0 & \\ & & & & & 0 \end{bmatrix}$$

M = 0.90

$$\begin{bmatrix} \bar{2}.30996 & & & & & \\ \bar{1}.23298 & & & & & \\ & 0 & & & & \\ & 0.927943 & & & & \\ & & 0 & & & \\ & & 0.941029 & & & \\ & & & 0 & & \\ & & & & 0 & \\ & & & & & 0 \end{bmatrix}$$

M = 0.98

$$\begin{bmatrix} \bar{2}.84845 & & & & & \\ \bar{0}.694493 & & & & & \\ & 0 & & & & \\ & 1.51140 & & & & \\ & & 0 & & & \\ & & 1.68606 & & & \\ & & & 0 & & \\ & & & & 0 & \\ & & & & & 0 \end{bmatrix}$$

Figure 32 $C_{H_\alpha}\left[{}_Q H\alpha\right]$

Antisymmetric

(Symmetric = 1.16 Antisymmetric)

Ft^3/Rad

M = 0.75

$$\begin{bmatrix} 0.107604 & & & & & \\ & 2.08589 & & & & \\ & & \bar{1}.01812 & & & \\ & & & 0 & & \\ & & & & 0 & \\ & & & & & 0 \end{bmatrix}$$

M = 0.82

$$\begin{bmatrix} \bar{0}.328451 & & & & & \\ & 1.92816 & & & & \\ & & \bar{0}.964570 & & & \\ & & & 0 & & \\ & & & & 0 & \\ & & & & & 0 \end{bmatrix}$$

M = 0.90

$$\begin{bmatrix} 0 & & & & & \\ 1.39979 & & & & & \\ & 2.26684 & & & & \\ & 3.71757 & & & & \\ & & \bar{0}.674434 & & & \\ & & 0.370762 & & & \\ & & & 0 & & \\ & & & & 0 & \\ & & & & & 0 \end{bmatrix}$$

M = 0.98

$$\begin{bmatrix} 1.23862 & & & & & \\ 4.03821 & & & & & \\ & 3.68750 & & & & \\ & 7.34494 & & & & \\ & & 0.742112 & & & \\ & & 3.70938 & & & \\ & & & 0 & & \\ & & & & 0 & \\ & & & & & 0 \end{bmatrix}$$

Figure 33 $C_{H_\beta}\left[Q^{H\beta}\right]$

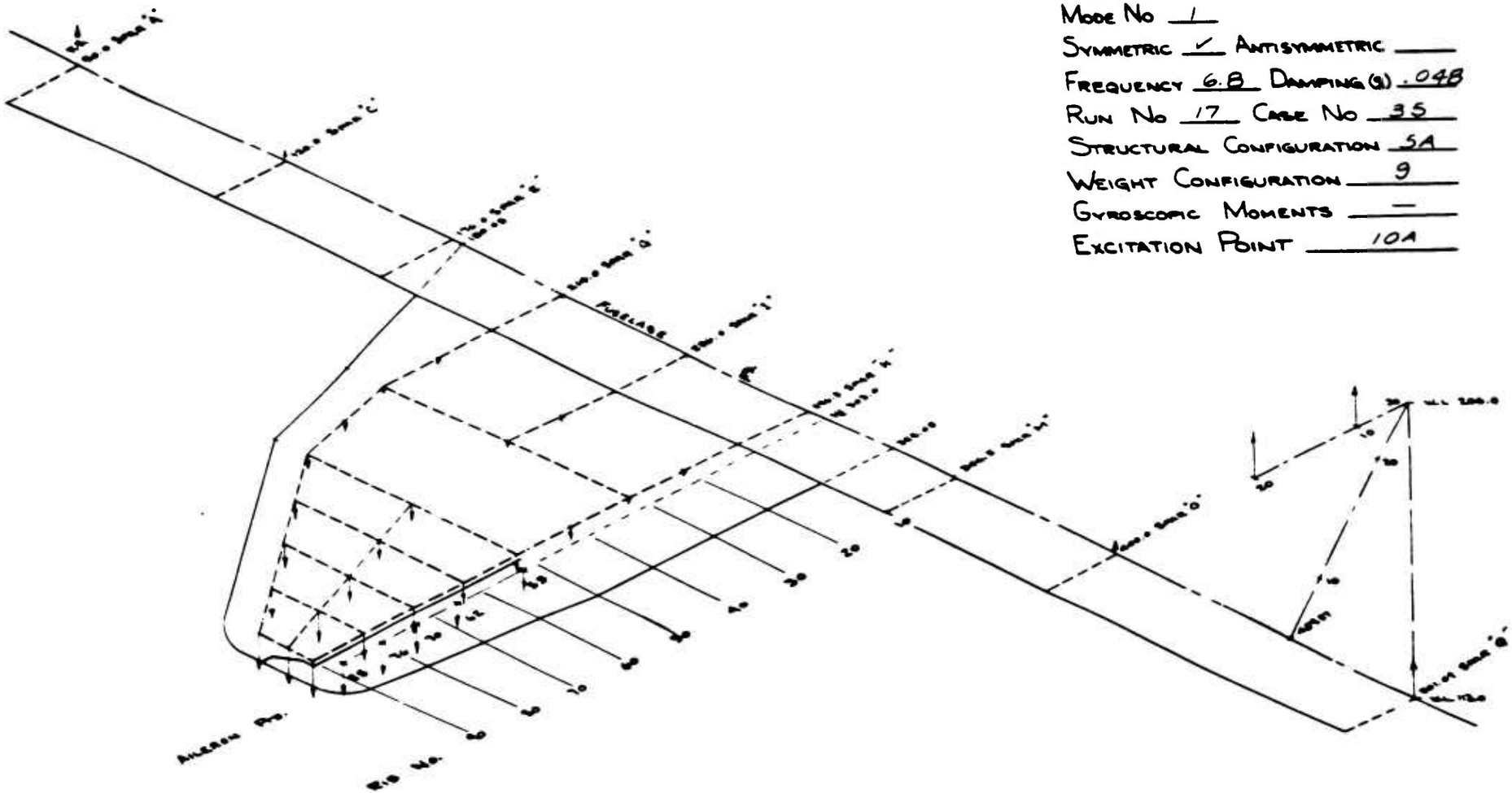

Figure 34 Symmetric Mode Shapes - Stiffness Configuration 5A - Gyroscopic Forces Out - Mode 1

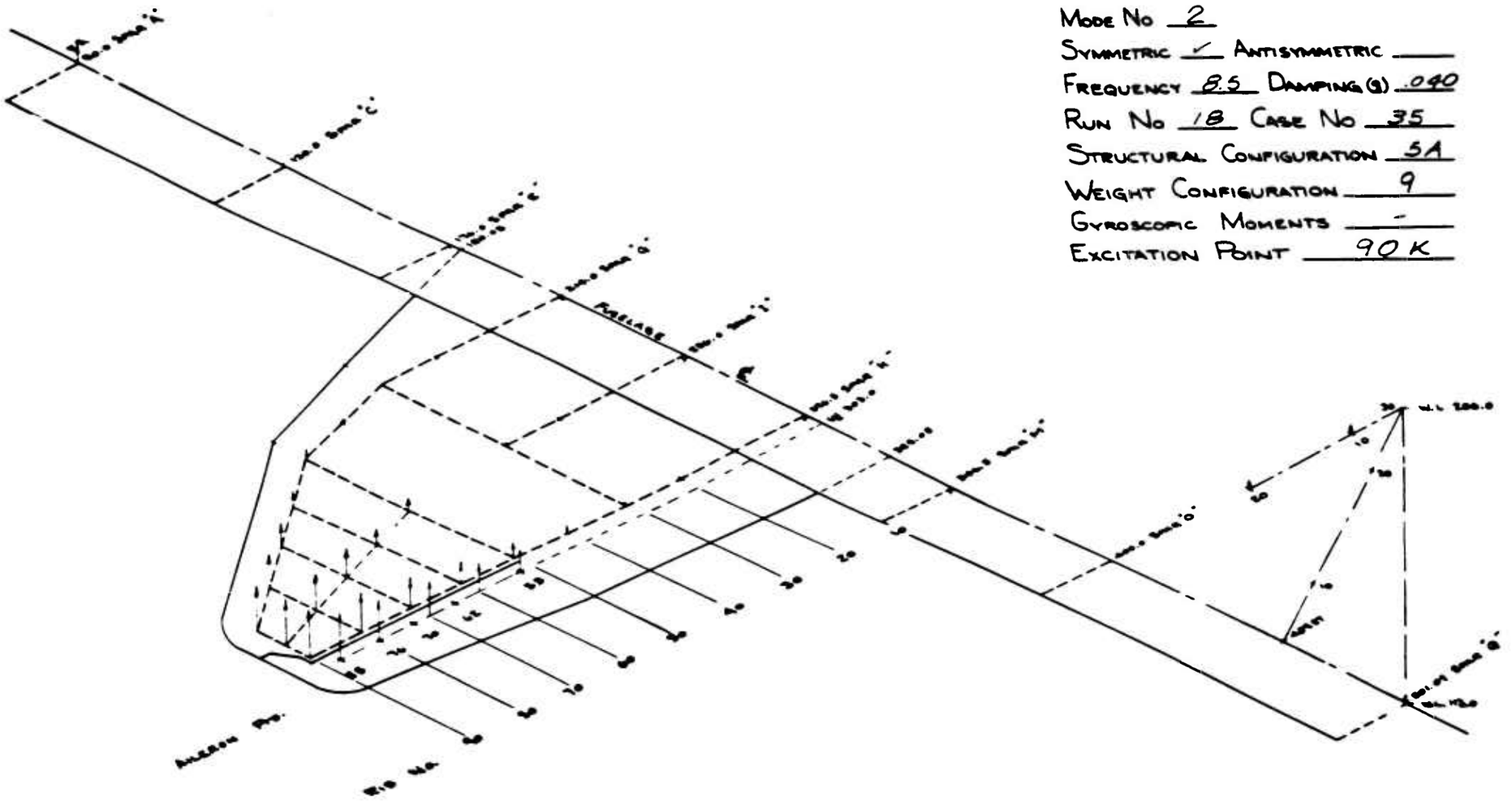

Figure 35 Symmetric Mode Shapes - Stiffness Configuration 5A - Gyroscopic Forces Out - Mode 2

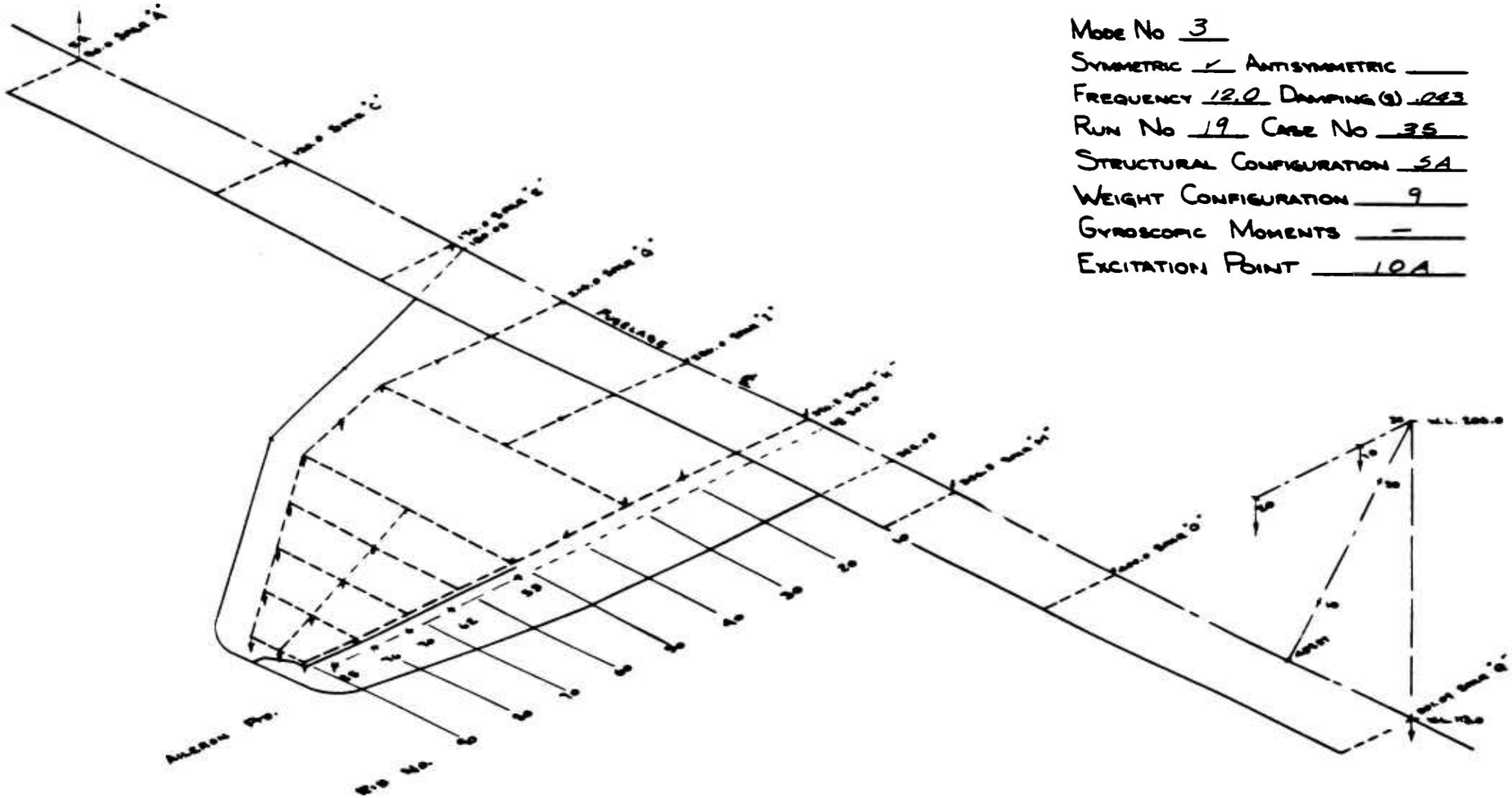

Figure 36 Symmetric Mode Shapes - Stiffness Configuration 5A - Gyroscopic Forces Out - Mode 3

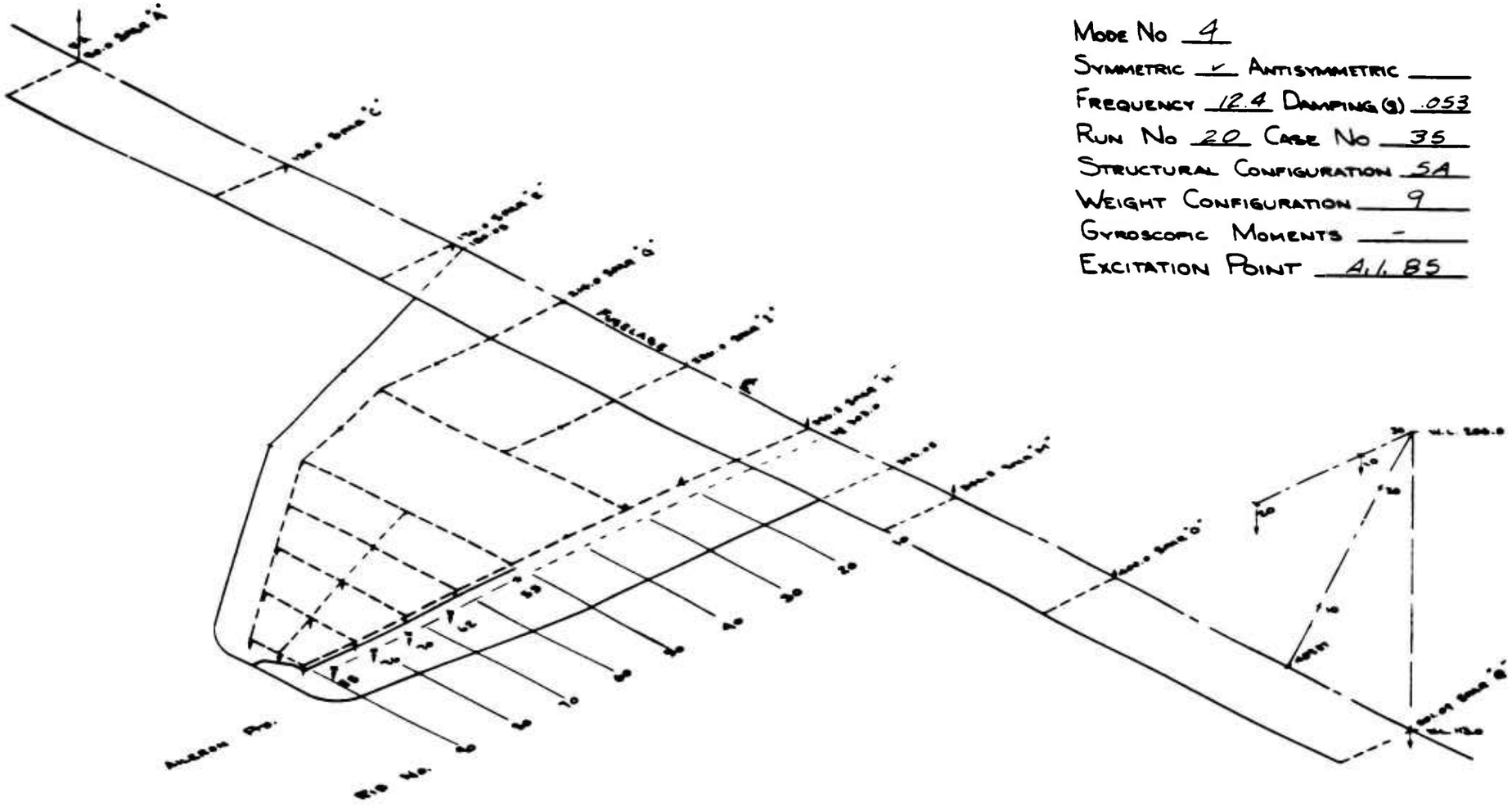

Figure 37 Symmetric Mode Shapes - Stiffness Configuration 5A - Gyroscopic Forces Out - Mode 4

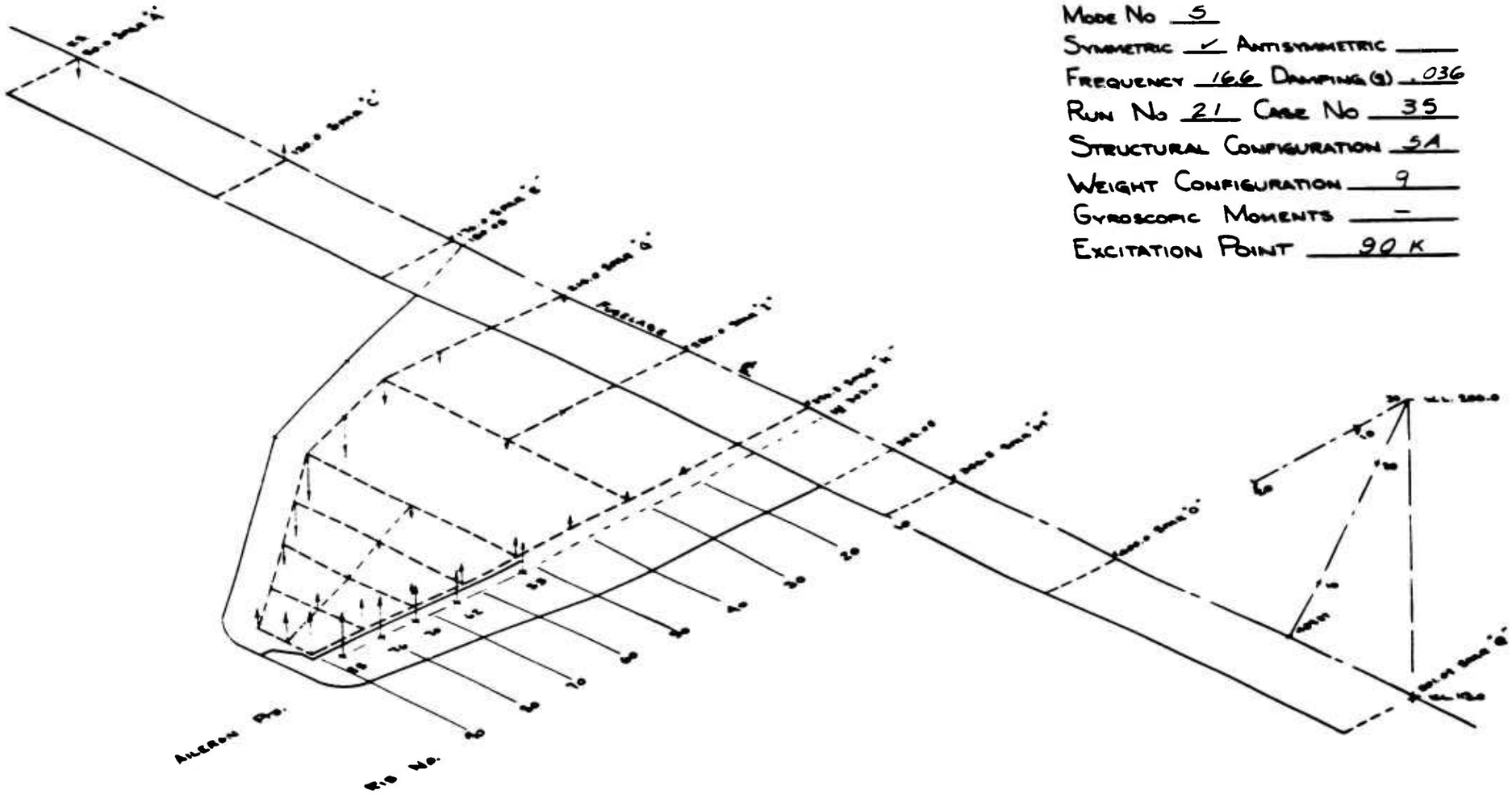

Figure 38 Symmetric Mode Shapes - Stiffness Configuration 5A - Gyroscopic Forces Out - Mode 5

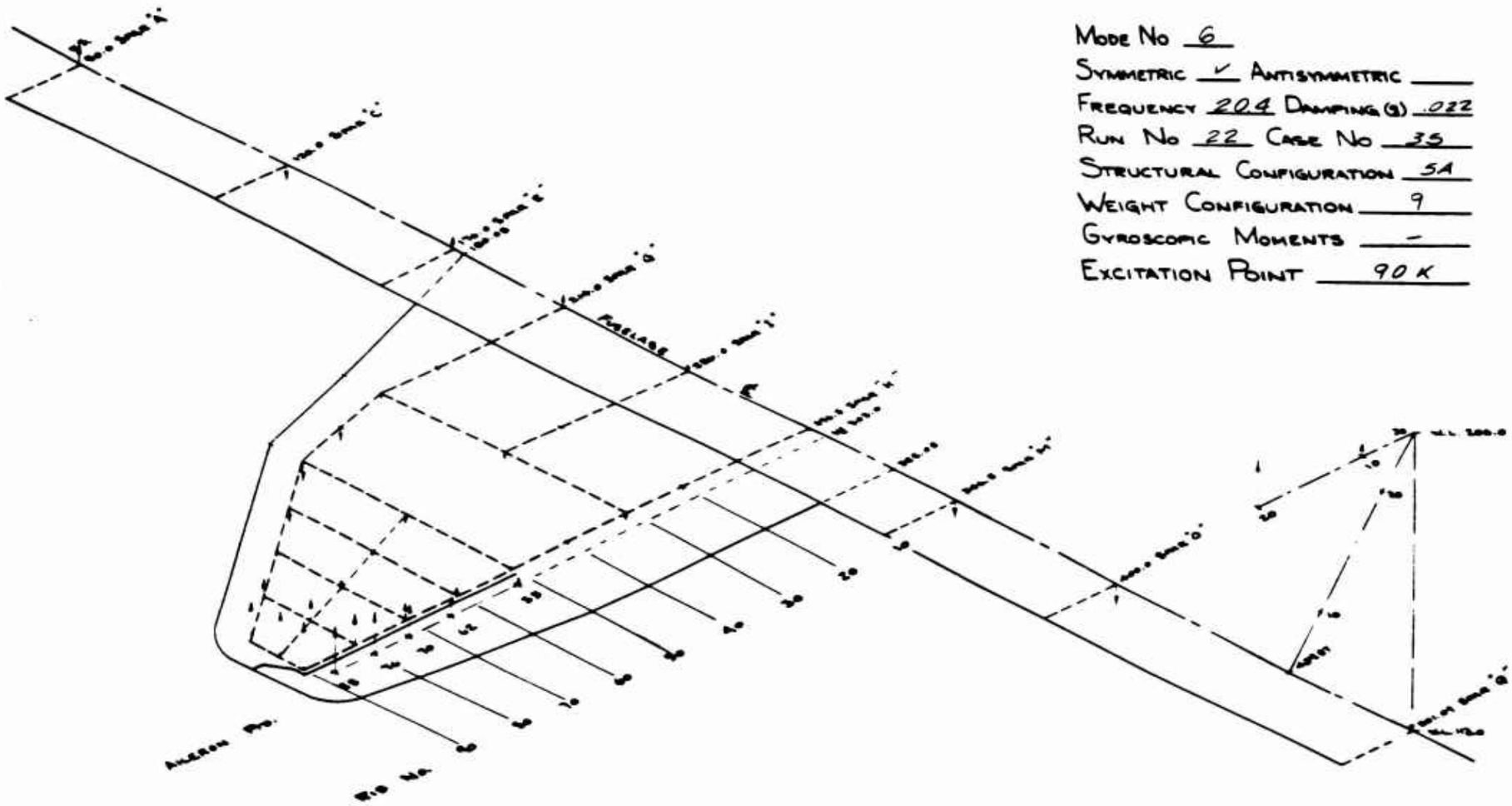

Figure 39 Symmetric Mode Shapes - Stiffness Configuration 5A - Gyroscopic Forces Out - Mode 6

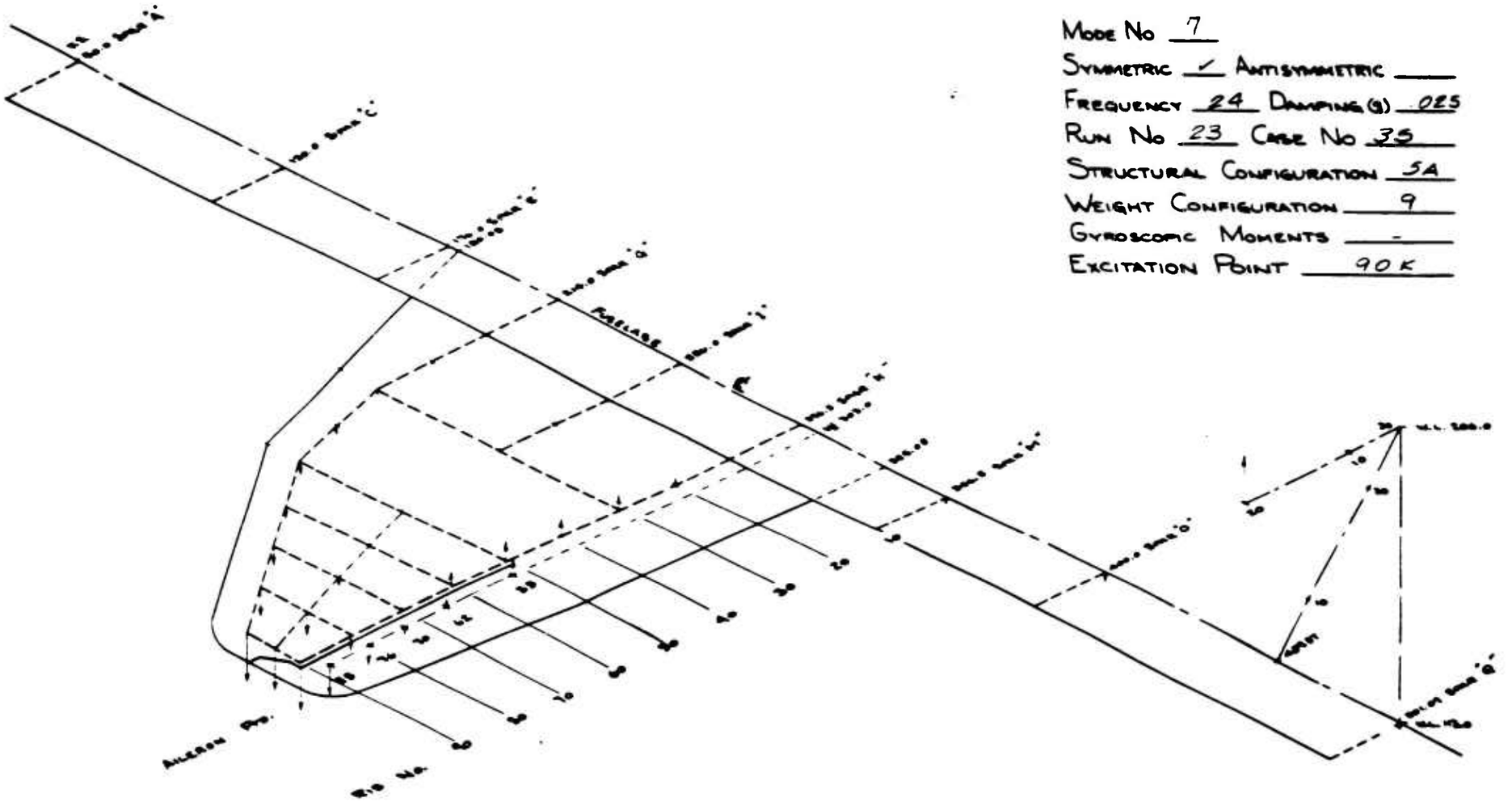

Figure 40 Symmetric Mode Shapes - Stiffness Configuration 5A - Gyroscopic Forces Out - Mode 7

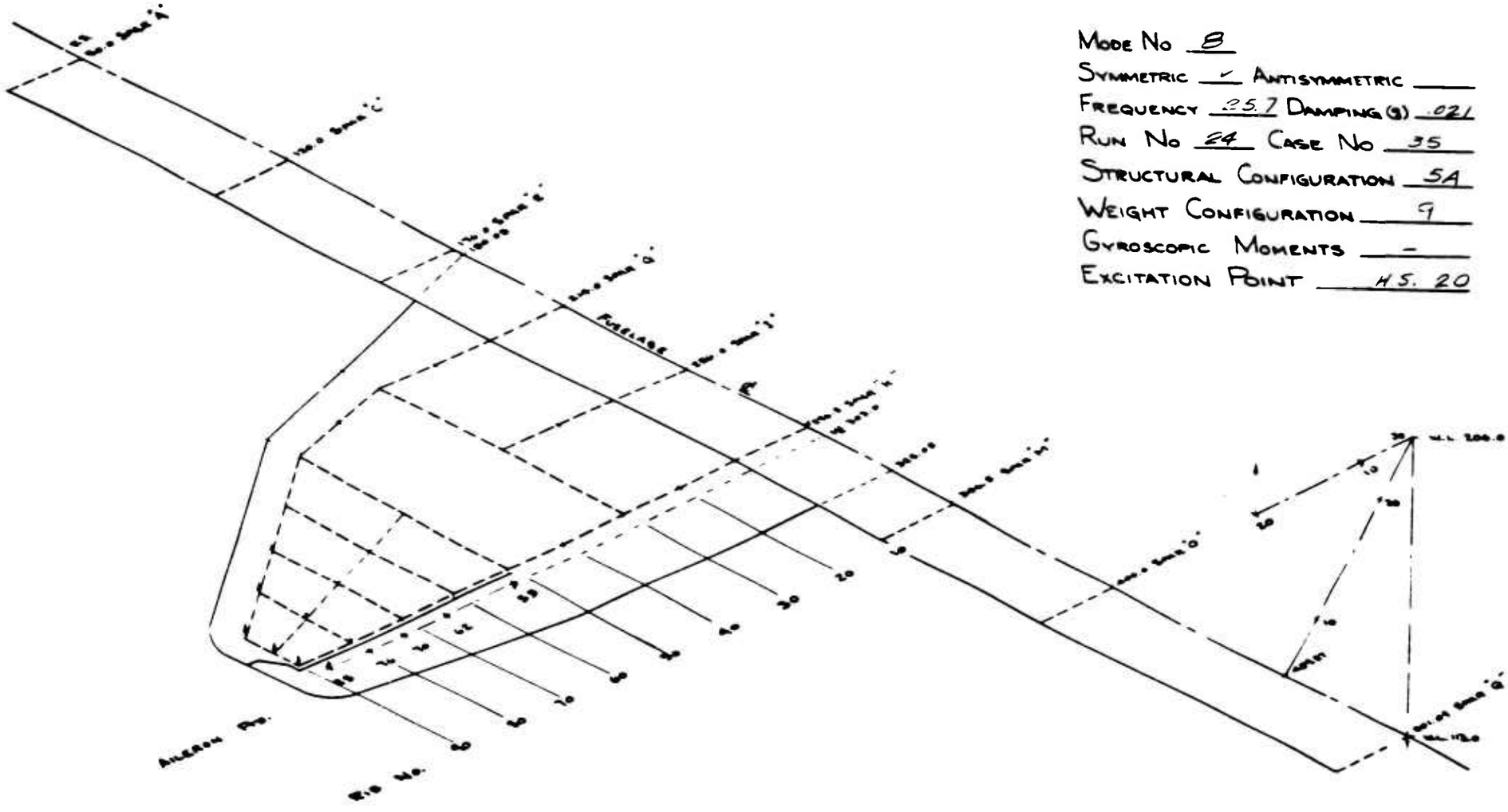

Figure 41 Symmetric Mode Shapes - Stiffness Configuration 5A - Gyroscopic Forces Out - Mode 8

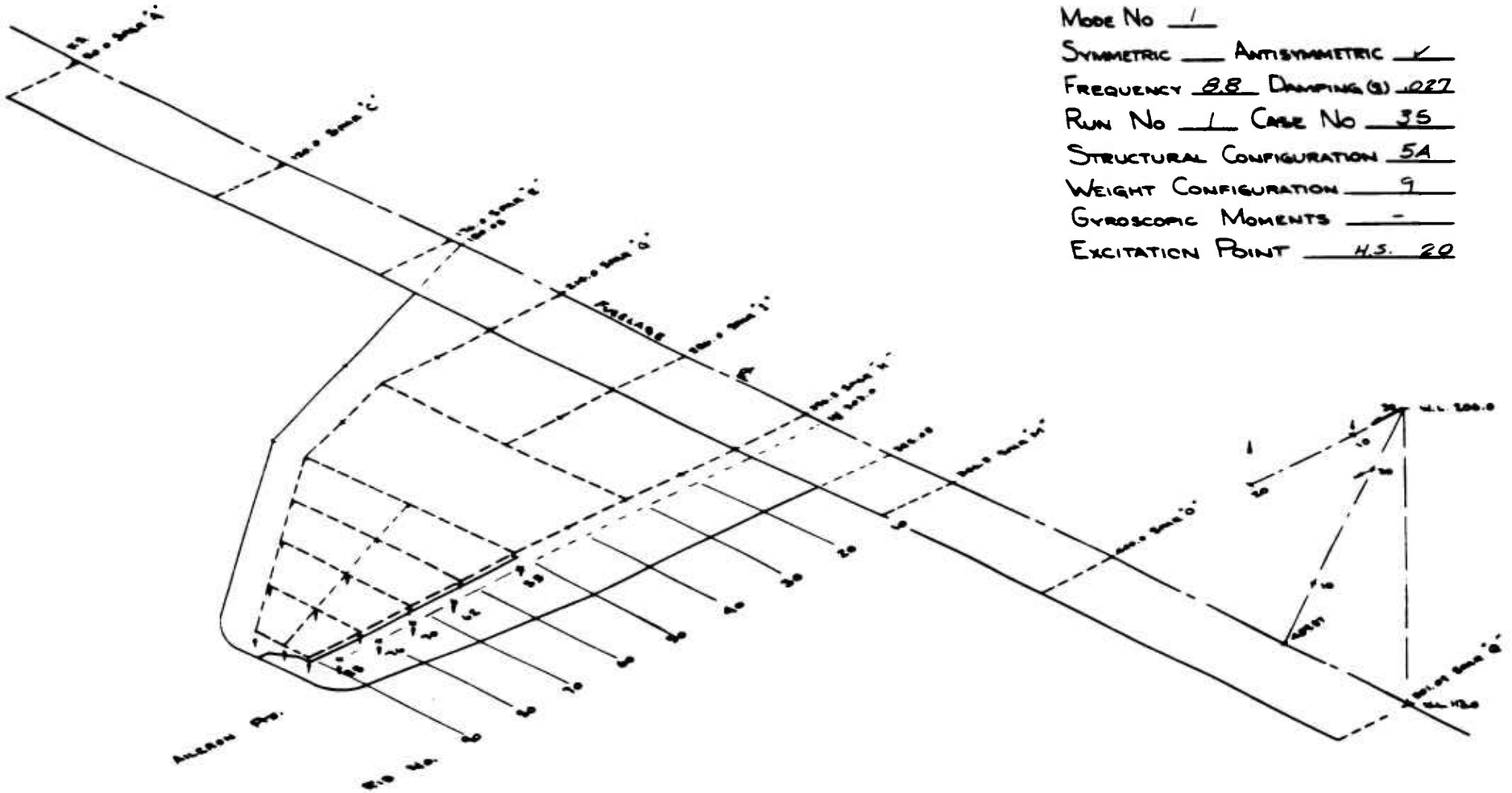

Figure 42 Antisymmetric Mode Shapes - Stiffness Configuration 5A - Gyroscopic Forces Out - Mode 1

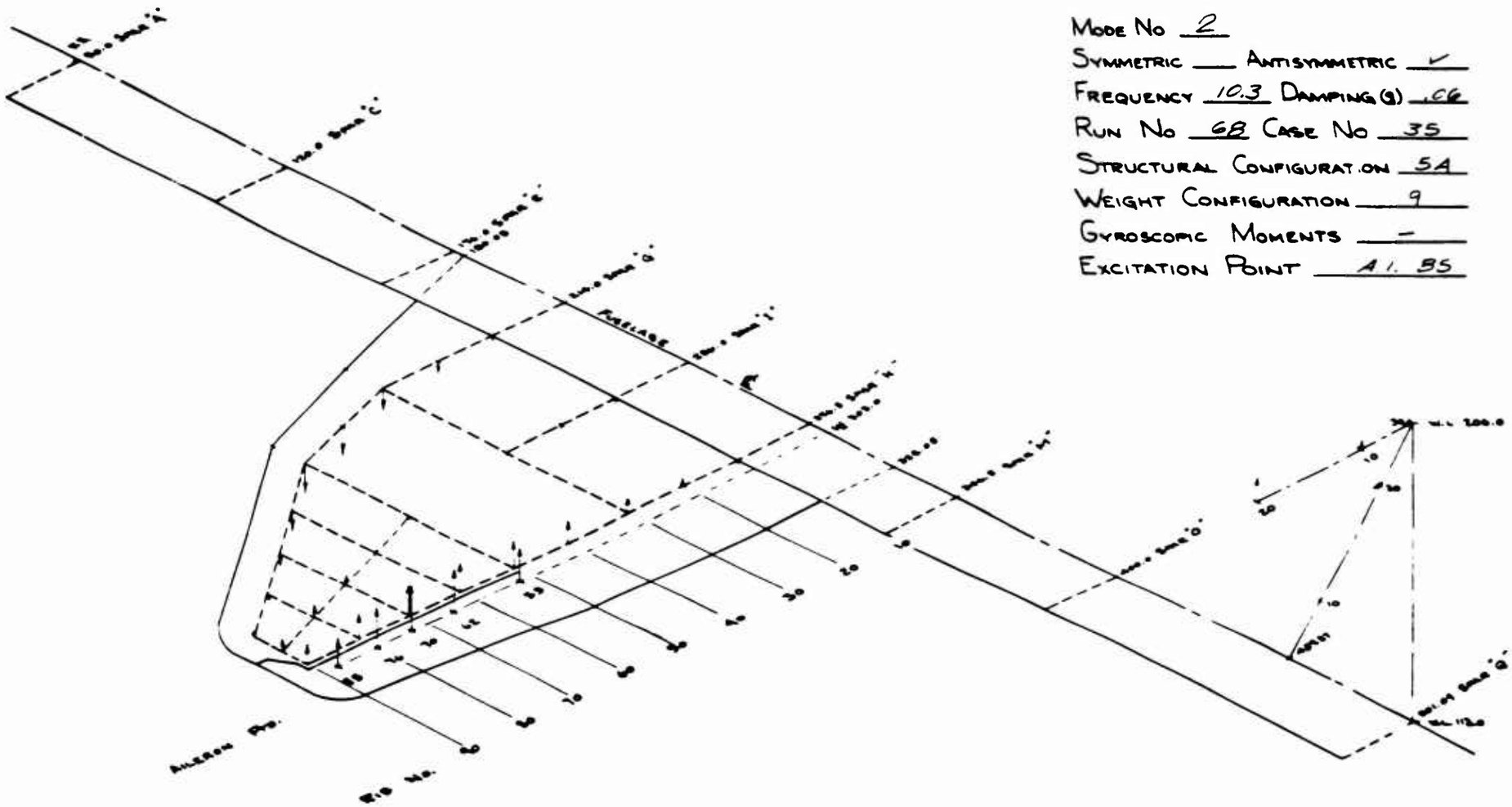

Figure 43 Antisymmetric Mode Shapes - Stiffness Configuration 5A - Gyroscopic Forces Out - Mode 2

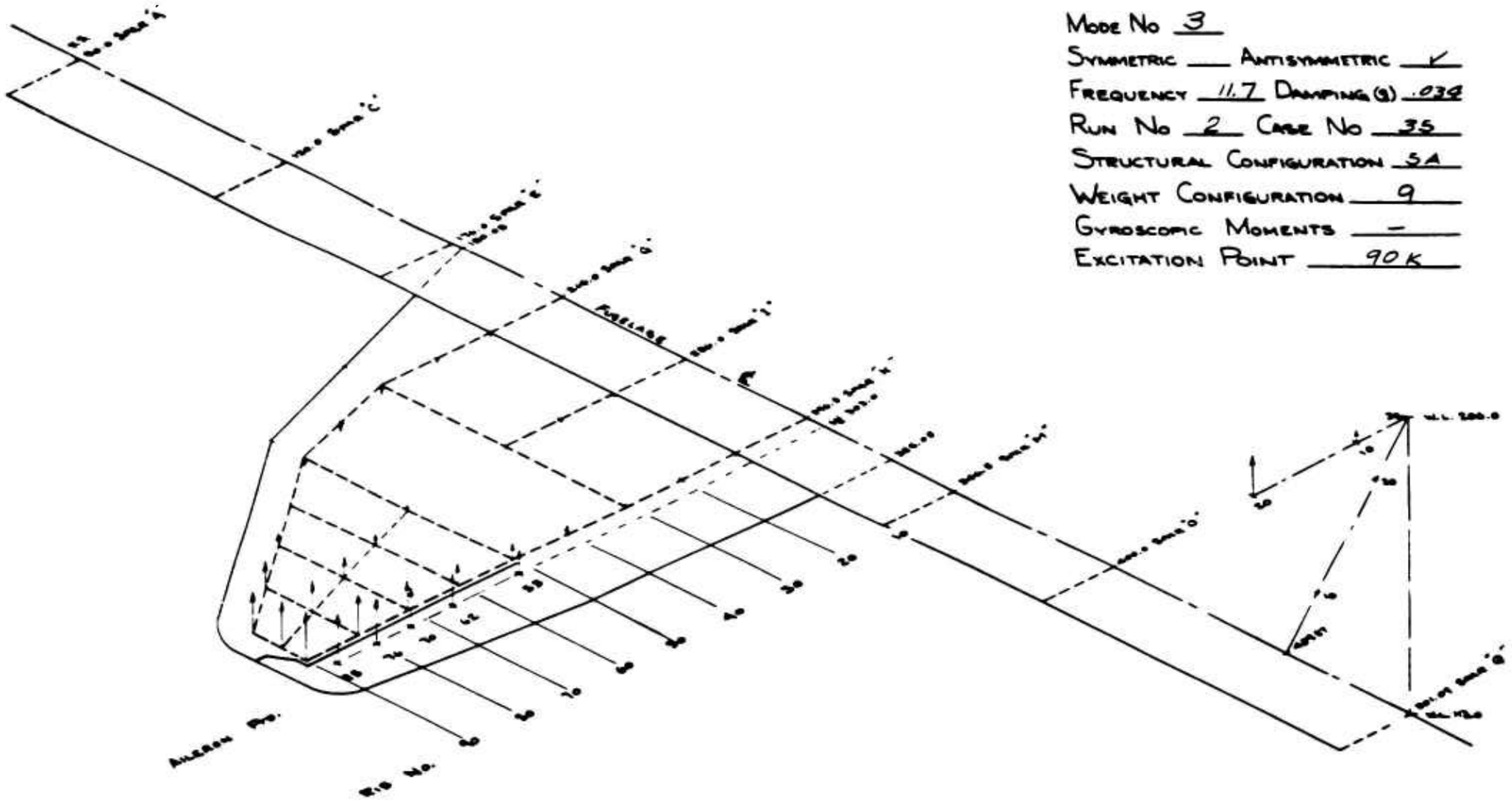

Figure 44 Antisymmetric Mode Shapes - Stiffness Configuration 5A - Gyroscopic Forces Out - Mode 3

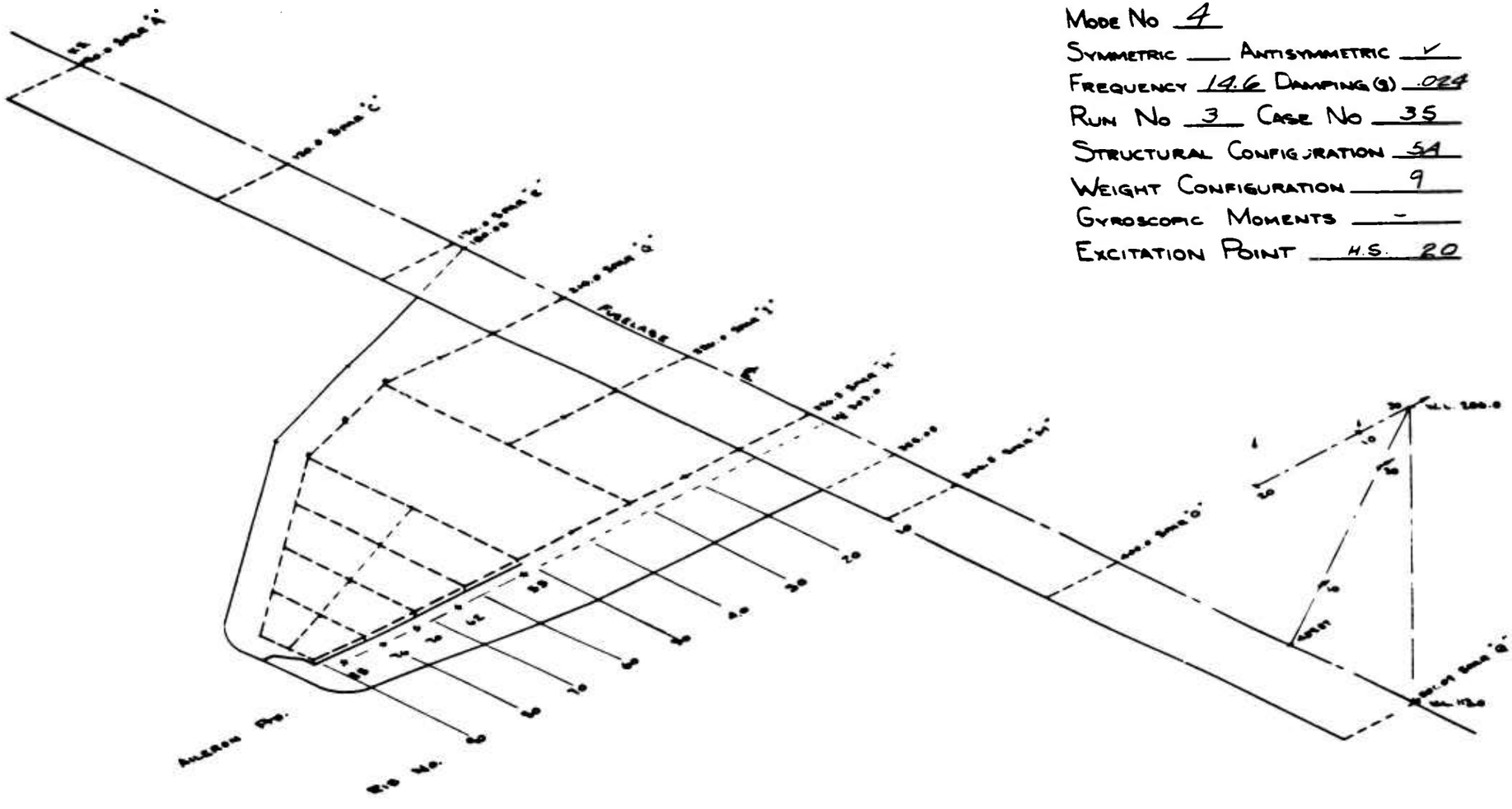

Figure 45 Antisymmetric Mode Shapes - Stiffness Configuration 5A - Gyroscopic Forces Out - Mode 4

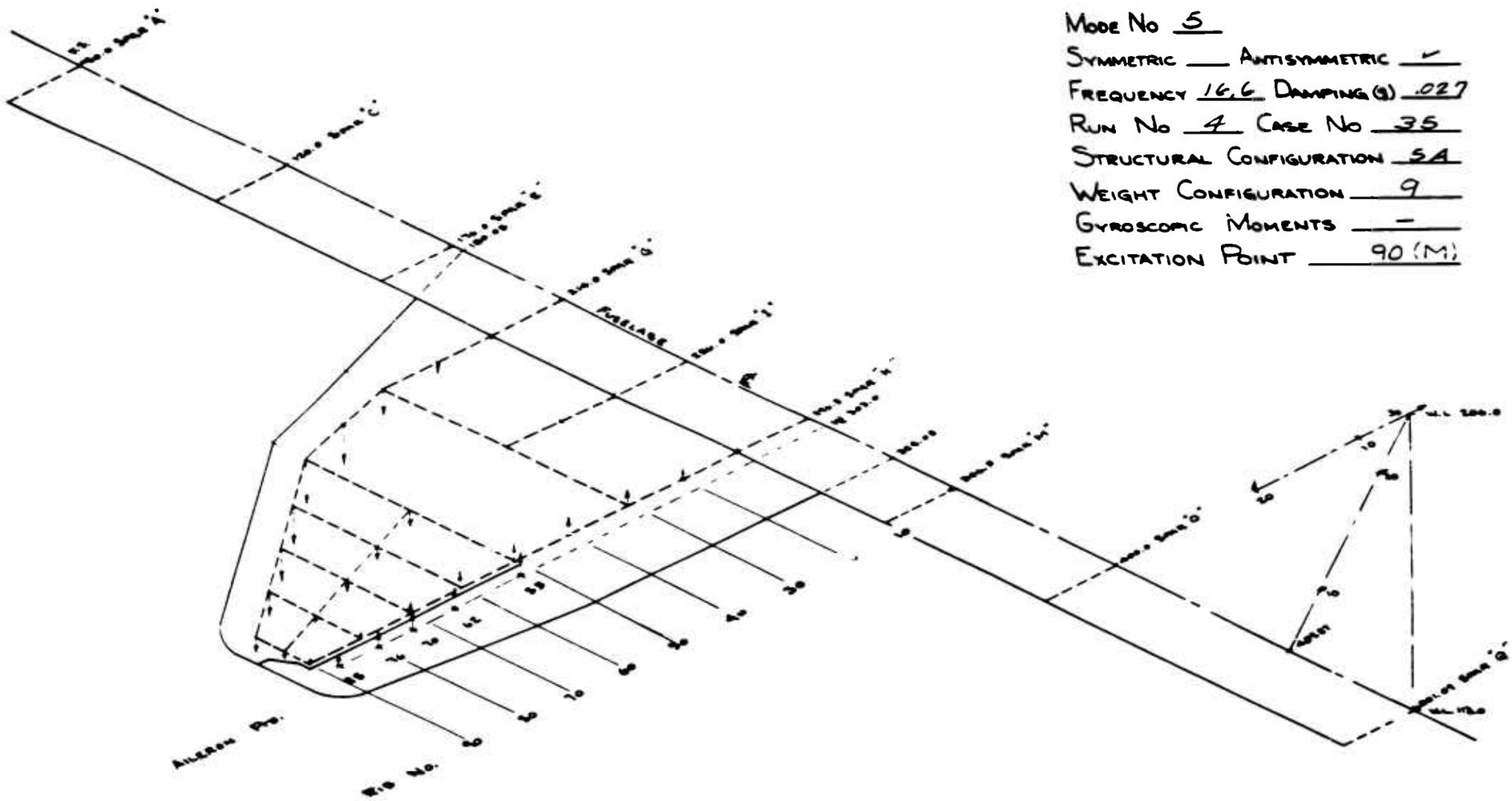

Figure 46 Antisymmetric Mode Shapes - Stiffness Configuration 5A - Gyroscopic Forces Out - Mode 5

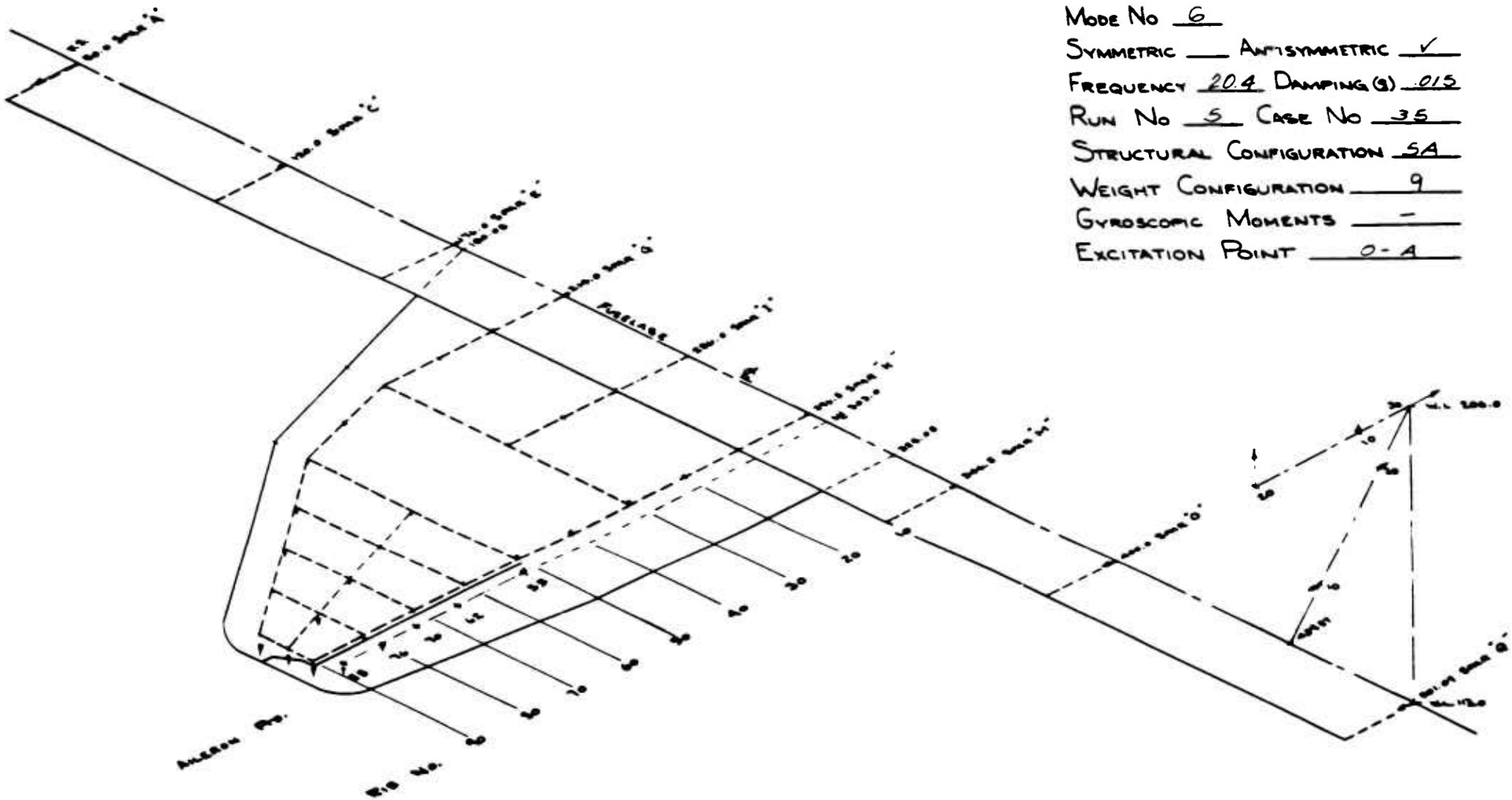

Figure 47 Antisymmetric Mode Shapes - Stiffness Configuration 5A - Gyroscopic Forces Out - Mode 6

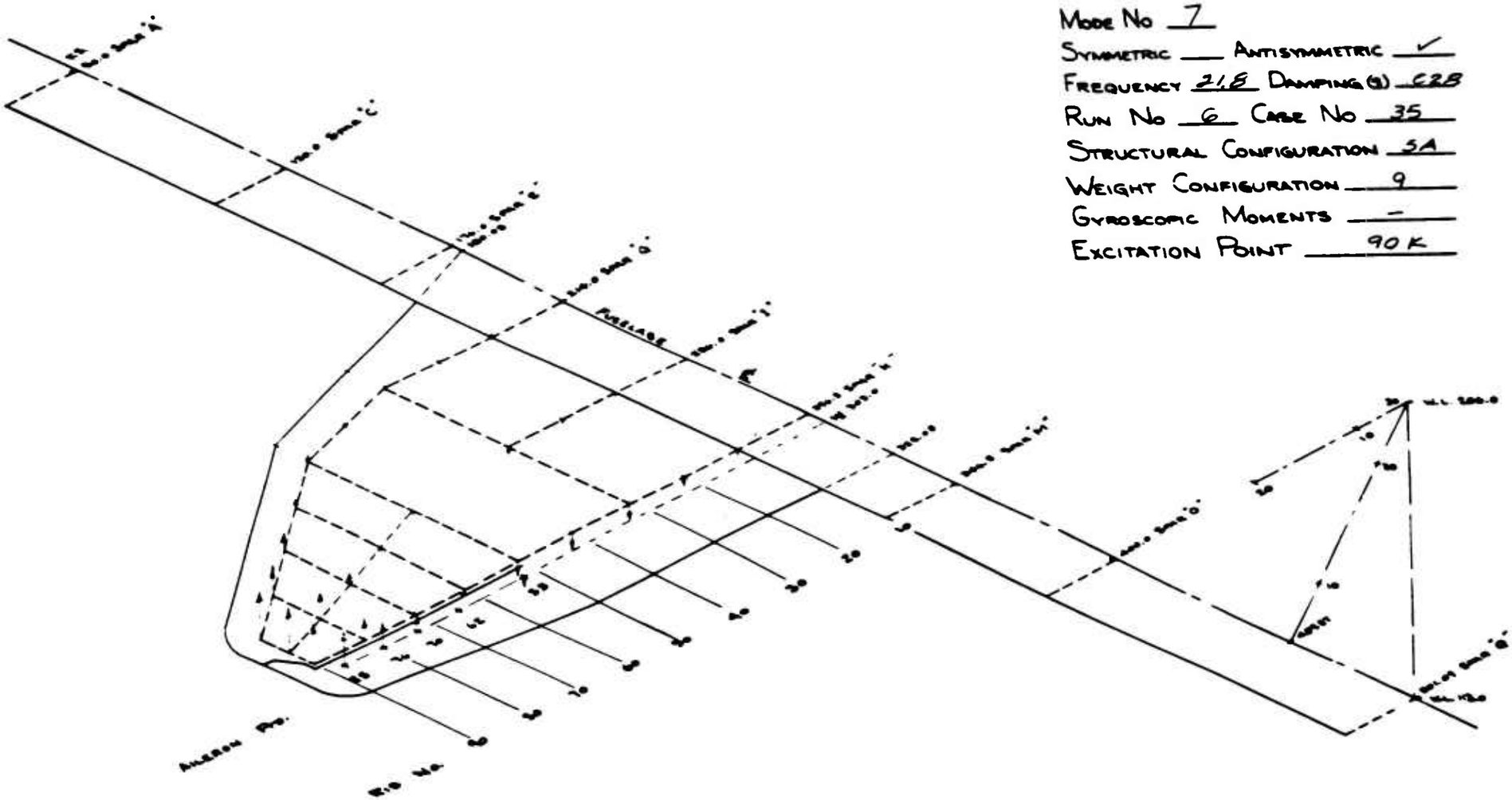

Figure 48 Antisymmetric Mode Shapes - Stiffness Configuration 5A - Gyroscopic Forces Out - Mode 7

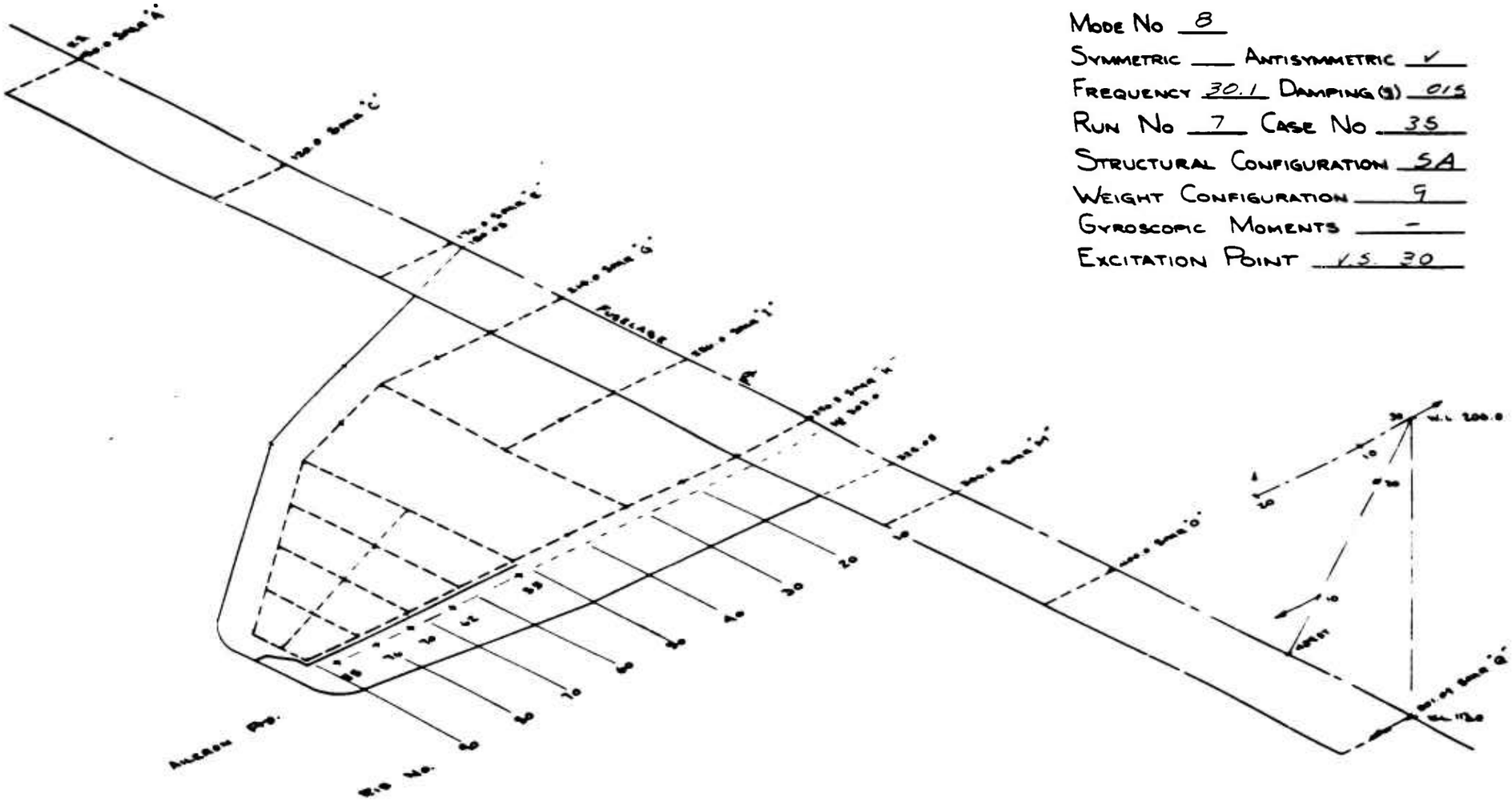

Figure 49 Antisymmetric Mode Shapes - Stiffness Configuration 5A - Gyroscopic Forces Out - Mode 8

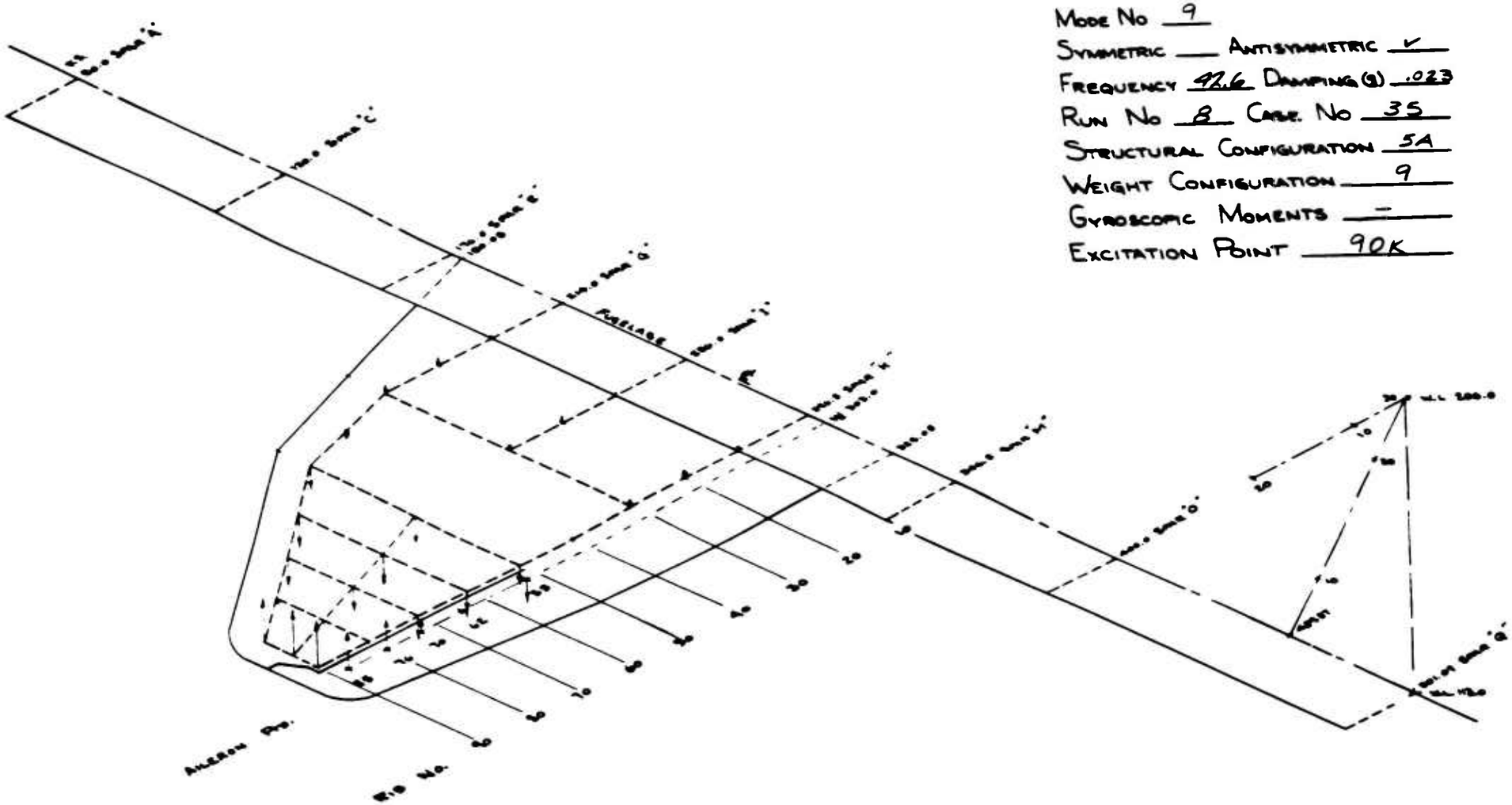

Figure 50 Antisymmetric Mode Shapes - Stiffness Configuration 5A - Gyroscopic Forces Out - Mode 9

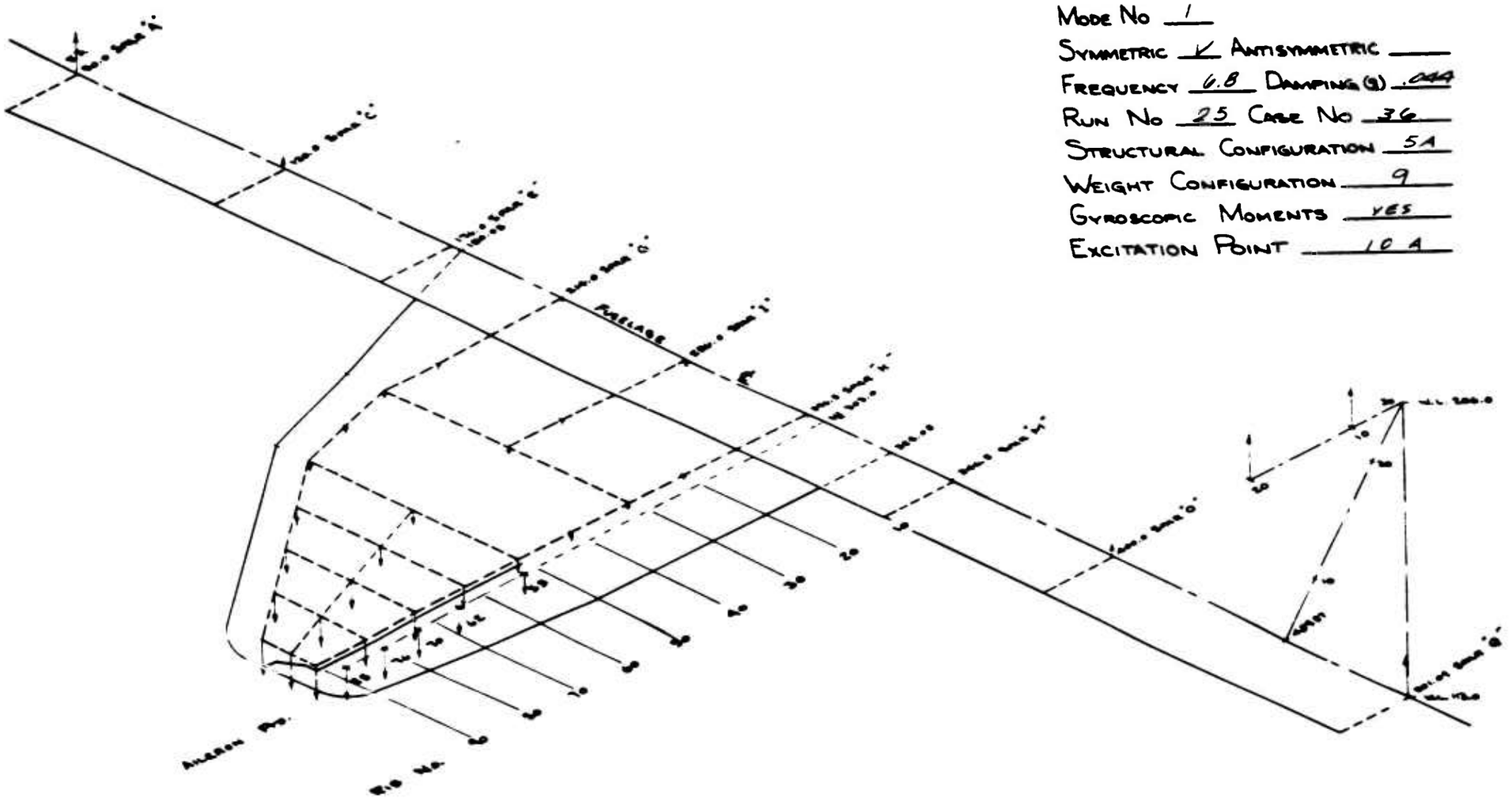

Figure 51 Symmetric Mode Shapes - Stiffness Configuration 5A - Gyroscopic Forces In - Mode 1

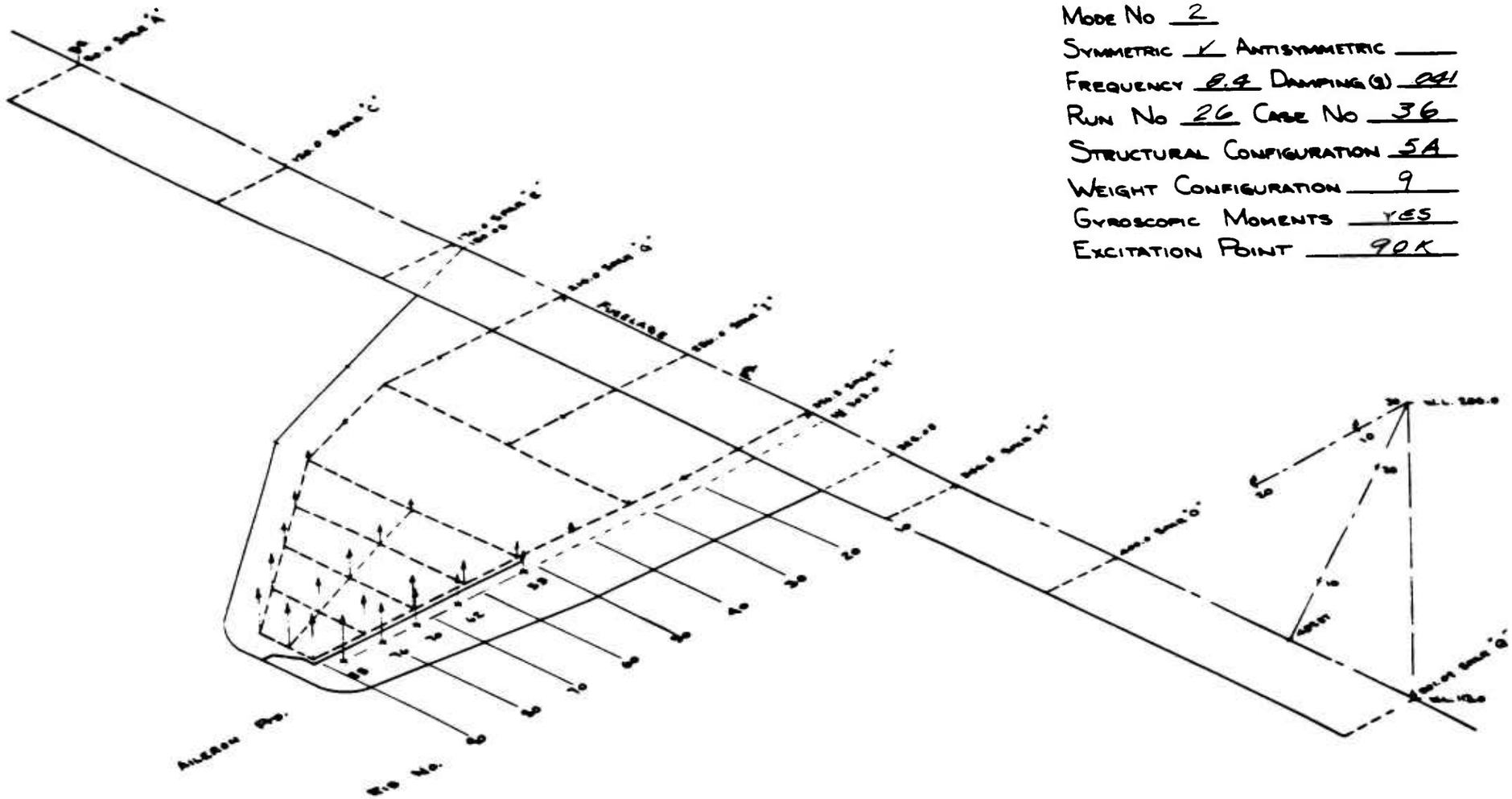

Figure 52 Symmetric Mode Shapes - Stiffness Configuration 5A - Gyroscopic Forces In - Mode 2

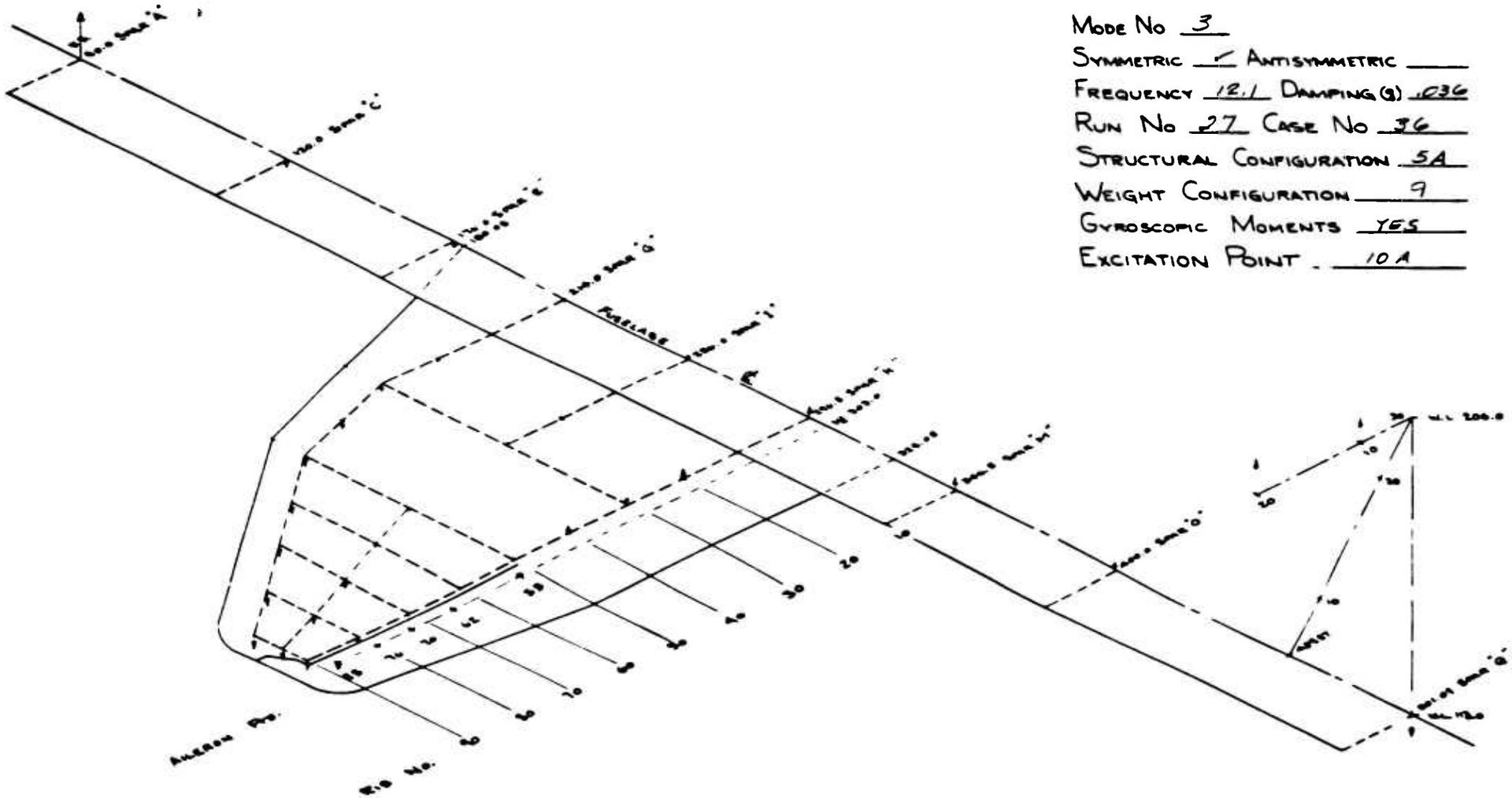

Figure 53 Symmetric Mode Shapes - Stiffness Configuration 5A - Gyroscopic Forces In - Mode 3

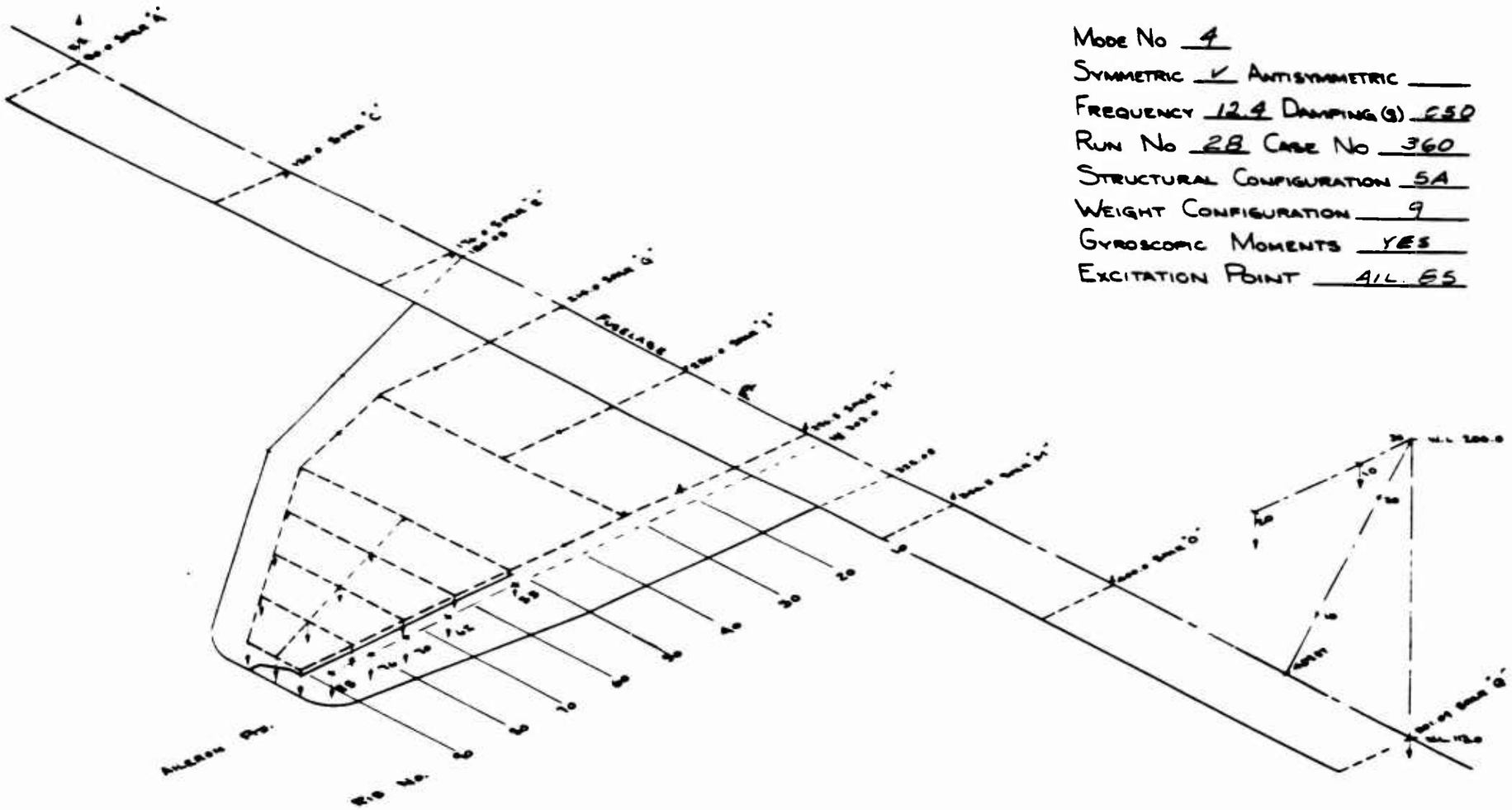

Figure 54 Symmetric Mode Shapes - Stiffness Configuration 5A - Gyroscopic Forces In - Mode 4

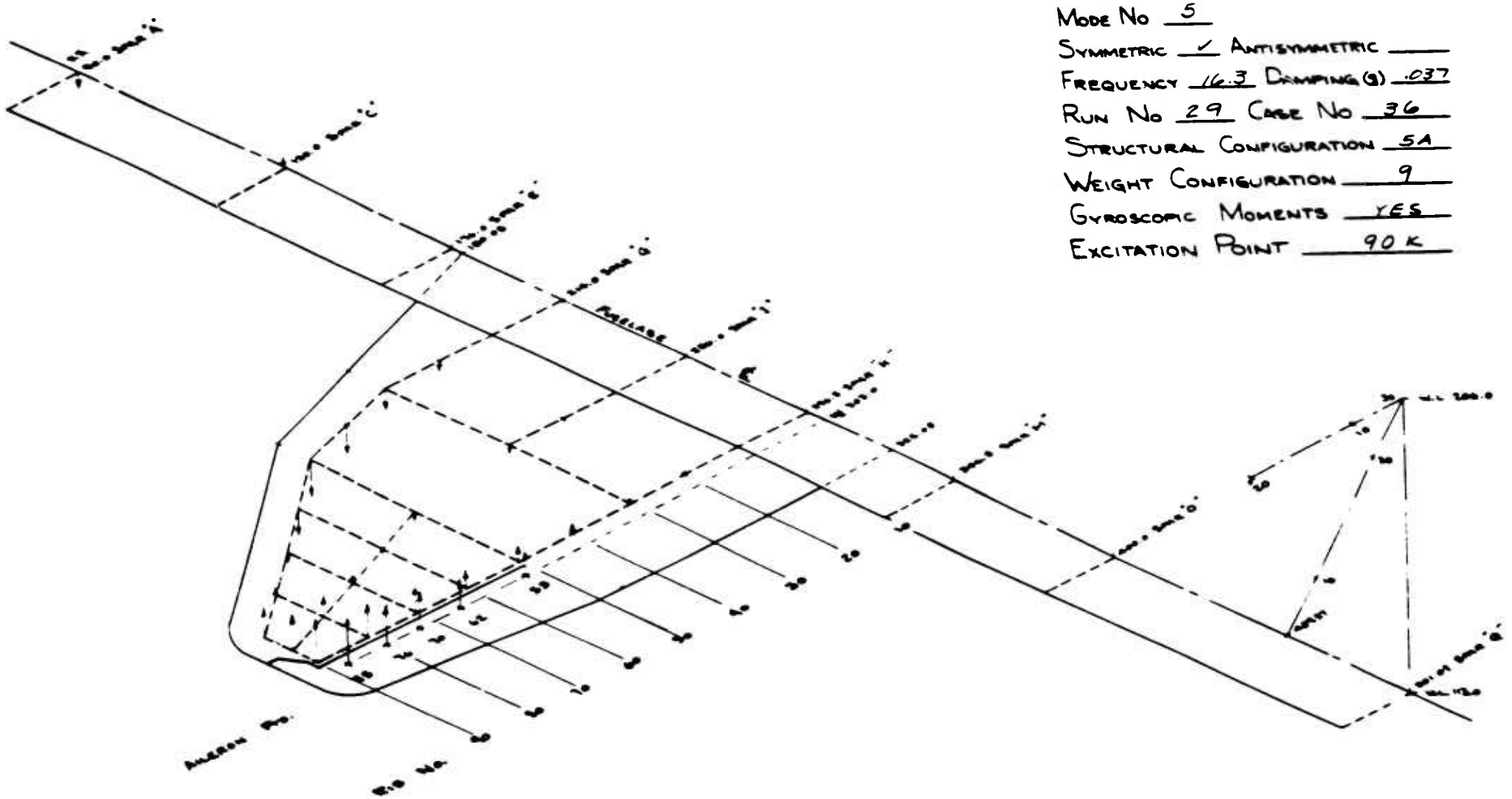

Figure 55 Symmetric Mode Shapes - Stiffness Configuration 5A - Gyroscopic Forces In - Mode 5

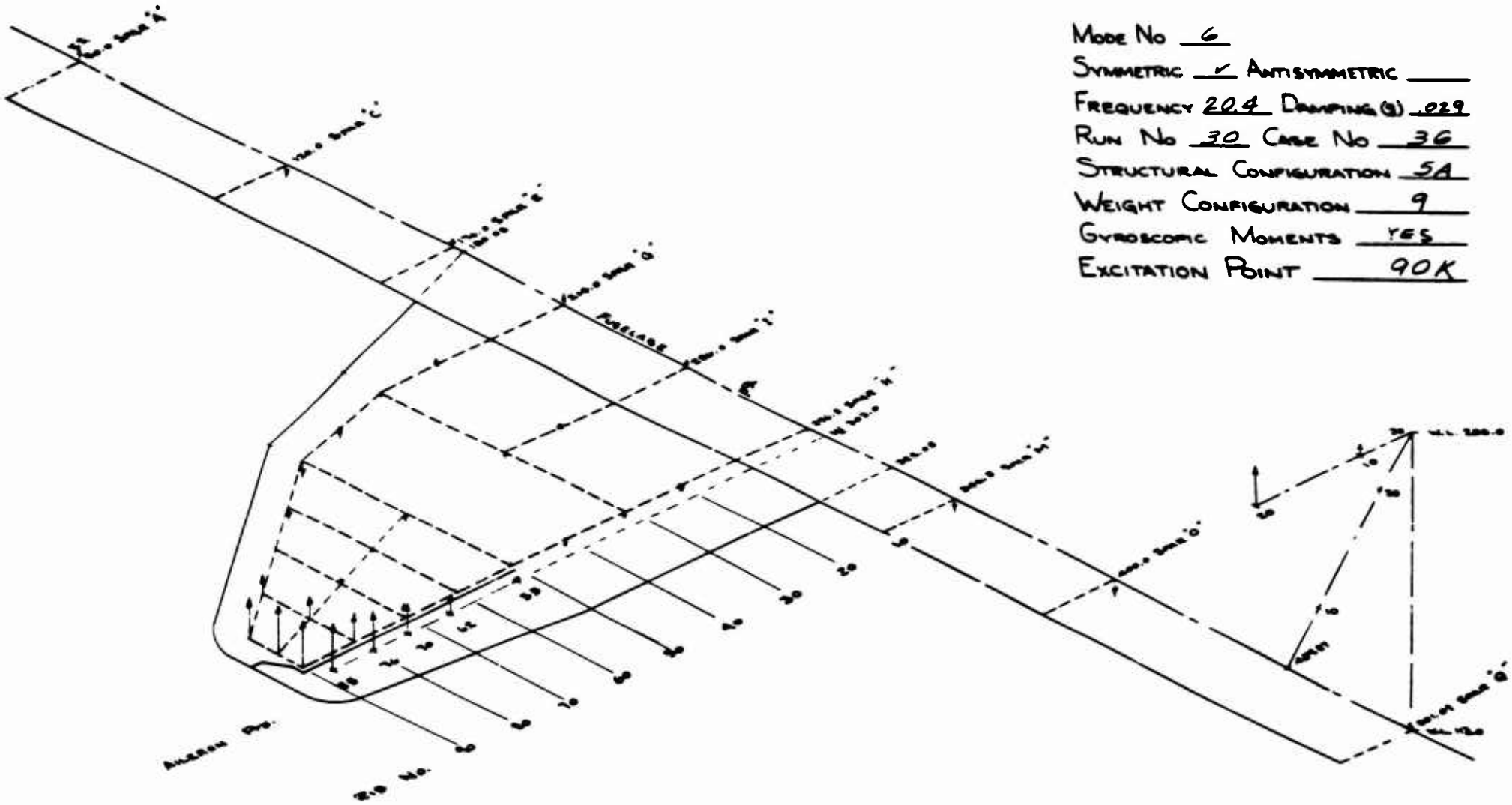

Figure 56 Symmetric Mode Shapes - Stiffness Configuration 5A - Gyroscopic Forces In - Mode 6

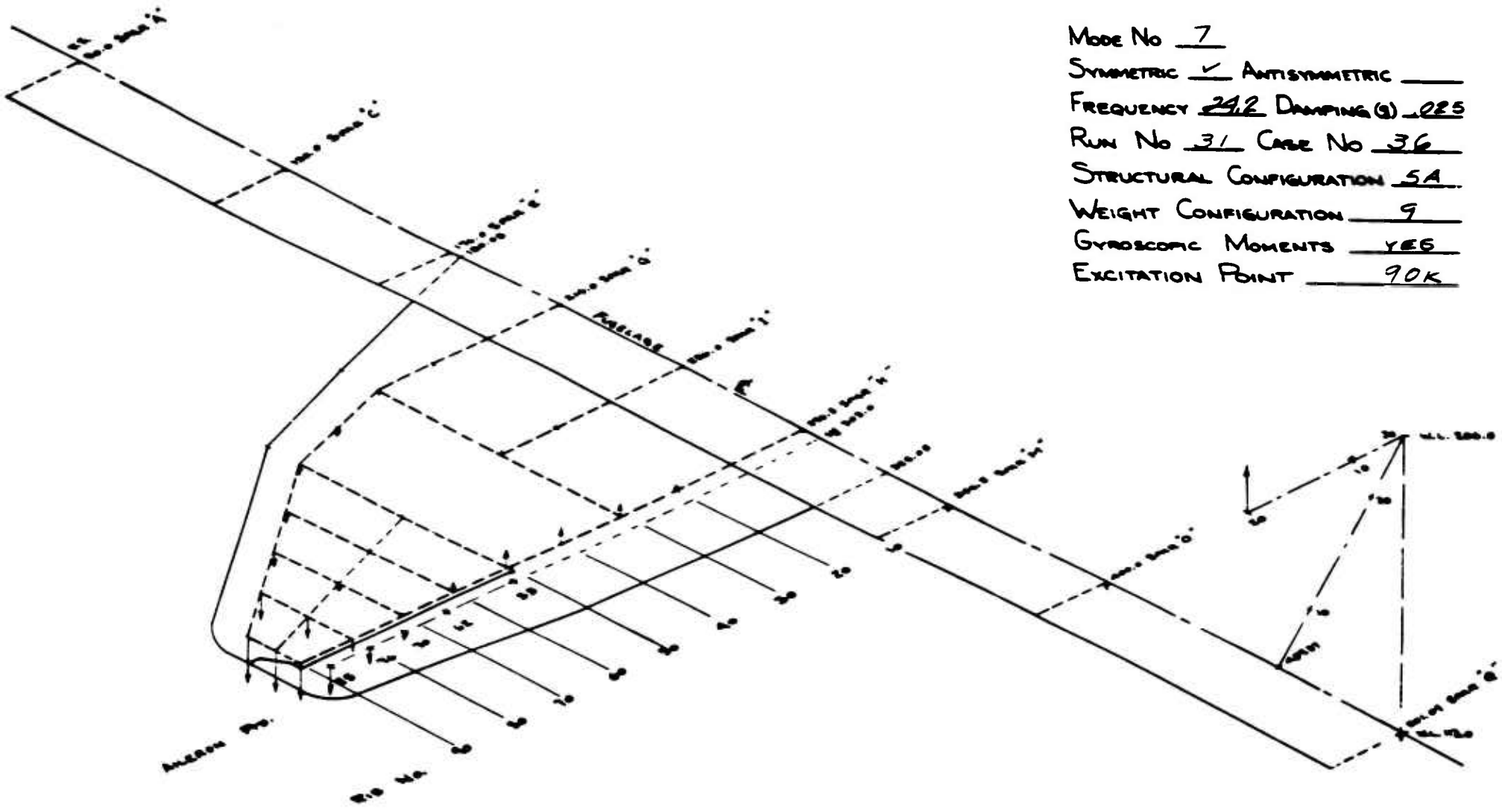

Mode No 7
Symmetric ✓ Antisymmetric ____
Frequency 24.2 Damping (g) .085
Run No 31 Case No 36
Structural Configuration 5A
Weight Configuration 9
Gyroscopic Moments YES
Excitation Point 90K

Figure 57 Symmetric Mode Shapes - Stiffness Configuration 5A - Gyroscopic Forces In - Mode 7

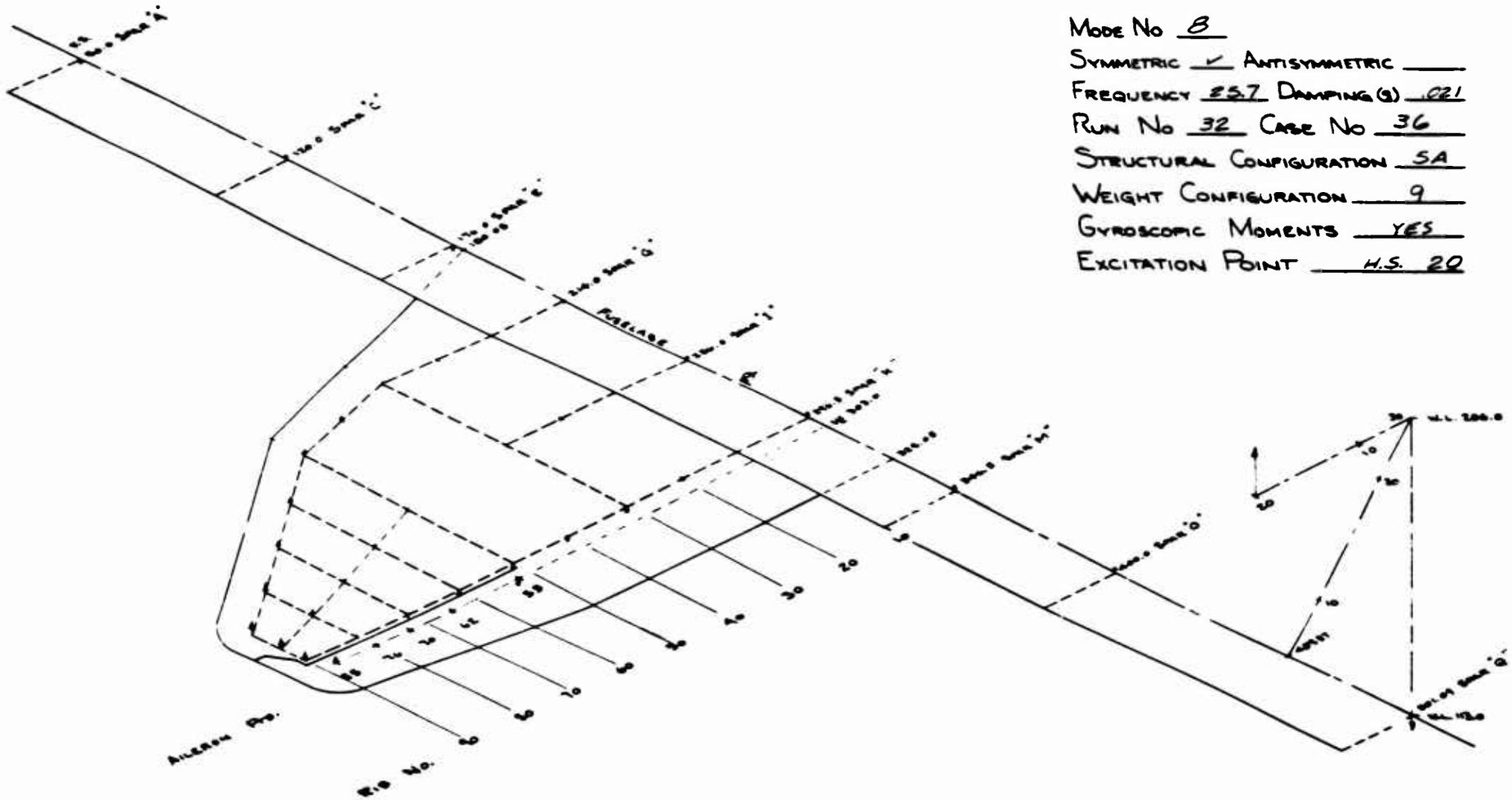

Figure 58 Symmetric Mode Shapes - Stiffness Configuration 5A - Gyroscopic Forces In - Mode 8

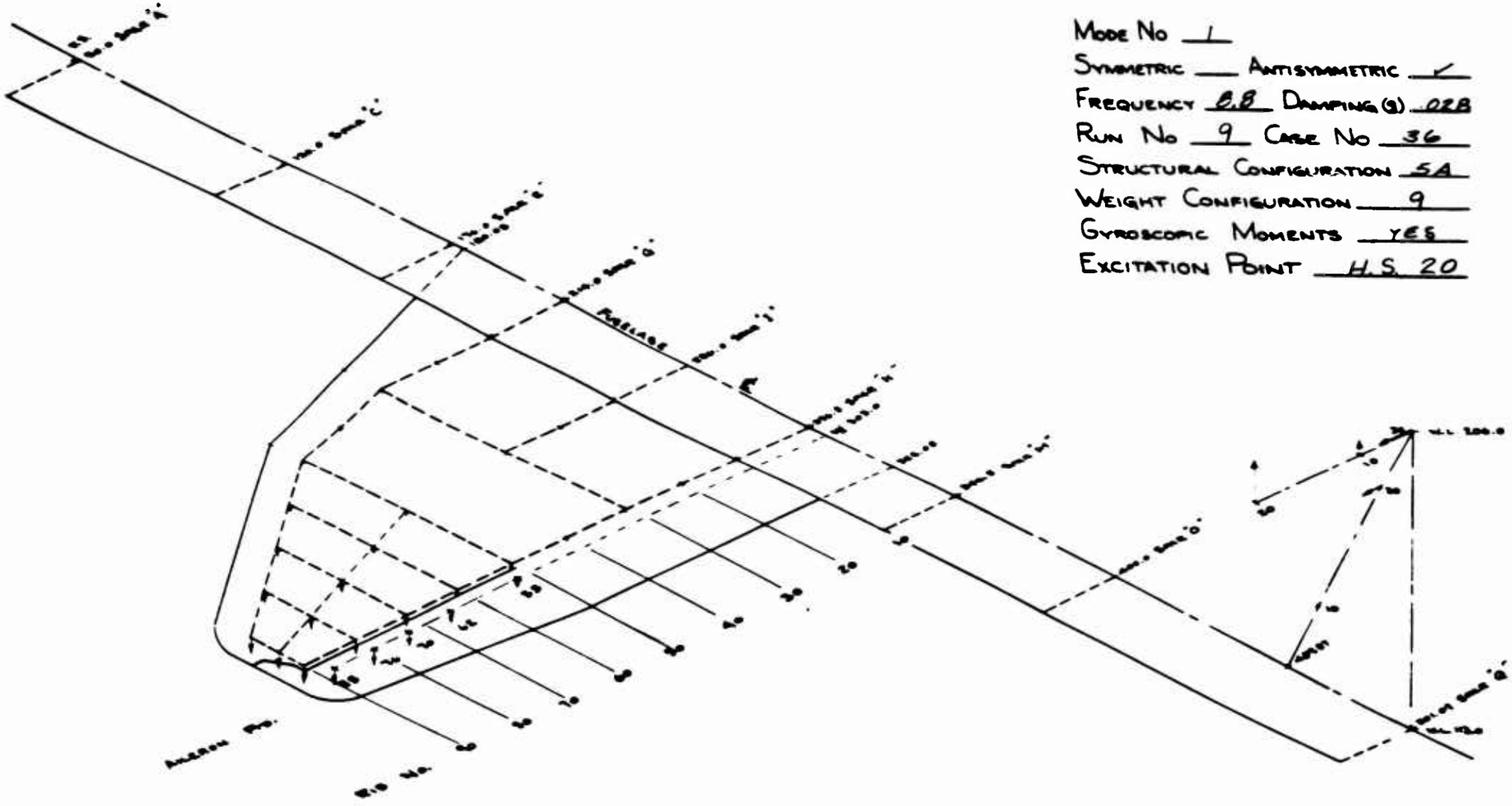

Figure 59 Antisymmetric Mode Shapes - Stiffness Configuration 5A - Gyroscopic Forces In - Mode 1

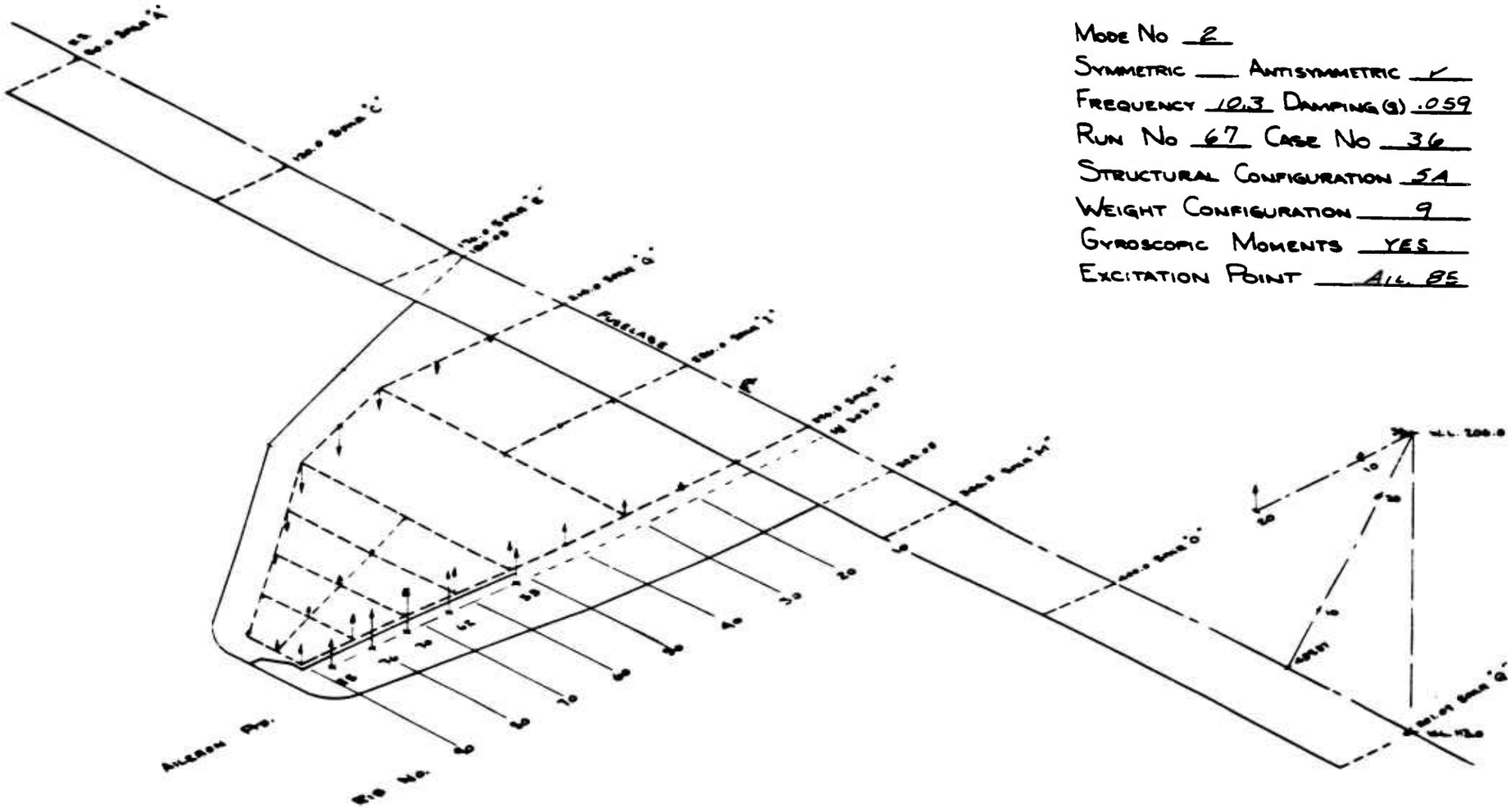

Figure 60 Antisymmetric Mode Shapes - Stiffness Configuration 5A - Gyroscopic Forces In - Mode 2

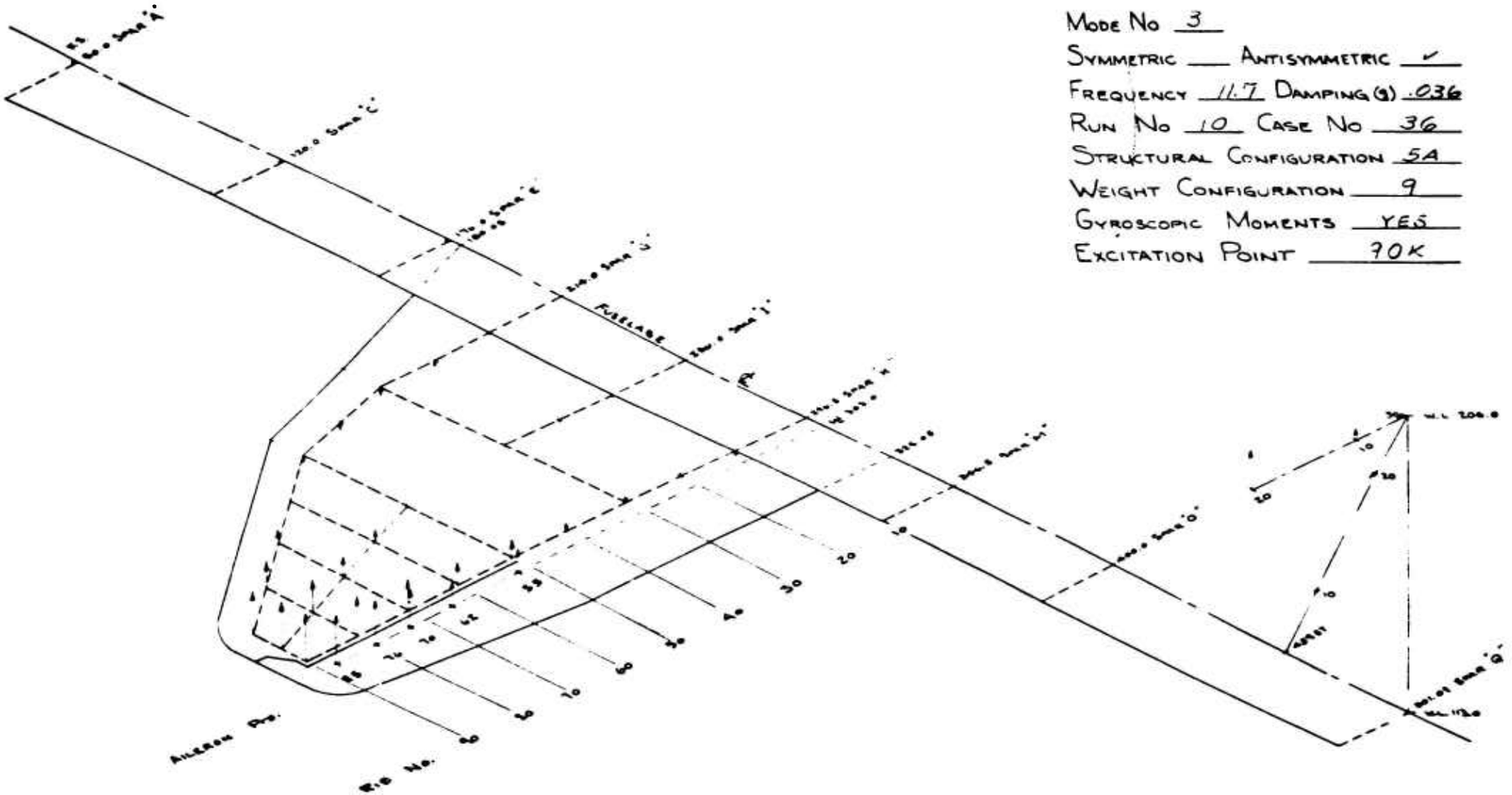

Figure 61 Antisymmetric Mode Shapes - Stiffness Configuration 5A - Gyroscopic Forces In - Mode 3

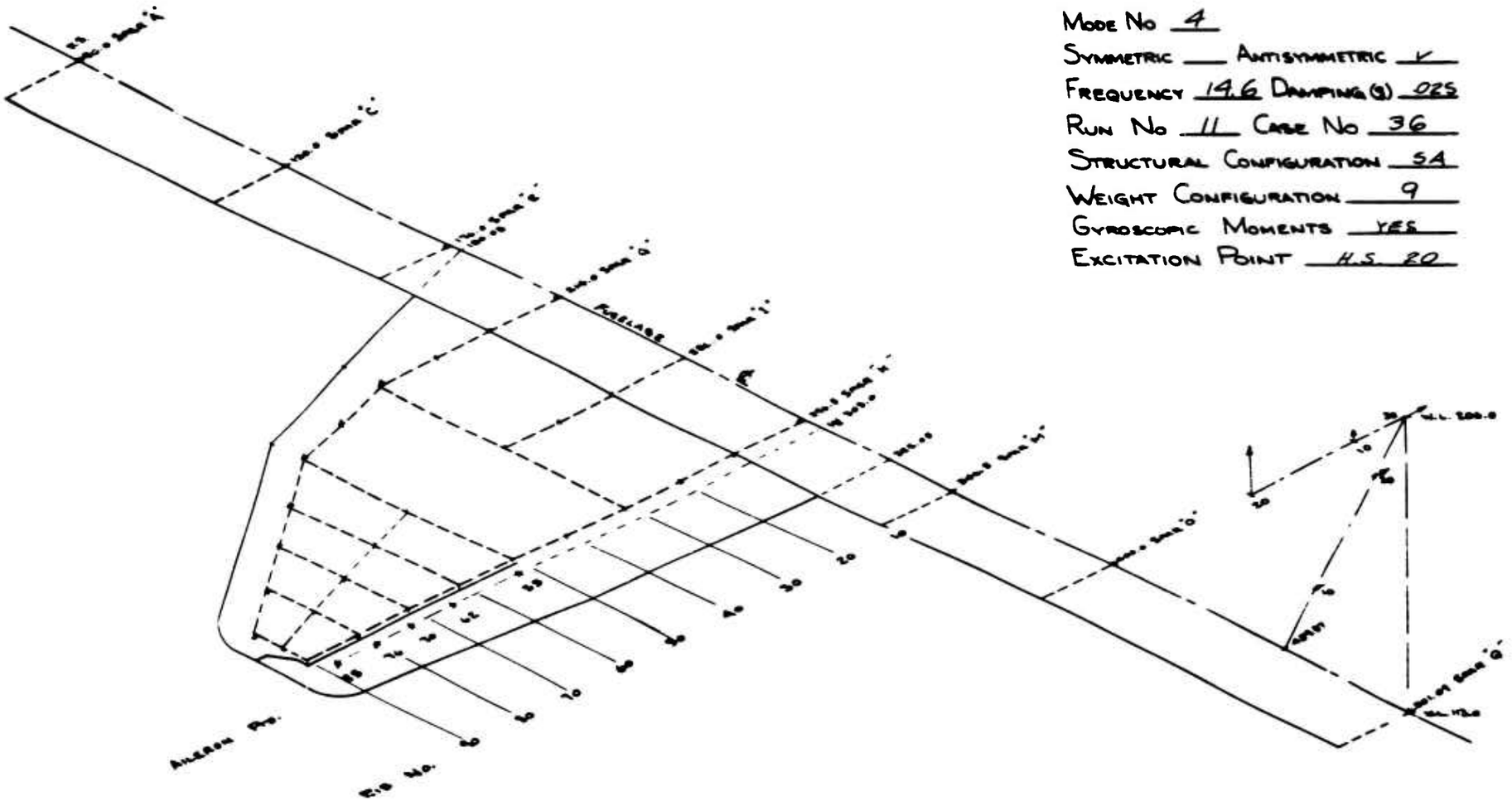

Figure 62 Antisymmetric Mode Shapes - Stiffness Configuration 5A - Gyroscopic Forces In - Mode 4

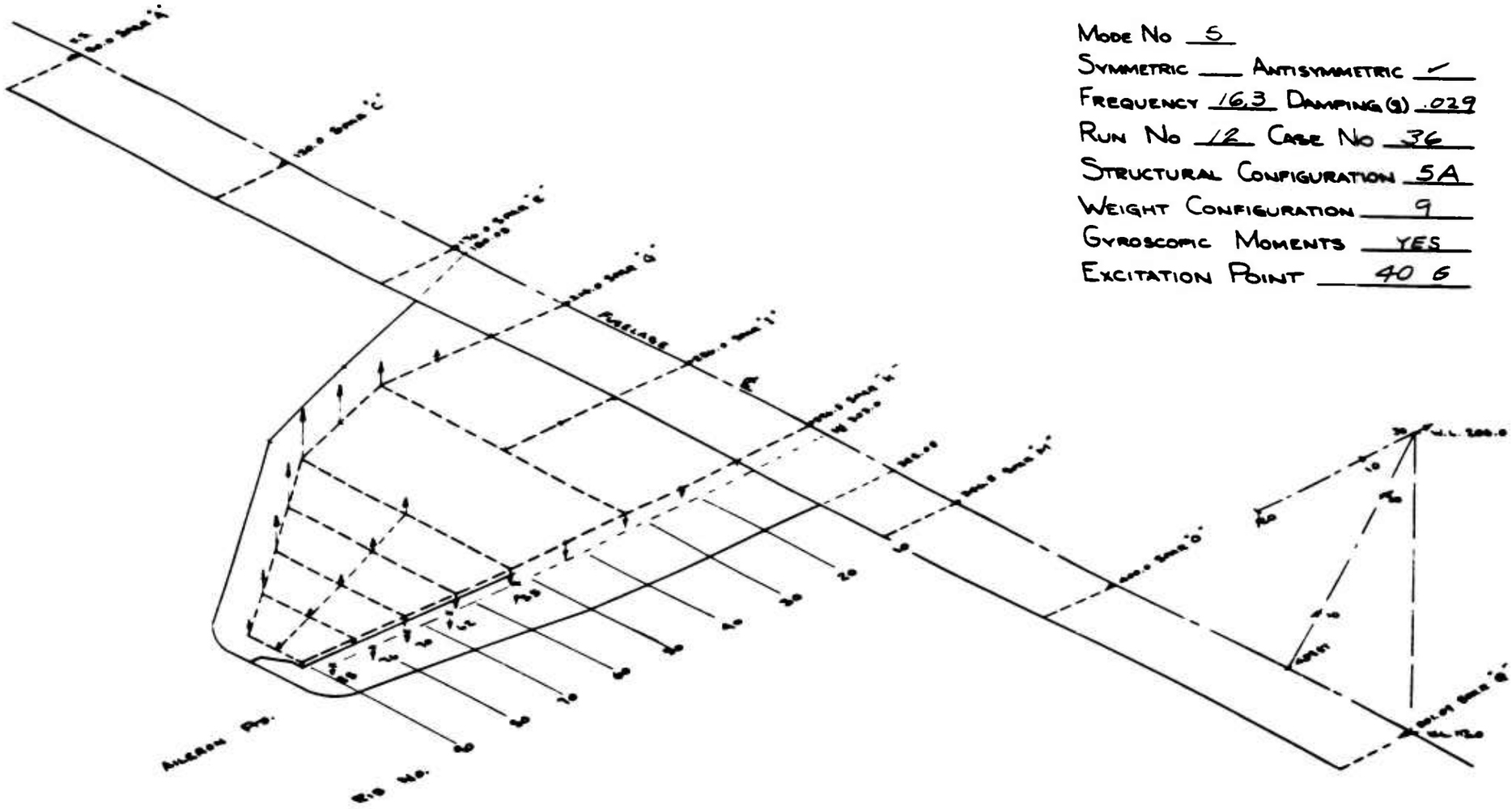

Figure 63 Antisymmetric Mode Shapes - Stiffness Configuration 5A. - Gyroscopic Forces In - Mode 5

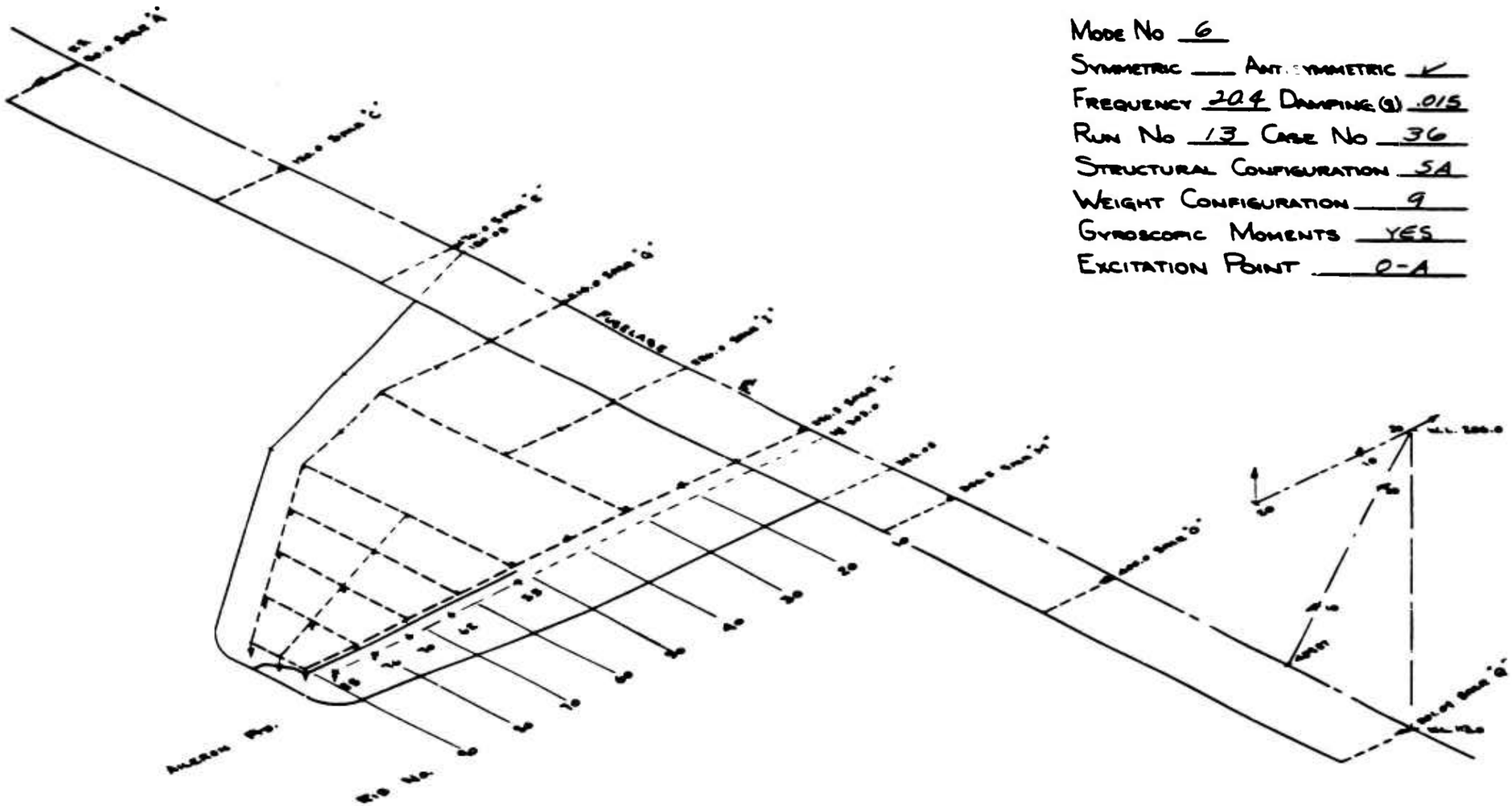

Figure 64 Antisymmetric Mode Shapes - Stiffness Configuration 5A - Gyroscopic Forces In - Mode 6

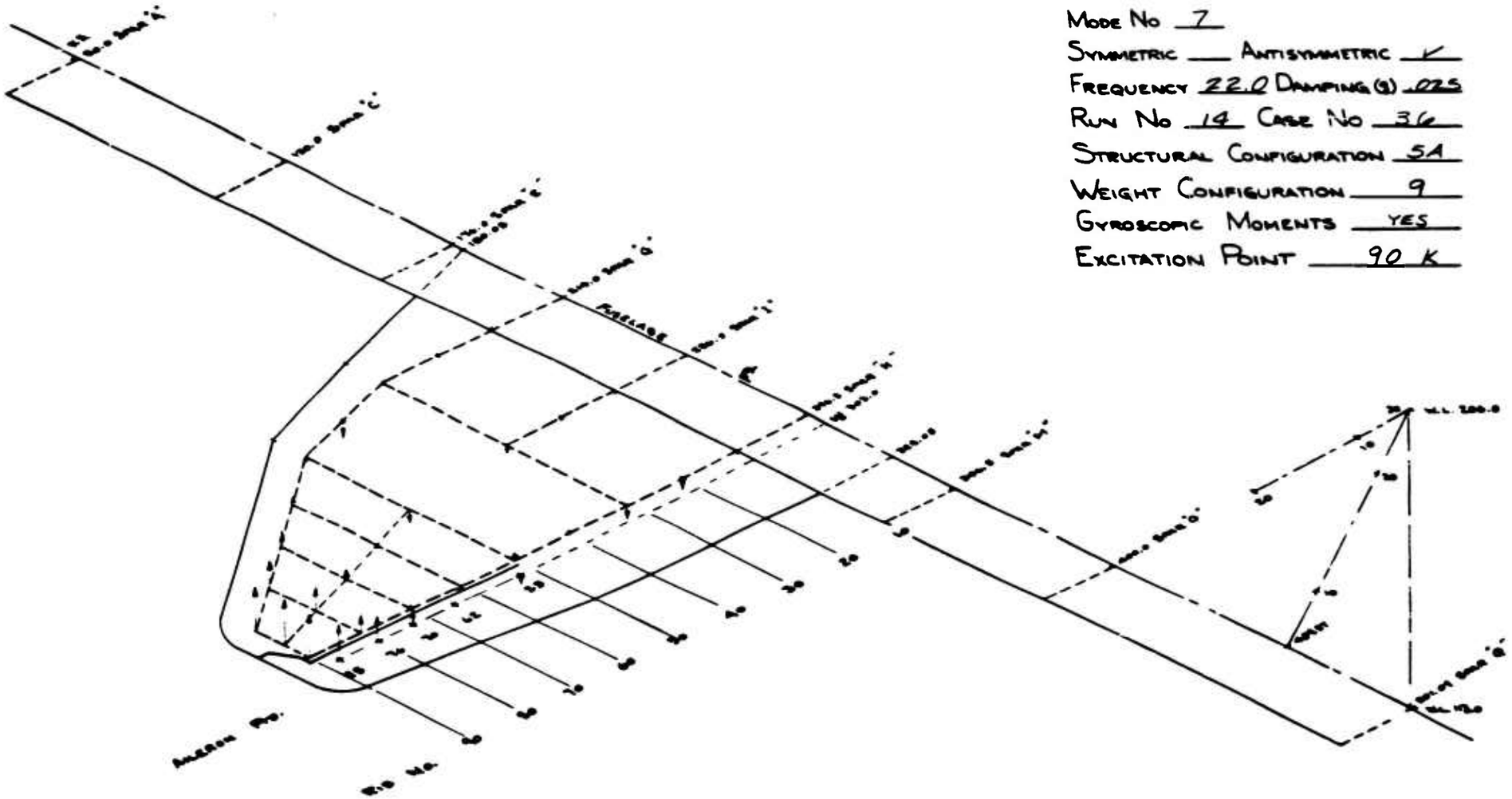

Figure 65 Antisymmetric Mode Shapes - Stiffness Configuration 5A - Gyroscopic Forces In - Mode 7

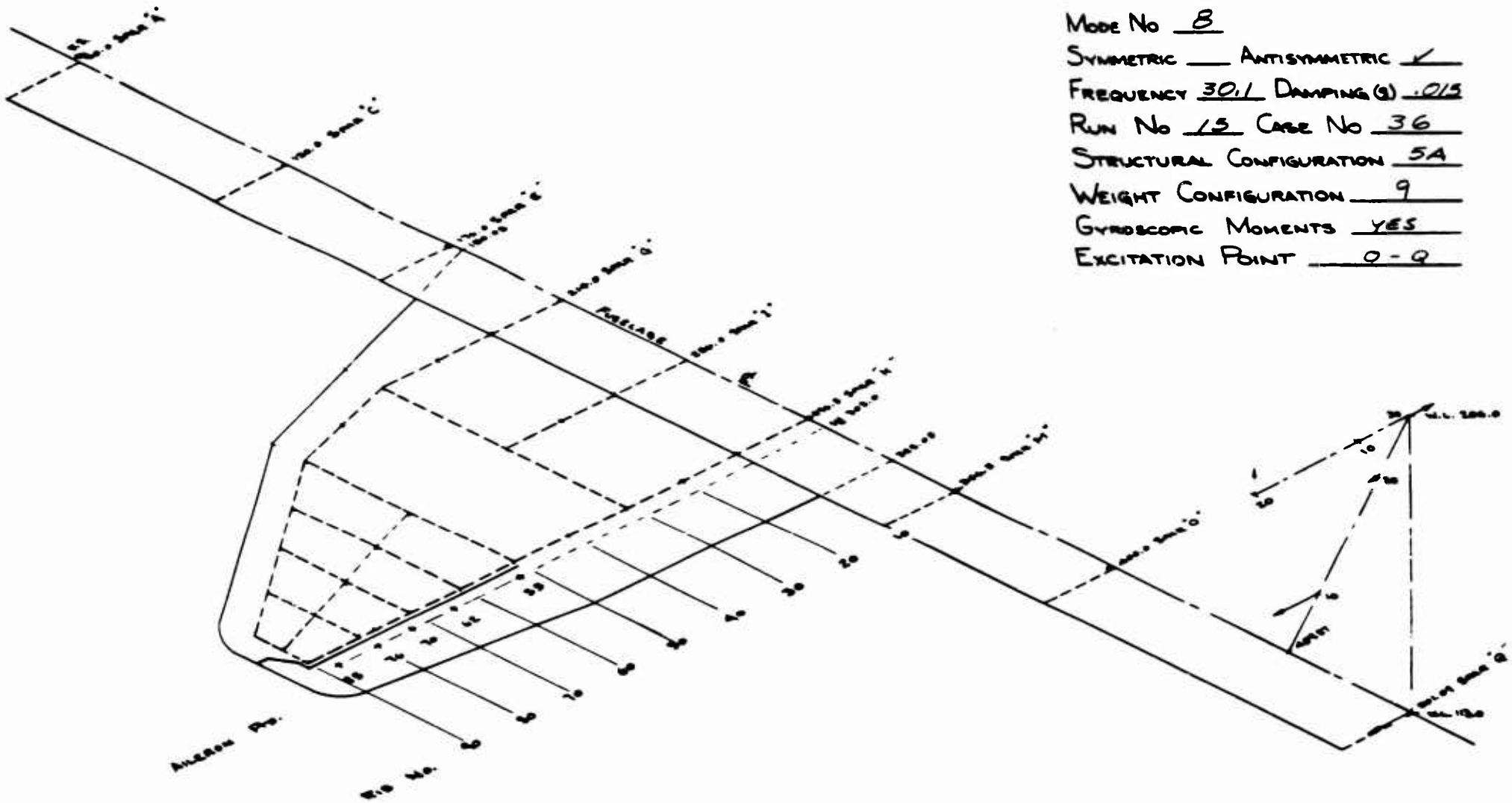

Figure 66 Antisymmetric Mode Shapes - Stiffness Configuration 5A - Gyroscopic Forces In - Mode 8

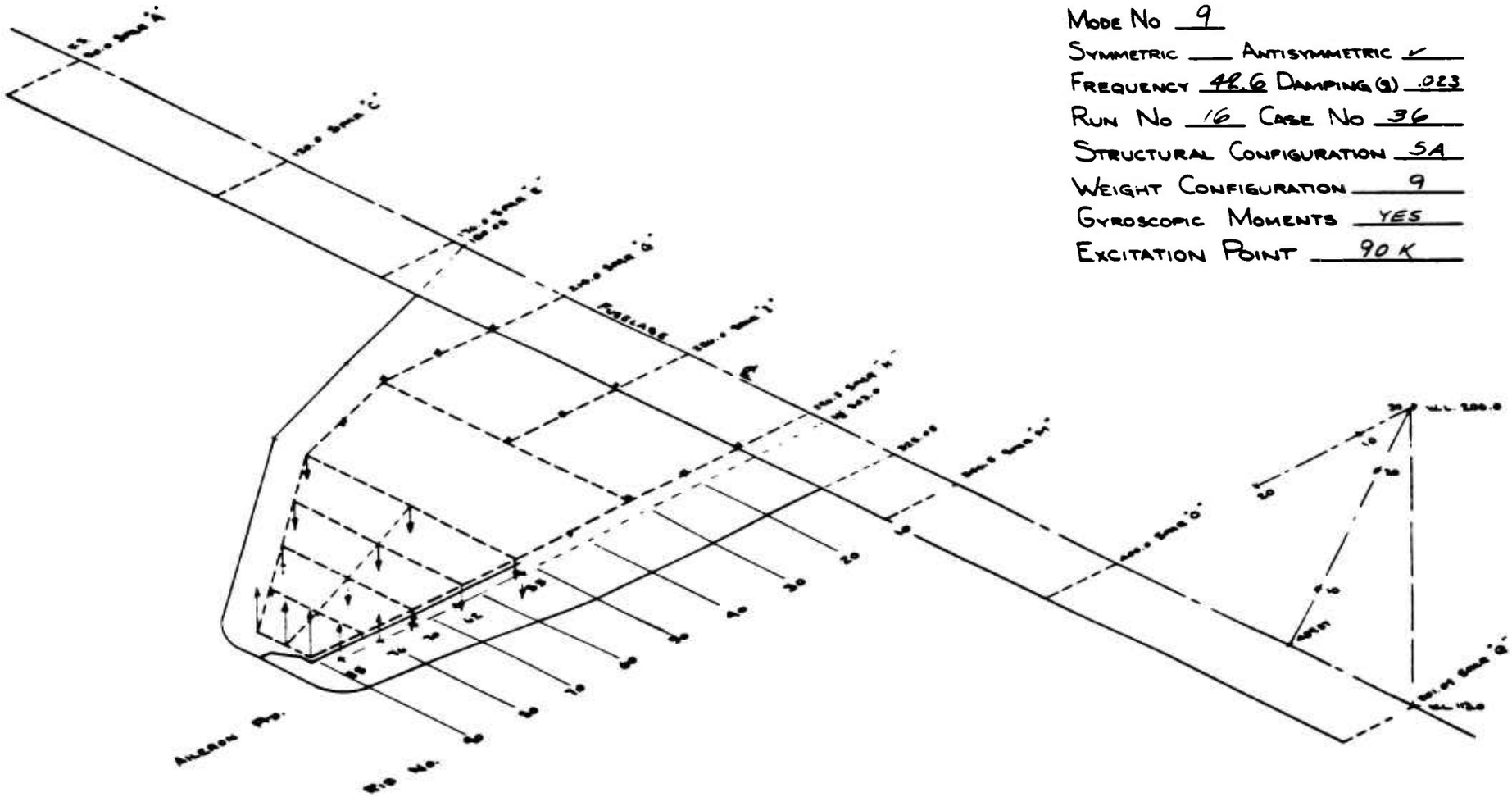

Figure 67 Antisymmetric Mode Shapes - Stiffness Configuration 5A - Gyroscopic Forces In - Mode 9

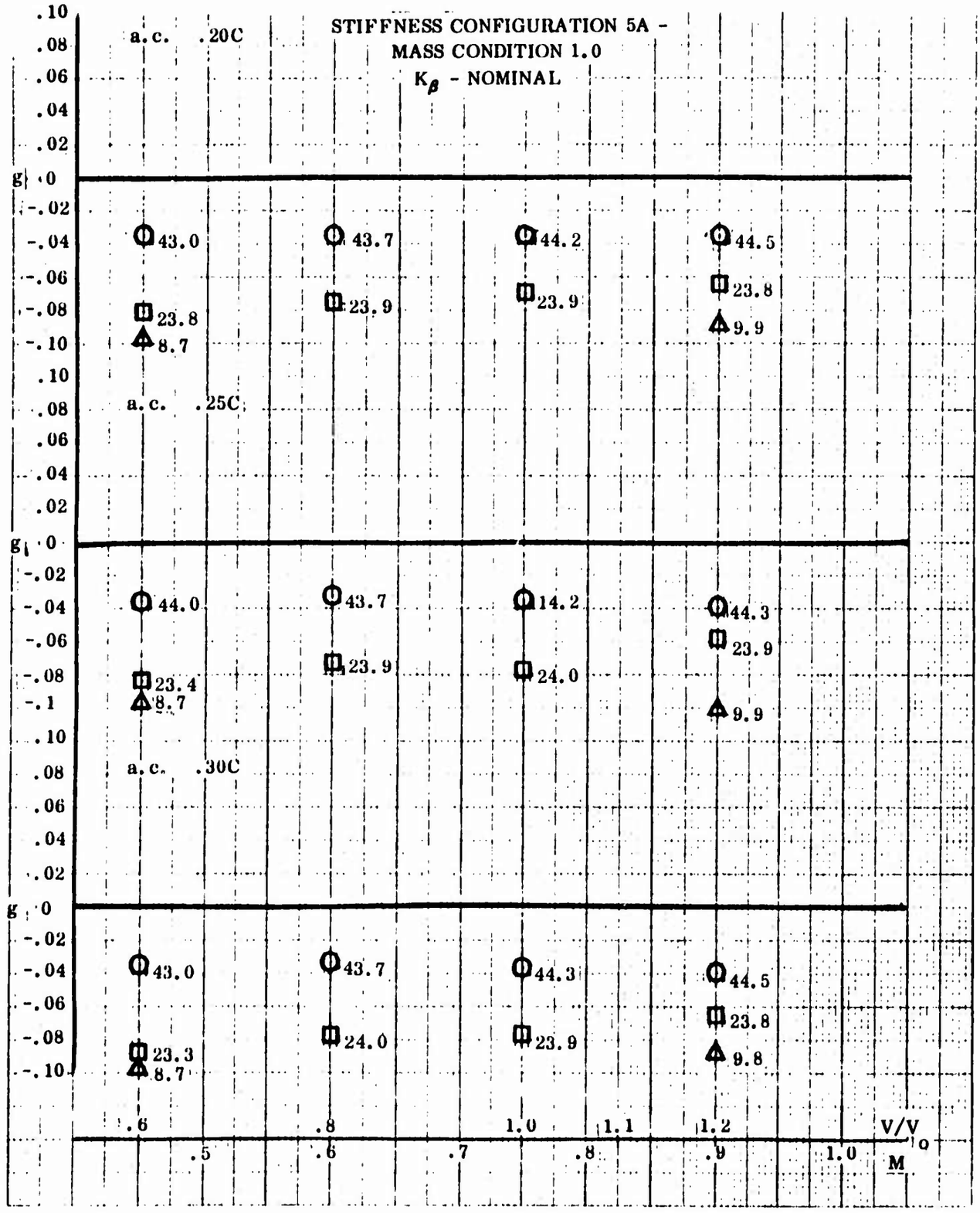

Figure 68 Phase I Studies - Symmetric: Flight Condition D (M = 0.75 at Sea Level)

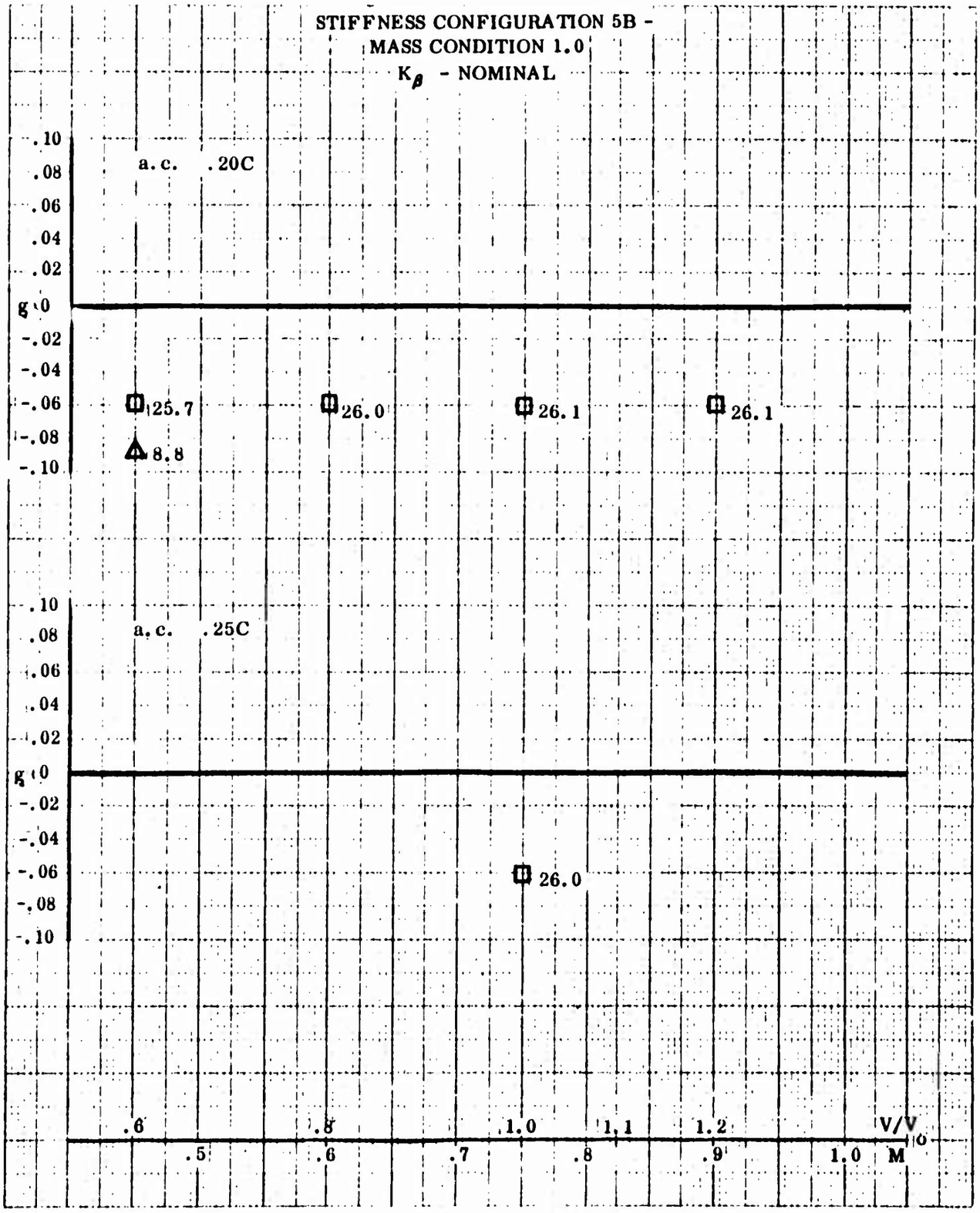

Figure 69 Phase I Studies - Symmetric: Flight Condition D (M = 0.75 at Sea Level)

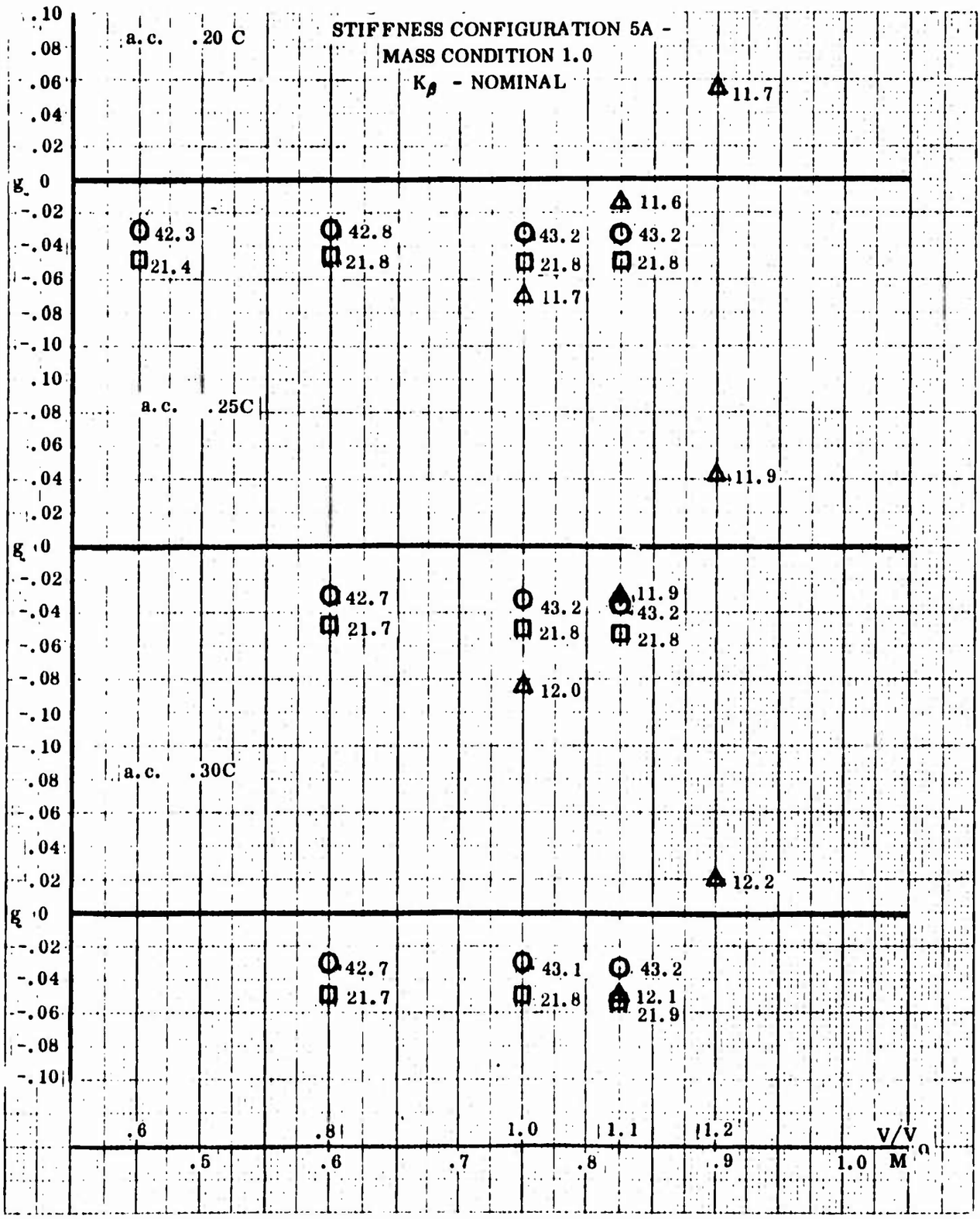

Figure 70 Phase I Studies - Antisymmetric: Flight Condition D (M = 0.75 at Sea Level)

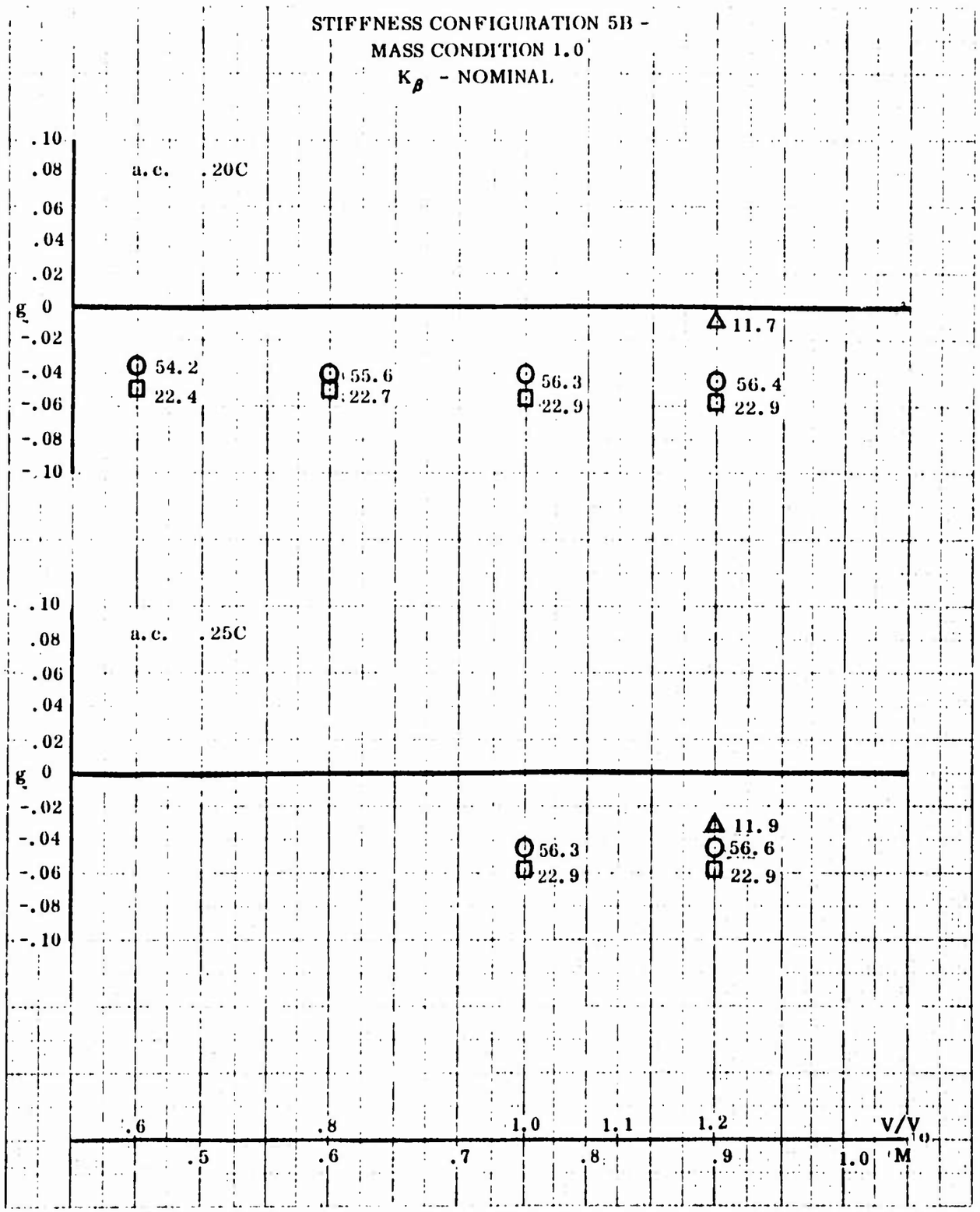

Figure 71 Phase I Studies - Antisymmetric: Flight Condition D (M = 0.75 at Sea Level)

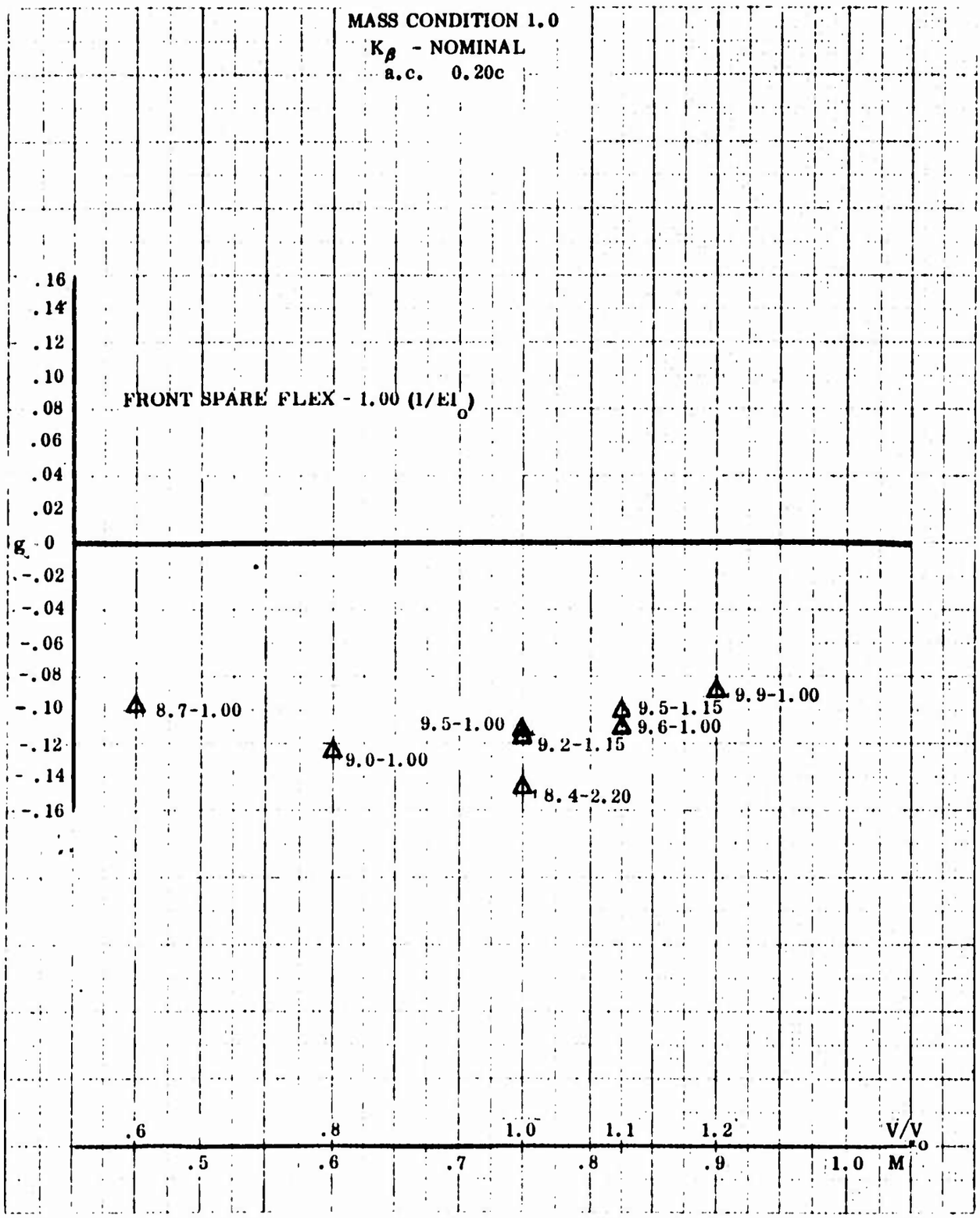

Figure 72 Phase II Studies - Symmetric: Flight Condition D (M = 0.75 at Sea Level)

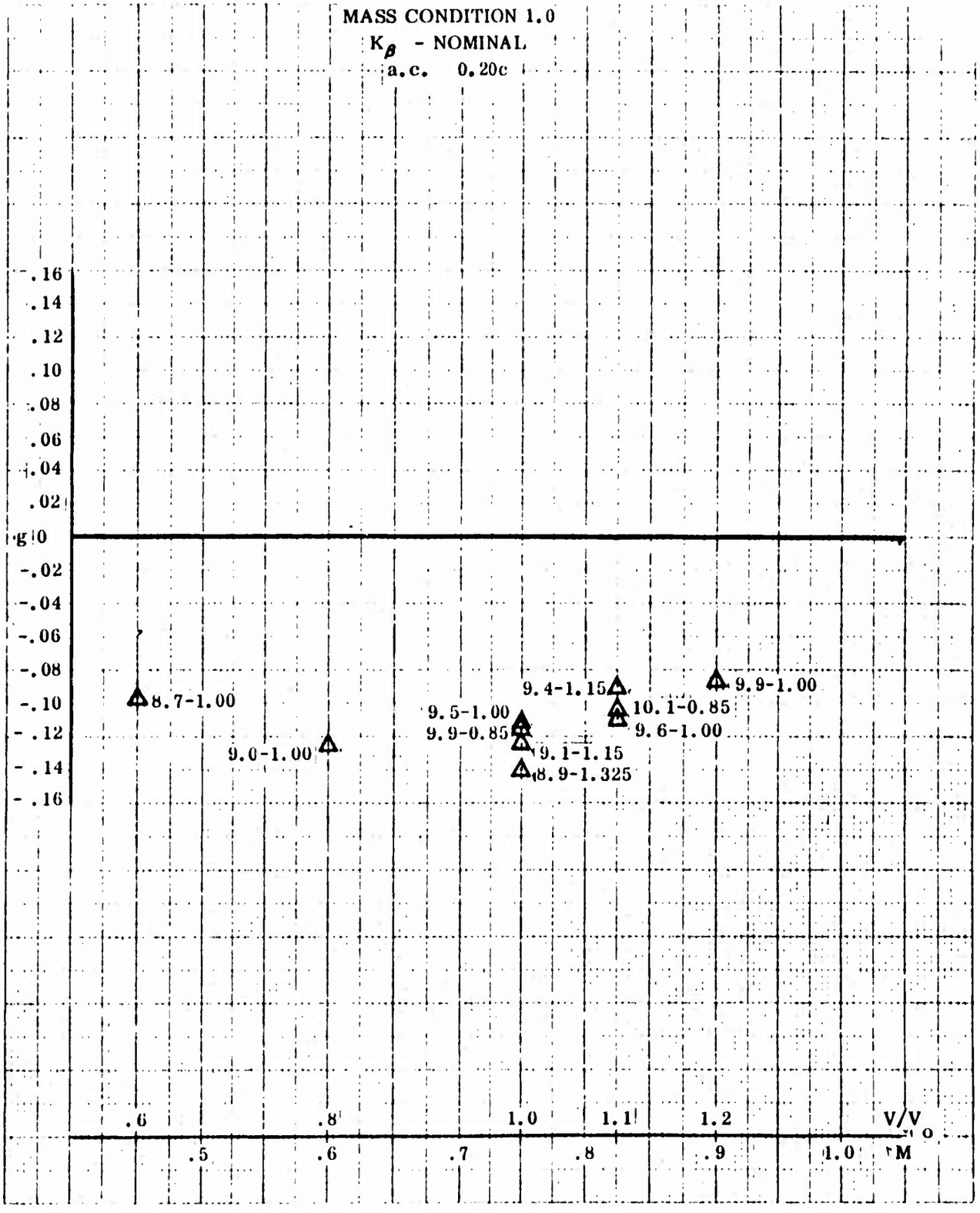

Figure 73 Phase II Studies - Symmetric: Flight Condition D (M - 0.75 at Sea Level)

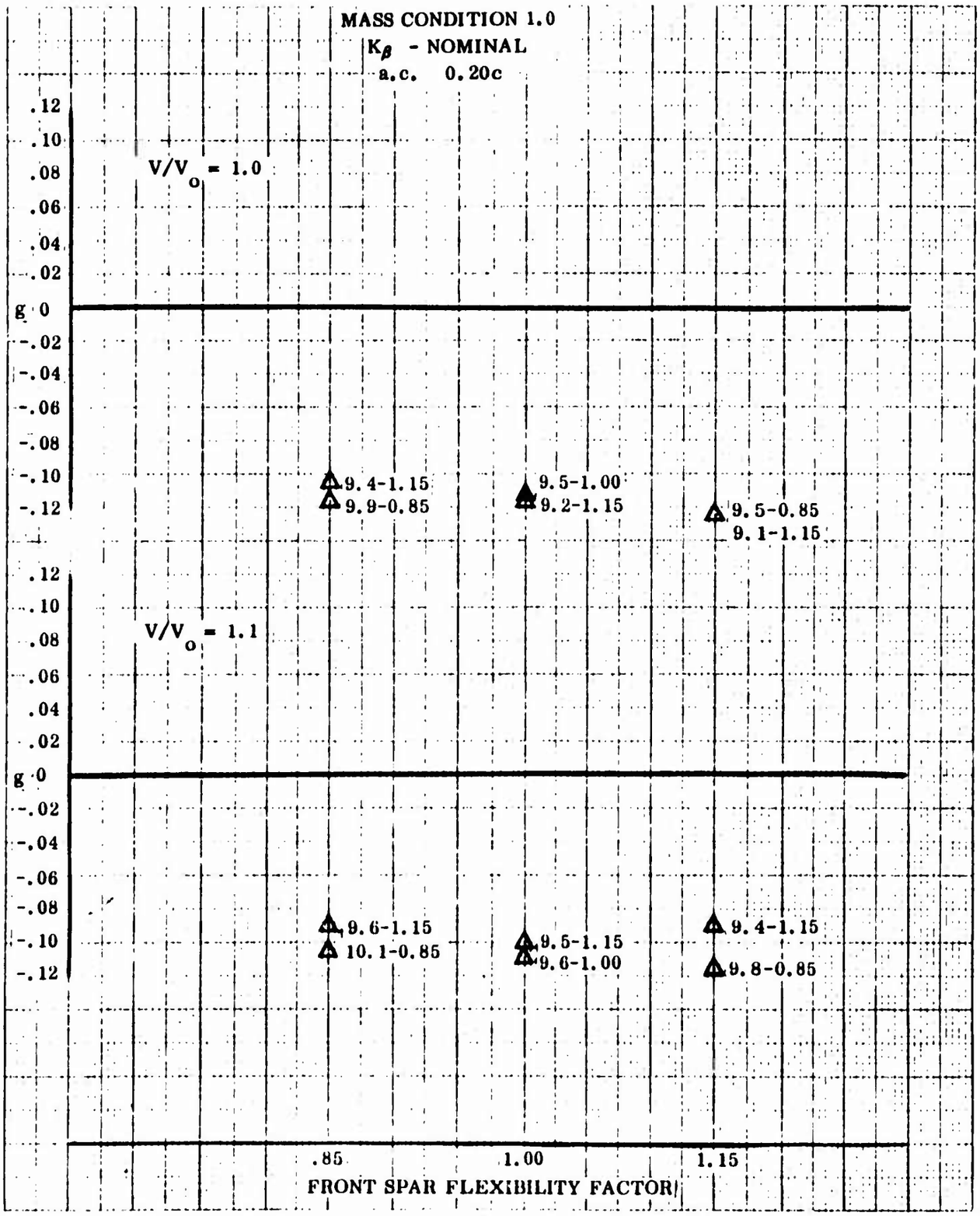

Figure 74 Phase II Studies - Symmetric: Flight Condition D (M = 0.75 at Sea Level)

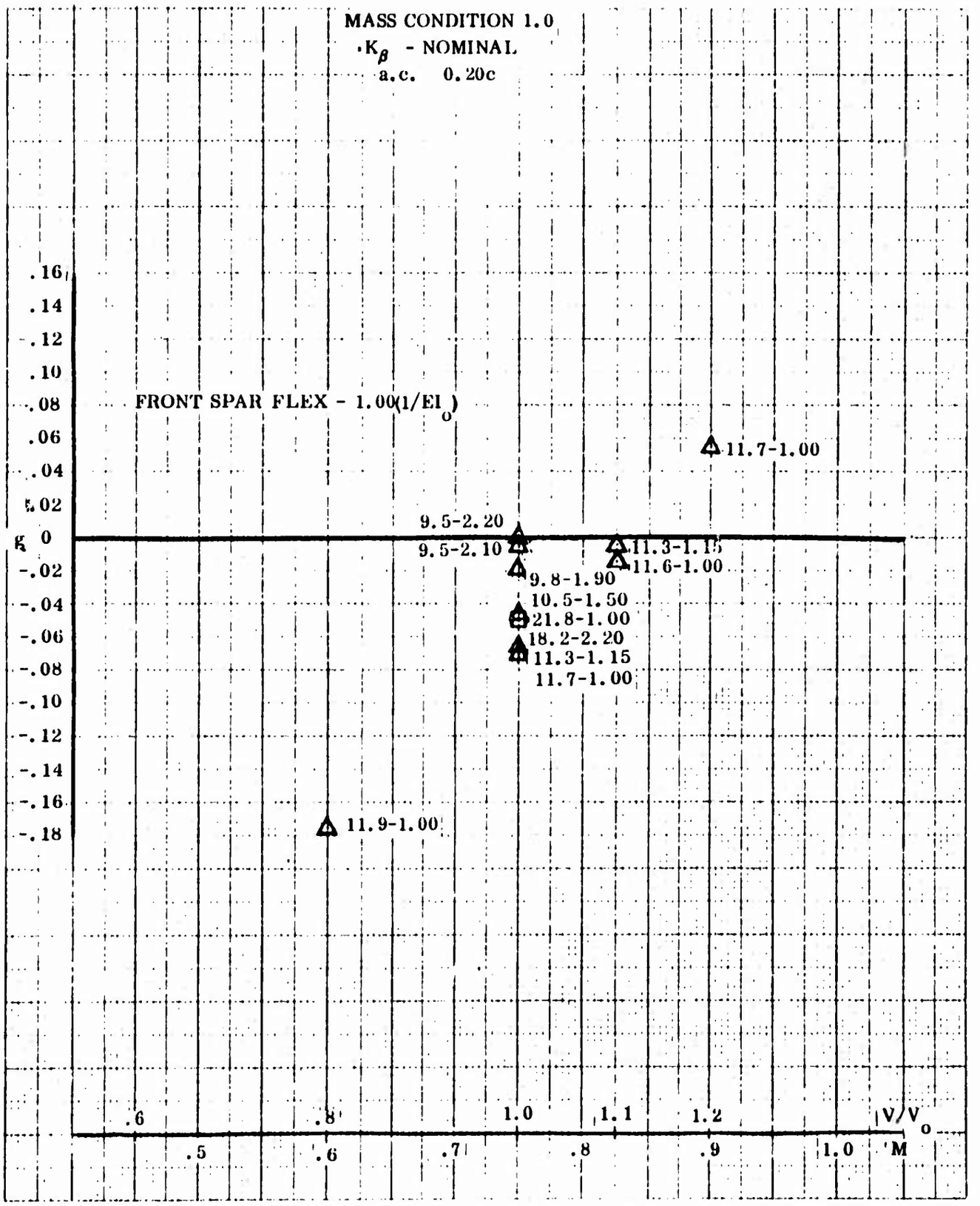

Figure 75 Phase I Studies - Antisymmetric: Flight Condition D (M = 0.75 at Sea Level)

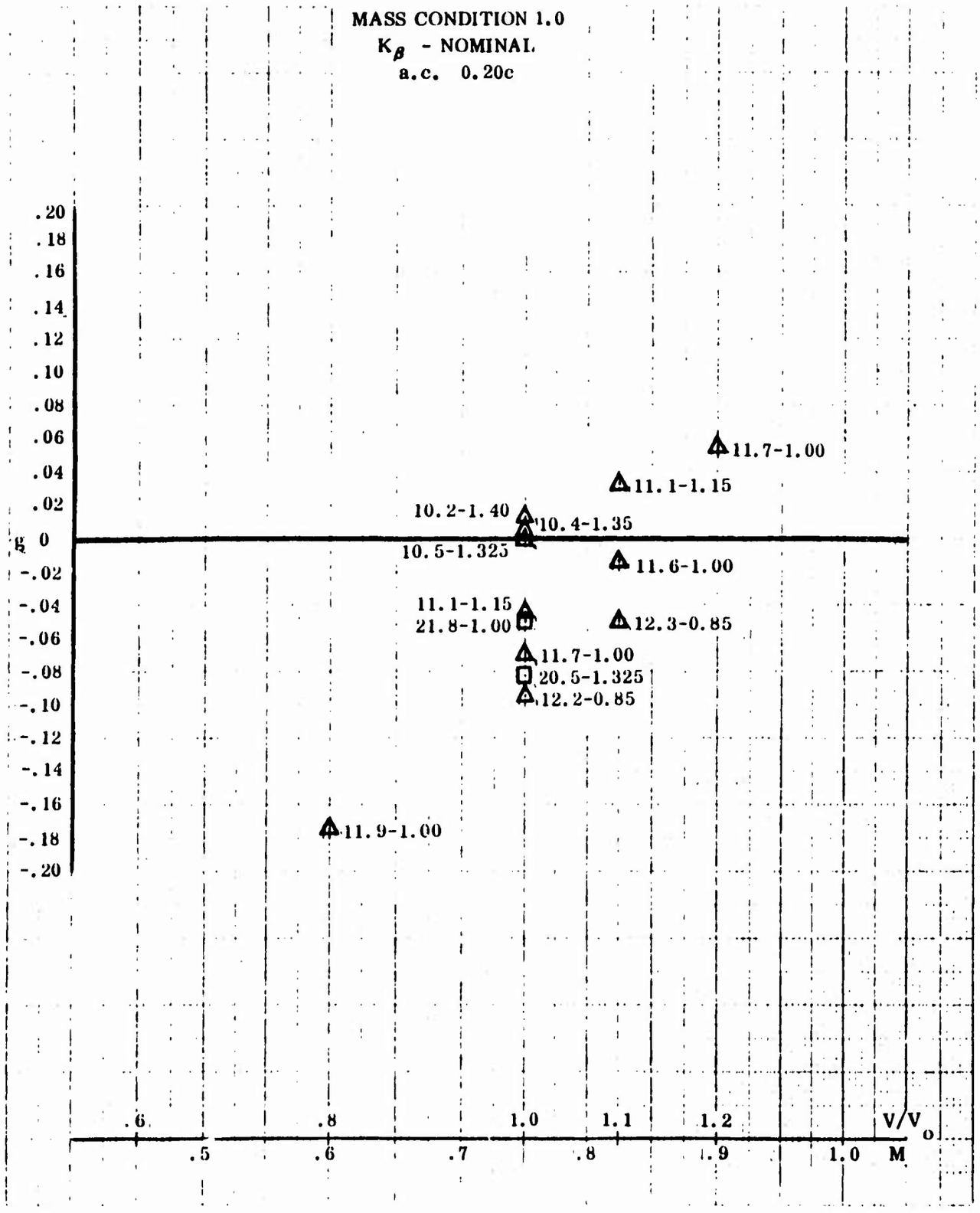

Figure 76 Phase II Studies - Antisymmetric: Flight Condition D (M = 0.75 at Sea Level)

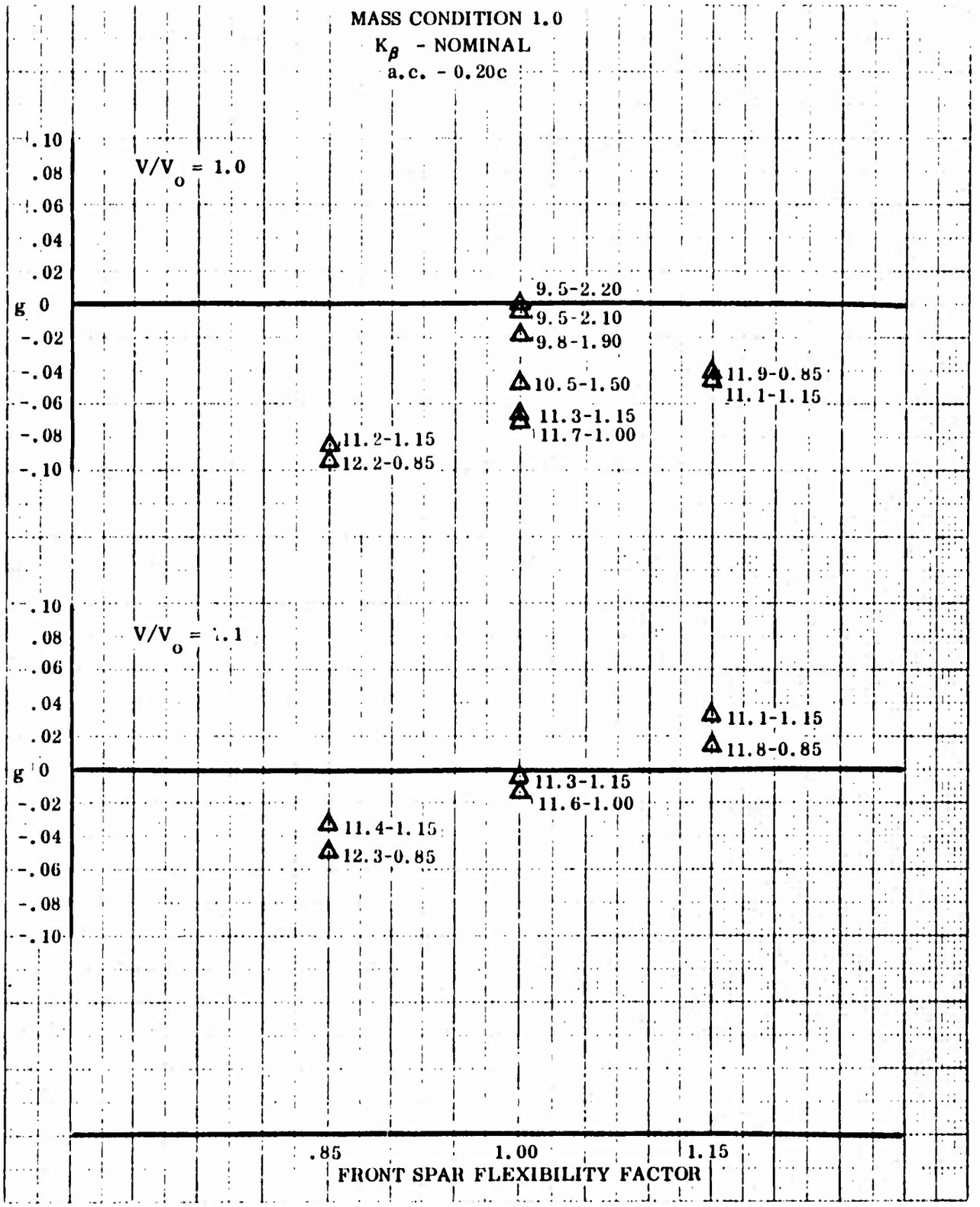

Figure 77 Phase II Studies - Antisymmetric: Flight Condition D (M = 0.75 at Sea Level)

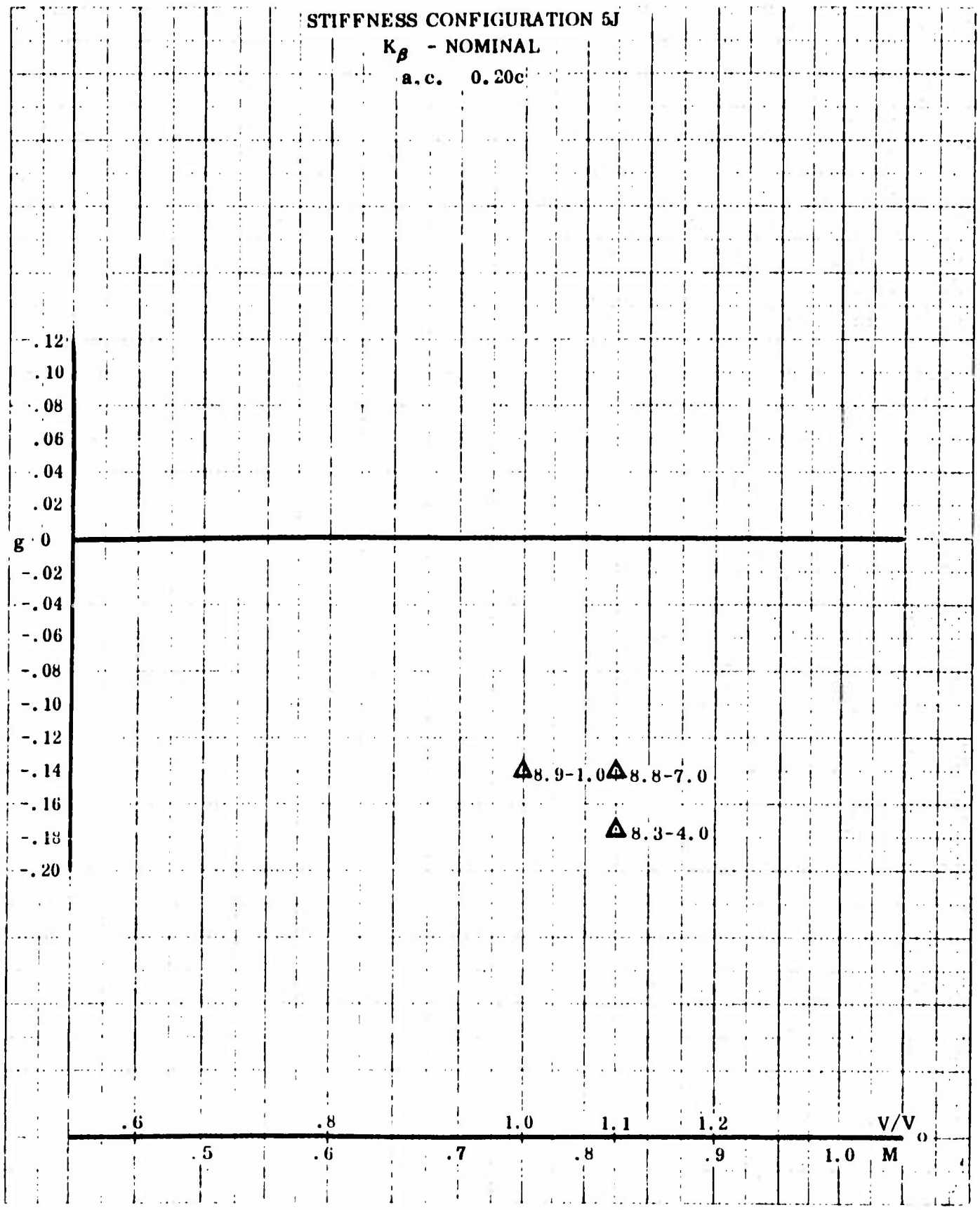

Figure 78 Phase III Studies - Symmetric: Flight Condition D (M = 0.75 at Sea Level)

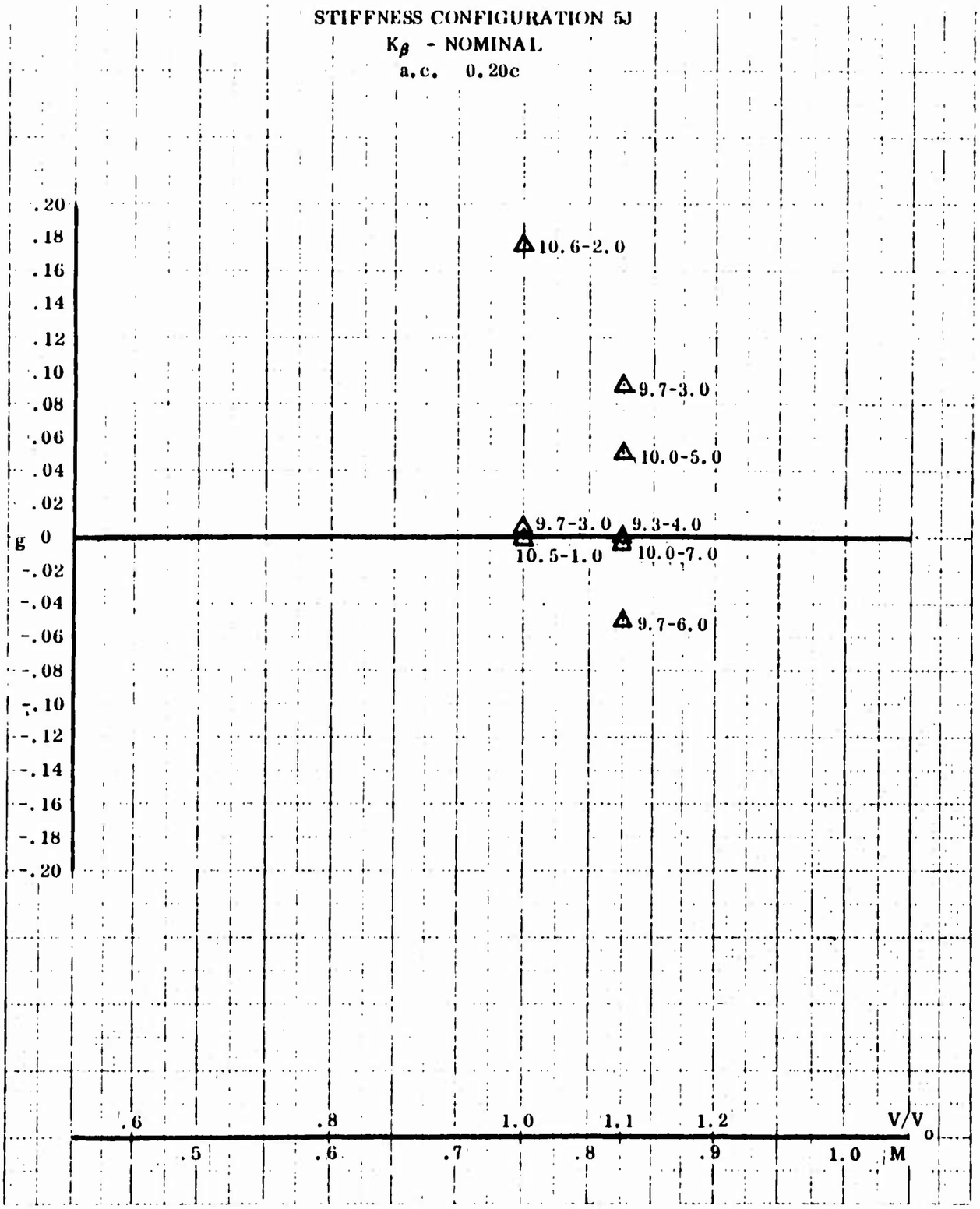

Figure 79 Phase III Studies - Antisymmetric: Flight Condition D (M = 0.75 at Sea Level)

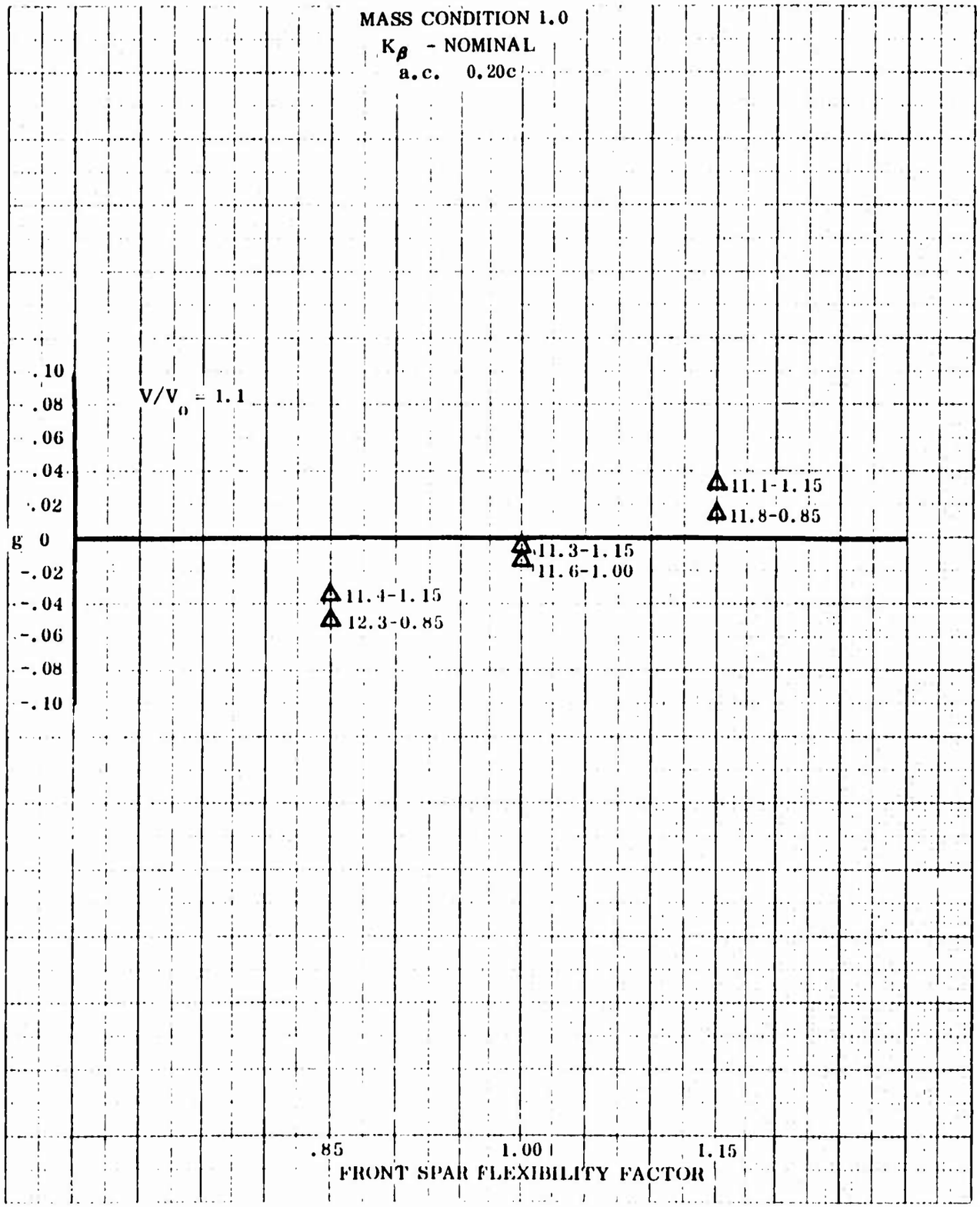

Figure 80 Phase IV Studies - Antisymmetric: Flight Condition D (M = 0.75 at Sea Level)

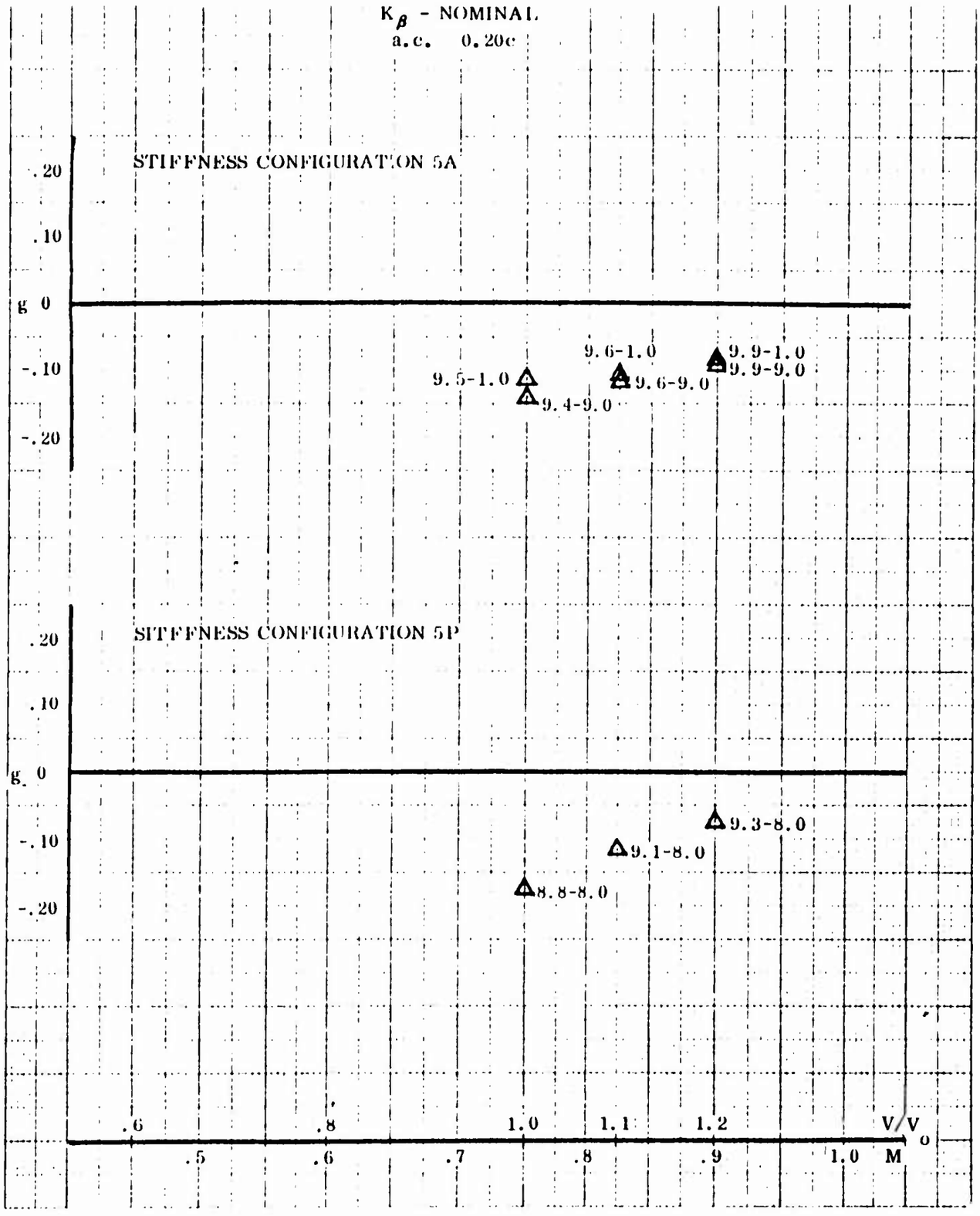

Figure 81 Phase IV Studies - Symmetric: Flight Condition D (M = 0.75 at Sea Level)

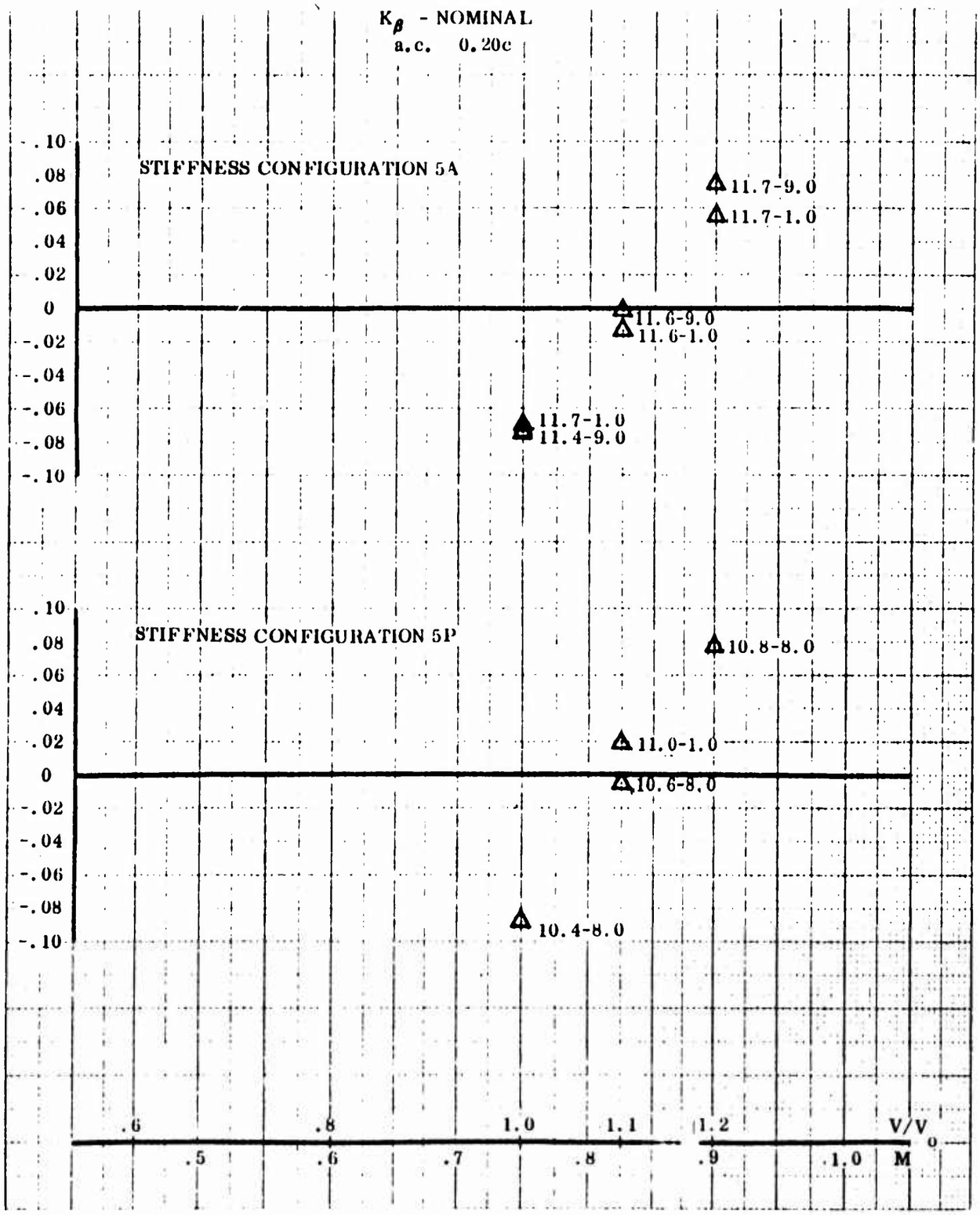

Figure 82 Phase IV Studies - Antisymmetric: Flight Condition D (M = 0.75 at Sea Level)

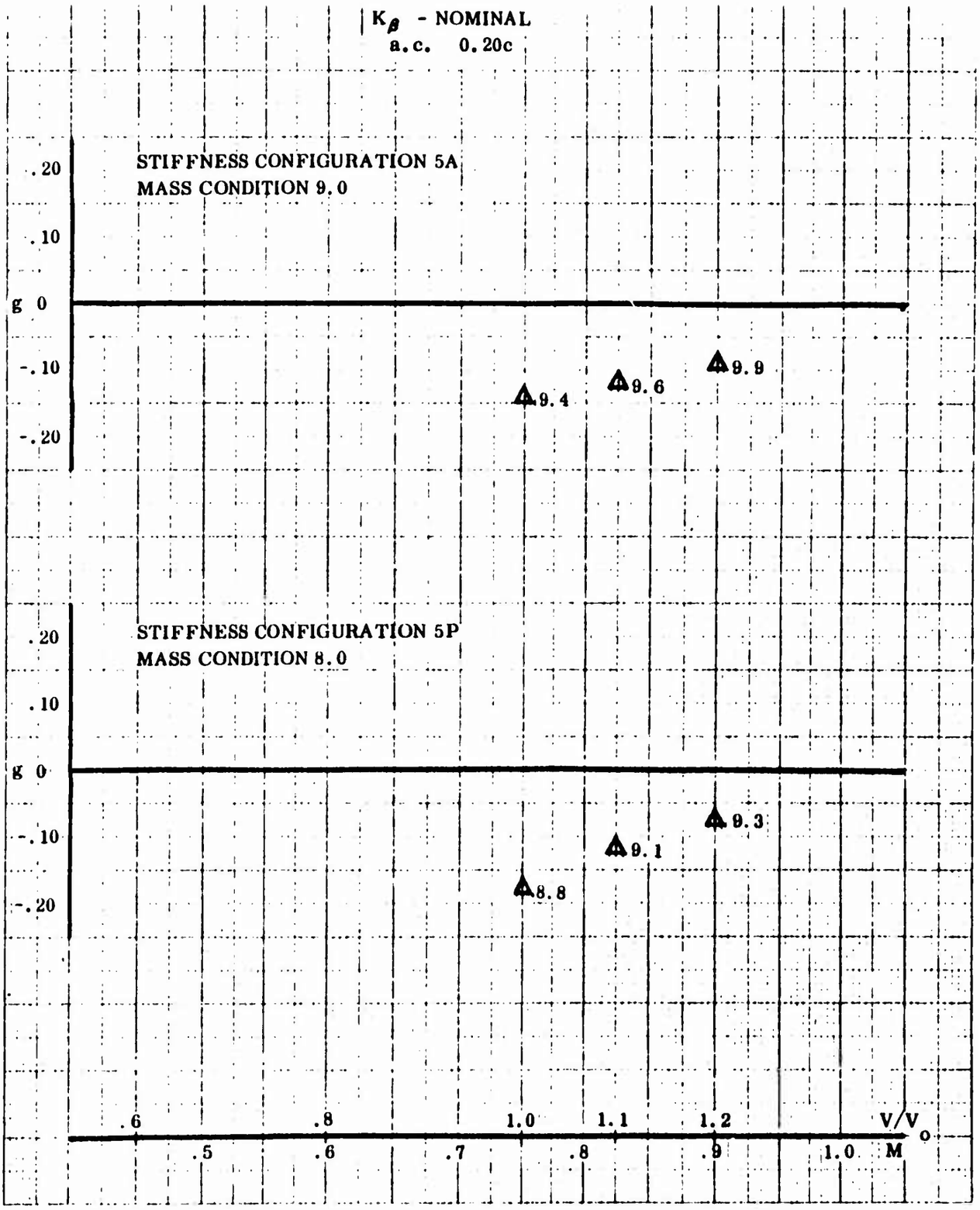

Figure 83 Phase V Studies - Symmetric: Flight Condition D (M = 0.75 at Sea Level)

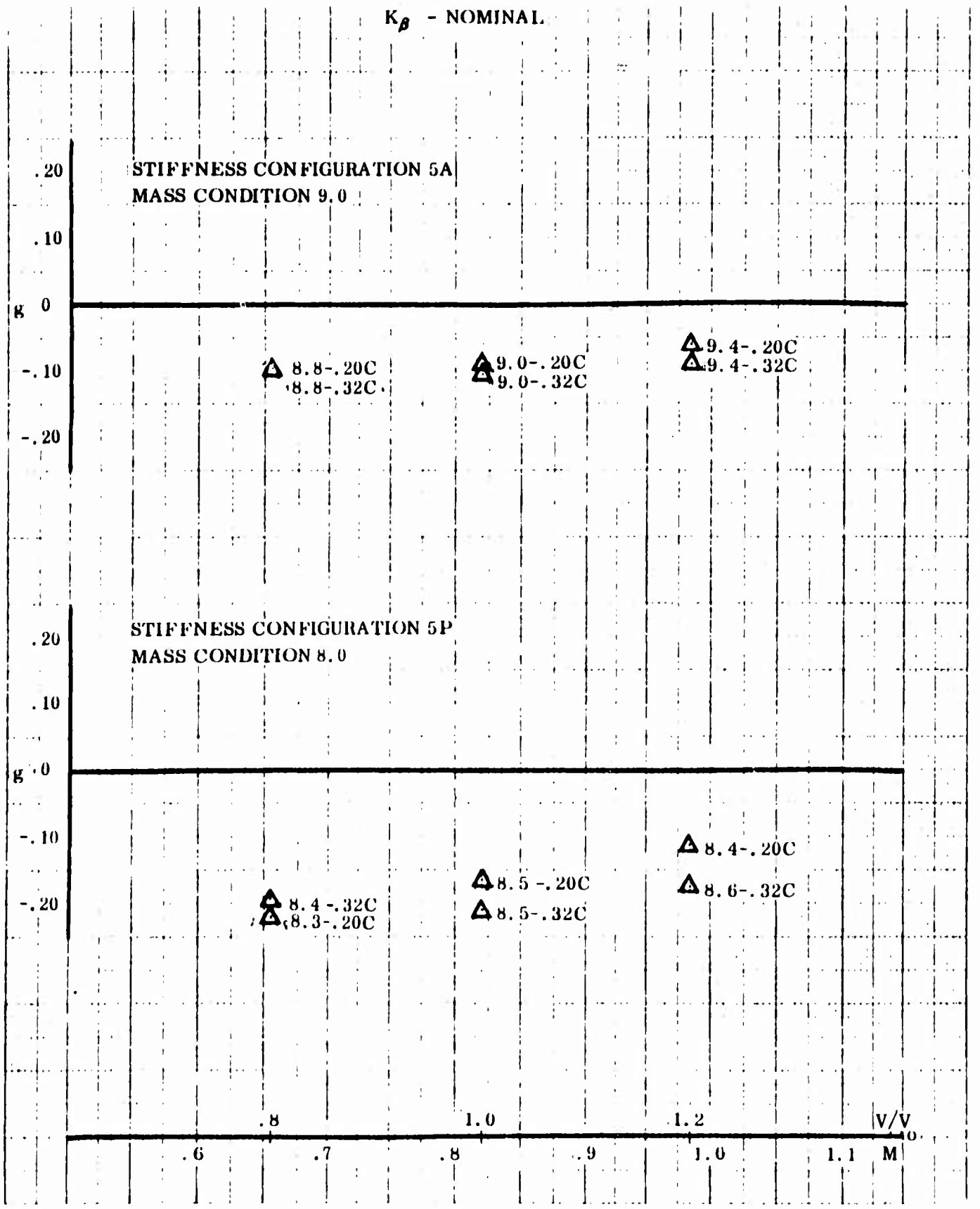

Figure 84 Phase V Studies - Symmetric: Flight Condition A (M = 0.82 at Sea Level)

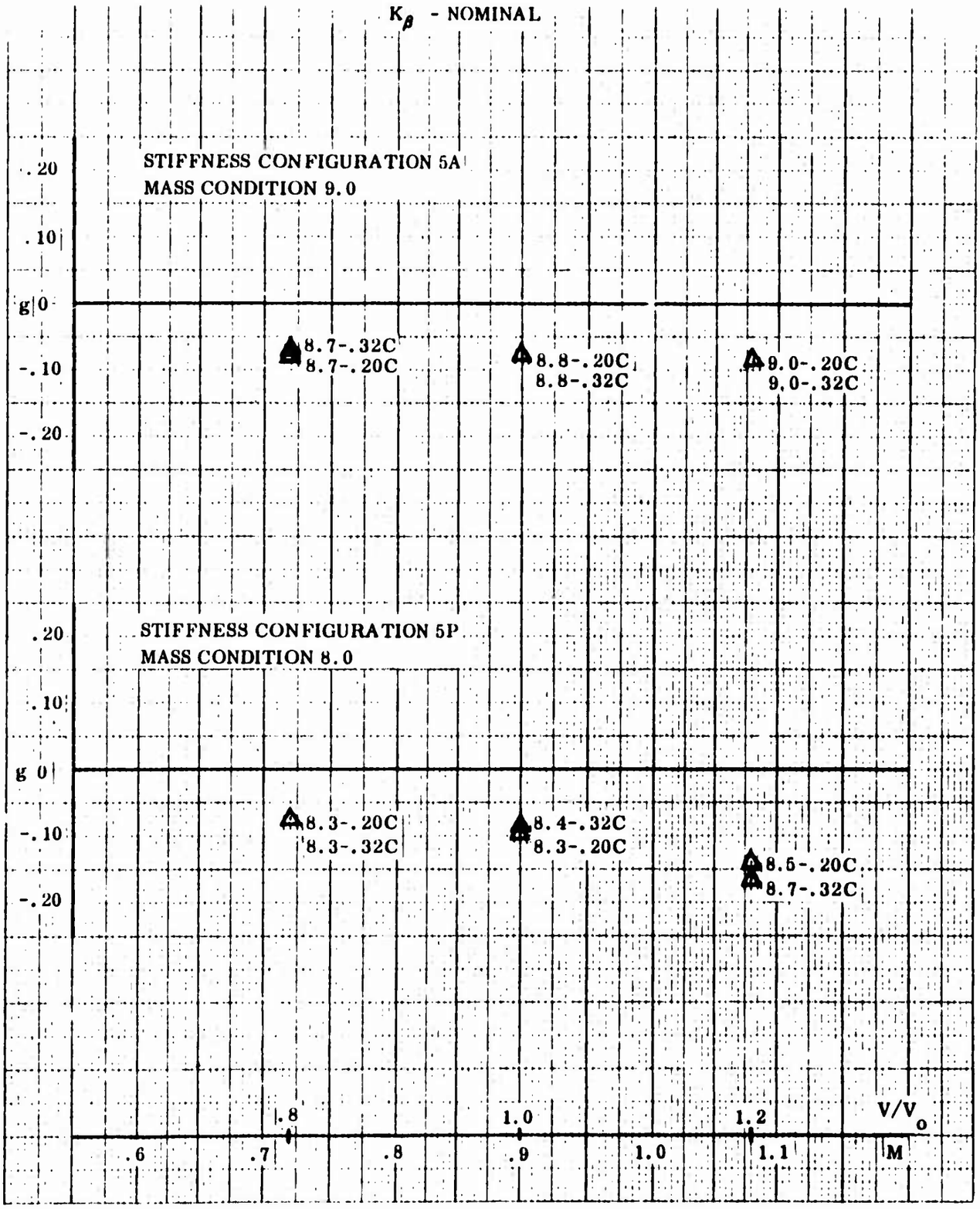

Figure 85 Phase V Studies - Symmetric: Flight Condition E (M = 0.90 at 5,000')

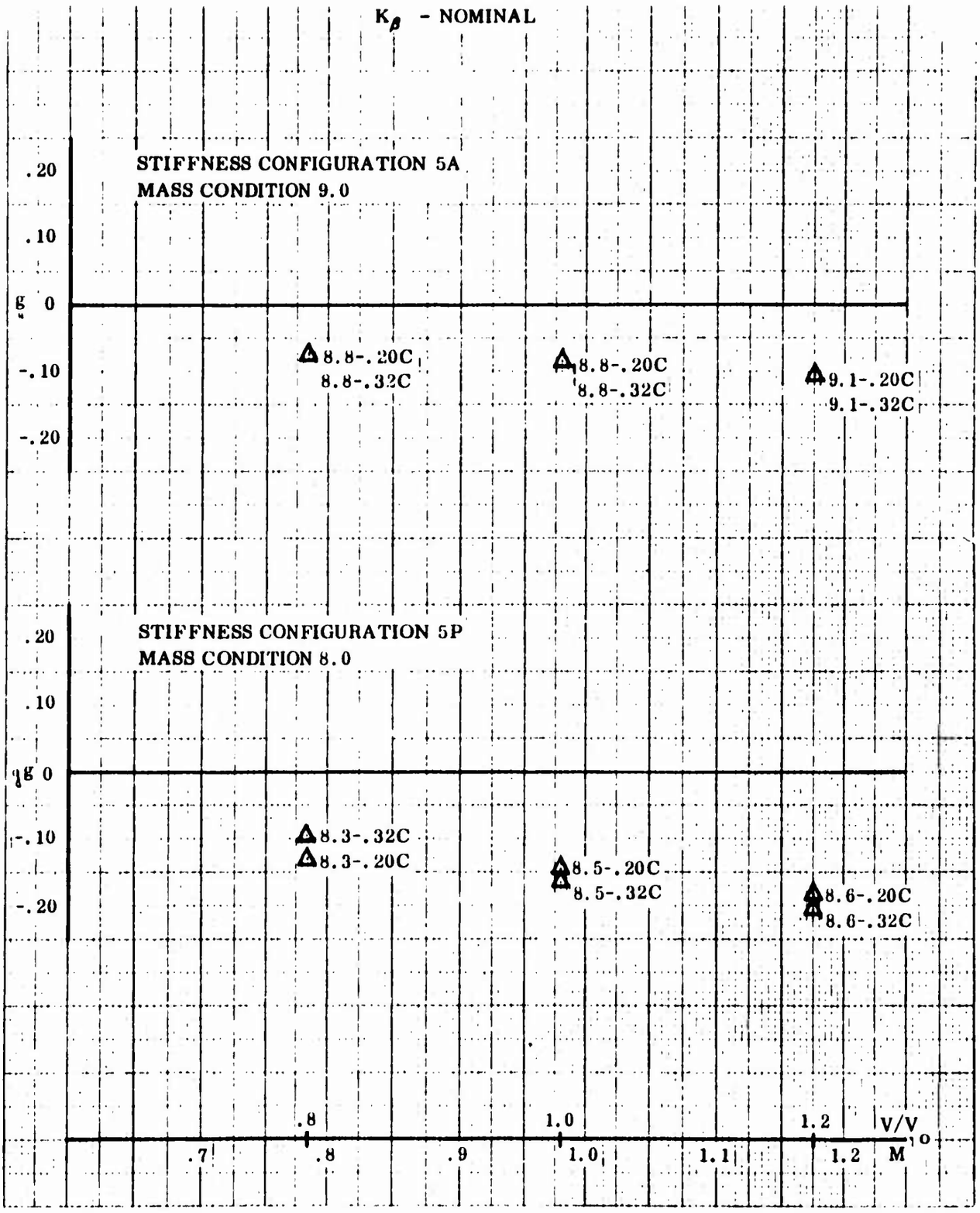

Figure 86 Phase V Studies - Symmetric: Flight Condition B (M = 0.98 at 9,500')

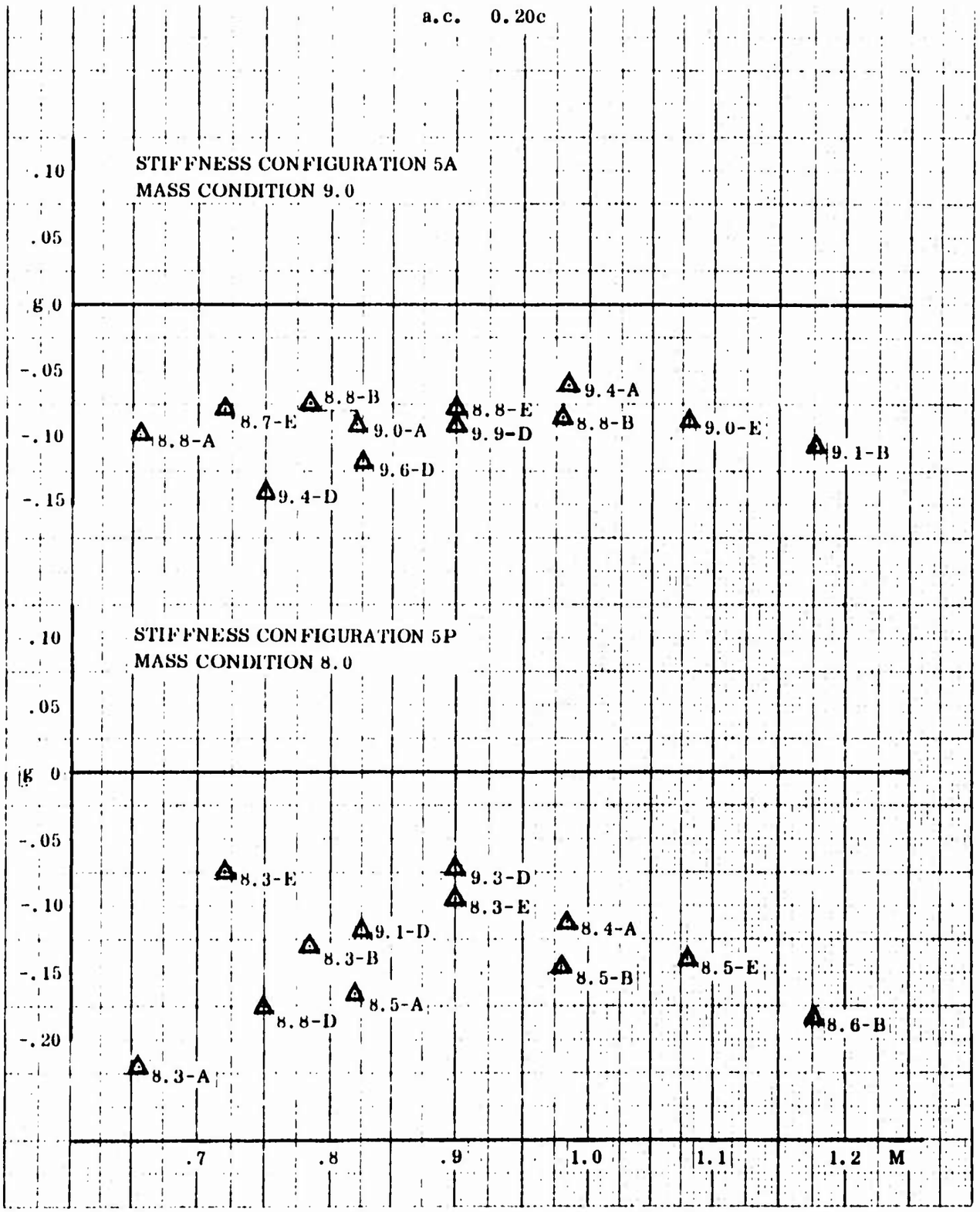

Figure 87 Phase V Studies - Symmetric: Flight Conditions D, A, E and B

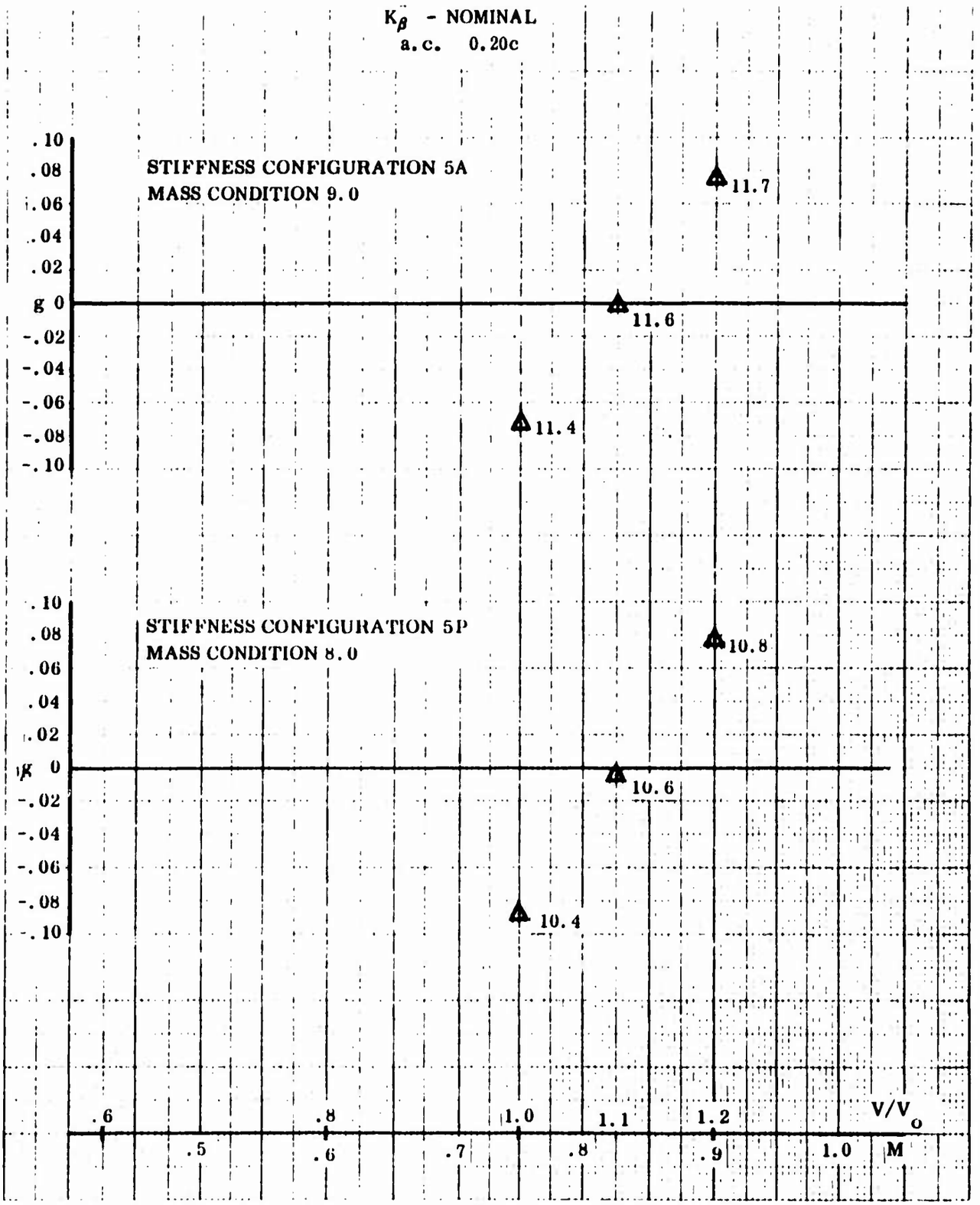

Figure 88 Phase V Studies - Antisymmetric: Flight Condition D (M = 0.75 at Sea Level)

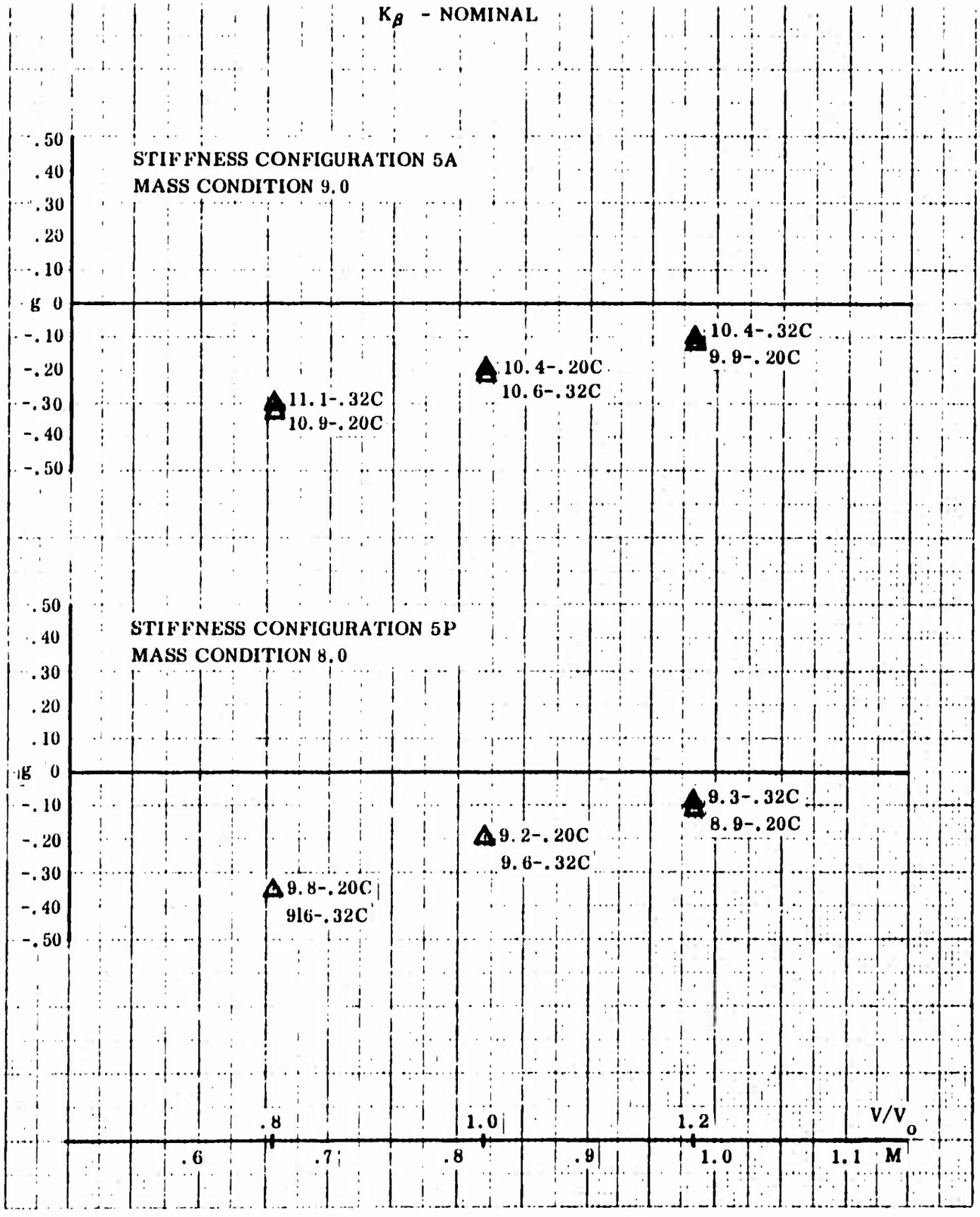

Figure 89 Phase V Studies - Antisymmetric: Flight Condition A (M = 0.82 at Sea Level)

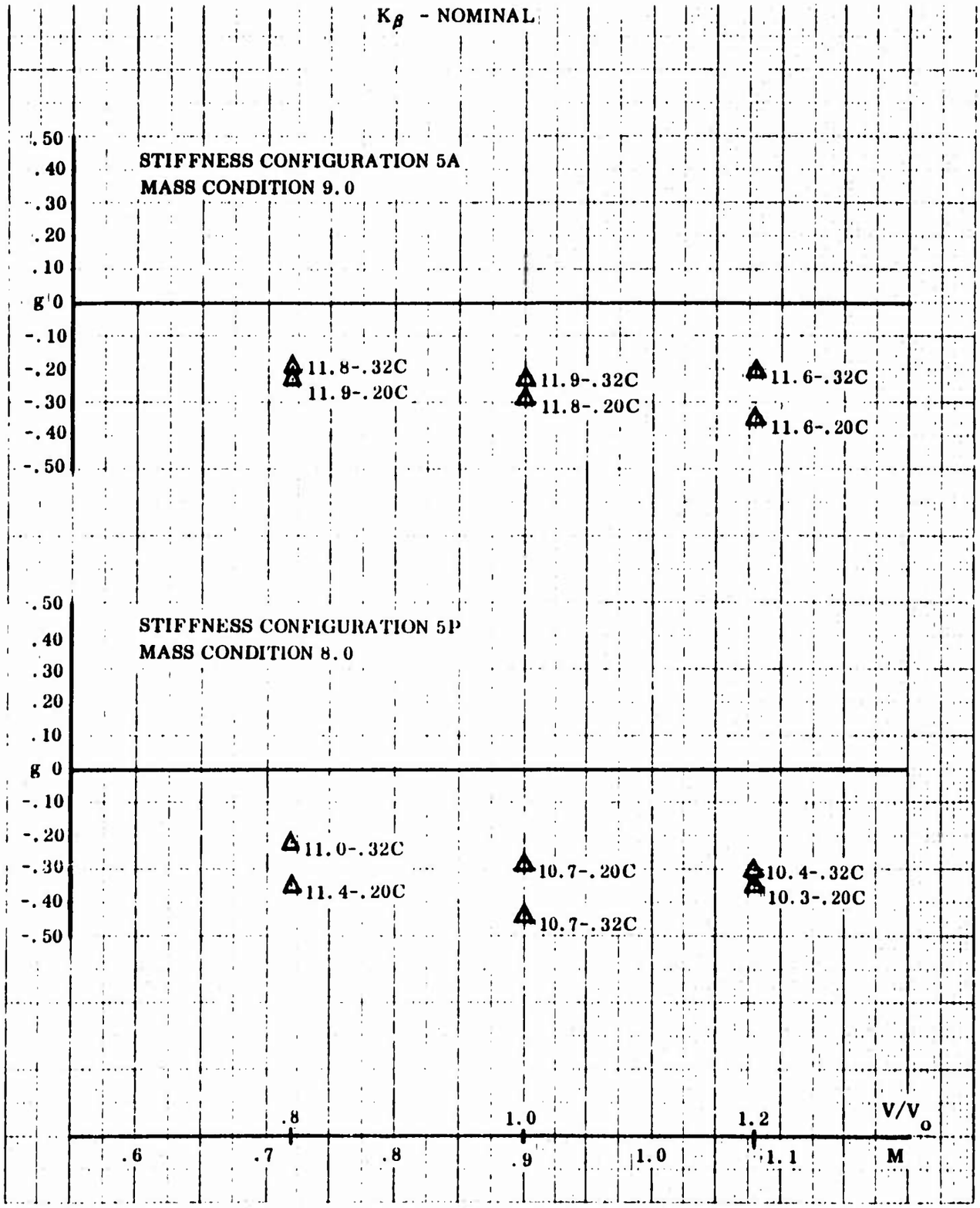

Figure 90 Phase V Studies - Antisymmetric: Flight Condition E (M = 0.90 at 5,000')

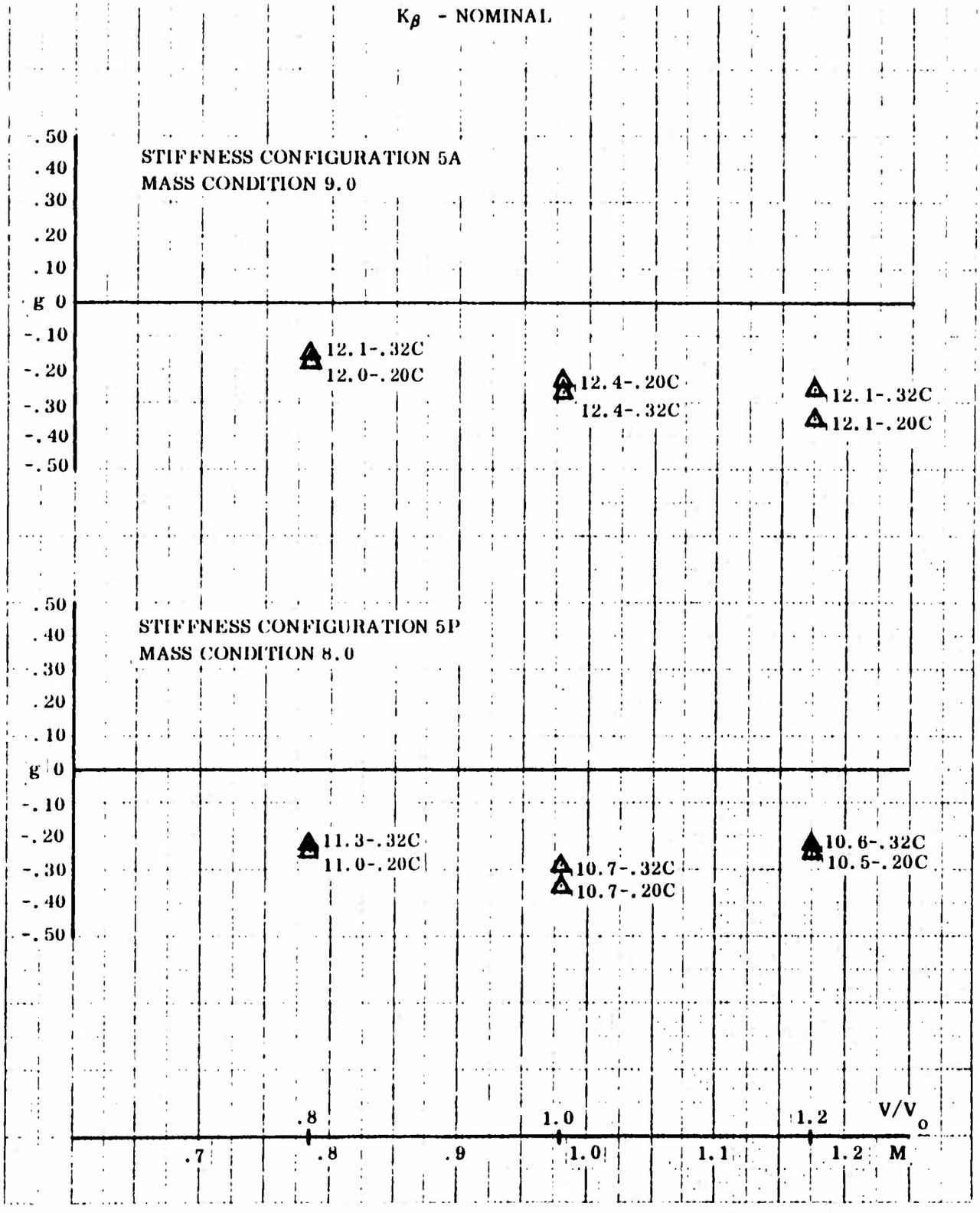

Figure 91 Phase V Studies - Antisymmetric: Flight Condition B (M = 0.98 at 9,500')

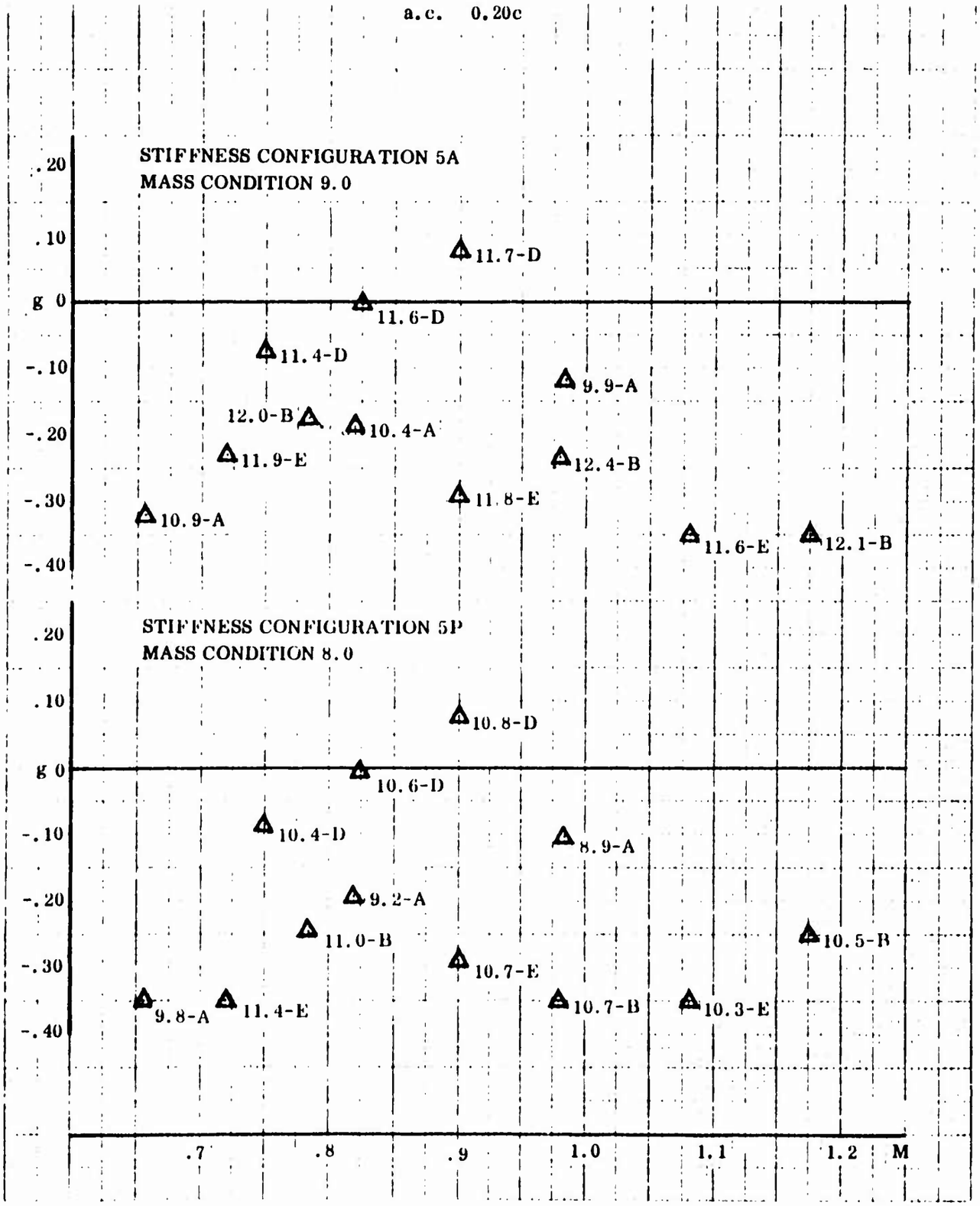

Figure 92 Phase V Studies - Antisymmetric: Flight Conditions, D, A, E and B

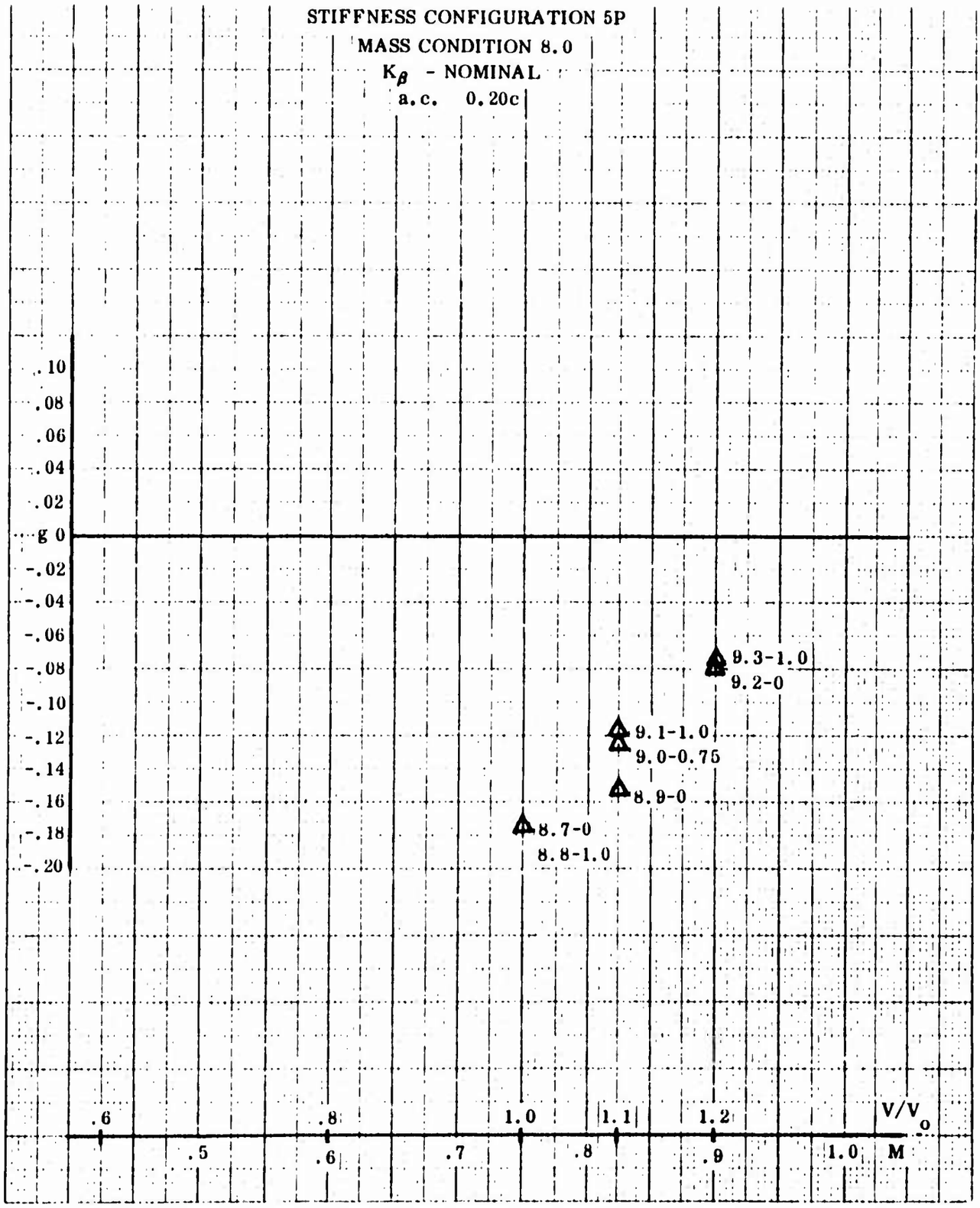

Figure 93 Phase VI Studies - Symmetric: Flight Condition D (M = 0.75 at Sea Level)

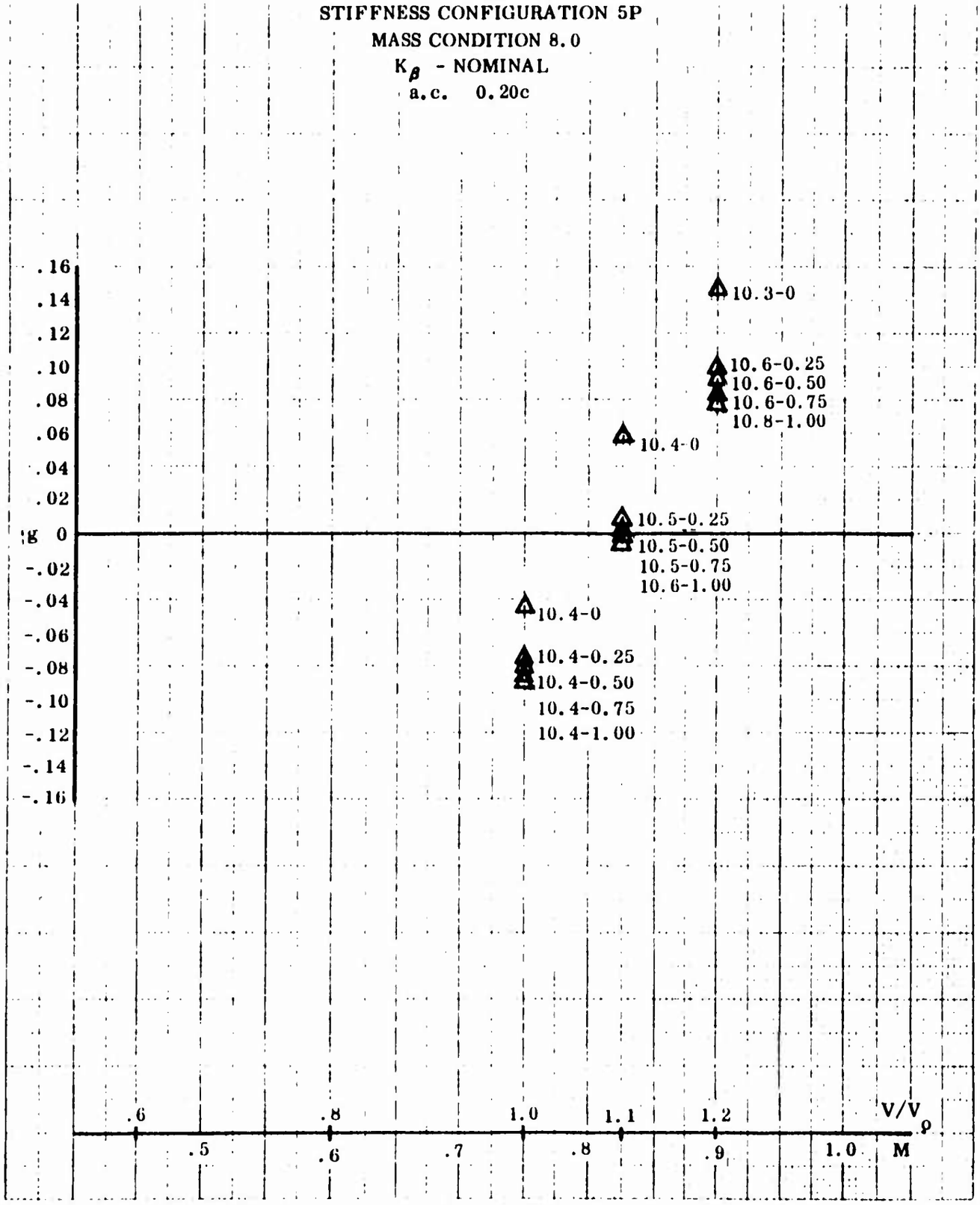

Figure 94 Phase VI Studies - Antisymmetric: Flight Condition D (M = 0.75 at Sea Level)

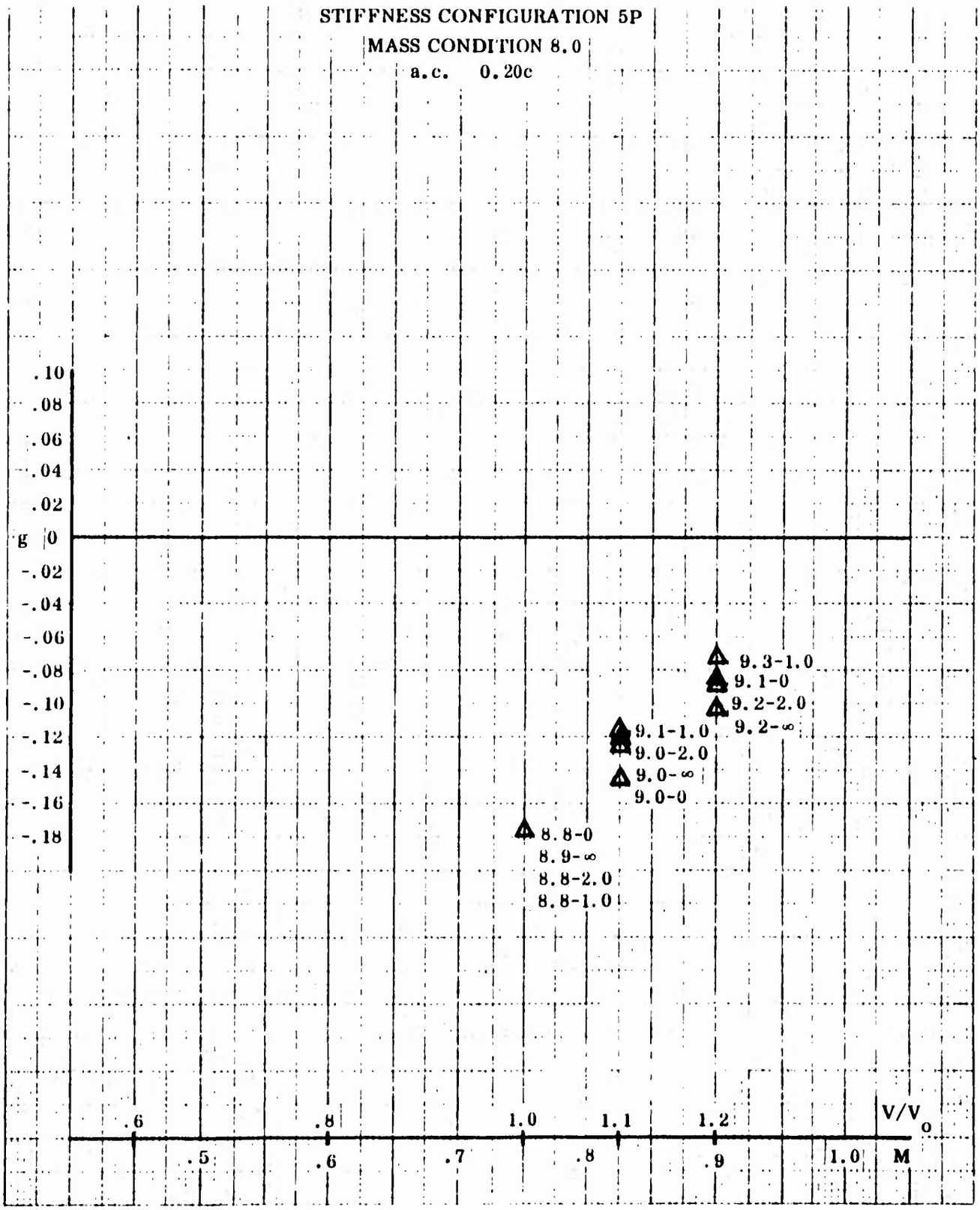

Figure 95 Phase VII Studies - Symmetric: Flight Condition D (M = 0.75 at Sea Level)

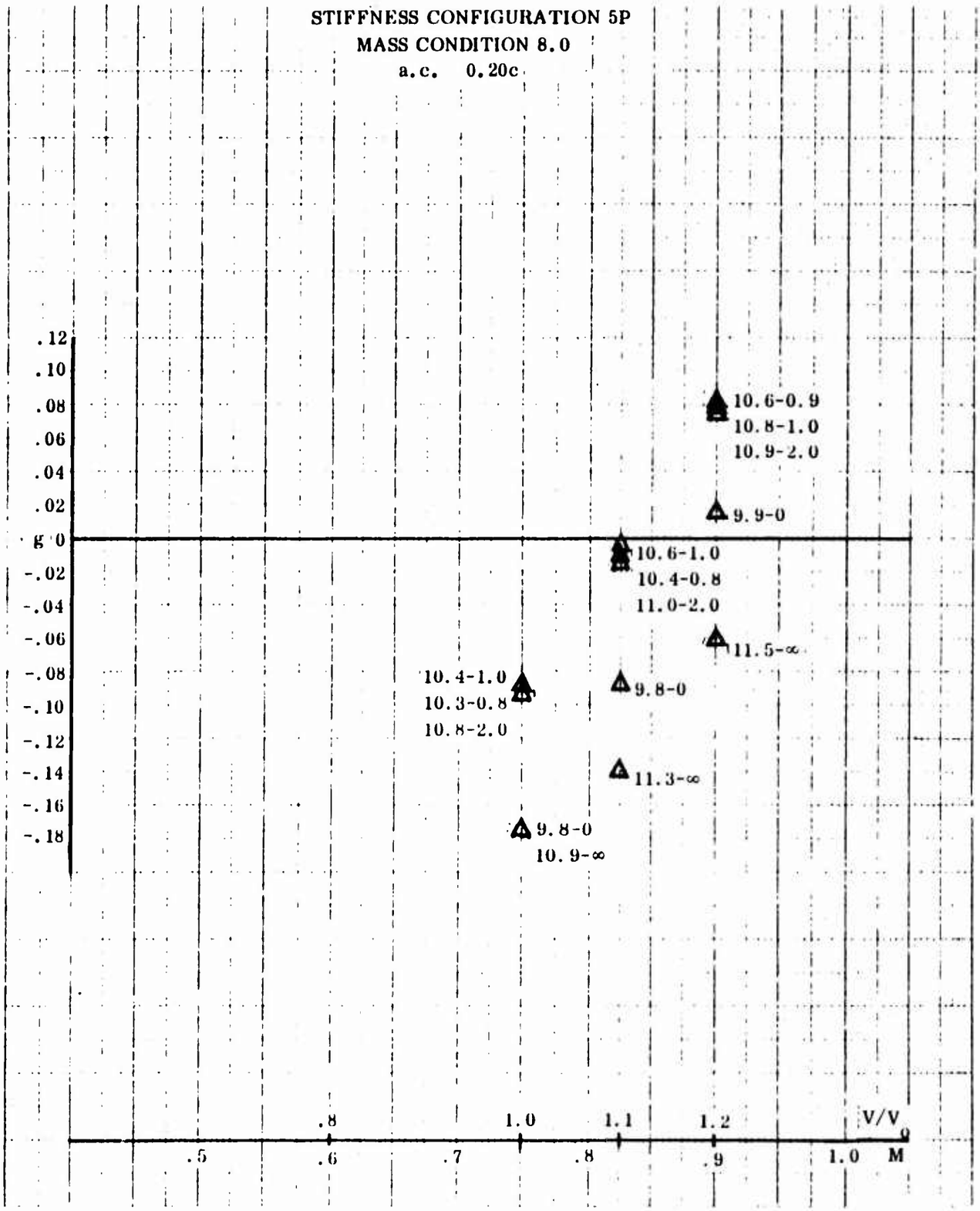

Figure 96 Phase VII Studies - Antisymmetric: Flight Condition D (M = 0.75 at Sea Level)

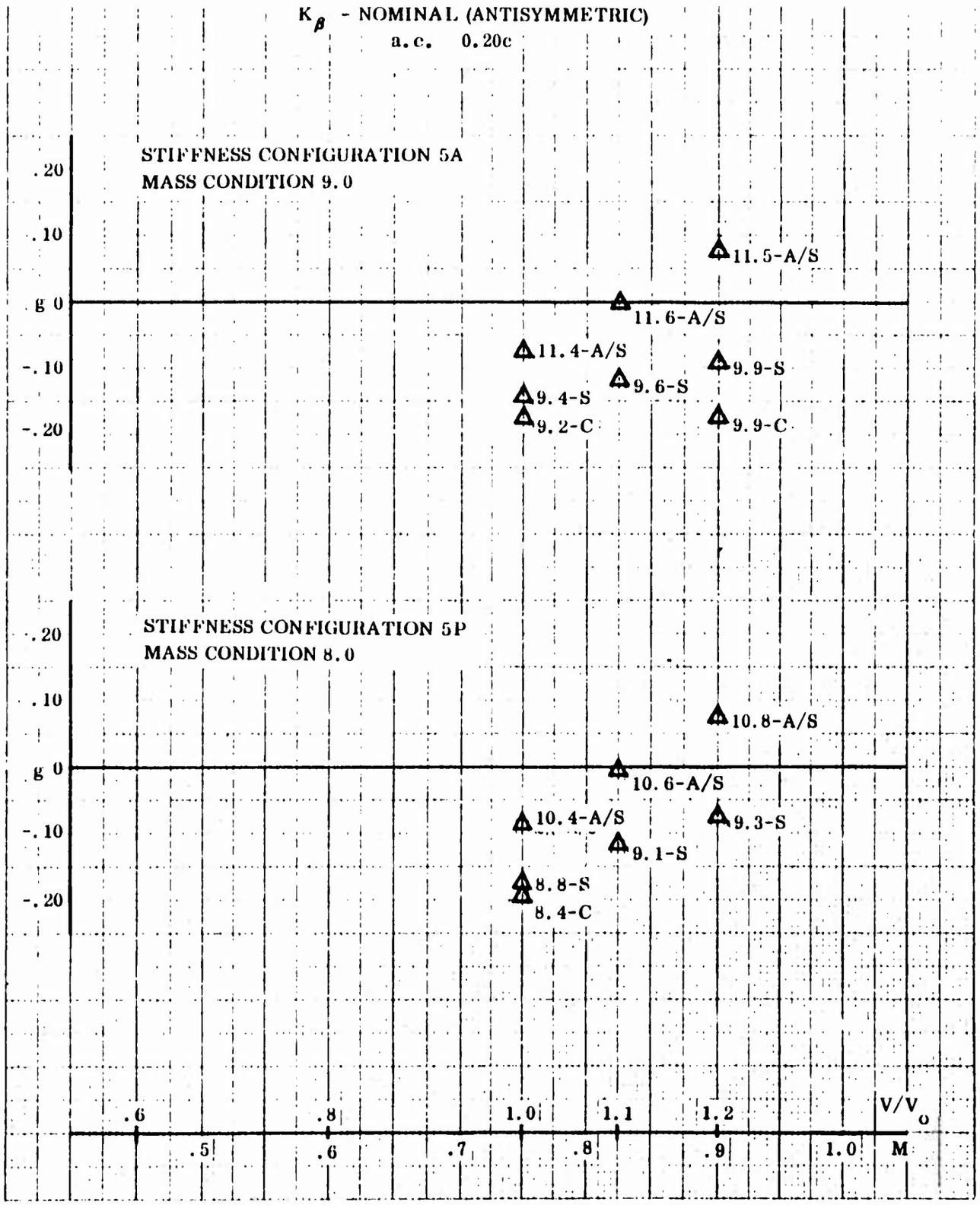

Figure 97 Phase VIII Studies - Cantilevered Wing - Flight Condition D
(M = 0.75 at Sea Level)

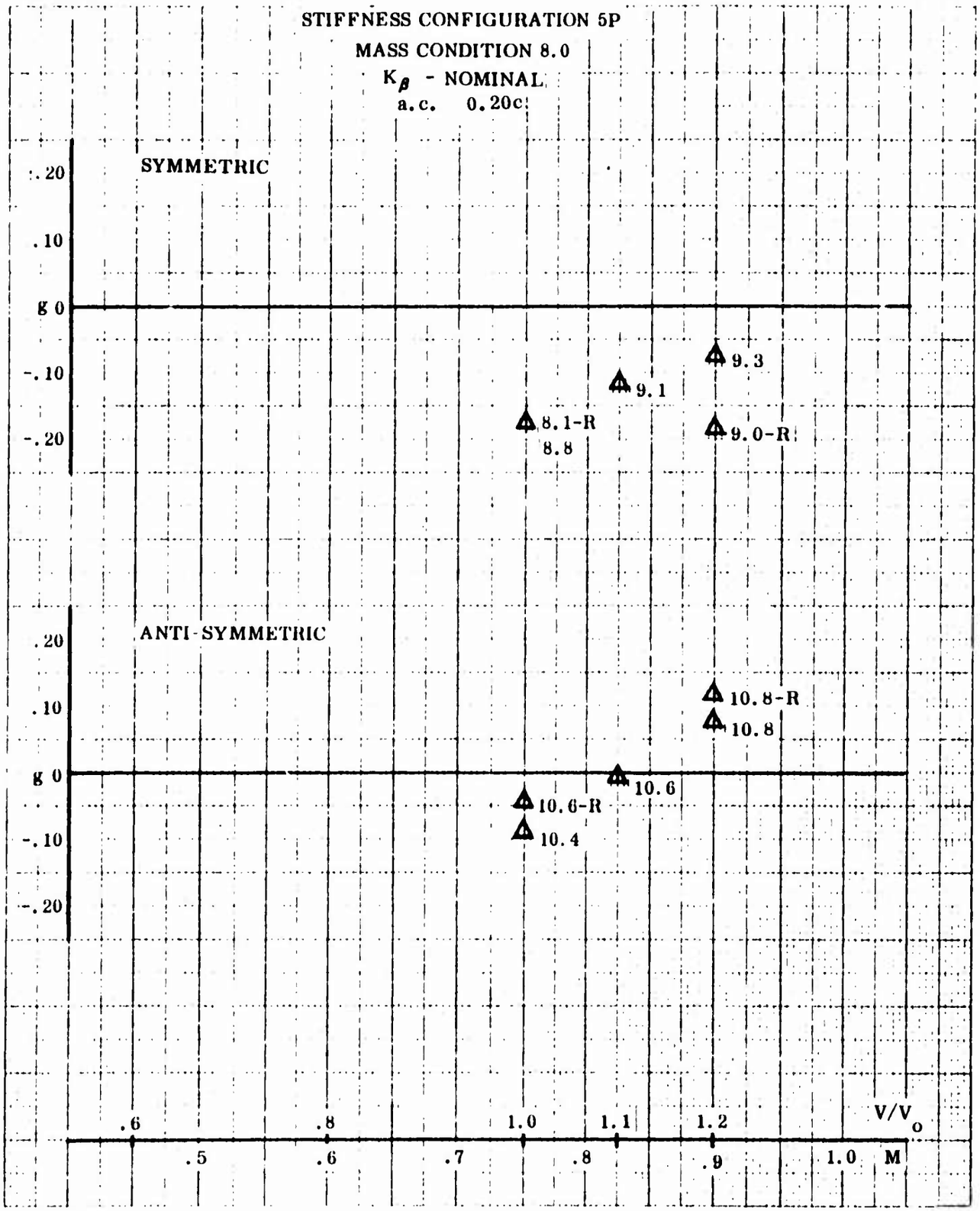

Figure 98 Phase VIII Studies - Rigid Fuselage and Empennage - Flight Condition D (M = 0.75 at Sea Level)

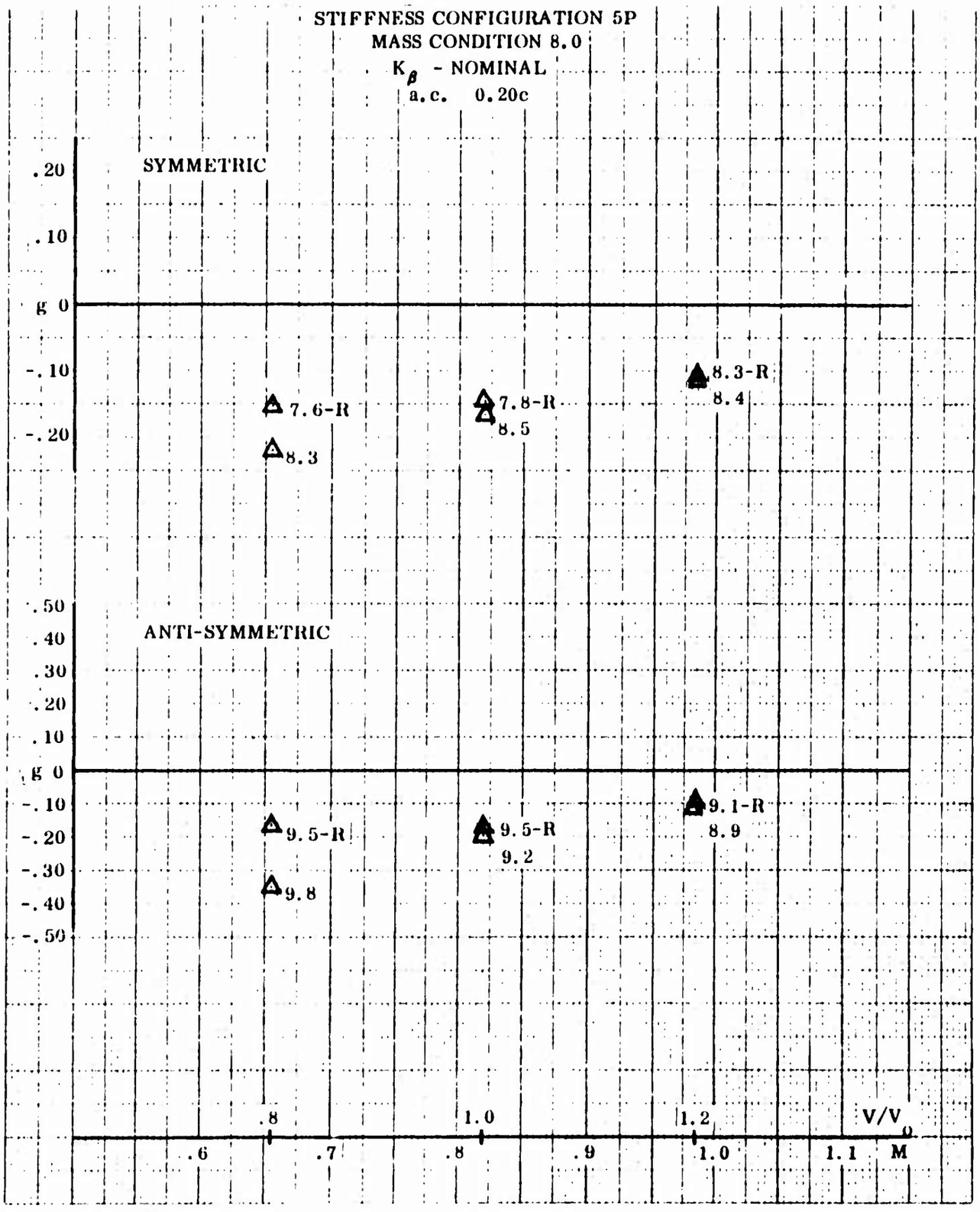

Figure 99 Phase VIII Studies - Rigid Fuselage and Empennage - Flight Condition A (M = 0.82 at Sea Level)

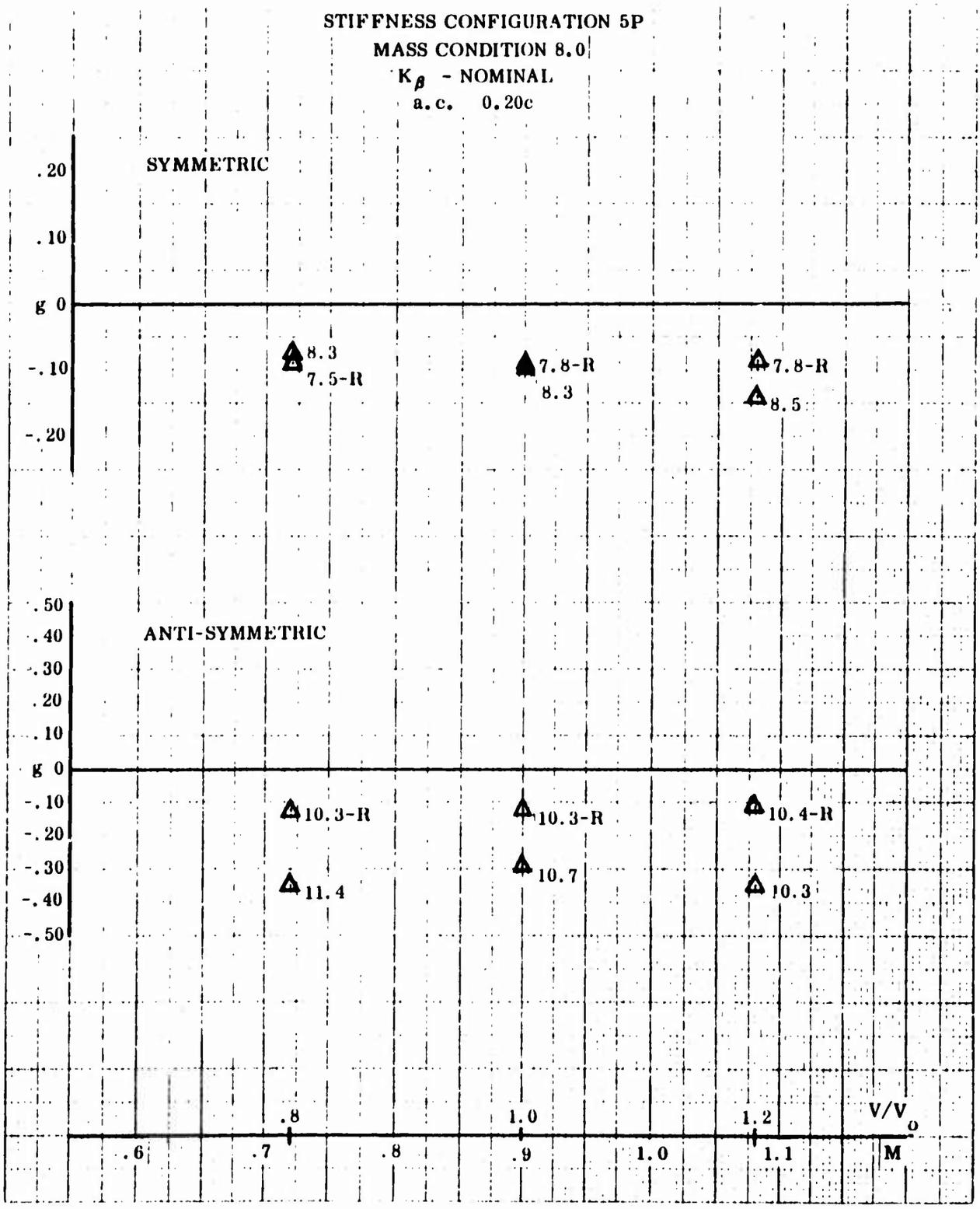

Figure 100 Phase VIII Studies - Rigid Fuselage and Empennage - Flight Condition E (M = 0.90 at 5,000')

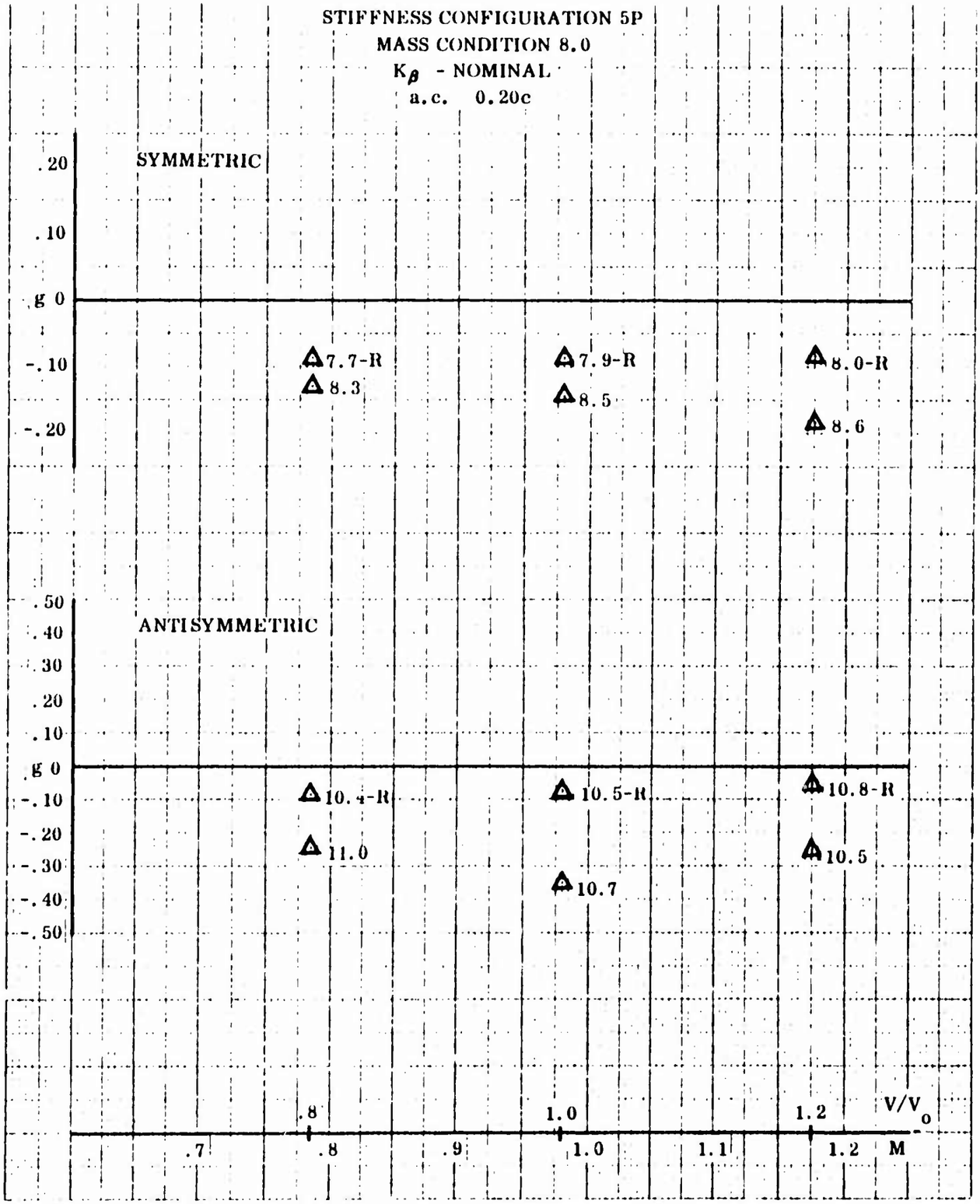

Figure 101 Phase VIII Studies - Rigid Fuselage and Empennage - Flight Condition B (M = 0.98 at 9,500')

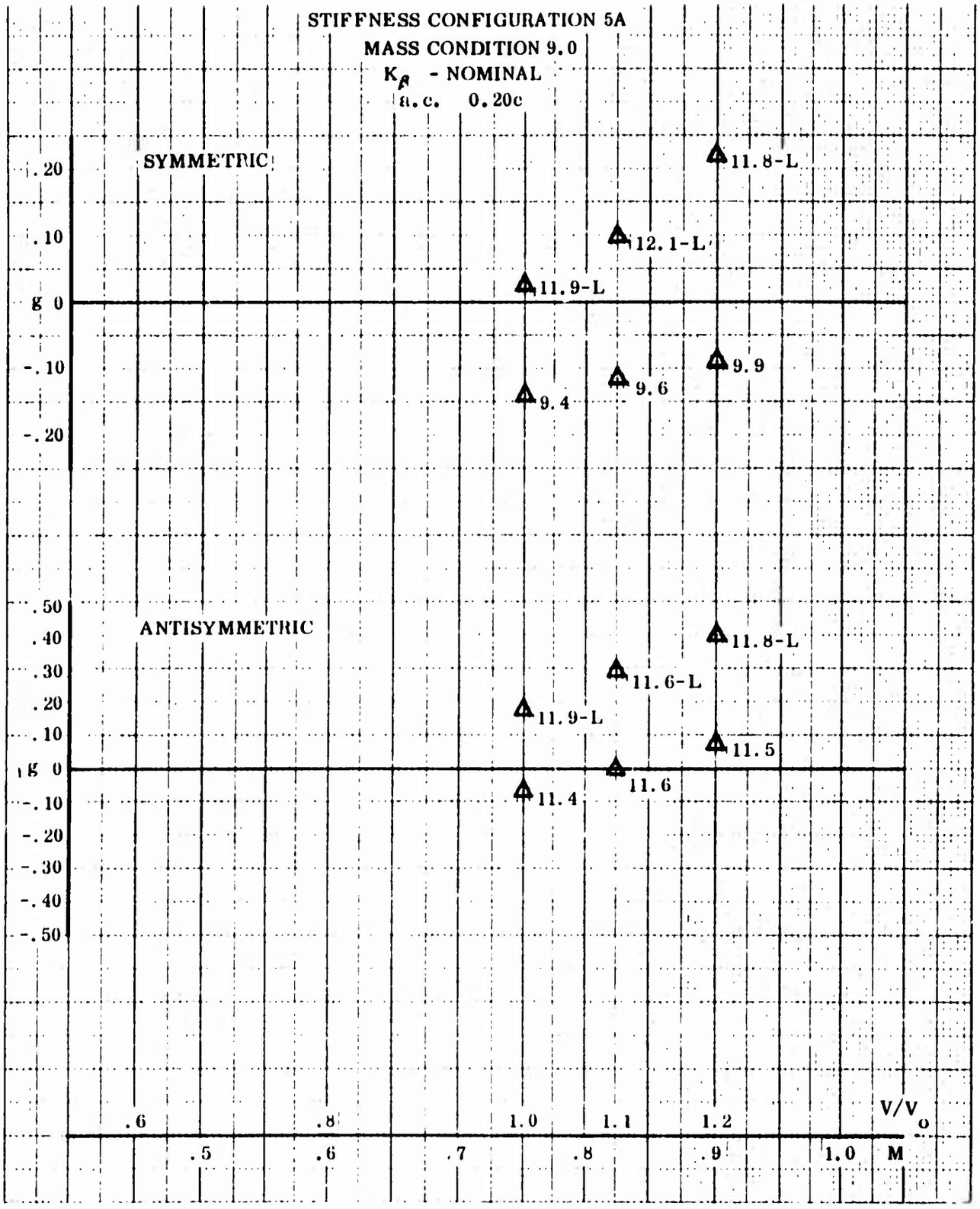

Figure 102 Phase IX Studies - Lag Function Effects - Flight Condition D (M = 0.75 at Sea Level)

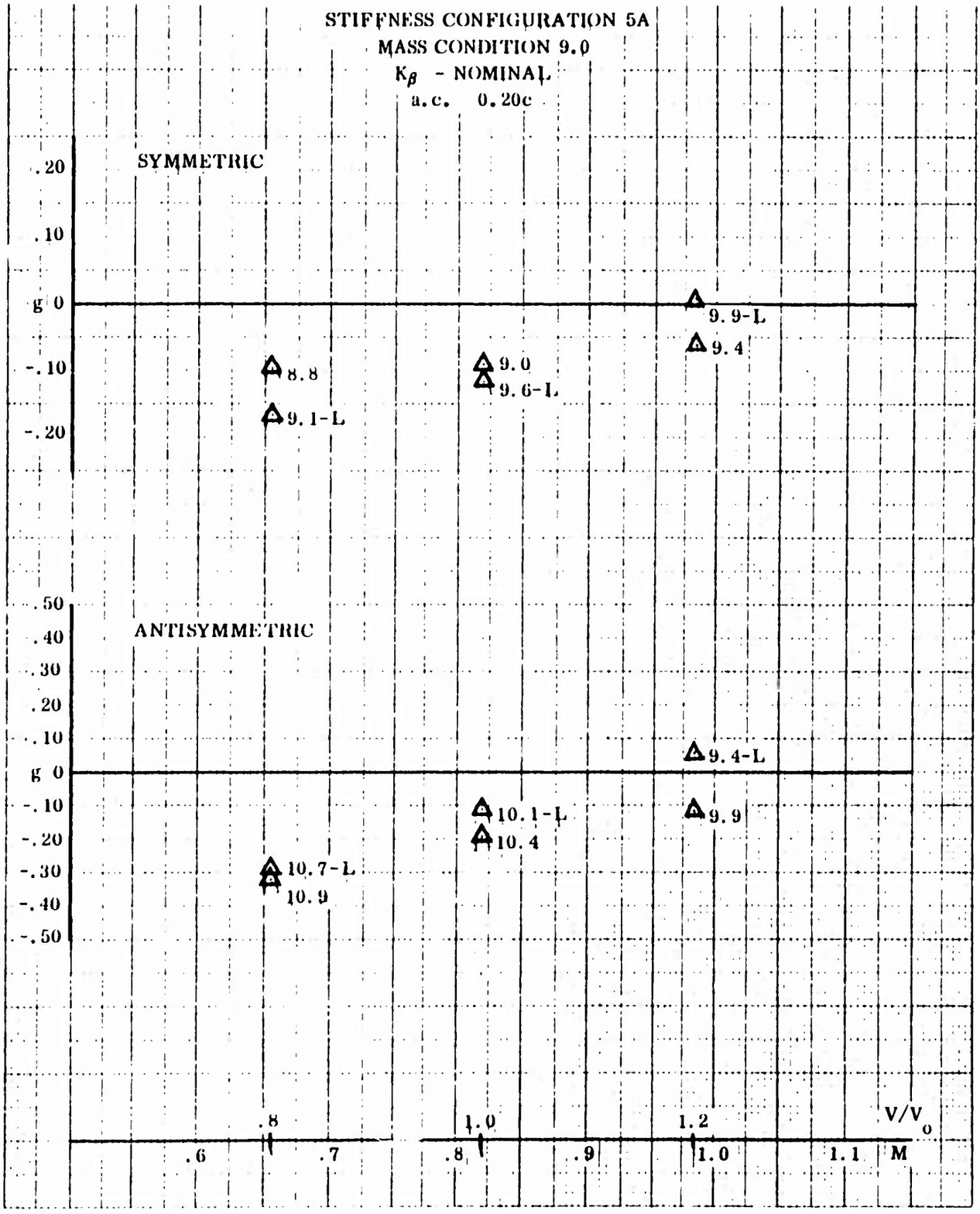

Figure 103 Phase IX Studies - Lag Function Effects - Flight Condition A (M = 0.82 at Sea Level)

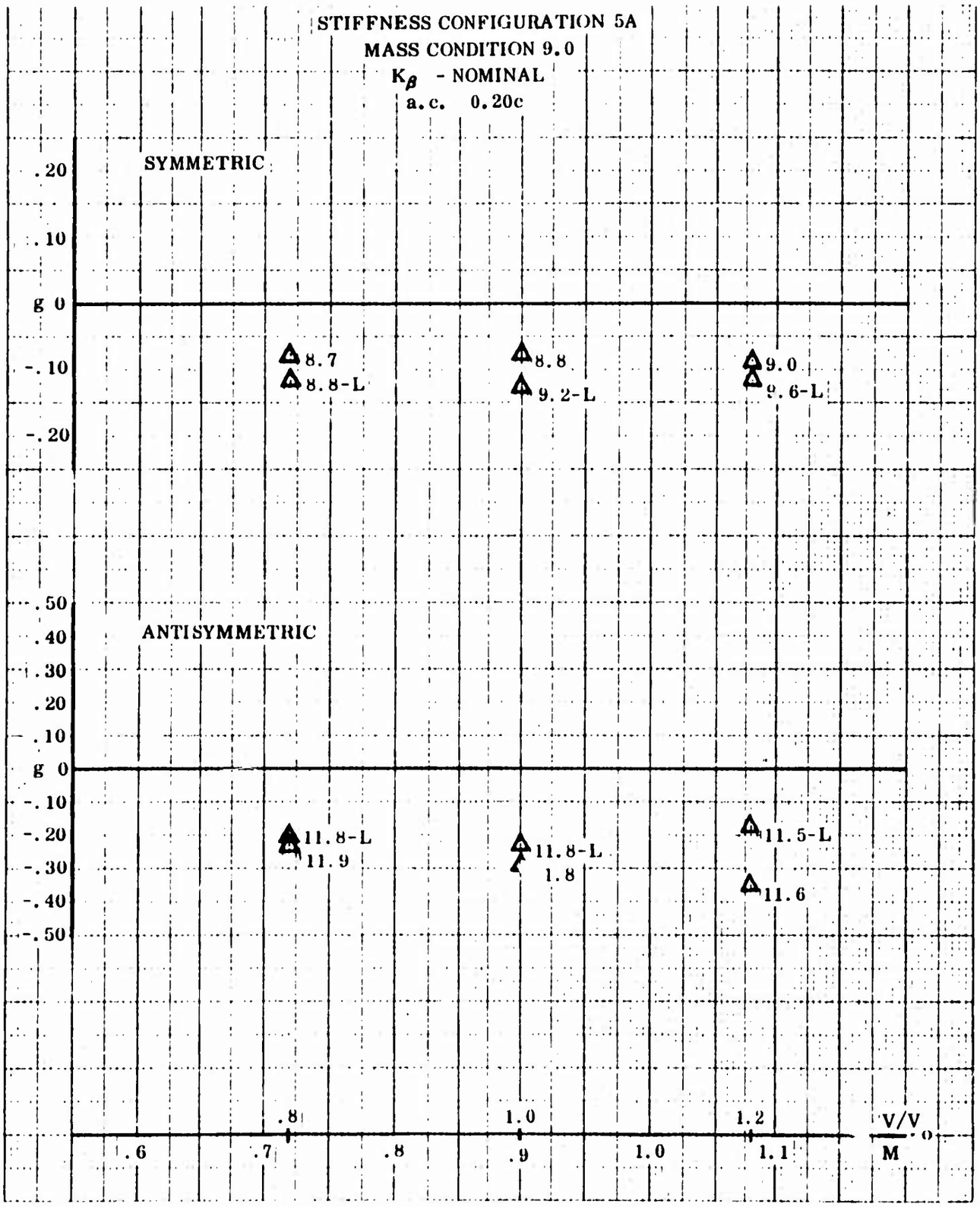

Figure 104 Phase IX Studies - Lag Function Effects - Flight Condition E (M = 0.90 at 5,000')

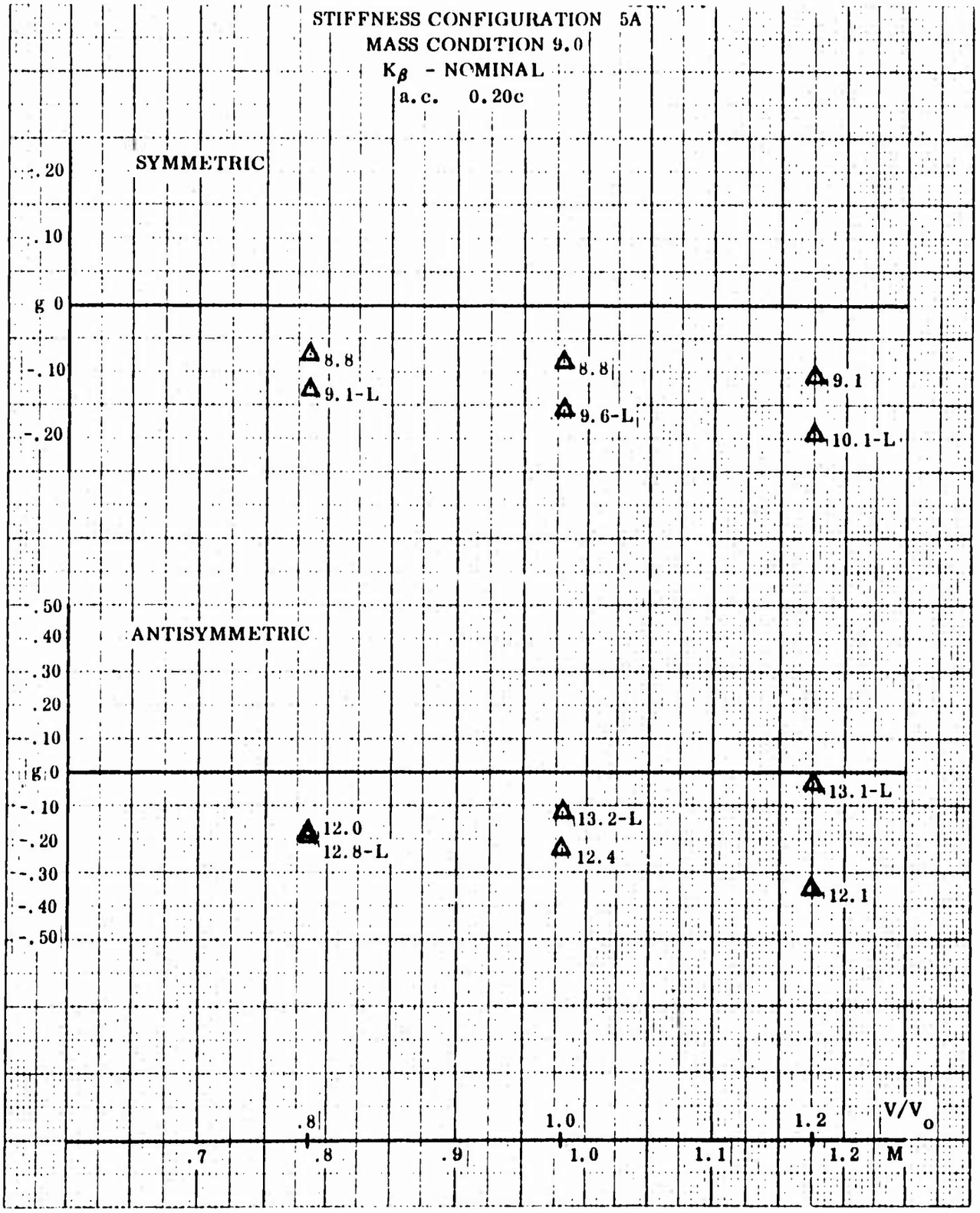

Figure 105 Phase IX Studies - Lag Function Effects - Flight Condition B (M = 0.98 at 9,500')

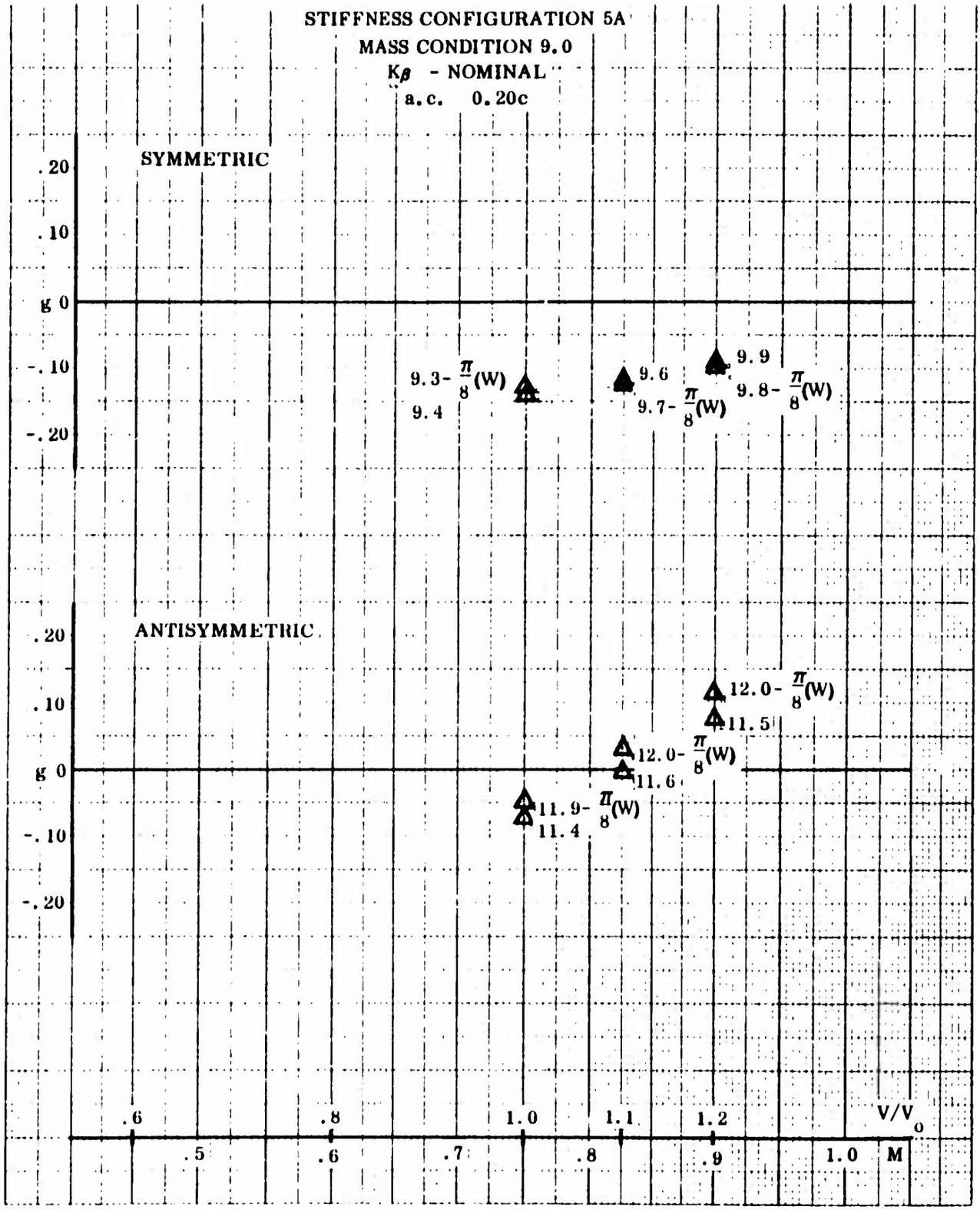

Figure 106 Phase IX Studies - C_{M_q} Effects - Flight Condition D (M = 0.75 at Sea Level)

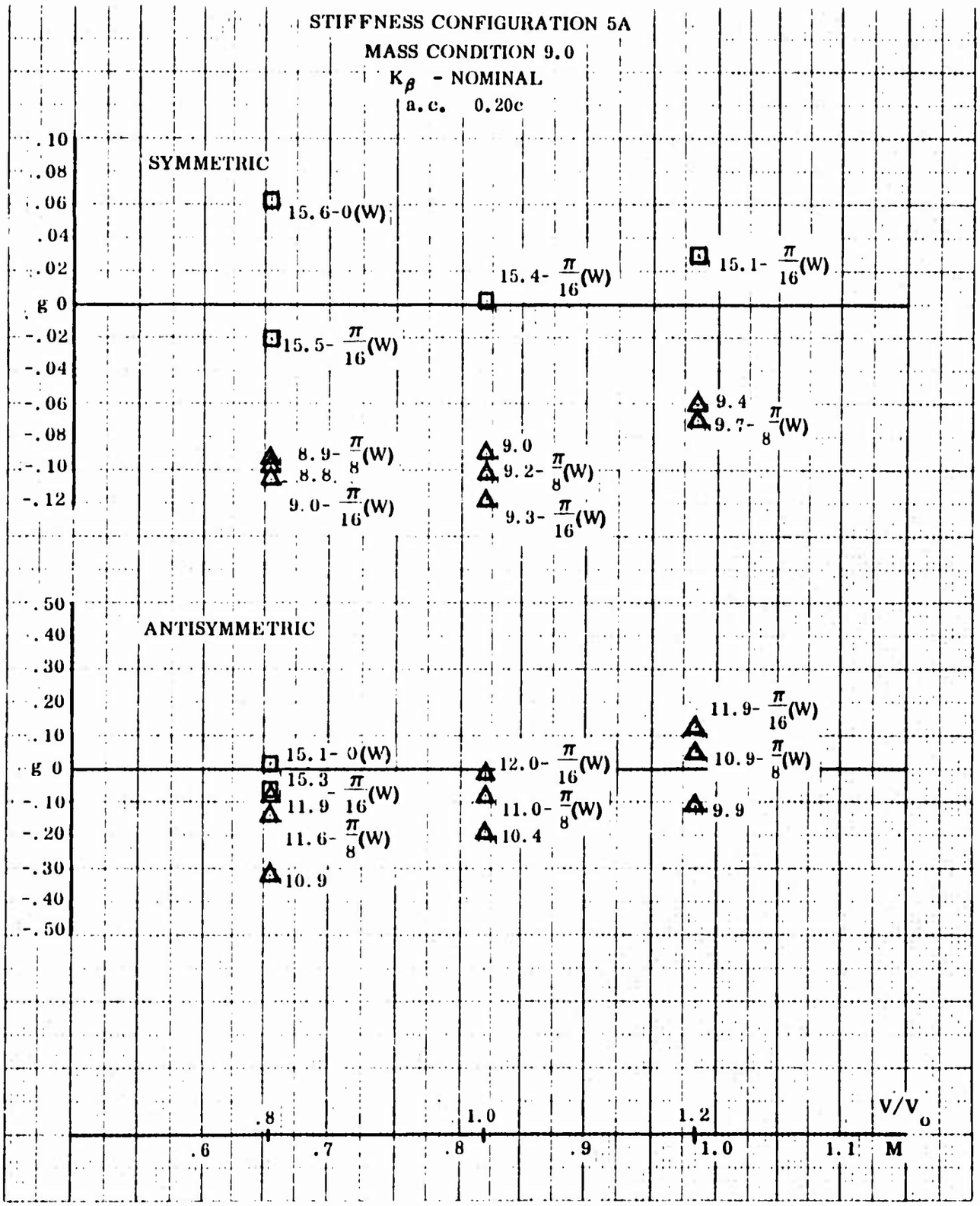

Figure 107 Phase IX Studies - C_{M_q} Effects - Flight Condition A (M = 0.82 at Sea Level)

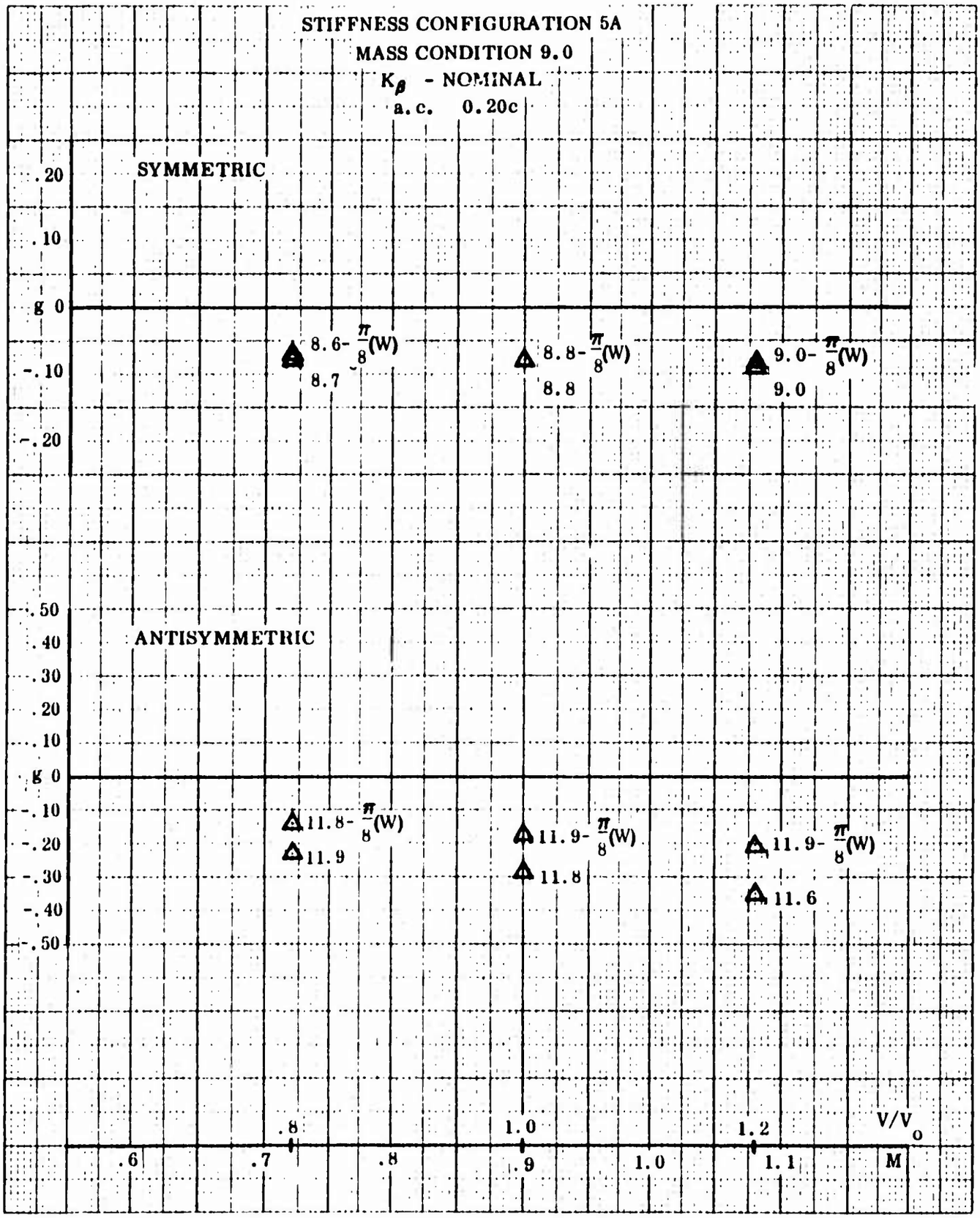

Figure 108 Phase IX Studies - C_{M_q} Effects - Flight Condition E (M = 0.90 at 5,000')

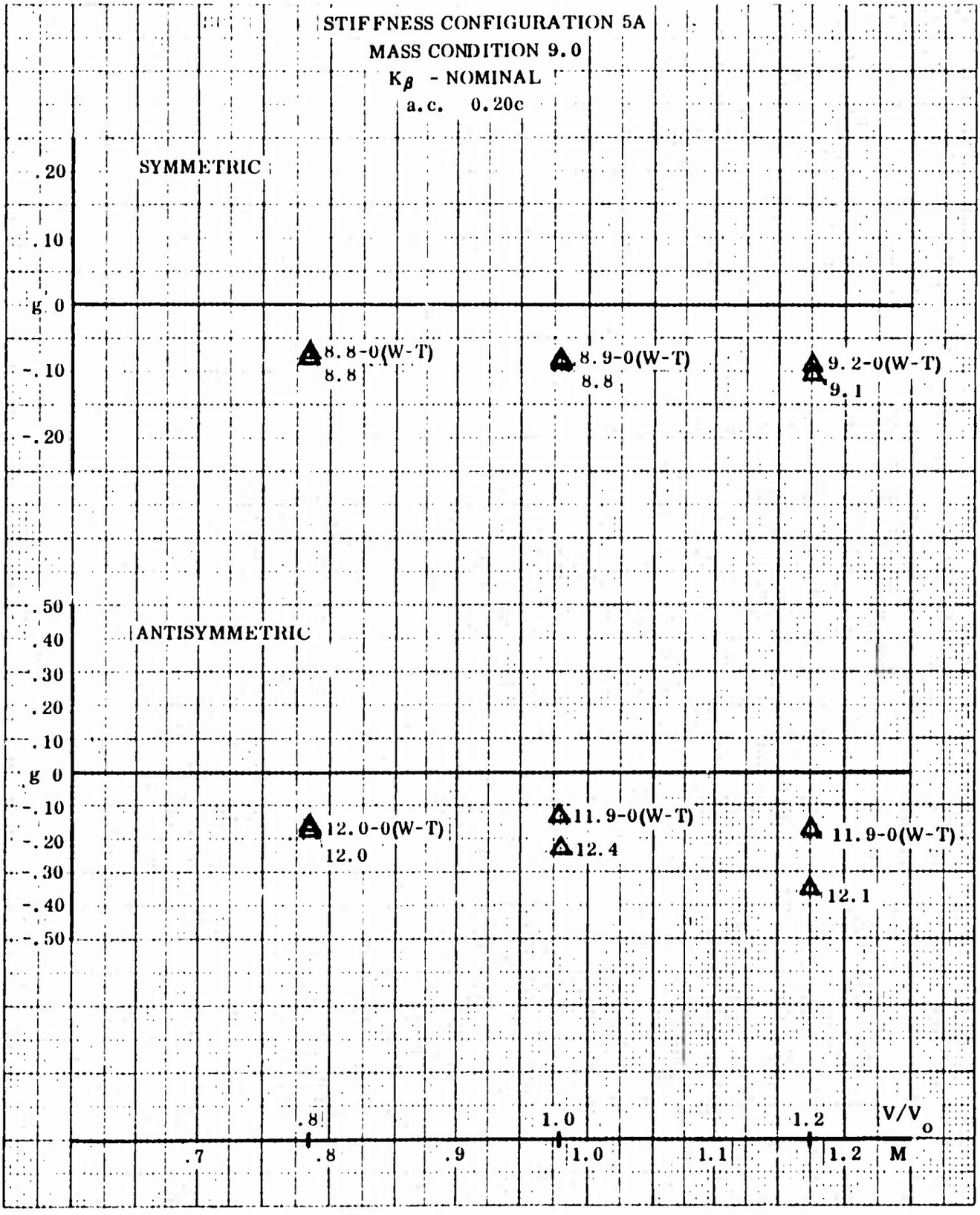

Figure 109 Phase IX Studies - C_{M_q} Effects - Flight Condition B (M = 0.98 at 9,500')

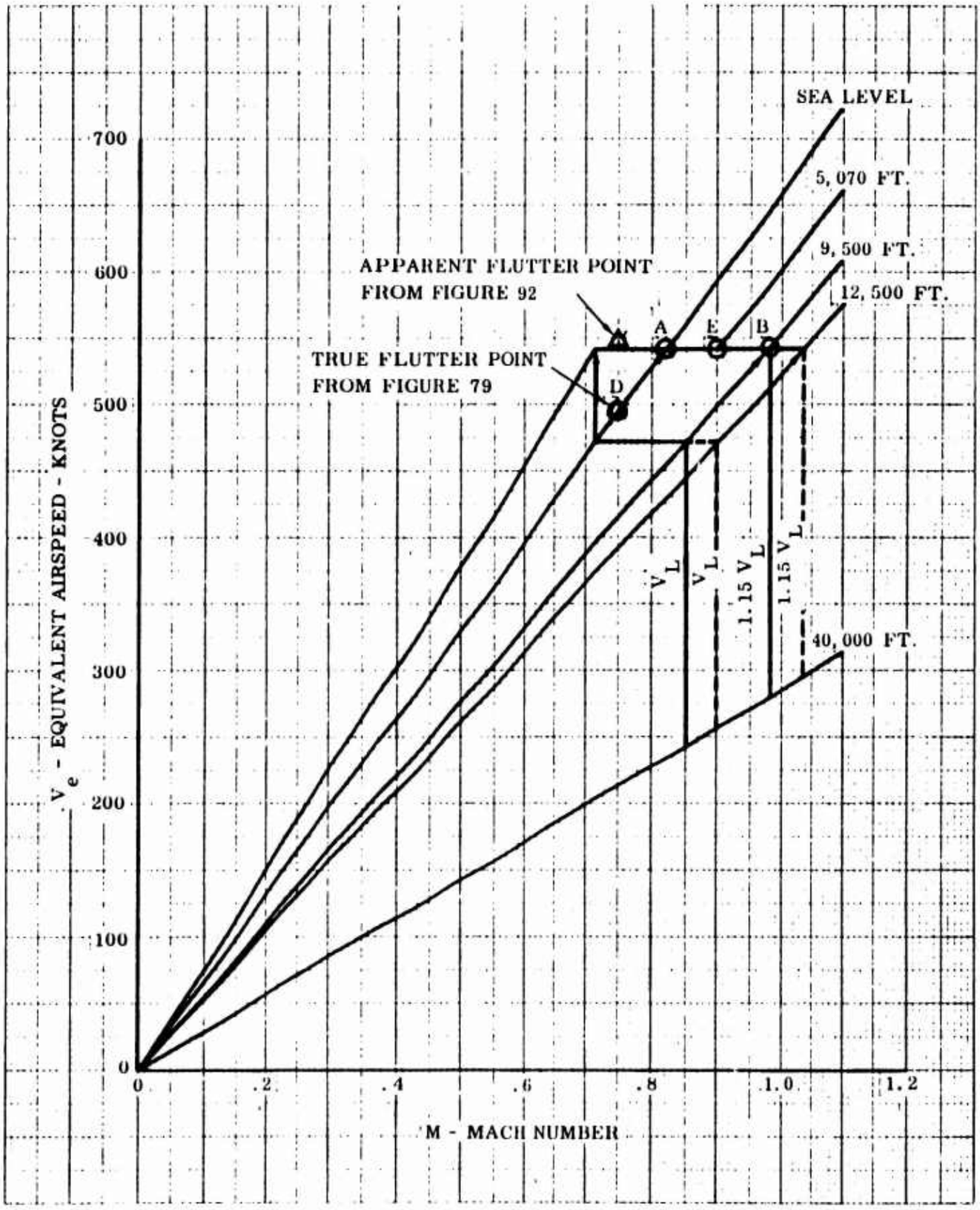

Figure 110 Flutter Boundary Envelope

TABLE 1

AERODYNAMIC DATA

X_a	W_2/W_1	$0.8W_5/W_4$	$0.4W_8/W_7$	W_6	$0.2W_5$
0.65	0.241	0.252	0.250	0.13	0.10
0.70	0.208	0.206	0.200	0.09	0.084
0.75	0.173	0.163	0.160	0.06	0.068
0.80	0.137	0.122	0.116	0.04	0.050

TABLE 2

STIFFNESS CONFIGURATIONS

Configuration Number	Flexibility Factor	
	Front Spar	Rear Spar
5A	Basic (Nominal)	Basic (Nominal)
5B	Basic	Basic
5C	0.85	1.15
5D	1.15	1.15
5E	1.15	0.85
5F	0.85	0.85
5G	1.00	1.15
5H	1.40	1.40
5I	1.35	1.35
5J	1.325	1.325
5K	1.00	1.50
5L	1.00	1.90
5M	1.00	2.10
5N	1.00	2.20
5P	1.11	1.18

$$\frac{1}{EI} = \frac{1}{EI}_{\text{Nominal}} \times \text{Flex. Factor}$$

TABLE 3

FLIGHT CONDITIONS

Flight Condition	Mach No.	Altitude (Ft.)	V_o (Knots)	q_o (lb/Ft^2)	$C_{M_q} / \frac{\pi}{8}$ (1/rad.)	C_{L_α}(Tail) (1/rad.)	Lag Function Coefficient	
							A	B
D	0.75	0	496	833	1.273	4.61	3.29	7.194
A	0.82	0	542	996	1.782	3.72	4.49	10.20
E	0.90	5,070	584	996	1.935	2.32	6.25	19.23
B	0.98	9,500	626	996	2.088	2.67	6.25	19.23

Lag Function

$$C(p) = \frac{A\left(\frac{c}{V}\right)p + 1}{B\left(\frac{c}{V}\right)p + 1}$$

$$p = \frac{d}{dt}$$

TABLE 4

MASS AND INERTIA DISTRIBUTION

(SYMMETRIC IDEALIZATION)

Wing: (Weights Distribution 3/6/62) *

Component	Basic Wing	Wing Fan	Fuselage Alloted Items	Total Wing	ΔFan (5/7/62)	Fuselage Alloted Items	Revised Total Wing
Panel Point	Wt.-Lb.	Wt.-Lb.	Wt.-Lb.	Wt.-Lb.	Wt.-Lb.	Wt.-Lb.	Wt.-Lb.
20G	31.8						31.8
20I	0						0
20K	19.6						19.6
30G	81.0						81.0
30I	0	720.0			35.9		755.9
30K	74.4						74.4
40G	17.7						17.7
40K	20.1						20.1
50G	24.1						24.1
50I	19.8						19.8
50K	47.3						47.3
60G	13.9						13.9
60I	16.9						16.9
60K	11.1						11.1
70G	9.6						9.6
70I	11.5						11.5
70K	9.3						9.3
80G	6.4						6.4
80I	5.8						5.8
80K	6.4						6.4
90G	4.5						4.5
90I	4.3						4.3
90K	3.9						3.9
Σ	439.4	720.0	97.3	1256.7	35.9	-97.3	1195.3

Wing Fan: (Lumped at Panel Point 30I - See Above)

W = 755.9 Lb.

$I_y = 0.4219 \times 10^6$ Lb-In^2

$I_x = 0.5063 \times 10^6$ Lb-In^2

* Per Side

TABLE 4 (Cont.)

MASS AND INERTIA DISTRIBUTION

(SYMMETRIC IDEALIZATION)

Fuselage: (Weights Distribution 4/13/62) *

Component Panel Point	Basic Fuselage Wt.-Lb.	Wing Fan Wt.-Lb.	Flap Wt.-Lb.	Wing Wt.-Lb.	Vertical Stab. Wt.-Lb.	Total Fuselage Wt.-Lb.
10A	95.06					95.06
10C	602.16					602.16
10E	514.62					514.62
10G	748.64			47.0		795.64
10I	304.88	90.3		8.8		403.98
10K	475.50		19.3	41.5		536.30
10M	208.55					208.55
10O	125.07					125.07
10Q	34.00				58.2	92.20
Σ	3108.48	90.3	19.3	97.3	58.2	3373.6

Horizontal Stabilizer: (Weights Distribution 4/17/62) *

Panel Point	Wt.-Lb.	I_{ea}-Lb.-In^2
H.S.10	29.9	8922
H.S.20	21.3	6024
Σ	51.2	14946.0

Total Airplane Distribution: (1/2 Airplane)

Fuselage:	3108.5 Lb.	Wing:	459.4 Lb.
Wing Fan to Fuselage:	90.3	Wing Fan:	720.0
Flap to Fuselage:	19.3	Wing Items:	97.3
Wing Items:	97.3	Total Wing:	Σ 1256.7
Vertical Stabilizer:	58.2	Δ Fan:	35.9
Total Fuselage:	Σ 3373.6	Wing Items:	-97.3
Horizontal Stabilizer:	51.2	Rev.Total Wing:	Σ 1195.3
Aileron (Nominal):	24.5		

Total Gross Weight: 2 (3373.6 + 51.2 + 24.5 + 1195.3) = 2 (4644.6) = 9289.2 Lb.

Center of Gravity: F.S. 239.04

* Fuselage - 1/2 Airplane; Horizontal Stabilizer - Per Side

TABLE 5

MASS AND INERTIA DISTRIBUTION

(ANTISYMMETRIC IDEALIZATION)

Wing: (Weights Distribution 3/6/62) *

Component Panel Point	Basic Wing Wt.-Lb.	Wing Fan Wt.-Lb.	Fuselage Alloted Items Wt.-Lb.	Total Wing Wt.-Lb.	Wing Fan Wt.-Lb.	Flap Wt.-Lb.	ΔFan (5/7/62) Wt.-Lb.	Revised Total Wing Wt.-Lb.
10G	0		47.0					47.0
10I	0		8.8		90.3			99.1
10K	0		41.5			19.3		60.8
20G	31.8							31.8
20I	0							0
20K	19.6							19.6
30G	81.0							81.0
30I	0	720.0					35.9	755.9
30K	74.4							74.4
40G	17.7							17.7
40K	20.1							20.1
50G	[illegible]							24.1
50I	[illegible]							19.8
50K	47.3							47.3
60G	13.9							13.9
60I	16.9							16.9
60K	11.1							11.1
70G	9.6							9.6
70I	11.5							11.5
70K	9.3							9.3
80G	6.4							6.4
80I	5.8							5.8
80K	6.4							6.4
90G	4.5							4.5
90I	4.3							4.3
90K	3.9							3.9
Σ	439.4	720.0	97.3	1256.7	90.3	19.3	35.9	1402.2

Wing Fan: (Lumped at Panel Point 30I - See Above)

$W = 755.9$ Lb.
$I_y = 0.4619 \times 10^6$ Lb.-In^2
$I_x = 0.5065 \times 10^6$ Lb.-In^2

* Per Side

TABLE 5 (Cont.)

MASS AND INERTIA DISTRIBUTION

(ANTISYMMETRIC IDEALIZATION)

Fuselage: (Weights Distribution 4/13/62) *

Component Panel Point	Basic Fuselage Wt.-Lb.	ΔW^{+} Wt.-Lb.	$\Delta W^{\neq}$ Wt.-Lb.	Total Fuselage Wt.-Lb.	Component Panel Point	Basic Fuselage $I_x \times 10^{-6}$-Lb-In^2
OA	95.06		50.00	145.06	OA	0.0810
OC	602.16		- 50.00	552.16	OC	0.4945
OE	514.62			514.62	OE	0.4899
OG	745.64	149.67	589.80	1488.11	OG	0.5274
OI	304.88	-304.88		0	OI	0.3430
OK	475.50	155.21	702.46	1333.17	OK	0.3279
OM	208.55			208.55	OM	0.2911
OO	125.07		- 47.42	77.65	OO	0.1814
OQ	34.00		47.42	81.42	OQ	0.0083
Σ	3108.48	0	1292.26	4400.74	Σ	2.7445

$\Sigma I_{z_{o_{Wing}}}$ = 5.563 x 10^6 Lb-In^2 (Applied at C.G. of A/C .S. 239.04)

Horizontal Stabilizer: (Weights Distribution 4/17/62) *

Panel Point	Wt.-Lb.	I_{ea}-Lb.In^2
H.S.10	29.9	8922.0
H.S.20	21.3	6024.0
Σ	51.2	14946.0

Vertical Stabilizer: (Weights Distribution 4/18/62) *

Component Panel Point	Basic V.S. Wt.-Lb.	H.S. Wt.-Lb.	Total V.S. Wt.-Lb.	Basic V.S. I_{ea}-Lb-In^2
V.S. 10	37.9		37.9	18974.0
V.S. 20	20.3		20.3	5436.0
V.S. 30	0	51.2	51.2	0
Σ	58.2	51.2	109.4	24410.0

* Fuselage - 1/2 Airplane; Horizontal and Vertical Stabilizer - Per Side

\+ Distribution of Lumped Fuselage Mass at Panel Point OI

≠ Weight Applied to Fuselage for Proper A/C Yaw Inertia Simulation

TABLE 6

AILERON

MASS AND INERTIA CONFIGURATIONS

Mass Condition 1 - Nominal: (Weights Distribution 4/18/62)

Component	Basic Aileron (Unbalanced)			Mass Balance*			Total Aileron (Balanced)		
Panel Point	Wt.~ Lb.	$\bar{X}$~In.	I_{HL}~Lb.-In.^{2}	Wt.~Lb.	$\bar{X}$~In.	I_{HL} Lb.-In.^{2}	Wt.~Lb.	$\bar{X}$~In.	I_{HL}~Lb.-In.^{2}
55	4.70	4.14	274.8	3.50	-6.7	159.0	8.20	-0.49	433.8
62	2.14	6.19	190.5	2.24	-5.9	78.0	4.38	0.01	268.5
70	1.92	5.48	149.9	2.22	-5.3	62.4	4.14	-0.30	212.3
76	2.16	5.18	148.2	2.38	-4.7	52.6	4.54	0	200.8
85	2.48	3.46	181.2	0.74	-13.3	130.9	3.22	-0.39	312.1
Σ	13.39			11.08			24.48		
	Σ $W\bar{X}$ = 63.0 Lb.-In.			Σ $W\bar{X}$ = -69.5			Σ $W\bar{X}$ = -6.5		

Mass Condition 2: (Balance at Outb'd. Panel Point)

Component	Mass Balance*				Total Aileron (Balanced)			
Panel Point	W ~ Lb.	$\bar{X}$~In.	$W\bar{X}$~Lb.-In.	I_{HL}~ Lb.-In.^{2}	W ~ Lb.	$\bar{X}$~In.	$W\bar{X}$~Lb.-In.	I_{HL}~ Lb.-In.^{2}
55	0	0	0	0	4.70	4.14	19.4	274.8
62	0	0	0	0	2.14	6.19	13.2	190.5
70	0	0	0	0	1.92	5.48	10.5	149.9
76	0	0	0	0	2.16	5.18	11.2	148.2
85	0.74	-13.3	-9.84	130.9	3.22	-0.39	-1.2	312.1
Σ	0.74		-9.84		14.14		53.1	

Mass Condition 3: (Balance at Outb'd. Panel Point)

Component	Mass Balance*				Total Aileron (Balanced)			
Panel Point	W ~ Lb.	$\bar{X}$~In.	$W\bar{X}$~Lb.-In.	I_{HL}~Lb.-In.^{2}	W ~ Lb.	$\bar{X}$~In.	$W\bar{X}$~Lb.-In.	I_{HL}~Lb.-In.^{2}
55	0	0	0	0	4.70	4.14	19.4	274.8
62	0	0	0	0	2.14	6.19	13.2	190.5
70	0	0	0	0	1.92	5.48	10.5	149.9
76	0	0	0	0	2.16	5.18	11.2	148.2
85	6.29	-10.0	-62.9	629.0	8.77	-6.19	-54.2	810.2
Σ	6.29		-62.9		19.69		0.10	

*Treated as a Point Mass

TABLE 6 (CONTINUED)

AILERON

MASS AND INERTIA CONFIGURATIONS

Mass Condition 4: (Balance at Outb'd. Panel Point)

Component	Mass Balance*				Total Aileron (Balanced)			
Panel Point	Wt.~Lb.	$\bar{X}$~In.	$W\bar{X}$~Lb.-In.	I_{HL}~Lb.-In.^{2}	Wt.~Lb.	$\bar{X}$~In.	$W\bar{X}$~Lb.-In.	I_{HL}~Lb.-In.^{2}
55	0	0	0	0	4.70	4.14	19.4	274.8
62	0	0	0	0	2.14	6.19	13.2	190.5
70	0	0	0	0	1.92	5.48	10.5	149.9
76	0	0	0	0	2.16	5.18	11.2	148.2
85	9.62	-10.0	-96.2	962.0	12.10	-7.24	-87.6	1143.2
Σ	9.62		-96.2		23.02		-33.2	

Mass Condition 5: (Balance at Inb'd. & Outb'd. Panel Points)

Component	Mass Balance*				Total Aileron (Balanced)			
Panel Point	Wt.~Lb.	$\bar{X}$~In.	$W\bar{X}$~Lb.-In.	I_{HL}~Lb.-In.^{2}	Wt.~Lb.	$\bar{X}$~In.	$W\bar{X}$~Lb.In.	I_{HL}~Lb.-In.^{2}
55	12.38	-7.0	-86.7	606.6	17.08	-3.93	-67.1	881.4
62	0	0	0	0	2.14	6.19	13.2	190.5
70	0	0	0	0	1.92	5.48	10.5	149.9
76	0	0	0	0	2.16	5.18	11.2	148.2
85	2.40	-4.1	-9.8	40.3	4.88	-0.26	-1.3	221.5
Σ	14.78		-96.5		28.18		-33.5	

Mass Condition 6: (Balance at Inb'd. & Outb'd. Panel Points)

Component	Mass Balance*				Total Aileron (Balanced)			
Panel Point	Wt.~Lb.	$\bar{X}$~In.	$W\bar{X}$~Lb.-In.	I_{HL}~Lb.-In.^{2}	Wt.~Lb.	$\bar{X}$~In.	$W\bar{X}$~Lb.-In.	I_{HL}~Lb.-In.^{2}
55			NOT AVAILABLE					
62	0	0	0	0	2.14	6.19	13.2	190.5
70	0	0	0	0	1.92	5.48	10.5	149.9
76	0	0	0	0	2.16	5.18	11.2	148.2
85			NOT AVAILABLE					

*Treated as a Point Mass

TABLE 6 (CONTINUED)

AILERON

MASS AND INERTIA CONFIGURATIONS

Mass Condition 7: (Balance at Inb'd. & Outb'd. Panel Points)

Component	Mass Balance*				Total Aileron (Balanced)			
Panel Point	Wt. ~ Lb.	$\bar{X}$~In.	W$\bar{X}$~Lb.-In.	I_{HL}~Lb.-In.^{2}	Wt.~Lb.	$\bar{X}$~In.	W$\bar{X}$~Lb.-In.	I_{HL}~Lb.-In.^{2}
55	8.53	-7.0	-59.71	418.0	13.23	-3.04	-40.2	692.8
62	0	0	0	0	2.14	6.19	13.2	190.5
70	0	0	0	0	1.92	5.48	10.5	149.9
76	0	0	0	0	2.16	5.18	11.2	148.2
85	2.4	-4.1	-9.84	40.3	4.88	-0.25	-1.2	221.5
Σ	10.93		-69.5		24.33		-6.5	

Mass Condition 8: (Balance at Outb'd. Panel Point)

Component	Mass Balance*				Total Aileron (Balanced)			
Panel Point	Wt. ~ Lb.	$\bar{X}$~In.	W$\bar{X}$~Lb.-In.	I_{HL}~Lb.-In.^{2}	Wt.~Lb.	$\bar{X}$~In.	W$\bar{X}$~Lb.-In.	I_{HL}~Lb.-In.^{2}
55	0	0	0	0	4.70	4.14	19.4	274.8
62	0	0	0	0	2.14	6.19	13.2	190.5
70	0	0	0	0	1.92	5.48	10.5	149.9
76	0	0	0	0	2.16	5.18	11.2	148.2
85	7.0	-10.0	-70.0	700.0	9.48	-6.47	-61.3	881.2
Σ	7.0		-70.0		20.4		-7.0	

Mass Condition 9: (Balance at Outb'd. Panel Point)

Component	Mass Balance*				Total Aileron (Balanced)			
Panel Point	Wt. ~ Lb.	$\bar{X}$~In.	W$\bar{X}$~Lb.-In.	I_{HL}~Lb.-In.^{2}	Wt.~Lb.	$\bar{X}$~In.	W$\bar{X}$~LB.-In.	I_{HL}~Lb.-In.^{2}
55	0	0	0	0	4.70	4.14	19.4	274.8
62	0	0	0	0	2.14	6.19	13.2	190.5
70	0	0	0	0	1.92	5.48	10.5	149.9
76	0	0	0	0	2.16	5.18	11.2	148.2
85	5.0	-10.0	-50.0	500.0	7.48	-5.53	-41.3	681.2
Σ	5.0		-50.0		18.39		13.0	

Note: Unbalance of aileron measured with respect to hinge-line, positive aft

*Treated as a Point Mass

TABLE 7

MODAL DATA

Stiffness Configuration 5A
Mass Condition 9
No Gyroscopic Forces

Symmetric:

Mode	Frequency cps	Damping g	Point Driven	Predominant Component
1	6.82	0.048	10A	Fuselage
2	8.50	0.040	90K	Wing
3	12.00	0.043	10A	Fuselage
4	12.58	0.053	Ail. 85 (M)*	Aileron-Fuselage
5	16.55	0.036	90K	Wing
6	20.35	0.022	90K	Wing-Fuselage
7	23.95	0.025	90K	Wing-Horiz. Stabilizer
8	25.65	0.021	H.S. 20	Horizontal Stabilizer

Anti-Symmetric:

Mode	Frequency cps	Damping g	Point Driven	Predominant Component
1	8.84	0.027	H.S. 20	Empennage
2	10.34	0.060	Ail. 85 (M)*	Aileron-Empennage
3	11.66	0.034	90K	Wing-Empennage
4	14.62	0.024	H.S. 20	Empennage
5	16.55	0.027	90K (M)*	Wing
6	20.41	0.015	0A	Fuselage
7	21.75	0.028	90K	Wing
8	30.10	0.015	V.S. 30	Fuselage-Empennage
9	42.60	0.023	90K	Wing

* Moment

TABLE 8

MODAL DATA

Stiffness Configuration 9P
Mass Condition 8
No Gyroscopic Forces

Symmetric:

Mode	Frequency cps	Damping ζ	Point Driven	Predominant Component
1	6.68	0.043	10Q	Fuselage
2	8.02	0.040	90K	Wing
3	11.44	0.045	Ail. 85 (M)*	Aileron-Fuselage
4	12.11	0.045	10A	Fuselage
5	15.92	0.038	90K	Wing
6	20.09	0.023	90K	Wing-Fuselage
7	22.95	0.029	90K	Wing-Horiz. Stabilizer
8	25.40	0.024	H.S. 20	Horizontal Stabilizer

Anti-Symmetric:

Mode	Frequency cps	Damping ζ	Point Driven	Predominant Component
1	8.64	0.030	H.S. 20	Empennage
2	9.70	0.037	Ail. 85 (M)*	Aileron-Empennage
3	11.02	0.032	90K	Wing-Empennage
4	14.52	0.023	H.S. 20	Empennage
5	15.88	0.030	40G	Wing
6	20.23	0.018	0A	Fuselage
7	20.84	0.019	90K	Wing
8	29.85	0.018	0Q	Fuselage-Empennage
9	41.15	0.023	90K	Wing

* Moment

TABLE 9

MODAL DATA

Stiffness Configuration 9A
Mass Condition 9
Gyroscopic Forces

Symmetric:

Mode	Frequency cps	Damping g	Point Driven	Predominant Component
1	6.83	0.044	10A	Fuselage
2	8.42	0.041	90K	Wing
3	12.06	0.036	10A	Fuselage
4	12.40	0.050	Ail. 85 (M)*	Aileron-Fuselage
5	16.34	0.037	90K	Wing
6	20.40	0.029	90K	Wing-Fuselage
7	24.15	0.025	90K	Wing-Horiz. Stabilizer
8	25.65	0.021	H.S. 20	Horizontal Stabilizer

Anti-Symmetric:

Mode	Frequency cps	Damping g	Point Driven	Predominant Component
1	8.84	0.028	H.S. 20	Empennage
2	10.32	0.059	Ail. 85 (M)*	Aileron-Empennage
3	11.65	0.036	90K	Wing-Empennage
4	14.60	0.025	H.S. 20	Empennage
5	16.32	0.029	40G	Wing
6	20.40	0.015	OA	Fuselage
7	22.00	0.025	90K	Wing
8	30.05	0.015	OQ	Fuselage-Empennage
9	42.60	0.023	90K	Wing

* Moment

TABLE 10

MODAL DATA

Stiffness Configuration 5P
Mass Condition 8
Gyroscopic Forces

Symmetric:

Mode	Frequency cps	Damping g	Point Driven	Predominant Component
1	6.63	0.049	10Q	Fuselage
2	8.00	0.038	90K	Wing
3	11.43	0.047	Ail. 85 (M)*	Aileron-Fuselage
4	12.12	0.049	10A	Fuselage
5	15.72	0.039	90K	Wing
6	20.12	0.023	90K	Wing-Fuselage
7	23.20	0.026	90K	Wing-Horiz. Stabilizer
8	25.45	0.020	H.S. 20	Horizontal Stabilizer

Anti-Symmetric:

Mode	Frequency cps	Damping g	Point Driven	Predominant Component
1	8.64	0.030	H.S. 20	Empennage
2	9.71	0.057	Ail. 85 (M)*	Aileron-Empennage
3	11.03	0.032	90K	Wing-Empennage
4	14.50	0.028	H.S. 20	Empennage
5	15.72	0.030	40G	Wing
6	20.28	0.015	0A	Fuselage
7	20.96	0.021	90K	Wing
8	29.90	0.017	0Q	Fuselage-Empennage
9	41.20	0.023	90K	Wing

* Moment